# NUMERICAL SIMULATION AND EXERGY ANALYSIS OF CI ENGINE OPERATIONS USING BIODIESEL BLENDS

**A thesis submitted in**

**part fulfillment of the requirements**

**for award of the degree of**

**Doctor of Philosophy**

**by**

**Tapan Kumar Gogoi**

Regn. No. 008 of 2011

**in**

**The School of Engineering**

**Department of Energy**

**Tezpur University**

Napaam-784028

**September, 2011**

**Dedicated to my Father in Heaven,**

**My family, friends and all well wishers**

**who supported and endured me**

## ABSTRACT

Biodiesel obtained from various edible and non edible sources are receiving significant attention world over as one of the possible renewable alternate fuels due to some obvious benefits viz. (i) similar fuel properties with fossil diesel, (ii) non-toxicity, (iii) biodegradability, (iv) absence of sulphur and aromatics (v) oxygenated fuel and (vi) better ignition quality. However, higher viscosity, lower calorific value and volatility are some of its drawbacks that are responsible for lower combustion and thermal efficiency with biodiesel. Only non-edible feedstock is considered as potential sources for biodiesel production in India, because it is difficult to justify the use of edible oils for biodiesel production as domestic requirements are higher than production.

Extensive researches are going on all over the world for evaluating engine performance with various blending of biodiesel including biodiesel in its pure form. The investigation of fuel combustion phenomena pertaining to such changes of fuel has also been a prime consideration in the context of ensuring biodiesel as a viable alternative. However, experimental investigations concerning fuel combustion vis-à-vis engine performance, with comprehensive representation of the system, are sometimes expensive and also time consuming. Mathematical simulation of engine behavior concerning combustion of conventional fuel vis-à-vis engine performance, where even the effect of engine design and operating conditions can also be assessed, has received meaningful attention in recent times. Success of such diesel-cycle simulation results indicates the possibilities of testing alternative fuels through appropriately developed simulation model. Therefore, in this study an attempt has been made to develop a diesel-cycle simulation model for prediction of engine performance with biodiesel blends as fuel.

A single-zone approach has been employed in modeling various engine processes for the present work. Two models are developed during the evolution of the study. Initially, the cycle-simulation model was developed to simulate engine performance (brake power and brake thermal efficiency) with varying speed and compression ratio for diesel and various diesel and biodiesel blends. The important considerations in the model are (i) simulation of compression and the expansion phases using polytropic relations of pressure and temperature with cylinder volume, (ii) heat release rate being determined employing simple Wiebe function and (iii) the parameter values in the model equations pertaining to fuel properties and operating conditions being based on some realistic conditions and relevant data as available in standard literature.

Diesel and 20% (B20), 40% (B40), 60% (B60) (by volume) blending of biodiesel from non edible Karanja (*Pongamia glabra*) oil with diesel were considered as fuels in this model. From the model results it was seen that the engine brake power (BP) increased with speed, reaching peak at particular speed and further increase in speed resulted in decrease of BP. Predicted BP at various speed was more in case of B40 and B60, whereas it was slightly lower in case of B20 compared to that of diesel. The blends B20, B40 and B60 also presented an increase in brake thermal efficiency (BTE) when compared to diesel. The model also predicted higher rate of pressure and temperature rise for the blends during combustion as compared to diesel. These model outputs are analyzed in terms of corresponding experimental results available in the literature.

Later, a second model was developed associating extensive experimental work conducted in laboratory and using specific biodiesel fuel blends prepared and characterized following standard procedure. The important components of this model are (i) iterative computation for the end states during the compression and expansion phases by applying first

law of thermodynamics for a closed system, (ii) heat release rate being determined employing double Wiebe function and (iii) the parameter values in the model equations based on experimental results of the present work.

Biodiesel is prepared from locally available Koroch seed oil (Pongamia glabra vent.) and then mixed in various proportions with diesel procured from Numaligarh Refinery Limited (NRL), Assam to prepare the blends *viz.* B10, B20, B30 and B40. These are characterized using standard procedure for generating some of the fuel-specific input data for the simulation study. The fuel properties of Koroch seed oil methyl ester (KSOME) blends are found quite similar to that of diesel, the viscosities being slightly higher and calorific values being comparatively lower. The experiments using different biodiesel blends are carried out in a single cylinder four stroke direct injection diesel engine. The set up is provided with necessary instruments for combustion pressure, fuel pressure, crank-angle, speed, airflow, fuel flow, temperatures and load measurements. It has also the facility for on line performance evaluation using data acquisition and processing software. A five gas analyzer is used to measure the concentration of gaseous emissions. Many important observations relating to performance, combustion and emission characteristics of the blended fuels are made from these experiments. Overall, engine BTE was found slightly lower for the KSOME blends than NRL diesel. BSFC of the blends was also more than diesel. Similarly, the engine IP was higher for the KSOME blends up to B30 over the entire range of load and it was less in case of B40. Early pressure rise was observed in case of the KSOME blends at various loads. Peak pressure of the combustion gases for NRL diesel and the KSOME blends was more or less same at full load. At lower loads, however, the peak pressure was slightly higher for the blends compared to NRL diesel peak pressure. Ignition delay period was less for the biodiesel blends, and due to shorter ignition delay, heat release occurred earlier. Compared to NRL diesel, the cumulative heat release was higher for the blends up to B30

and it was significantly less for the blend B40 at all the loads. The results concerning performance have mainly been used for validating the model results. Emission characteristics of the KSOME blends showed that it was the fuel blend B10 which produced lower emissions of carbon monoxide (CO), unburned hydrocarbon (HC), NOx, and smoke opacity. $CO_2$ emissions with the biodiesel blends were slightly higher than that of NRL diesel at various loads. In case of the other biodiesel blends (B20, B30 and B40), the CO and HC emissions were more at full and 75% of full load while these were less at 50% and 25% of full load. As opposed to this, the NOx emission was less for the blends at full and 75% of full load and the same being more at 50% and 25% of full load.

The second model was used to predict in-cylinder pressure evolution as a function of CA, IP, BP and BTE for a number of cases corresponding to different fuel operations at various loads. Experimental data such as speed, relative air fuel ratio, injection timings, combustion durations etc. obtained from experiments were used as input parameters for this model. The exact reproduction of the cylinder pressure trace was however not possible, particularly at lower loads and more significantly at 25% of full load. But, the overall agreement of model predictions with experimental data was good in terms of ignition delay, peak pressure, location of peak pressure, IP, BP and BTE. Steady increase with load as observed in case of experimental IP, BP and BTE results was observed in case of predicted IP, BP and BTE results too for all the biodiesel fuel blends. The model had been successful in predicting the trend correctly for IP, BP and BTE at various loads for NRL diesel as well as the blends of diesel and biodiesel.

A comprehensive energy and exergy balance study was also carried out to quantify the various losses and exergy destruction associated with various engine processes on the basis of experimental performance and emission data. An energy balance study was done for

understanding how the fuel energy is lost in engine operation with the biodiesel blends. Energy analysis based on first law alone does not permit quantitative measurement of factors that preclude the attainment of the best theoretical performance of an energy conversion device. Therefore, exergy balance study was performed to evaluate the irreversibility associated with various engine processes. Based on the exergy analysis, possible causes of exergy destruction are identified in case of fuel operation with biodiesel blends.

From the energy analysis, it was seen that the unaccounted heat losses were significantly high at all engine loads with respect to the fuel blend B40 which might be the reason of lower IP and BTE for this blend. The viscosities of the KSOME blends were more and due to this higher viscosity, particularly for the blend B40, the fuel did not atomize properly resulting in poor combustion. This might ultimately resulted in higher combustion losses and consequently lower IP and BTE for fuel blend B40 compared to those using B10, B20 and B30 blends. Combustion efficiency of the blends was determined and this was found to be higher for the blends B10, B20 and B30. However, there was marked reduction in combustion efficiency of B40 at various loads which confirms the possibility of incomplete combustion with this particular bio-diesel blend.

From the exergy analysis it was observed that the exergy destroyed with the KSOME blends was more compared to that of NRL diesel fuel operation at various loads. Most significantly, the rate of exergy destroyed for fuel operation with B40 was the maximum at all loads. These exergy destructions mainly represent the exergy destroyed due to phenomenon of air fuel mixing and combustion. Compared to NRL diesel fuel, exergetic efficiencies were found to be lower for the KSOME blends at various loads and particularly with B40.

From the comprehensive experimental investigation and also from various analyses it was confirmed that the engine performance and fuel combustion was favorable with KSOME blends up to B30. It is recommended that KSOME blending up to B30 can be used as fuel in the test engine which is mainly used as generating set and agricultural application in India without any significant drop in performance.

Moreover, the cycle simulation models developed in this study could be effectively used for performance analysis of biodiesel and its blends with petro-diesel. This was confirmed form the validation of the model simulation results using the experimental results.

**DEPARTMENT OF ENERGY**

**TEZPUR UNIVERSITY**

**NAPAAM-784028**

**TEZPUR**

## CERTIFICATE

This is to certify that the work contained in the thesis entitled "**Numerical Simulation and Exergy Analysis of CI engine Operations Using Biodiesel Blends**" submitted by **Sri Tapan Kumar Gogoi** for the award of the degree of Doctor of Philosophy of Tezpur University has been carried out under our supervision and guidance. This work has not been submitted elsewhere for the award of any other degree or diploma.


Prof. D.C. Baruah

Department of Energy

Tezpur University

Napaam-784028

Tezpur, Assam, India

Prof. S. Ghosal

Department of Mechanical Engineering

Jadavpur University

Kolkata-700 032

West Bengal, India

## *ACKNOWLEDGMENTS*

First of all I would like to acknowledge with many thanks my supervisors, Prof. Debendra Ch. Baruah and Prof. Sujit Ghosal for their assistance and advice throughout my research. I wish to express my deepest gratitude to Late Prof. Dulan Konwar, Prof. SK Dolui and Prof. S.K. Samdarshi for their guidance and help in my work and also for being associated with me as members of doctoral committee. I am also grateful to Apex Innovations Ltd., Sanghli, Maharastra for their constant support, particularly Mr. S.S. Mulay who provided many important information and constantly helped me in understanding the computerized engine set up. I would also like to thank all those students and technical staff members who have worked with me in the set up, particularly I thank Mihir Mouchum Hazarika, Dhirukamal Deka, Shovana Talukdar and Kamaljyoti Talukdar for their cooperation during the course of experimentation in the set up. I can't fail to acknowledge the support provided by the technical staff of the Mechanical Engineering Department. They were always with me to assist, whenever some problems related to the engine operations arised. I would also like to take this opportunity to thank the management of NEDFI, Khetri for providing their laboratory facility for transesterification of the raw Koroch seed oil into its methyl ester and particularly the technician Mr. Bharat Phukan. I also want of offer my sincere gratitude to the management of Quality Control Laboratory, Numaligarh refinery Ltd. who helped me in evaluating the properties of the biodiesel blends. My special thanks also go to Prof. V. Ganesan of IIT, Chennai who helped me in clearing some of my doubts about diesel engine cycle simulation through e mail. I especially wish to thank our Tezpur University authority for providing the logistics and other facilities throughout the course of this study. My small accomplishment would have not been possible if it was not for the endless patience of my beloved family, particularly my wife, Minakshi. I especially wish to thank my supervisors for the corrections and improvements suggested for this thesis.

Thank you all whom I did not mentioned here.

## TABLE OF CONTENTS:

LIST OF TABLES

LIST OF FIGURES

## Abbreviations

AFR Air fuel ratio

BDC Bottom dead centre

BMEP Brake mean effective pressure

BP Brake power

BSFC Brake specific fuel consumption

BTE Brake thermal efficiency

CA Crank angle

CI Compression ignition

CR Compression ratio

DI Direct injection

D2 No. 2 diesel

EVO Exhaust valve opening

FFA Free fatty acid

FMEP Frictional mean effective pressure

ICE Internal combustion engine

IDI Indirect injection

IP Indicated power

IVC Inlet valve closing

KSOME Koroch seed oil methyl ester

MEP Mean effective pressure

MF Marine fuel

NHRR Net heat release rate

SME Soybean methyl ester

SOC Start of combustion

SOI Start of injection

TDC Top dead centre

YGME Yellow grease methyl ester

**Nomenclature**

$A$ Area, $m^2$

$b$ Specific exergy, kJ/kmol

$\dot{B}$ Exergy rate, kW

$B$ Total exergy, kJ

$C_p$ Specific heat at constant pressure of the combustion product species, kJ/kmol

$C_{pr}$ Moles averaged specific heat at constant pressure, kJ/kmol

$C_{pa}$ Specific heat at constant pressure of air, kJ/kmol

$C_v$ Specific heat at constant volume of the combustion product species, kJ/kmol

$C_{vr}$ Moles averaged specific heat at constant volume, kJ/kmol

$D$ Cylinder bore, m

$D_p$ Valve port diameter, mm

$D_s$ Valve stem diameter, mm

$D_v$ Valve diameter, mm

$D_{vi}$ Inlet valve diameter, mm

$\dot{E}$ Energy, kW

$H$ Total enthalpy, kJ

$h$ Specific enthalpy, kJ/kgK or heat transfer coefficient, $W/m^2K$

$k$ Thermal conductivity, W/mK

$L$ Length of connecting rod, mm

$L_v$ Instantaneous valve lift, mm

$\dot{m}$ Mass flow rate, kg/sec

$m$ Constant used in heat release based combustion model

$M$ Mass, kg

$N$ Speed, RPM or No. of moles, kmol

$n$ No. of intake valve/cylinder or constant used in ignition delay model

$\dot{n}$ Molar flow rate, kmol/sec

$n_{pr}$ No. of piston ring

$p$ Pressure, bar

$p_a$ Atmospheric pressure, bar

$p_e$ Exhaust back pressure, bar

$p_{imf}$ Inlet manifold pressure, bar

$p_{imep}$ Indicated mean effective pressure, bar

$P_{sl}$ Piston skirt length, mm

$\dot{Q}$ Energy transfer rate, kW

$\frac{dQ_c}{d\theta}$ Heat release rate due to combustion of fuel, kJ/ degree crank angle

$\frac{dQ_h}{d\theta}$ Rate of heat transfer from in cylinder gases to the wall, kJ/ degree crank angle

$\frac{dQ_n}{d\theta}$ Net heat release rate, kJ/ degree crank angle

$\overline{R}$ Universal gas constant, kJ/kmolK

Re Reynolds's Number

$S$ Stroke length, mm

$T$ Temperature, K or Torque, Nm

$t$ Time, sec

$\frac{dU}{d\theta}$ Rate of change of internal energy, kJ/ deg. crank angle

$V$ Volume, $m^3$

$V_s$ Stroke volume, $m^3$

$V_p$ Mean piston speed, m/s

$\frac{dW}{d\theta}$ Rate of Work transfer, kJ/ deg. crank angle

**Greek Letters**

$\rho$ Density, $kg/m^3$

$\mu$ Dynamic viscosity, kg/ m sec

$\gamma$ Ratio of specific heat, dimensionless

$\theta$ Crank angle (CA), degree

$\phi$ Fuel air equivalence ratio, dimensionless

$\omega$ Crank shaft angular speed, rad. /sec

$\tau$ Ignition delay, CA degree

**Subscripts**

a Air

cal Calorimeter

ex Exhaust gas

f Fuel

p Combustion products or valve port

w Cylinder wall or water

x Residual exhaust gas

**Superscripts**

tm thermo-mechanical

ch chemical

# CHAPTER 1

# INTRODUCTION

## 1.1 BIODIESEL: AN ALTERNATIVE FUEL

The world reserves of fossil fuels like coal, petroleum, natural gas are undoubtedly very large, but the fact remains that these natural gifts are neither unlimited nor renewable and can only deplete with use. According to an estimate [1], the reserves will last for 218 years for coal, 41 years for oil, and 63 years for natural gas, under a business-as-usual scenario. The enormous growth of world population, technical development, standard of living of mankind and increasing number of vehicles employing internal combustion engines (ICE) have drastically increased the demand for fossil fuels. This has ultimately made an alarming situation of imbalance between energy supply and demand. The world today is also confronted with the crises of global climate change and environmental degradation. The current and anticipated problems related to energy crisis and the increasing concern for the environment has stimulated active research interest in search for non-petroleum, renewable, and non-polluting fuels of bio origin such as biomass, vegetable oils, alcohol, biogas etc. Biodiesel is considered promising in this regard. Biodiesel is basically monoalkyl esters of long chain fatty acids derived from plants or animal matters. It is the name given to transesterified vegetable oil to describe its use as a diesel fuel. Biodiesel produced from different vegetable oils has been accepted as a clean alternative fuel worldwide. It is an eco-friendly green diesel fuel which contains no petroleum, but can be blended at any level with petroleum diesel to create a biodiesel blend for use in compression ignition (CI) engines. The properties of biodiesel are found to be slightly different from that of petro-diesel depending upon the source of biodiesel from which it is obtained. The advantages with biodiesel are that it is biodegradable, nontoxic, and essentially free of sulfur and aromatics, but contains about 10% built in oxygen, a factor which could favour combustion. Its higher cetane number improves the ignition quality even when blended with petroleum diesel. Biodiesel offers higher lubricity and hence, engines using biodiesel tend to last longer because the engine parts are lubricated better with this fuel as opposed to standard fossil diesel.

### 1.1.1 Biodiesel: International scenario

Biodiesel has been accepted as a clean alternative fuel by most of the developed and developing countries. Countries around the world, primarily by the EU members and the

USA, are promoting increased production and use of bio-fuels, mainly biodiesel. Countries like Germany, France, Italy, UK, Austria, USA, Malaysia, Czechoslovakia, including other European and Asian countries have put a major thrust on production of biodiesel from vegetable oils through extensive research & development. These countries while initiating active biodiesel programmes, have also provided legislative support and have drawn up national policies on biodiesel development. In France, conventional diesel is mixed with 2% to 5% biodiesel. In the United States (US), bulk of most biodiesel is made from soybean oil; however canola oil, sunflower oil, recycled cooking oil and animal fats are also used. Sunflower, rapeseed oil and likes are used as raw materials in Europe. Rapeseed based biodiesel are produced in Germany and a good number of biodiesel filling stations have started functioning. Sunflower based biodiesel has made good success in France and UK. Thailand uses palm oil and Ireland uses waste frying oil and animal fats as feedstock for biodiesel.

As the demand for vegetable oils for food has increased tremendously in recent years, it is not sensible to use these oils for biodiesel production. In line with this, edible vegetable oils and animal fats, being food materials, are not allowed for biodiesel production in India. The non-edible oils such as *Jatropha curcus (Ratanjot), Pongamia pinnata (karanja), Azadirachta indica (Neem), Hevea brasiliensis (Rubber seeds), Madhuca indica (Mahua), Calophyllum inophyllum(Nagchampa), Simmondsia chinensis (Jajoba), Orbignya oleifera (Babassu), Gossypium spp. (Cotton seed) etc.* are available in many parts of the world including India and these could be promising sources for the purpose.

Stricter emission regulations in the world have placed design limitations on heavy duty diesel engines. The trend towards cleaner burning fuel is growing worldwide and this is possible through use of fuel from bio-origin. Thus, the envisaged benefits of biodiesel indicate a start towards a cleaner, healthier planet and its use a positive step in the right direction.

### 1.1.2 Biodiesel: Indian initiative

The Indian biofuel market has been consistently witnessing growth and developments for the past few years. In view of the fluctuating oil prices in the international market and continuously increasing oil import, the Indian biofuel sector is expected to see robust growth in coming years. The Government of India is investing huge amount of money and resources into the development of this sector in an attempt to reduce dependency on imported oil. India

has great potential for production of bio-fuels like bio-ethanol and biodiesel from non-edible oil seeds. Currently, ethanol dominates the Indian biofuel sector, but biodiesel is expected to join the commercial stream. With huge potential for production and market, the Indian biofuel industry could prove to be a good option for biofuel producers. There has been greater awareness on biodiesel in India in the recent times and significant activities have been initiated for its production, especially, with a view to boosting the rural economy. The Government of India proposed a National Mission on biodiesel comprising six micro-missions covering the essential aspects of plantation, seed procurement, oil extraction, transesterification, blending & trade, and research and development (R&D). In this regard, the Government of India has approved the controlled cultivation of plant species such as Jatropha curcus, Karanja, Nagchampa, Neem, Mahua and Rubber seeds. Indian Oil Corporation (IOC), in its R&D Centre at Faridabad, has already initiated production of biodiesel from Jatropha seed oil.

Government of India has announced its National Biofuel Policy in 2008 with an objective to meet 20% of India's diesel demand with fuel derived from plants. Jatropha incentives in India are a part of India's goal to achieve energy independence by the year 2012. Large plots of waste land have been selected for jatropha cultivation anticipating employment generation for the rural people. IOC, in a joint venture with the Chhattisgarh Renewable Development Authority has taken up a pilot project of Jatropha plantation on 600 hectares of revenue wasteland in Jhabua district in Madhya Pradesh to ascertain the feasibility of revenue land-based commercial biodiesel units and to develop benchmarks for plantation costs and output. It is also looking to acquire 50,000 hectares of wasteland in Uttar Pradesh for plantation of non-edible oilseeds, such as Jatropha and Karanja.

The automobile industry, in India, has come forward with projects to make biodiesel techno-economically viable for their engines. Mahindra & Mahindra Ltd. has set up a pilot plant in Mumbai for biodiesel utilizing Karanja. Further, the company has also launched a biodiesel compliant 75 HP tractor in 2007 with a fuel injection system which allows 5% blending of biodiesel. Tata Motors, a leading automobile manufacturer in India, has also started its biodiesel program in collaboration with IOC. General Motors India Pvt. Ltd.'s has recently entered into an agreement with Central Salt and Marine Chemical Research Institute, Bhavnagar, and is considering a project on commercial production of Jatropha based biodiesel.

Scientists from various industries, research, and educational institutes in India have started its research and developmental work on production of transesterified non edible oil

and its use in diesel engines. IOC, Indian railway, Mahindra and Mahindra, Tata Motors are some of the leading industries involved in R&D activities on biodiesel. Many leading educational and research institutes in India are carrying out different aspects of biodiesel research. Most of the Indian Institutes of Technology (IITs), Indian Institute of Petroleum (IIP) Dehradun, Indian Institute of Chemical technology (IICT) Hyderabad, Indian Institute of Science (IISc) Bangalore, Indian Biodiesel Corporation (IBDC) are few of them.

## 1.2 BENEFITS OF USAGE OF BIODIESEL

Extensive research works on biodiesel initiated in recent times could be justified from some inherent benefits of biodiesel as an alternative fuel, particularly in respect of environment, safety and economy. These aspects are further discussed below.

### 1.2.1 Environment, safety and sustainability

In a report of National Biodiesel Board (NBB) US, it is mentioned that biodiesel is considered an important alternative fuel in the US conforming to EPA-required Tier I and Tier II norms. This is related to human health and comes under the Clean Air Act. Some independent tests carried out on biodiesel conclusively demonstrated its capability of significant reduction of almost all regulated emissions. There is less smoke and odor from engines powered by biodiesel and they tend to run quieter as well. Another study conducted by the US Department of Energy showed that the production and use of biodiesel, compared to petroleum diesel, resulted in 78.45% reduction in carbon dioxide emissions. Biodiesel contains virtually no sulfur or aromatics, and use of biodiesel in a conventional diesel engine results in substantial reduction of unburnt hydrocarbons, carbon monoxide and particulate matter. Since biodiesel does not contain sulfur, its emission does not contribute to acid rain. Biodiesel fuel also reduces the cancer causing particulates from being released into the air. It is non toxic and completely biodegradable.

Further, biodiesel has high flashpoint of about 150°C compared to petroleum diesel fuel, which has a flash point of 55°C, and, as such, it is much safer to handle, transport, and store. Thus, the safety issues make this a very attractive alternative fuel. Moreover, biodiesel is a renewable fuel produced from agricultural resources such as vegetable oils, which positively addresses the very important issues concerning sustainability.

### 1.2.2 Economic aspects

Biodiesel industry has the potential for contributing significantly to a country's domestic economy. It is quite encouraging to use one's own domestic resources for growing its own fuel through contributing to additional economic activities. Biodiesel has good potential for rural employment generation. Once bio-diesel is used, it will enhance agricultural produce and create new jobs in the field of cultivating crops used in the manufacturing and processing of bio-diesel. The NBB report says that in the US, a good number of jobs are being currently supported by its biodiesel industry which clearly reflects the potential of this industry to create jobs and economic growth. Biodiesel is relatively easy to produce. People have started making their own biodiesel at home from waste vegetable oil (WVO) which could be a viable option.

The use of biodiesel as IC engine fuels can play a vital role in helping the developing countries to reduce the dependence on foreign oil imported in huge quantities every year and to make a considerable savings in the annual oil import bill. According to an Integrated Energy Policy (IEP) document published by the Planning Commission, demand for crude oil in India in the year 2031–2032 will be in the range of 350 to 486 million metric tones (MMT), and assuming domestic production being at the level of 35 MMT, it is expected that the range of import dependence may increase up to 90% to 93%. These are serious concerns in view of the (i) increasing prices of crude oil in the international market, (ii) supply disruptions due to various geopolitical disturbances, (iii) the oil import bill, and (iv) oil supply uncertainty.

## 1.3 ENGINE PERFORMANCE USING BIODIESEL

Biodiesel if it conforms to the established standard generally performs well in engines without posing many problems. Most of the reported literature concerns about the blends of biodiesel and diesel. Some of important observations relating to engine performances that have been noticed by researchers are discussed below:

**Engine power and torque**: In general, there is reduction in engine power and torque with biodiesel as the fuel. This is due to the fact that biodiesel has less energy per unit volume than traditional diesel fuel. However, torque and power performance also depends on engine types, blending level, density, viscosity and other fuel properties. Lower calorific value of biodiesel is compensated by its higher density due to which the mass of fuel injected for the same volume increases at the given injection pressure.

**Engine thermal efficiency**: Thermal efficiency of diesel engine operating on biodiesel blends is slightly less compared to thermal efficiency of engine operated with diesel. Thermal efficiency depends upon the type and blends of biodiesel, density, viscosity, and calorific value. Poor combustion characteristics of biodiesel because of its higher viscosity and lower volatility are referred to as the cause of lower thermal efficiency with biodiesel.

**Fuel efficiency**: Fuel efficiency tends to be slightly lower when using biodiesel due to the lower energy content and higher density and viscosity of the fuel. Since engine torque is often the output the user demands, the lower heating value of biodiesel generally translates into increased brake specific fuel consumption (BSFC). Several literatures report this fuel consumption characteristic of biodiesel where biodiesel fuelled engine requires more amount of fuel in order to produce a given power output.

**Engine wear:** Information on engine wear pattern linking biodiesel as fuel is scanty. However, biodiesel improves the important property of fuel lubricity, thus improving lives of engine components related to fuel system. Long term endurance tests have confirmed additional lubricating properties of biodiesel.

**Deposits and clogging:** Deposits and clogging due to biodiesel have been widely reported but are generally traceable to biodiesel that has either degraded or become oxidized during storage. If standard biodiesel specification is maintained, engine deposit is normally not recognized as a major problem.

**Pollution from engine exhaust**: Air pollution from biodiesel fuelled engine is less due to its higher oxygen content and absence of both "aromatic compounds" and sulfur. The one exception to this is nitrogen oxide (NOx) emissions, which tend to be slightly higher when using biodiesel. However, its lower sulfur content allows the use of NOx control technologies and hence, NOx emissions can be effectively managed by proper tuning and optimization of engine operating parameters.

**Cold-weather performance**: Engines tested in cold weather typically experience significant operational problems which are primarily caused by clogging of the fuel filters and/or coking of the injectors. The uses of flow improving additives, "winter blends" of biodiesel and kerosene have proved effective in extending the range of operating temperatures for biodiesel. Reports say, pure biodiesel tends to operate well at temperatures down to about 5°C depending on the type of fuel being used. Cold weather performance is further improved by use of additives up to 8°C, while winter blends have proved effective at temperatures as low as -20°C.

From the above discussion it is found that bio-diesel could a potential alternative for petro-diesel. Different aspects of biodiesel fuel are getting attention for its processing, production and application the world over. The basic areas of such studies include

i) Biodiesel production

ii) Chemical composition and fuel properties of biodiesel

iii) Performance of engines using biodiesel fuel blends in terms of power, efficiency, fuel consumption, combustion, emission, etc. based on experiments with such fuels

iv) Development of proper engine cycle simulation model for predicting the performance

v) Exergy analysis for assessing and improving the efficiency of processes, energy conversion devices etc.

Before we go to discuss about the state of the art in the related research activities in the next chapter, we describe in what follows, in brief, each of these areas of research in some general terms.

## 1.4 BIODIESEL PRODUCTION

A number of methods are currently available and have been adopted for the production of biodiesel fuel like, transesterification, pyrolysis [3-5] and micro-emulsification [6, 7]. However, transesterification is the most commonly used method of biodiesel production [8]. Transesterification with alcohols (usually methanol and ethanol) is considered to be the basic process for conversion of triglycerides (the basic constituents of vegetable oils and animal fats) to biodiesel. Methanol is usually preferred as it reacts quickly with the triglyceride because of its short chain length and polar nature. The cost of methanol is also less and sodium hydroxide which is used as catalyst in the transesterification reaction easily dissolved in it [2]. The transesterification reaction can be catalyzed by bases, acids, or enzymes. The base catalyzed transesterification is the mostly used method today for industrial production of biodiesel as it gives high yield of ester in short reaction times, where sodium hydroxide, potassium hydroxide and carbonates are used as catalysts. These catalysts require anhydrous conditions and feedstock with low levels of free fatty acids (FFAs). Oils containing high levels of FFAs cannot be directly used with the base catalysts [9]. When oils with high content of FFAs and water are used, soaps are produced as byproduct which has to be removed after the reaction. In transesterification, the following important factors should be satisfied for maintaining the biodiesel standard and its ASTM specifications. (a) complete transesterification reaction, (b) removal of catalyst, (c) removal of alcohol, (d) removal of glycerol, and (e) complete esterification of FFAs.

Enzymatic transesterification processes avoid soap formation and hence the purification process becomes simple and easy. However, they are less used commercially because of the longer reaction times and higher cost. New biocatalysts have recently been developed which can reduce the production cost and no purification is necessary for using these biocatalysts.

The disadvantages with the catalytic transesterification can be eliminated with the use of non-catalytic supercritical alcohol transesterification method. In this method, reaction is allowed to occur above the critical pressure and temperature of the alcohol used. Reaction time reduces drastically and presence of FFAs and water in the crude vegetable oil has no effect on the ester conversion. However, more energy and alcohol are required during production. Moreover, increased capital costs and maintenance associated with pressurized reaction vessels are some of its disadvantages [10].

## 1.5 CHEMICAL COMPOSITION AND FUEL PROPERTIES OF BIODIESEL

The basic constituent of vegetable oils and animal fats is triglycerides, which are composed of three fatty acids (R–COOH) and one glycerol $\{C_3 H_5 (OH)_3\}$ [11]. The chemical structures of the common fatty acid chains found in a triglyceride molecule are shown in Table 1.1. The physical and chemical fuel properties of biodiesel basically depend on the fatty acids composition of the triglyceride used in the production.

Fatty acids vary in their carbon chain length and in the number of double bonds. In the term within bracket in Table 1.1, the former represents the number of carbon atoms and the latter shows the number of double bonds. Since the chemical composition of fatty acid chains differ from feedstock to feedstock, therefore fuel properties of biodiesel produced from different feedstock will also be different. In addition to this, the ester moiety derived from the alcohol also influences the fuel properties of biodiesel because biodiesel consists of fatty acids esters [12]. Fuel properties of biodiesel can also be influenced by contaminants and other minor components arising from production or other sources [10]. Contaminants are the incomplete or undesired reaction products, such as FFA, soaps, triglyceride, diglyceride, monoglyceride, alcohol, catalyst, glycerol, metals, and water. Naturally occurring minor components found in vegetable oils and animal fats include tocopherols, phospholipids, steryl glucosides (also called sterol glucosides, steryl glycosides, sterol glycosides, or phytosterols), chlorophyll, fat soluble vitamins, and hydrocarbons (such as alkanes, squalene, carotenes, and polycyclic aromatic hydrocarbons [10]. The important properties of a

biodiesel fuel that are influenced by the structure of fatty acids and fatty esters include cetane number that measures fuel ignition quality, heating value, cold flow properties , oxidative and storage stability, viscosity and lubricity.

Table 1.1: Chemical structures of common fatty acid chains

| Fatty acid chain | Chemical Structure |
|---|---|
| Caprylic (8:0) | $CH_3(CH_2)_6COOH$ |
| Capric (10:0) | $CH_3(CH_2)_8COOH$ |
| Lauric (12:0) | $CH_3(CH_2)_{10}COOH$ |
| Myristic (14:0) | $CH_3(CH_2)_{12}COOH$ |
| Palmitic (16:0) | $CH_3(CH_2)_{14}COOH$ |
| Palmitoleic (16:1) | $CH_3(CH_2)_5CH=CH(CH_2)_7COOH$ |
| Stearic (18:0) | $CH_3(CH_2)_{16}COOH$ |
| Oleic (18:1) | $CH_3(CH_2)_7CH=CH(CH_2)_7COOH$ |
| Linoleic (18:2) | $CH_3(CH_2)_4CH=CHCH_2CH=CH(CH_2)_7COOH$ |
| Linolenic (18:3) | $CH_3CH_2CH=CHCH_2CH=CHCH_2CH=CH(CH_2)_7COOH$ |
| Arachidic (20:0) | $CH_3(CH_2)_{18}COOH$ |
| Eicosenoic (20:1) | $CH_3(CH_2)_7CH=CH(CH_2)_9COOH$ |
| Behenic (22:0) | $CH_3(CH_2)_{20}COOH$ |
| Erucic (22:1) | $CH_3(CH_2)_7CH=CH(CH_2)_{11}COOH$ |
| Lignoceric (24:0) | $CH_3(CH_2)_{22}COOH$ |

## 1.6 DIESEL CYCLE SIMULATION MODELING

The thermodynamic cycle analysis and the performance prediction of diesel engines using cycle simulation programs has become an established part of the diesel engine research and development. Diesel engine simulation models are mainly classified into following three categories viz. zero-dimensional single-zone models, quasi-dimensional multi-zone models and multi-dimensional models. Zero dimensional single zone combustion models are widely used by most engine manufacturers because they are simple, easy to handle, require less number of model constants and involve minimum operating cost and computational time. These are generally utilized for prediction of in-cylinder pressure which can later be used for stress analysis of main engine parts, optimization of design aspects via parametric analysis. However zero dimensional models are not appropriate to account for exhaust emissions due to the lack of spatial information as they avoid the detailed description of mixture preparation and don't take into account the three-dimensional effects due to the geometry of the combustion chamber. The quasi-dimensional multi-zone models are formulated by employing simplified quasi steady equations describing the individual processes that occur in the engine cylinder such as fuel injection, fuel atomization, air entertainment, fuel-air mixing, combustion and heat transfer. In these models, charge in the cylinder is divided into several zones during various processes, especially for combustion process. The system of ordinary differential equations that is obtained from the first law of thermodynamics and the other basic thermodynamic relations are solved for pressure, temperature and mass in the zones. These models can predict engine performance and emissions satisfactorily and are considered to be a good engine cycle simulation tool. However, computational time is more due to emission related calculations in a number of zones compared to zero-dimensional model. Multi-dimensional models are based on the numerical solution of a set of governing coupled partial-differential equations, which are integrated in fine geometric grids in the combustion chamber space. These models are capable of providing detailed information about both spatial and temporal resolution of the quantities of interest; however, they require large amounts of computer time and storage capacity. Thus, if it is desired to examine the effects of design and operating parameters on engine performance, zero dimensional single zone models could be useful because they offer greater computational efficiency and this is an important consideration in so far as parametric studies of operating characteristics are concerned. Although these models are proposed and tested with various degrees of success but most of them refer to diesel as its working fluid. In particular, one of the missing such

models is that these have not been applied for predicting and validating engine performance with biodiesel blends as fuel. As biodiesel blends including pure biodiesel are being experimented and used as fuel for diesel engines, it is quite obvious that research can also be extended towards engine modeling considering diesel biodiesel blending as fuel.

## 1.7 EXERGY ANALYSIS AND ENGINE SYSTEM

The rapid depletion of world's energy resources has caused the entire world community to review their energy policy and to take drastic measures in eliminating the waste. It has also forced the scientific community to take a closer look at the energy conversion devices and develop new techniques for better utilization of the existing limited resources. Exergy analysis (also called second law or availability analysis) is a powerful thermodynamic technique for assessing and improving the efficiency of processes, energy conversion devices and thermal systems. It can be used to determine the direction of process, establish the condition of equilibrium, to specify the maximum possible performance of thermal systems and identify those aspects of processes that are significant to overall performance. Thermodynamic analysis of engine performances based on first law of thermodynamics do not explicitly identify those processes within the system that cause unrecoverable degradation of the thermodynamic state of the working fluid. It only permits the designer to evaluate the variation in internal energy as a function of energy transfers and enthalpies associated with mass flow crossing the system boundaries. Moreover, evaluation of some features of energy resource utilization is also not possible with the first law alone, as it deals with only the quantity of energy and completely ignores the qualitative aspect of it. It is the second law which deals with the quality of energy and provides the framework for evaluating the irreversible losses occurring in a process. Thus, second law analysis of any thermal system offers plenty of room for improvement of the system operations.

Exergy or availability is a composite property depending upon the state of the system and surroundings. Exergy of a given system is defined as the maximum useful work that can be produced through interaction of the system with its surroundings, as it reaches thermal, mechanical and chemical equilibrium. Exergy analysis performed on ICE has been reported in many studies. Most of these studies were carried out mainly to quantify the exergy losses due to irreversibility associated with engine processes such as combustion, heat transfer, heat loss accompanying exhaust gas and so on. Exergetic performance of an engine also depends upon the fuel used. Since recently, biodiesel obtained from different non edible sources such

as Karanja, Jatropha etc. have received significant attention as possible renewable alternate fuel in India, and therefore, the present work is aimed at evaluating the exergetic performance of a diesel engine fuelled with different blending of diesel and biodiesel. Both the terms i.e. exergy and availability will be used in the preceding text wherever it deems fit in the exergy analyses with the same meaning.

The present work, however, does not deal with the first two areas of research and concentrates mainly on (i) experimentation for performance of bio-diesel run engines, (ii) cycle simulation modelling and (iii) exergy analysis.

## 1.8 MOTIVATION AND OBJECTIVE OF THE RESEARCH

As can be seen from the discussion so far, diesel engine simulation modeling has long been used by engine designers as an effective tool for studying engine performances. In most of these models, the diesel engine processes are simulated using different modeling approaches in order to test their predictive capability under different operating conditions. But majority of them are specific to diesel as its fuel. Research works on diesel engine simulation modeling using biodiesel blend as fuel are very few. Although, there are models for predicting performance of diesel engine, but these have not been validated so far for biodiesel blended fuels. Since extensive experimental research have been going on for evaluating diesel engine performance with different blending of biodiesel as fuel, a diesel engine cycle simulation model capable of predicting engine performance fuelled with biodiesel blends is required to be developed. Such a model can be used to study the effect of engine design and operating parameters such as load, speed, compression ratio, varying fuel composition and fuel properties on engine performance.

The different aspects of diesel engine performance and combustion, combined with widely differing physical and chemical properties of diesel and different blending of diesel and biodiesel are required to be addressed for prediction and interpretation of the engine behaviour. Extensive experimentation is required for the purpose and the results obtained from experiments can be used for validating simulation model results as well.

Further, as mentioned earlier, it is also important to evaluate the performance of a diesel engine system in the light of second law of thermodynamics in order to identify and quantify the irreversibility of various processes involving a diesel engine system. Particularly when a conventional diesel engine is operated with various biodiesel blends, second law analysis of engine performance may be very useful in understanding the various engine

processes and thereby to propose methods for improvement. This has become necessary in view of the recent shifting of attention towards biodiesel as fuel supplement for normal diesel fuel.

Thus, the research objectives of this dissertation can be summarized as follows:

(i) Developing a cycle simulation model to simulate all the processes consisting of a diesel engine for predicting the performance of the engine in terms of brake power (BP) and brake thermal efficiency (BTE) fuelled with diesel and various blending of bio-diesel.

(ii) Performing experiments with biodiesel and its diesel blends as fuels for evaluating the engine performance, fuel combustion and emission characteristics and also to obtain important input parameters for the cycle simulation model.

(iii) Analyzing the exergetic performance of the engine in terms of various exergy losses, exergy destruction and exergetic efficiency using experimental performance and emission data.

(iv) Validating the cycle simulation model with experimental results.

Following this introduction, Chapter 2 describes the literature review and scope of present work, Chapter 3 the modeling and Chapter 4 the biodiesel production and characterization for the present work. Chapter 5 presents the experimentation details. Chapter 6 describes the energy and exergy analyses while Chapter 7 describes the results of different models used for cycle simulation and validation with experimental data. Finally the conclusions and recommendations are presented in Chapter 8.

# CHAPTER 2

# LITERATURE REVIEW

A host of literature is available related to study of different aspects of biodiesel fuel. They essentially include biodiesel production and characterization, engine performance fuel combustion and emission among others. In the context of the present scope of work the literature survey is presented in the following sections.

## 2.1 PERFORMANCE OF BIODIESEL RUN DIESEL ENGINE

Several experimental investigations have been carried out by researchers around the world to evaluate the performances and emissions of compression ignition engines, fuelled with pure and blended biodiesel. Ramadhas et al. [13] using rubber seed oil and its diesel blends in a single cylinder diesel engine observed that the blends containing 20%–40% of rubber seed oil in the blend yielded similar engine performance with that of diesel. Raheman and Ghadge [14] evaluated the performance of a single cylinder, four stroke Ricardo E6 engine with various blends of diesel and biodiesel viz. B20, B40, B60, B80 and pure biodiesel (B100) derived from Mahua seed oil. They observed that brake specific fuel consumption (BSFC) of the engine increased with increasing proportion of B100 in the fuel blends and consequently the brake thermal efficiency (BTE) was lower in case of the biodiesel fuel blends. BSFC of biodiesel fuelled engine increases and BTE reduces due to increase in the fuel consumption rate. Labeckas and Slavinskas [15] conducted experiment on a four cylinder, four stroke direct injection (DI) diesel engine to examine the effects of rapeseed oil methyl ester (RME), diesel fuel and their blends (B5, B10, B20, B35) on BSFC and BTE at three different speeds viz. 1400, 1800 and 2200 rpm while changing engine operation from light to heavy load. BSFC increased with speed at a given load for all the fuels tested. It was comparatively less in case of B5 and B10 but found to be higher for B20, B35 and neat RME at these speeds. BSFC was the maximum in case of neat RME. At the rated speed (2200 rpm), the maximum BTE values were reported to be 0.375, 0.380 and 0.378 for diesel, B5 and B10 blends, respectively. They also observed lower BTE with B20, B35 and neat RME with average maximum efficiency of 35.5% Cetinkaya et al. [16] observed slight reduction in torque and power using waste cooking oil originated biodiesel in a Renault Me´gane F9Q732 type diesel engine over the entire speed range from 1000-4500

rpm. They used viscosity improver and pour point additives to improve the fuel property of biodiesel. Usta [17] found that the power and torque of a turbocharged indirect injection (IDI) variable speed engine increased slightly and the thermal efficiency significantly with the addition of tobacco seed oil methyl ester (TSOME) blends. The main reasons for higher torque, power and efficiency was attributed to higher density, higher viscosity and better combustion in respect of the biodiesel blends. Raheman and Phadatare [18] investigated the use of Karanja methyl ester and its diesel blends (B20, B40, B60 and B80) in a single cylinder, four-stroke, and DI diesel engine for obtaining comparative measures of torque, power and BSFC. They found that the torque produced in case of B20 and B40 were 0.1%–13% higher, however for the blends from B60 to B100, it reduced by 4%–23% from that of diesel. At an average speed of 2525 rpm (±2%), the BSFC for B20 and B40 was 0.8%–7.4% lower and for the blends from B60 to B100, it was 11%–48% higher than that of diesel. The BTEs were also higher for B20 and B40. This was due to a decrease in the calorific value of the fuels with an increase in biodiesel percentage in the blends. Pramanik [19] evaluated the performance of a Kirloskar make single cylinder diesel engine using Jatropha curcus oil and its diesel blends. He also found higher BSFC in the case of biodiesel blends in the entire range of load and attributed this to the combined effects of the fuel density, viscosity and heating value of the blends. It was further observed that the blends B30 and B40 had BSFC close to diesel. The BTE of the blends were lower than diesel throughout the entire load range. Sahoo et al. [20] made a performance analysis using neat biodiesel from Jatropha, Karanja and Polanga and their blends (B20 and B50) at different speed in a three cylinder tractor engine at full and part throttle operations. BSFC for all the biodiesel blends was higher compared to neat diesel operation. Among the biodiesel blends, the maximum increase in power was observed for B50 Jatropha blend at the rated engine speed of 2200 rpm. Banapurmath et al. [21], while investigating a diesel engine operated with methyl esters of Honge, Jatropha and Sesame oils, found that, methyl esters of Honge, Jatropha and Sesame oils resulted in poor performance along with higher emissions compared to diesel operation. Working on a single cylinder four stroke diesel engine with Jatropha oil, Agarwal and Agarwal [22] found performance and emission parameters very close to diesel for the lower blend concentrations. However, for higher blend concentrations, performance and emissions were observed to be marginally inferior.

From the above discussion it is seen that the lower biodiesel blends yielded either slightly better or similar engine performance compared to diesel. Engine performance

deteriorates when the percentage of biodiesel in the blend exceeds certain level depending upon the type of biodiesel feedstock. Usta [17] observed slightly better performance with TSOME, which could possibly be attributed to the use of an IDI engine having a pre-chamber allowing better mixing of biodiesel fuel with air before combustion.

## 2.2 EMISSION CHARACTERISTICS OF BIODIESEL FUEL

Impact of biodiesel on engine emissions varies depending on the type of biodiesel and also on the type of diesel to which it is added. Engine operating conditions and the design parameters also have a strong influence on emissions. Various experimental investigations [17, 18, 20, 23-26] have confirmed substantial reductions in emissions of unburned hydrocarbons (HC), carbon monoxide (CO), and particulate matter (PM) from diesel engines using biodiesel as fuel. CO is a toxic combustion product that results from incomplete combustion of hydrocarbons. In presence of sufficient oxygen, CO is converted into $CO_2$. Biodiesel is an oxygenated fuel containing about 11% built-in oxygen [13] which helps in complete combustion; hence CO and HC emissions reduce in the exhaust. However exception in this regard is also reported. Fuelling the engine with methyl esters of Honge, Jatropha and Sesame oils, Banapurmath et al. [21], observed increase in CO, HC, PM emissions. They also reported reduction in NO emissions. Lower NOx was also reported in literatures [18, 23]. But some other research works [17, 20, 24-26] indicate a complete reversal of trend for NOx emission. There is a very small change in $CO_2$ emissions using biodiesel and it varies depending upon the type of biodiesel and cleanliness of the base fuel [1]. Canakci [24] reported that $CO_2$ emission for pure soybean biodiesel (B100) and B20 fuels was slightly higher (0.5% and 0.12%, respectively) than the No. 2 diesel fuel (D2). $CO_2$ and NOx emissions are of primary importance as they are major contributor to global warming and climate change having significant impact on human health and environment. However, net $CO_2$ emission of biodiesel is reported to be 78% less compared to diesel if its closed carbon cycle is considered [1]. This is because, $CO_2$ is released into atmosphere when biodiesel is burned and is recycled by growing plants, which are later processed into fuel.

Biodiesel obtained from various sources have different fatty acid compositions and fuel properties. Therefore, emissions from biodiesel fuelled engines vary accordingly. Moreover, engine emissions also depend on the type of combustion chamber and engine operating conditions.

## 2.3 DIESEL ENGINE COMBUSTION AND CYCLE SIMULATION

Diesel engine simulation modeling has long been established as an effective tool for studying engine performance. Such simulations and models are routinely used by design engineers to examine new design concepts and perform optimization studies in order to avoid costly and time consuming experimental tests. Several modeling approaches have been reported in the literature [27, 28] which has been tested with various degrees of success. Single zone heat release based zero dimensional models [28-30] are useful because of their simplicity. However, they cannot relate engine design and operating variables explicitly to the details of the combustion process and hence cannot be used to account for fuel spray evolution and spatial variation in mixture composition and temperature, which are essential to predict exhaust emissions. Moreover, they should be checked against experimentally derived heat release profiles before being used for predictions. However, such models are capable of reproducing cylinder pressure and overall engine performance accurately with high computational efficiency over a wide range of operating conditions [31, 32] and are considered appropriate for use in total diesel system simulations [28]. The need for accurate predictions of exhaust emission has forced researchers to the development of two zone combustion models [33, 34] and eventually, over the years, many multi-zone combustion models e.g. [31-37] have been developed and this is still an active area of research. In multi-zone models, the engine cycle and characteristics are computed generally for the closed cycle. The primary objective of these models has been to predict engine combustion and emissions, especially NO and soot. Fluid dynamics based multi-dimensional (CFD) models [38-43] have been used mainly to address the engine fluid flow, heat transfer and combustion processes. Details of the flow field, heat transfer and combustion prediction in engines by numerical solution of governing conservation equations is fast becoming a reliable proposition [28, 38]. Development of such methods is in progress to improve their ability for analyzing the flow field in realistic engine geometries [28]. In a single zone approach for the diesel engine combustion, the cylinder charge is assumed to be a homogeneous mixture of ideal gases at all times [28, 44]. The instantaneous state of the mixture is described by its pressure, temperature, and equivalence ratio. Fuel burns instantaneously as it is added to the cylinder [44]. On the contrary to this, quasi-dimensional multi-zone models incorporate the development of the fuel spray with time and simplified quasi steady equations are used to describe processes which include fuel injection, atomization, air entrainment, droplet

formation, evaporation, wall impingement, ignition, heat release and heat transfer. The fuel spray is divided into various elemental zones in the radial and penetrating directions, tracking the evolution of the zones over time. The solution of these quasi steady equations together with the conservation equations for mass, energy and species within each zone provide the detailed data needed for emission calculations [31, 32]. Although CFD models using codes such as KIVA, FIRE, STAR-CD etc. provide large amount of predicted data mainly regarding the flow field, but these models lack preciseness in modeling the diesel engine combustion because of complex combustion mechanisms [44]. Furthermore, computational time and storage constraints still restrain these codes from routine use for design purposes [32]. As can be inferred from the discussion so far, due to its efficient computational capability and simplicity of application, a single-zone approach for diesel engine combustion and cycle simulation is quite popular and always a better choice for total system simulation and complex engine system studies [28]. Discussion from now on will be concentrated upon a single zone approach.

Single-zone models use one or more algebraic formulae to predict the heat release rate [28]. The heat release rate is defined as the rate at which the chemical energy of the fuel is released during the combustion process. In spark ignition (SI) engines, the heat release rate is computed from the mass burning history which is often represented by the well known Wiebe function as given below [28, 44].

$$x_b = 1 - \exp\left[-a\left(\frac{\theta - \theta_0}{\Delta\theta}\right)^{m+1}\right] \tag{2.1}$$

where, $x_b$ is the mass fraction burnt, $\theta$ is the CA, $\theta_0$ is the CA corresponding to start of combustion (SOC), $\Delta\theta$ is the combustion duration and $a$ and $m$ are adjustable parameters. This model for global heat release rate function has also earned wider acceptance in diesel engine simulation [45] notwithstanding the basic difference in the combustion mechanism between SI and CI engines. The two adjustable parameters in the function depend upon the engine type; however the function cannot explain the effect of speed and load. In addition it does not reflect the effect of the shape of the combustion chamber and fuel injection rate on the history of the heat release as desired in the current state of engine development.

Researchers have also proposed different heat release rate models for diesel engines. Kreiger and Borman developed a heat release rate model using the following expression for fuel injection rate proposed by Ferguson [44, 46].

$$\frac{\dot{m}_f}{M_f} = \frac{\omega}{\Gamma(n)}\left(\frac{\theta-\theta_s}{\theta_d}\right)^{n-1}\exp\left(\frac{\theta_s-\theta}{\theta_d}\right) \tag{2.2}$$

Where $\theta_s$ is the CA where combustion starts, $\theta_d$ is the combustion duration, $\Gamma(n)$ is a polynomial function of shape factor $n$.

However, the effect of ignition delay was not taken into consideration in the heat release model. Watson et al. [47] developed a diesel engine heat release model by considering two unique algebraic functions, one describing the rapid premixed burning phase and the other describing the slower mixing controlled burning phase. These two functions were weighted with a phase proportionality factor which was a function of the ignition delay period [28]. The limitation of Wiebe function to predict the rate of heat release during early premixed combustion in diesel engine was somewhat overcome by Watson et al. [47] through the concept of double Wiebe function. This however added more number of adjustable parameters that are dependent on the engine type, but still such algebraic functions are easy to compute. A double Wiebe function is the superimposition of two simple Wiebe functions. Double Wiebe function in certain cases can not exactly reproduce combustion lasting until the exhaust phase [48]. This is because of the mathematical form of the equation. The central exponential term describing the diffusion phase of the double Wiebe function under certain circumstances cannot exactly describe large energy release rates. On such occasion a threefold Wiebe function [49] is sometimes used. The model parameters used in these formulae, which may vary with engine design details and operating conditions, are required to be determined empirically by fitting with experimental data. Some other heat release models are also reported in literature e.g. the polygon-hyperbola substitute heat release rate suggested by Schreiner [48] which was developed keeping in view of the calculation of NOx formation by means of multi-zone models. Yet another suggested by Barba et al. [48] was a combination of the Wiebe substitute heat release rate and the hyperbola substitute heat release rate. This model was developed in order to describe the long burn-out phase and the variable pre-injection in a common-rail injection system. A relatively simple and computationally efficient heat release model was presented by Chmela et al. [48] in which a few characteristic parameters of importance such as fuel mass available at every point of

time, specific turbulent kinetic energy (representing mixing speed of air and fuel) were introduced in the equation as given below and this model could fairly depict the effect of injection system parameters on the heat release rate.

$$\frac{dQ_{fuel}}{d\theta} = \left( M_{fuel} - \frac{Q_{fuel}}{lhv} \right) \exp \frac{\sqrt{k}}{\sqrt[3]{V_{cyl}}} \tag{2.3}$$

where, $k$ is the specific turbulent kinetic energy, $lhv$ stands for lower heating value, $V_{cyl}$ is the instantaneous cylinder volume. But the major disadvantage is that it cannot describe the premixed phase of diesel engine combustion.

Heat transfer through the cylinder side walls is an important process in determining overall performance of an ICE as it affects the indicated efficiency. It reduces the cylinder temperature and pressure, and thereby decreasing the work transferred on the piston per cycle. The description of heat transfer in ICE places the highest demands on modeling. The heat transfer by radiation taking place from the high temperature solid soot particulates during combustion process has a dominant effect on diesel engine performance and ranges from about 10% to 40% of total heat loss to the walls, whereas this ratio is generally less and just about 5% to 10% in SI engines [50]. Many formulae for calculating instantaneous engine heat transfer coefficients have been proposed by a number of investigators. The well accepted Woschni's correlation for heat transfer coefficient is given by [28,44]

$$h = 3.26 B^{-0.2} p^{0.8} T^{-0.55} \omega^{0.8} \tag{2.4}$$

with $\omega = \left[ C_1 V_p + C_2 \frac{V_d T_{ign}}{P_{ign} V_{ign}} (p - p_m) \right]$; where $B$ is the cylinder bore in metre, $p$ is the instantaneous cylinder pressure in kPa , $T$ is the mean cylinder gas temperature in K, $V_d$ is the displacement volume, $V_p$ is the mean piston speed, $p_m$ is the motored cylinder pressure. $P_{ign}, T_{ign}$ and $V_{ign}$ are the working fluid pressure, temperature and volume at the SOC. $C_1$ and $C_2$ are constants having different values for different processes. Hohenberg made some changes in the Woschni's formula, such as use of length based instantaneous cylinder volume instead of bore, the effective gas velocity and the exponent of the temperature term. Hohenberg's equation for heat transfer coefficient is:

$$h = 3.26 p^{0.8} T^{-0.4} V^{-0.06} (V_p + C)^{0.8} \tag{2.5}$$

where, $C$ is the calibration constant which Hohenberg suggested to be 1.4 for the engine he studied [50]. Other empirical correlations of interest are Ashley-Campbell equation, Sitkei Ramaniah equation and Annand's equation etc. [51] as given below.

Ashley-Campbell Equation: $$h = \frac{0.13B^{02}p^{0.8}Z^{0.8}}{T^{05}} \quad (2.6)$$

where, $B$ is the cylinder bore in metre, $p$ is the instantaneous cylinder pressure in atm, $T$ is the working fluid temperature in K, $Z$ is the working fluid velocity in m/s.

Sitkei- Ramaniah Equation: $$h = 0.04(1+b)\frac{p^{0.7}V_p^{0.7}}{T^{02}d_e^{0.3}} \quad (2.7)$$

where, $b$ is a parameter that depends upon the type of combustion chamber and $d_e$ is the equivalent cylinder diameter. Annand's equation takes into account the forced convection as well as the grey body radiation and predicts fairly the engine heat transfer. Since the radiation heat transfer during combustion has a significant effect in diesel engine, Annand's equation is used in the present study to calculate heat transfer between the trapped gas and the surrounding wall.

The starting point of the cycle simulations is the first law of thermodynamics either for an open system or a closed system depending upon the simulation. It may start either with the simulation of intake process or with the compression process. The first law is applied to the cylinder volume for the intake, compression, combustion, expansion and exhaust processes which in sequence constitute the engine's operating cycle. Then, during each process, sub-models are used to describe geometric features of the cylinder and valves, the thermodynamic properties of working fluid, the mass and energy transfers across the system boundary and the combustion process [28]. Mathematical modeling of the diesel engine cycle simulating all these processes has nowadays become an important tool to predict engine performance and efficiency. The present work aims at assessing the prediction capability of this kind of model when it is applied to biodiesel and its diesel blends as fuels to the engine.

## 2.4 EXERGY ANALYSIS OF ICE THERMODYNAMICS

### 2.4.1 Introduction

As already mentioned in section 1.5, related to the analysis based on second law is the concept of exergy. Since, the overall engine system is composed of both the closed and open system operations, exergy of both the forms are needed for analysis. In exergy analysis, usually the exergy terms associated with thermo-mechanical and chemical equilibration are

calculated. For a closed system experiencing heat and work interactions with the environment, the following equation holds, for the thermo-mechanical exergy [52, 53].

$$B^{tm} = (E - U_0) + p_0(V - V_0) - T_0(S - S_0) \tag{2.8}$$

where, $E = K.E. + P.E. + U$ ; with $K.E.$ the kinetic and $P.E.$ the potential energy, $p_0$ and $T_0$ are the fixed pressure and temperature of the environment; and $U_0, V_0$ and $S_0$ are the internal energy, volume and entropy of the contents at the standard reference dead state at $p_0$ and $T_0$. Similar relation for an open system is given by:

$$B^{tm} = (H - H_0) - T_0(S - S_0) + \frac{mV^2}{2} + mg(z - z_0) \tag{2.9}$$

where, $H$ is the enthalpy and $S$ is the entropy of the system at the specified state. $H_0$ is the enthalpy of the reference dead state. But usually the kinetic and potential energy effects are neglected. The choice of a reference dead state is of paramount importance when dealing with exergy calculations as it determines the kind of equilibrium that will be established with the environment. The dead state referred in the calculation of thermo-mechanical exergy is that state at which no work potential exists between the system and the environment due to temperature or pressure differences. If it is assumed that there also exists chemical equilibrium between the two, then no work potential exists due to compositional differences and in such situation chemical exergy of the gas mixture is neglected. However, if no chemical equilibrium exists, some work recovery is possible due to the difference between the composition of the system at the dead state and that of the reference environment (true dead state). If the system at the dead state is also permitted to pass into but not react chemically with the surrounding environment, then for ideal gas mixtures, the chemical availability is defined as [53, 54].

$$b^{ch} = \sum_i m_i(\mu_{i0} - \mu_i^0) = T_0 \sum_i R_i m_i \ln \frac{x_i}{x_i^0} \tag{2.10}$$

where, $\mu_{i0}$ is the respective chemical potential at the dead state and $m_i$ is the mass of species $i$. $\mu_i^0$ the chemical potential of species $i$ at the reference environment. $x_i$ and $x_i^0$ are the mole fractions of species $i$ in the mixture and the environment, respectively. This chemical availability is a measure of the maximum possible work output when the system comes to equilibrium with the environmental composition. The thermo-mechanical and chemical

exergy can also be calculated on molar basis. The total exergy is the sum of the thermo-mechanical and chemical exergy.

### 2.4.2 Research works on exergy analysis of ICE system

Investigations based on the second law of thermodynamics to analyze the combustion and other processes in ICE have been published for over 50 years. Caton [55] identified over two dozens of previous investigations on exergy analysis of ICE and described these investigations in his review work while illustrating, in details, the type of information obtained. He showed that the exergy destruction due to heat transfer from the gas temperature ($T_g$) to the wall temperature ($T_w$), increases as the difference ($T_g - T_w$) increases.

Rakopoulos and Giakoumis [56] reported on the use of a computer based analysis to assess the performance of a six cylinder marine-duty, turbocharged, IDI diesel engine operated over a wide range of operating conditions from a second-law analysis point of view. A number of engine sub-assemblies (i.e. compressor, inlet, exhaust, combustion, and turbine) were studied quantifying the various kinds of irreversibility associated with each of them. They found that the combustion irreversibility was the main source of exergy destruction at every operating point. The exergy destruction due to throttling, friction and mixing in the turbocharger and inlet- exhaust manifolds were found to be about 20% of the total irreversibility.

In a separate study [57], they also analyzed the cumulative and availability rate balances of the same engine but specifically for full load operation at a speed of 1500 rpm. The paper systematically describes and evaluates the various kinds of availability degradations for every device and each process. They reported the overall engine second law efficiency to be 40.31%. The total irreversibility of various components was 27.3% and this increased up to 44.9% considering the destruction due to heat transfer to the cooling medium. Exhaust manifold irreversibility, due to exhaust valve throttling during blowdown, mixing of exhaust gases with manifold contents and friction accounted for about 10% of the total irreversibility.

Rakopoulos and Giakoumis [58] studied the energy and exergy performance of an IDI, naturally aspirated diesel engine subsystems using a computer based analysis. The engine was operated under steady state as well as transient conditions comprising sudden changes in speed and load. The engine was a four stroke single cylinder Ricardo E-6 research diesel engine. As a part of their transient analysis, they increased the load from an initial 15%

to the full engine load (100%) within 0.2 seconds keeping the engine speed constant at 1500 rpm. They also took up an acceleration test in which the engine speed was varied from 1500 rpm to 2150, 2250 and 2350 rpm in three different governor settings within no time in order to find out the engine responses in respect of first and second law terms. They concluded that the combustion irreversibility decrease and the exergy loss due to heat transfer to the wall increase for a ramp increase in load. They also found that the loss of exergy accompanying the exhaust gas from the cylinder to the ambient increase with increasing load or speed.

Kumar et al. [59] made a second law analysis of a single cylinder DI diesel engine using a comprehensive numerical simulation and evaluated the irreversible losses in engine processes such as combustion, heat transfer, and inlet and exhaust valve flow. At an operating condition of 2000 rpm with a fuel air equivalence ratio of 0.7, they found that 16.1% of the fuel availability was destroyed during the combustion process [44].

Caton [60] made an investigation based on second law to explore the destruction of exergy due to combustion processes. The study was made in an adiabatic, constant volume system for a range of initial pressure, temperature and equivalence for octane air mixtures. He summarized that the loss of exergy of fuel decreases when combustion is conducted at higher temperature. This may necessitate use of preheated air and in-cylinder materials that are capable of withstanding high temperature. At the same time, he also pointed out that higher combustion temperature leads to loss of more exergy with heat transfer and exhaust gas.

Rakopoulos and Giakoumis [61] also presented a detailed survey concerning the works pertaining to the application of the second-law of thermodynamics in ICE. The exergy balance equations of the engine cylinder and various subsystems were reviewed in detail, stating the relations concerning the definition of state properties, chemical availability, flow and fuel availability and dead state. Their review also includes identification and quantification of second-law efficiencies and the irreversibility of various processes and subsystems.

Som and Dutta [62] has made a comprehensive review pertaining to fundamental studies on thermodynamic irreversibility and exergy analysis in the processes of combustion of gaseous, liquid and solid fuels and have discussed the various approaches of exergy analysis and the results arrived at by different research workers in the field. They found that chemical reaction and physical transport processes are the main sources of irreversibility in

combustion with low flame temperature and heat conduction arising out of internal mixing contributing to destruction of exergy.

The following works are however specific to exergy analyses of biodiesel fuelled diesel engine. Canacki and Hosoz [63] made steady state energy and exergy analyses of a four cylinder turbocharged diesel engine at full load condition, engine speed maintained at 1,400 rpm with a brake power of 37.78 kW in each fuel test. The fuels considered were pure soybean methyl ester (B100 SME) and the yellow grease methyl ester (B100 YGME) and their 20% blending with D2 (B20 SME, B20 YGME). Fuel exergy input, exergetic efficiency, exergy destruction and exergy losses were evaluated for all the fuels. From their analysis, the typical results of which are reproduced in Figs. 2.1-2.4, they observed similar exergetic performance with D2, biodiesel and their blends. Fuel exergy of biodiesel and its diesel blends were slightly less compared to D2. However, the fuel exergy of B20 SME was the same with D2. Exergy losses due to irreversibility associated with combustion, exhaust gas and heat transfer were found to be the major contributors in their decreasing order for all the fuel operations. Engine operations with the two varieties of biodiesel and their 20% blending as fuels resulted in slightly lesser exergy destruction and higher power output percentages. Consequently, slightly higher exergetic efficiencies were witnessed for biodiesel operations as compared to D2.

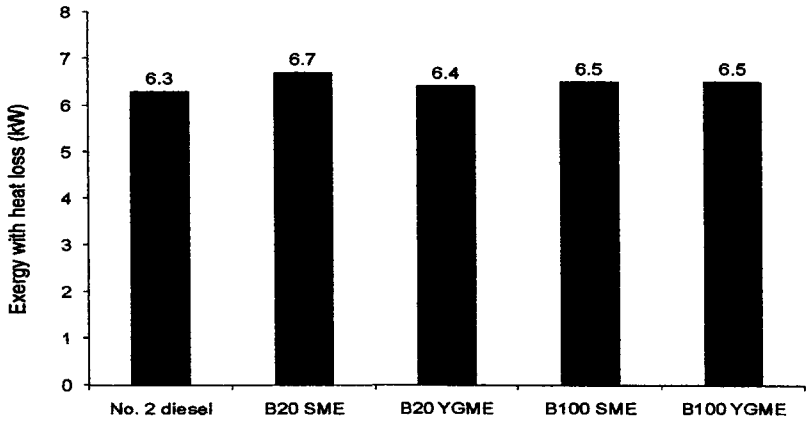


Fig. 2.1: Exergy loss accompanying heat loss

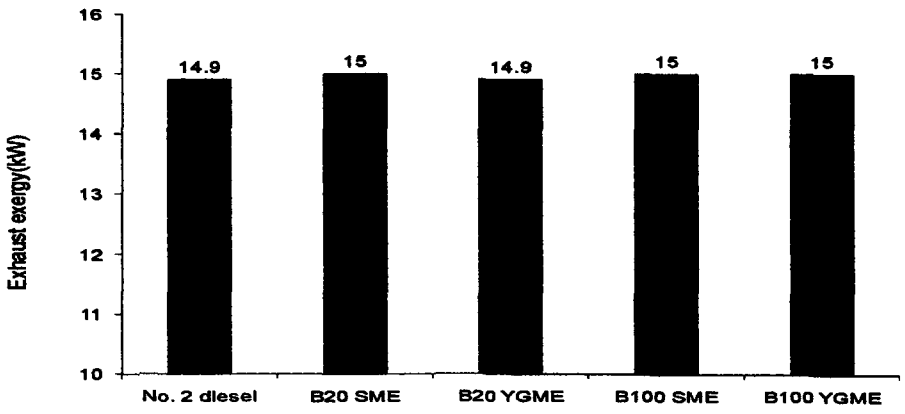


Fig. 2.2: Exergy loss with exhaust gas

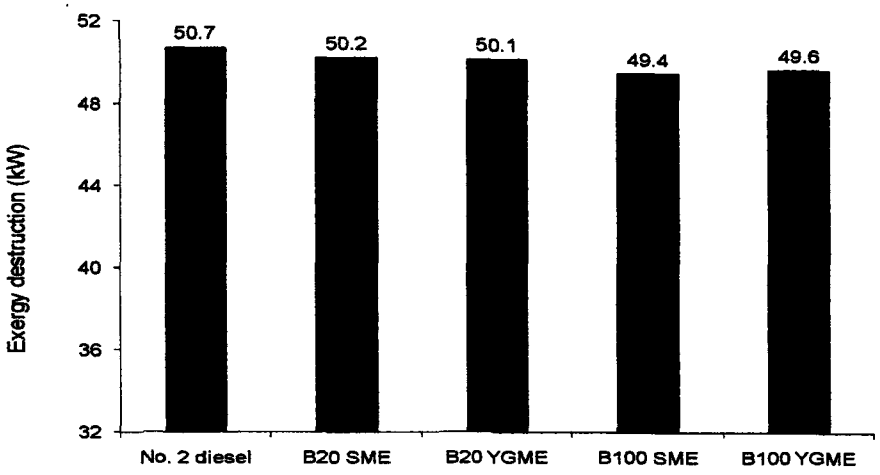


Fig. 2.3: Exergy destruction with various fuels

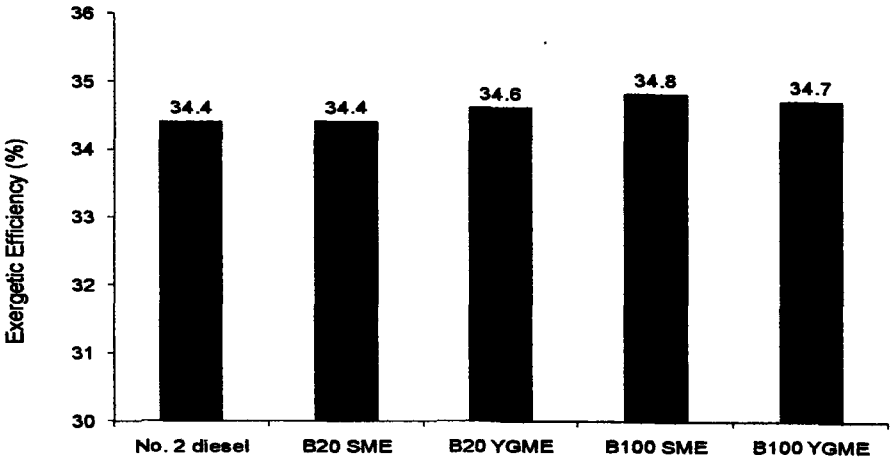


Fig. 2.4: Exergetic efficiency for the various fuels

Gokalp et al. [64] also performed a first and second law analysis of a four cylinder four stroke DI diesel engine using No. 2 diesel (D2), marine fuel (MF) and pure biodiesel i.e. soy oil methyl ester (SME) and their 5%, 20% and 50% blending separately with D2 and MF. They changed the engine speed from 1200 and 2400 rpm, with intervals of 400 rpm, while operating the engine at full load. The performance parameters such as BSFC, BTE, mechanical efficiency, exhaust temperature and the various exhaust emissions were evaluated and expressed as function of speed. They observed that the engine BTE was the maximum at 1600 rpm for all the fuel operations and hence presented the experimental and computational analyses on first- and second-law efficiencies performed for the engine at 1600 rpm using the fuels.

Fig. 2.5, adapted from this work, shows the effect of biodiesel addition on exergy destruction due to irreversibility of combustion. As seen from the figure, exergy destruction decreased with increasing biodiesel content in the fuel and exergy destruction by combustion was the minimum for pure SME (B100 SME). According to them, this was due to better combustion with biodiesel as biodiesel fuel increases homogeneity of the mixture in the combustion chamber of the cylinder. Exergy destruction occurs due to irreversibility present in the system and decreases the system efficiency. Exergy destruction by exhaust gas and heat transfer also contributes to the total exergy destroyed.

Fig. 2.6, from the same work clearly shows that the addition of biodiesel to the standard diesel fuel gives better exergy efficiency of the engine. They also observed that biodiesel addition to diesel fuels (D2 and MF) at lower proportion resulted in increase in fuel exergy which is depicted in Fig. 2.7. Although fuel exergy of B100 SME was less, lower exergy destruction by combustion with biodiesel of pure form however, resulted in better exergy efficiency of the engine. Exhaust exergy and exergy due to heat transfer however increased with biodiesel addition.

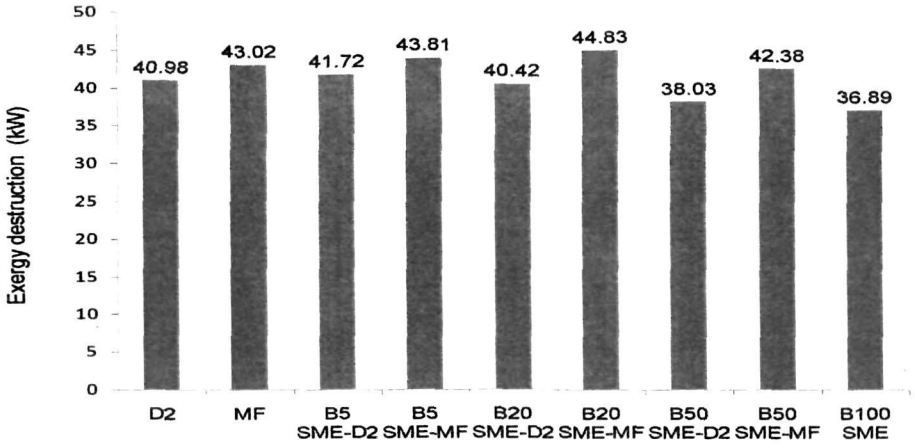


Fig. 2.5: Exergy destruction due to combustion

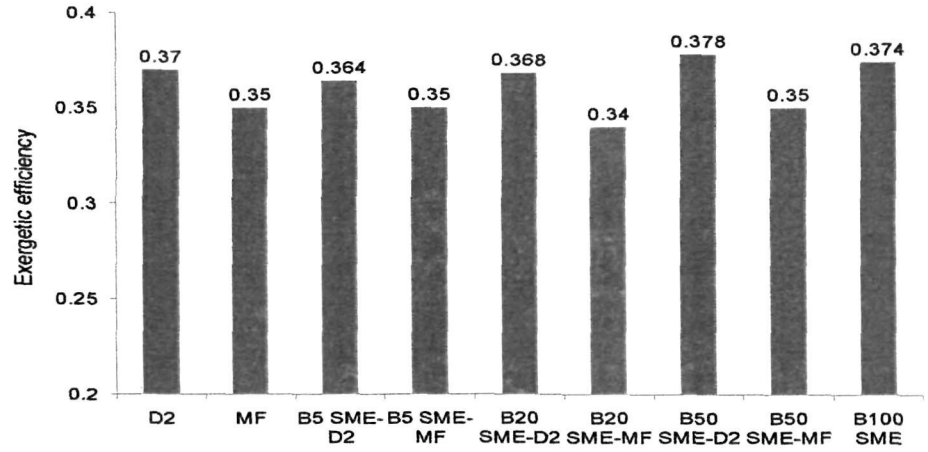


Fig. 2.6: Exergetic efficiencies for the various fuels

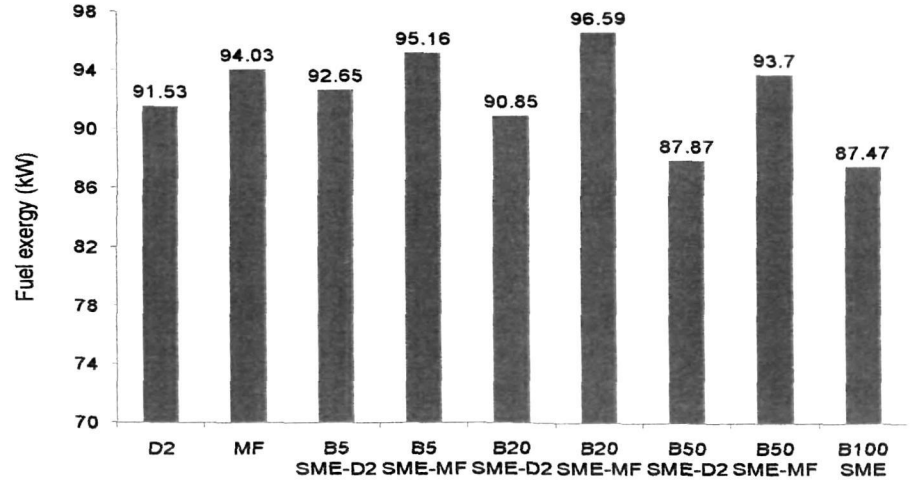


Fig. 2.7: Fuel exergy of the various fuels

## 2.5 BIODIESEL PRODUCTION

Biodiesel production is an important factor for implementation of renewable energy in transport sector and standby power application. Many technologies have been successfully developed and employed for processing and production of biodiesel [3-11]. However the state of the art in this regard has been discussed in detail in Chapter 4 where biodiesel processing and production for the present work have also been described. This has been done with the thought of keeping continuity and contiguousness of the contents in this regard.

## 2.6 SUMMARY OF LITERATURE REVIEW AND SCOPE OF PRESENT WORK

By reviewing the literature related to diesel engine cycle simulation and combustion model and also the experimental works on biodiesel fuelled diesel engine performance evaluation, it was realized that study of engine performance of biodiesel fuelled diesel engine with the help of simulation tool that avoids expensive and time consuming experiments, is becoming important. A mathematical model which is time-efficient and simple-to-use for computation is best suited for this purpose if the same is to predict engine performance involving less computational time and reduced cost. Therefore, the present work is chosen to model diesel engine processes with biodiesel and diesel blends as fuel adopting a single–zone approach. The detailed methodology of the modeling approach will be presented in the following chapter. From the literature survey conducted it was also realized that a detailed engine performance and combustion study involving a new biodiesel can be useful in understanding the behavior of the biodiesel blends in an unmodified diesel engine, while correlating the combustion characteristics with the performance of the engine considering these biodiesel blends as fuels. It is not possible to find out the effect of biodiesel properties on engine performance and fuel combustion behavior unless a comprehensive performance and combustion analyses is done to draw any conclusion out of it. Comprehensive investigation concerning performance and combustion with biodiesel from Koroch seed oil is not available. Also from the literature reviewed on exergy analyses of diesel engine system fuelled with biodiesel it was seen that these were specific to diesel engines of definite engine configuration with biodiesel from edible sources. However, the exergetic performance of an engine may vary considerably depending upon engine design configuration, type of biodiesel and other operating parameters. Through this work, the performance of a single cylinder four stroke DI Kirloskar TV1 diesel engine with different blends of non-edible biodiesel from Koroch seed oil will be evaluated in the light of second law of thermodynamics.

# CHAPTER 3

# MATHEMATICAL MODEL FOR SIMULATION OF DIESEL ENGINE PROCESSES

## 3.1 INTRODUCTION

In this chapter, the detailed diesel engine cycle simulation modeling will be described with their mathematical background. The cycle simulation model has been developed for a direct injection (DI) diesel engine which describes all the diesel engine processes in detail to permit calculations of pressure with changing crank angle (CA) and various performance parameters such as indicated power (IP), brake power (BP) and brake thermal efficiency (BTE). The developed cycle simulation model is a thermodynamic based model which follows the changing thermodynamic states of the working fluid through the engine intake, compression, combustion, expansion and exhaust processes while predicting the performance of the diesel engine. The characteristic feature of the simulation model is that it can be applied for predicting performance of the engine fuelled with diesel as well as various blends of diesel and biodiesel. Although there are many experimental studies concerning biodiesel fuel, but cycle simulation model predicting engine performance with biodiesel fuel blends are scarce. Cycle simulation model using biodiesel fuel blending could be an important tool for engine system design. Expensive and time consuming experiments involving biodiesel can be avoided through such a model. A thermodynamic based single zone combustion approach is adopted for simulating the combustion process while using these fuels.

## 3.2 GENERAL MODEL DESCRIPTION

Emphasis is laid on simulating all the processes consisting of a small DI diesel engine in the present model. A spatial uniformity of pressure, temperature and composition of the cylinder content at each CA is assumed. At any instant, the cylinder charge is assumed to be a homogeneous mixture of ideal gases and there always exists thermodynamic equilibrium without thermal or chemical gradient within the engine cylinder. Fuel mass is injected instantaneously from the injector and calculation of fuel mass that takes part in chemical reaction during combustion is based on complete combustion of the fuel. However, an approach that is more realistic is the incorporation of a fuel injection rate profile in the model with a finite injection duration period. Fuel is immediately evaporated once it is injected and

modeling of the combustion process is based on a uniformly distributed heat releasing phenomenon.

The molecular formula of diesel is approximated as $C_{12}H_{23}$ [65, 66]. Koroch seed oil Karanja oil, the relevant biodiesels for the presnt work, are mostly oleic and linoleic in composition [67]. The chemical formula of neat biodiesel is considered as $C_{17.75}H_{33.43}O_{1.98}$ and this has been derived from the fatty acid composition of Koroch seed oil as reported in earlier work [67] which is presented in Table 3.1. Koroch seed oil has its own characteristics as a potential source of biodiesel fuel due its unique fatty acid composition which is different from other variety of *Pongamia glabra* oil [67]. The chemical formulae for the various biodiesel blending have been obtained from the chemical formula of diesel and neat biodiesel and these are shown in Table 3.2. The calorific value, density, cetane number (CN) and the composition of the fuels are the parameters that define the characteristics of the fuels. It is further assumed that the air fuel mixture is lean and this leads to temperatures at which dissociation of products does not have much effect on engine performance [68]. Hence, dissociation of combustion products is not taken into consideration in order to make the analysis simple [69, 70]. However, it represents a more realistic cycle if combustion products are defined by dissociation consideration [69, 71]. Specific heats and internal energy are defined as a function of temperature [28, 51, 59, 71] and calculated using polynomial expressions for each species ($O_2$, $N_2$, $CO_2$, $H_2O$) considered in the present analysis.

Table 3.1: Fatty acid composition of Koroch seed oil [67]

| Sl. No | Fatty acid | Molecular formula | Composition (wt %) |
|---|---|---|---|
| 1. | Palmitic | $C_{16}H_{32}O_2$ | 11.30 |
| 2. | Stearic | $C_{18}H_{36}O_2$ | 9.80 |
| 3. | Oleic | $C_{18}H_{34}O_2$ | 45.25 |
| 4. | Linoleic | $C_{18}H_{32}O_2$ | 24.75 |
| 5. | Srachidic | $C_{20}H_{40}O_2$ | 1.75 |
| 6. | Linolenic | $C_{18}H_{30}O_2$ | 2.90 |
| 7. | Behenic | $C_{22}H_{44}O_2$ | 3.20 |
| 8. | Unidentified | | 1.05 |

The model calculation starts with the simulation of the compression phase which begins at the event of inlet valve closing (IVC) and continues simulating all the subsequent processes until the temperature specified at IVC event between two successive cycles becomes approximately equal. The CA at which fuel injection begins and the combustion duration are specified as inputs to the model. The period from the end of combustion to the exhaust valve opening (EVO) is the expansion phase.

Table 3.2: Chemical formulae for diesel, biodiesel and its diesel blends

| Fuel | Chemical formula |
|---|---|
| Diesel | $C_{12}H_{23}$ |
| B10 | $C_{12\,373}H_{23\,676}O_{0\,1284}$ |
| B20 | $C_{12\,776}H_{24\,408}O_{0\,267}$ |
| B30 | $C_{13\,213}H_{25\,2}O_{0\,418}$ |
| B40 | $C_{13\,689}H_{26\,064}O_{0\,582}$ |
| B60 | $C_{14\,78}H_{28\,043}O_{0\,957}$ |
| B100 | $C_{17\,75}H_{33\,43}O_{1\,98}$ |

## 3.3 MODEL FORMULATION

The mathematical formulation for the cycle simulation model consists in finding the engine performance parameters like BP, IP, BTE, ignition delay etc. in dependence of input parameters like fuel molecular formula, calorific value, speed, load and CR.

Two models are developed for cycle simulation in the present work. They will be termed as (a) Model I and (b) Model II. The first model predicts some aspects of engine performance theoretically while the second model uses experimental results of the present work for calculation of parameter values in the model and also for subsequent model validation in respect of prediction of engine performance. The basic features of the models and their objectives are outlined below.

(a) Model I

(i) The compression and the expansion phases are simulated using polytropic relations of pressure and temperature with cylinder volume, (ii) heat release rate is determined employing simple Wiebe function and (iii) some model input parameters are

chosen arbitrarily and the parameter values in the model equations are taken from published literature. Property values of Karanja biodiesel have been used in this model for fuel parameter inputs.

This model is used to study theoretically the effect of variation of speed and compression ratio (CR) on engine performance related to BP and BTE for diesel as well as 20% (B20), 40% (B40), 60% (B60) blending of biodiesel from Karanja oil [18, 67] with diesel.

(b) Model II

In this model formulation, (i) the compression and the expansion phases are simulated following the procedure outlined by Rakopoulos et al. [71] which essentially consists of iterative computation for the end state temperature by applying first law of thermodynamics for a closed system, (ii) heat release rate is determined employing double Wiebe function and (iii) model input parameters are obtained and the parameter values in the model equations are computed using experimental results of the present work. Heat release rate in diesel engine with clear premixed and diffusion combustion cannot be accurately predicted using simple Wiebe function, hence double Wiebe function was used in Model II.

This model is used to predict engine performance in terms of BP, IP and BTE for various engine loads and fuel blends at a fixed compression ratio. The predictions are compared with experimental results for model validation. Experiments for the purpose are carried out using diesel obtained from Numaligarh refinery limited (NRL), Assam and various blending of NRL diesel with biodiesel obtained from Koroch seed oil viz. B10, B20, B30 and B40. The description detailing all these model formulations follows in the next sections.

## 3.4 GOVERNING ENERGY CONSERVATION EQUATION

By applying the first law of thermodynamics applied for the closed cycle period (from IVC to EVO), the following energy balance equation can be written.

$$f(U) = U_2 - U_1 + dW - dQ = 0, \tag{3.1}$$

and the rate equation during combustion phase becomes

$$\frac{dQ_n}{d\theta} = \frac{dU}{d\theta} + \frac{dW}{d\theta} \tag{3.2}$$

where, $\frac{dQ_n}{d\theta}$ is the net heat release rate and is the difference between $\frac{dQ_f}{d\theta}$ and $\frac{dQ_h}{d\theta}$

$\frac{dQ_f}{d\theta}$ = Instantaneous heat release rate due to combustion of fuel

$\frac{dQ_h}{d\theta}$ = Instantaneous heat transfer rate from in cylinder gases to the wall

$\frac{dU}{d\theta}$ = Rate of change of internal energy

$\frac{dW}{d\theta}$ = Rate of Work transfer

These two energy conservation equations are used to find out the temperature history during the cycle. The first equation is used to determine the temperature history during compression and expansion phases for Model II, while the second equation is used to determine the same during combustion phases for both Model I and Model II as detailed later in this chapter. The temperature history during compression and expansion phases for Model I is determined explicitly considering polytropic processes.

### 3.4.1 Heat release based combustion sub-model (for heat release rate)

In the present work, the combustion process is modeled using a single zone approach, which is based on a uniformly distributed heat releasing phenomenon. Spray combustion is not considered in detail. Detailed phenomenological combustion modeling is undoubtedly useful, particularly in the design of combustion chamber; however, single zone heat release combustion models are appropriate for use in total diesel system simulation where the combustion process detail is not the primary focus [28]. The simple Wiebe function is often used to calculate heat release rate due to combustion of fuel as given in Equation (3.3) which is derived with the help of reaction kinetic considerations.

$$\frac{Q_f}{Q_{f,total}} = 1 - \exp\left[-a\left(\frac{\theta - \theta_0}{\Delta\theta}\right)^{m+1}\right] \qquad (3.3)$$

The total amount of energy released $Q_{f,total}$ is the product of the fuel mass brought into the combustion chamber, the lower heating value of the fuel and the combustion efficiency i.e.

$$Q_{f,total} = \eta_{comb} m_f LHV$$

where, $Q_f$ is the instantaneous heat release, $\theta_0$ is the CA at SOC and $\Delta\theta$ is the combustion duration. $a$ is an adjustable parameter that characterizes the degree of completeness of combustion. The parameter $m$ represents the rate of combustion. Differentiating equation (3.3) with respect to $\frac{\theta-\theta_0}{\Delta\theta}$ and multiplying with $\frac{Q_{f,total}}{\Delta\theta}$, the heat release rate is calculated as,

$$\frac{dQ_f}{d\theta} = a(m+1)(\frac{Q_{f,total}}{\Delta\theta})(\frac{\theta-\theta_0}{\Delta\theta})^m \exp\left[-a(\frac{\theta-\theta_0}{\Delta\theta})^{m+1}\right] \tag{3.4}$$

However in diesel engines with premixed and diffusion combustion phases, reproduction with a simple Wiebe function is usually inadequate. In such case, the simple Wiebe function is replaced by the double Wiebe function which is obtained by superimposition of two Wiebe functions. Description of an actual heat release rate with a double Wiebe function necessitates a subdivision of the energy shares of the two Wiebe functions.

$$\frac{dQ_{f,1}}{d\theta} = a_1(m_1+1)\left(\frac{Q_{f,1}}{\Delta\theta_1}\right)\left(\frac{\theta-\theta_{0,1}}{\Delta\theta_1}\right)^{m_1} \exp\left[-a\left(\frac{\theta-\theta_{0,1}}{\Delta\theta_1}\right)^{m_1+1}\right] \tag{3.5}$$

with, $\theta_{0,1} \le \theta \le \theta_{0,1} + \Delta\theta_1$

$$\frac{dQ_{f,2}}{d\theta} = a_2(m_2+1)\left(\frac{Q_{f,2}}{\Delta\theta_2}\right)\left(\frac{\theta-\theta_{0,2}}{\Delta\theta_2}\right)^{m_2} \exp\left[-a\left(\frac{\theta-\theta_{0,2}}{\Delta\theta_2}\right)^{m_2+1}\right] \tag{3.6}$$

with, $\theta_{0,2} \le \theta \le \theta_{0,2} + \Delta\theta_2$ and $\theta_{0,2} = \theta_{0,1} + \Delta\theta_1$

where, $Q_{f,1} = xQ_{f,total}$ and $Q_{f,2} = (1-x)Q_{f,total}$

$$\frac{dQ_f}{d\theta} = \frac{dQ_{f,1}}{d\theta} + \frac{dQ_{f,2}}{d\theta} \tag{3.7}$$

The suffices 1 and 2 refer to the premixed and diffusion combustion respectively. $x$ is the fraction of total energy released during premixed combustion. In the present study, the simple Wiebe function is used in Model I and the double Wiebe function in Model II to simulate the combustion process. In Model I, the value of $m$ in equation (3.4) is taken as 2.0 for all the fuels and the value of $a$ for diesel, B20, B40 and B60 were taken as 5.0 [28], 5.508, 6.008 and 6.508 respectively. These values are chosen arbitrarily for the biodiesel blends. Biodiesel is oxygenated in nature which helps in complete combustion and therefore higher value of $a$ was considered with increasing concentration of biodiesel in the blends. For Model II, the value of $x$ was determined from experiment and the values of $a_1$, $m_1$ and $a_2$, $m_2$ were adjusted such that the theoretical and experimental pressure CA curves best match. However the values of $a_1$ and $a_2$ were taken to be same during the process of adjustment. The determination of these parameters used in the double Wiebe function is discussed in detail in Chapter 7.

### 3.4.2 Heat Transfer

The heat transfer between the trapped gas and the surrounding wall is calculated by using Annand's equation.

$$\frac{dQ_h/d\theta}{A} = a\frac{k}{D}\mathrm{Re}^b(T_w - T) + c(T_w{}^4 - T^4) \tag{3.8}$$

where, $A = \pi\frac{D^2}{4} + \pi Dx$ is the heat transfer surface and $x$ is the instantaneous cylinder height in contact with the gas. $T_w$ is the temperature of the cylinder wall. $\mathrm{Re} = \frac{\rho V_p D}{\mu}$ is the Reynolds number with $D$ the cylinder bore and $V_p$ the mean piston speed. $\rho, \mu$ and $k$ are the gas density, dynamic viscosity and thermal conductivity respectively. The value of $a$ varies with speed and engine design. With normal combustion, $0.35 \le a \le 0.8$ with $b$ = 0.7 [28]; $c$ = 0 for the compression period and otherwise $c = 3.3\times10^{-8}$ W/m$^2$K$^4$ is the most usual value [69]. In the present study for Model I, the cylinder wall temperature $T_w$ for various fuels at different speed and CR is arbitrarily set a value equal to the temperature at the top dead centre (TDC) and is calculated using the following isentropic relation.

$$T_w = T_{tdc} = T_{ivc}\, CR^{\gamma-1}$$

However, for Model II, values of $T_w$ are calculated on the basis of cooling water temperature data from experiment. $T_w$ varies significantly with engine load and slightly with fuel used. Further, the constants, $a, b$ and $c$, are calibrated experimentally for all the fuels at various loads.

The gas dynamic viscosity is calculated using the following equation.

$$\mu = \frac{\mu_{air}}{\left[1 + \frac{0.027}{RAF}\right]} \tag{3.9}$$

where, $RAF$ is the relative air fuel ratio. In the above equation, the dynamic viscosity of pure air is taken as [28]

$$\mu_{air} = 3.3 \times 10^{-7} T^{0.7}$$

. The thermal conductivity $k$ is determined from the following relation [28].

$$k = \frac{9\gamma - 5}{4} \mu C_V$$

### 3.4.3 Compression phase calculation

The compression of charge begins at IVC. Pressure $(p_1)$, temperature $(T_1)$, and cylinder volume $(V_1)$ at the IVC event are known. CA $(\theta_1)$ with respect to IVC is specified. Initially it is assumed that $N_x = 0$, $T_1 = T_a$ and $p_1 = p_a$; where $N_x$ is the no. of moles of residual exhaust gas left in the engine from the previous cycle which is evaluated at the point exhaust valve closing (EVC). $T_a$ and $p_a$ are the ambient temperature and pressure respectively. For the next cycle, $T_1$ and $p_1$ are assigned the pressure and temperature values at the event of IVC. No. of moles of air trapped in the engine is calculated as:

$$N_a = \frac{p_1 V_1}{\bar{R} T_1} - N_x \tag{3.10}$$

and there are $N_a + N_x$ moles of charge at the beginning of the compression process. This is required to calculate the total kmol of fuel injected per cycle from the global air fuel ratio (AFR) which is known a priori.

**Computations for pressure and temperature**

Computations for state variables, temperature, and pressure during and at the end of the processes are carried out for the two models following a step by step process by advancing the piston position in small increment (1°) of CA.

**Model I**

Instantaneous cylinder volume $V$ is given by,

$$V(\theta) = V_s\left[\frac{R_c}{R_c - 1} - \frac{1-\cos\theta}{2} + \frac{L}{S} - \frac{1}{2}\sqrt{(2\frac{L}{S})^2 - \sin^2\theta}\right] \tag{3.11}$$

The terms used in equation (3.11) are as given below.

$R_c$ is the CR, $L$ is the length of connecting rod, $S$ is the stroke length , $V_s$ is the stroke volume of the cylinder and $\theta$ is the CA. Choosing a CA step size of $\Delta\theta$ equal to 1°, the cylinder volume $V_2$ for the next CA, $\theta_2 = \theta_1 + \Delta\theta$ is computed using equation (3.11). The compression process is taken as polytropic process and given by the relations,

$$T_2 = T_1\left(V_1/V_2\right)^{\gamma-1} \tag{3.12}$$

$$P_2 = P_1\left(V_1/V_2\right)^{\gamma} \tag{3.13}$$

with $\gamma = \dfrac{C_{pr}(T_1)}{C_{vr}(T_1)}$ = constant.

where, $C_{pr} = \frac{(C_{pa}N_a + C_p N_r)}{N_a + N_r}$ and $C_{vr} = C_{pr} - \overline{R}$

$C_{pa}$ and $C_p$ are molar specific heat of air and the combustion products respectively.

Specific heat for air as functions of temperature [54] and specific heat for each species of interest in the combustion products [28] are given in the form:

$$\frac{C_{pa}}{\overline{R}} = \alpha + \beta T + \gamma T^2 + \delta T^3 + \varepsilon T^4 \tag{3.14}$$

$$\frac{C_p}{\overline{R}} = a_1 + a_2 T + a_3 T^2 + a_4 T^3 + a_5 T^4 \tag{3.15}$$

The values of the coefficients $\alpha, \beta, \gamma, \delta$ and $\varepsilon$ are given in [54] and the constants $a_1, a_2$ etc. are listed in [28]. To account for the heat transfer during the compression process, a pressure drop given by the equation below was considered [51].

$$\frac{\Delta p}{p} = \frac{\frac{dQ_h}{dt}}{MC_v T}\Delta t \tag{3.16}$$

Having known the initial thermodynamic conditions of temperature, pressure and volume, the temperature and pressure after a crank rotation of $\Delta\theta$ are explicitly determined using equations (3.11) through (3.16).

**Model II**

Compression phase calculations are carried out following the technique proposed by Rakopoulos et al. [71], wherein the temperature at every CA is found out initially using equation (3.12) and is given by,

$T_2 = T_1\left(V_1/V_2\right)^{\gamma-1}$ with $\gamma = \frac{C_{pr}(T)}{C_{vr}(T)}$ given as a function of temperature.

To find pressure $p_2$, the perfect gas equation is used as follows:

$$p_2 = p_1\left(\frac{V_1}{V_2}\right)\left(\frac{T_2}{T_1}\right) \tag{3.17}$$

The $pdV$ work during the CA step is calculated as,

$$dW = pdV = 0.5(p_1 + p_2)(V_2 - V_1)$$

Heat transfer $'\delta Q'$ in the step is calculated employing the heat transfer model of Annand [28, 69] as explained in section 3.4.2. Equation (3.1) as mentioned in section 3.4 is solved with respect to $T_2$ using Newton-Raphson method for a better estimate of $T_2$ and then again $p_2$ is calculated using equation (3.17) with the revised value of $T_2$. All these steps are repeated until the error $f(U)$ in equation (3.1) is negligible. Then for both the models, the properties with index 2 are set as initial conditions for calculation of all the above mentioned parameters at the next CA and this continues till the CA reaches the value corresponding to SOC by keeping track of the ignition delay period. The total work done during the compression process is the integration of the $pdV$ work from IVC to SOC. The internal energy, U, as function of temperature is calculated as follows.

$$U = \frac{\left(U_a N_a + U_p N_x\right)}{N_a + N_x} \tag{3.18}$$

where, $U_a = \bar{R}\left[(\alpha - 1)T + \frac{\beta}{2}T^2 + \frac{\gamma}{3}T^3 + \frac{\delta}{4}T^4 + \frac{\varepsilon}{5}T^5\right] + \kappa$ (3.19)

$$\frac{U_p}{RT} = (a_1 - 1) + \frac{a_2}{2}T + \frac{a_3}{3}T^2 + \frac{a_4}{4}T^3 + \frac{a_5}{5}T^4 + \frac{a_6}{T} \tag{3.20}$$

Equations (3.19) and (3.20) are obtained by using equations (3.14) and (3.15), respectively.

### 3.4.4 Auto-ignition and ignition delay

The phenomenon of auto ignition of a fuel spray consists of sequences of physical and chemical processes of substantial complexity. The diesel fuel spray behavior needs to be considered for a detailed and exact description of ignition phenomenon in a diesel engine combustion chamber. Fuel preparation, mixture non-homogeneity, heat loss and non-uniform flow patterns are some of the factors that affect the ignition delay which is the time between start of injection (SOI) and SOC. However, with the single-zone combustion model, use of the detailed and complete ignition model would not be a proper choice as it demands an efficient estimation of the ignition timing. Therefore, relatively simple, effective and already available model of diesel engine ignition is applied with appropriate modification. Various

complex models have been developed for simulating the auto-ignition process. A number of expressions for ignition delay are available in literature involving parameters of IC engine and state of the working mixture in the cylinder. Most of them are correlated by Arrhenius type of equation of the form:

$$\tau_{id} = Ap^{-n} \exp\left(\frac{E_A}{\bar{R}T}\right) \tag{3.21}$$

where, $E_A$ is the apparent activation energy for the fuel auto-ignition process, $A$ is the frequency factor and $n$ is a constant depending upon the type of fuel and reaction environment as given in Table 3.3.

Many important correlations proposed by various authors are found in [72]. Some of these expressions were based on pressure and temperature at start of injection (influenced directly by speed and load) while the expression of Sitkei was based on pressure and temperature of air at the IVC (indirectly by residual gas fraction) and some others were based on average pressure and temperature in the cylinder and the fuel CN.

Table 3.3: Constants for Arrhenius equation [28]

| Conditions | | | | Parameters | | |
|---|---|---|---|---|---|---|
| Apparatus | Fuel | $p$, atm | $T$, K | $n$ | $A$ | $E_A/R$ |
| Steady flow reactor | No. 2 diesel | 10-30 | 650-900 | 2.000 | $2.43\times10^{-9}$ | 20926 |
| Steady Flow reactor | No. 2 diesel | 10-30 | 650-900 | 1.000 | $4.00\times10^{-10}$ | 20080 |
| Steady Flow | Diesel with CN 45-50 | 30-60 | 770-980 | 0.757 | 0.0405 | 5473 |
| Const. volume bomb | Fuel with CN >50 | 8-48 | 590-782 | 1.190 | 0.4400 | 4650 |
| Const. volume bomb | Kerosene | 1-30 | 673-973 | 1.230 | 0.0276 | 7280 |

The group of Assanis and co-authors defined an expression incorporating the fuel air equivalence ratio in it to account for the effect of engine load on ignition delay.

$$\tau_{id} = \frac{2.4}{p_m^{1.02}\phi^{0.2}} \exp\left(\frac{2100}{T_m}\right) \tag{3.22}$$

The correlation for ignition delay for DI diesel engines from Hardenberg and Hase [28] that gives ignition delay in CA degrees is:

$$\tau_{id} = (0.36 + 0.22V_p)\exp\left[E_A\left(\frac{1}{\bar{R}T} - \frac{1}{17190}\right)\left(\frac{21.2}{p-12.4}\right)^{0.63}\right] \tag{3.23}$$

where, $V_p$ is the mean piston speed, $E_A$ the apparent activation energy, $\bar{R}$ the universal gas constant and $p$ and $T$ are the charge pressure and temperature respectively. The expression for activation energy in joules per mole is given as:

$$E_A = \frac{618840}{CN + 25} \tag{3.24}$$

The expression given by Bibic et al. [72] for an M-type diesel engine is as follows.

$$\tau_{id} = 1.04 \times 10^{-3} N p_{fi}^{-0.2} \exp\left(\frac{16550 - 20CN}{\bar{R}T_{fi}}\right) \tag{3.25}$$

where, $N$ the engine speed, $p_{fi}$ and $T_{fi}$ are cylinder pressure and temperature at SOC. The constants used in these empirical relations should be modeled and identified from experimental engine test over an extended operating condition in order to predict the precise point of auto-ignition timing in a diesel engine of specific configuration.

A closer look into the various expressions for ignition delay indicates that certain different specific engine operational and fuel parameters have been used to obtain different correlations. The present study deals with engine operation involving variable operating conditions and fuel. Therefore, it was felt that an expression combining the basic features of these correlations could be developed in the present analysis as a function of mixture pressure, temperature, engine load defined by the fuel air equivalence ratio and the fuel type defined by the fuel CN as follows.

$$\tau_{id} = \frac{A}{p^n \phi^{0.2}} \exp\left(\frac{16550 - 20CN}{RT}\right) \tag{3.26}$$

This correlation has been found to work satisfactorily in matching the predicted results of Model II with experiment. In Model I, the values of the constant $A$ and the exponent $n$ in the above correlation were considered as 2.64 and 0.8 respectively for all the fuels at different speeds and various CR to achieve realistic output. However, for Model II, the constant $A$ and the exponent $n$ are calibrated against experimental results and the value of $A$ is considered as 2.4 for all the fuel operations at various loads. The value of the exponent $n$ was found to vary between 0.6 and 0.66 depending upon the type of fuel. A fixed exponent of 0.2 was used for the fuel air equivalence ratio for both Model I and Model II.

Under actual operational conditions, the cylinder pressure and temperature change during the delay period due to the piston movement during the compression stroke. Therefore, to account for these changing conditions, the ignition delay is calculated by summing up the instantaneous ignition delay time at each time step and the following integral relation is usually used for the purpose.

$$\int_0^{\tau_{id}} \left( \frac{1}{\tau_{id}} \right) dt = 1$$

### 3.4.5 Combustion phase computation (for Model I and Model II)

We introduce the ideal gas law and the perfect gas equation for internal energy expression as, $pV = MRT$ and $U = MC_V T$, respectively.

where, $M, C_V, p, T$ and $V$ are mass, specific heat at constant volume, instantaneous pressure, instantaneous temperature, instantaneous volume of the cylinder content respectively.

Equation (3.2) can be rearranged as

$$\frac{dQ_f}{d\theta} - \frac{dQ_h}{d\theta} = M\frac{d(C_V T)}{d\theta} + p\frac{dV}{d\theta} \tag{3.27a}$$

The first term in the right-hand side in the equation can be rewritten by applying the chain rule of the differentiation.

$$M\frac{d(C_V T)}{d\theta} = M\left[ C_V \frac{dT}{d\theta} + T\frac{dC_V}{d\theta} \right]$$

Therefore, $$\frac{dQ_f}{d\theta} - \frac{dQ_h}{d\theta} = M\left[ C_V \frac{dT}{d\theta} + T\frac{dC_V}{d\theta} \right] + p\frac{dV}{d\theta} \tag{3.27b}$$

Since $C_V$ is expressed as a function of temperature; which is say $C_V = f(T)$, one can write, $\frac{dC_V}{d\theta} = f'(T)\frac{dT}{d\theta}$

Substituting this in equation (3.27b),

$$\frac{dQ_f}{d\theta} - \frac{dQ_h}{d\theta} = M\left[ C_V \frac{dT}{d\theta} + Tf'(T)\frac{dT}{d\theta} \right] + p\frac{dV}{d\theta}$$

$$\Rightarrow M(C_V + Tf'(T))\frac{dT}{d\theta} = \frac{dQ_f}{d\theta} - \frac{dQ_h}{d\theta} - p\frac{dV}{d\theta}$$

$$\Rightarrow \frac{dT}{d\theta} = \frac{1}{M(C_V + Tf'(T))}\left[\frac{dQ_f}{d\theta} - \frac{dQ_h}{d\theta} - \frac{MRT}{V}\frac{dV}{d\theta}\right] \quad (3.28)$$

This first order ordinary differential equation is solved numerically using fourth order Runge -Kutta method for temperature at definite CA interval. In order to solve this governing equation, Equation (3.28), constitutive relations for each term in the equation need to be introduced.

Rewriting the Equation (3.11) for instantaneous cylinder volume and its first order derivative, one obtains,

$$V(\theta) = V_s\left[\frac{R_c}{R_c - 1} - \frac{1-\cos\theta}{2} + \frac{L}{S} - \frac{1}{2}\sqrt{(2\frac{L}{S})^2 - \sin^2\theta}\right]$$

and $$\frac{dV}{d\theta} = \frac{V_S}{2}\left[\frac{1}{2}\frac{\sin 2\theta}{\sqrt{\left(\frac{2L}{S}\right)^2 - \sin^2\theta}} - \sin\theta\right]$$

Representative relations for the other terms in the governing equation are discussed in the following sections. The heat release rate for the two models are determined using heat release combustion model as outlined earlier.

## 3.5 EXPANSION PROCESS

The burning gases force the piston towards bottom dead centre (BDC) during the expansion stroke and both pressure and temperature of the combustion products decrease. The procedure of pressure, temperature, and $pdV$ work computation for the expansion process is same with the one described for the compression process in section 3.4.3 for Model I and Model II.

## 3.6 GAS EXCHANGE PROCESS

The intake and exhaust processes in a four stroke cycle engine are together referred to as gas exchange process. The behavior of these two systems are extremely important as they

govern the air flow into and exhaust flow out of the engine cylinder and also many of the systems design variables determine the overall performance. Intake and exhaust system models developed for calculating details of intake and exhaust flow include (i) quasi steady models based on flow analysis through restrictions provided by valve and port etc. (ii) Filling and emptying models that represent the manifolds by finite volume (iii) gas dynamic models based on conservation equations of mass, momentum and energy that provide spatial variations in flow and pressure in the manifolds. If the manifold flows are the primary focus then models that describe the unsteady gas flow phenomenon are required. However, the necessity for such sophisticated intake and exhaust system models does not arise if the goal is only to provide the input or boundary conditions for the detailed model of in-cylinder processes. Due to time varying valve opening area, cylinder volume, gas inertia effects, wave propagation in the intake and exhaust system the pressure in the cylinder during the gas exchange process change in a complicated way. During these processes, the cylinder pressure is not only a function of in-cylinder processes but also of mass flow rate through the valves. Applying energy equation to these processes and treating the gas as ideal [51, 58, 59, 69] one obtains,

For the exhaust process,

$$\frac{dp}{dt} = \gamma p\left[\frac{1}{M}\frac{dM}{dt} - \frac{1}{V}\frac{dV}{dt}\right]_{exhaust} \tag{3.29}$$

For the intake process,

$$\frac{dp}{dt} = \gamma\left[\frac{RT}{V}\frac{dM}{dt} - \frac{p}{V}\frac{dV}{dt}\right]_{\text{int ake}} \tag{3.30}$$

Both these equations require the relevant mass flow rate $\frac{dM}{dt}$, which can be determined from either of the equations given below [28, 51, 59].

$$\frac{dM}{dt} = C_d A p_0 \sqrt{\left[\frac{2\gamma}{RT(\gamma-1)}\left(\frac{p}{p_0}\right)^{\frac{\gamma}{\gamma-1}}\left\{\left(\frac{p}{p_0}\right)^{\frac{\gamma}{\gamma-1}} - 1\right\}\right]} \tag{3.31}$$

$$\frac{dM}{dt} = C_d A p_0 \sqrt{\left[\frac{2\gamma}{RT(\gamma-1)}\left\{\left(\frac{p}{p_0}\right)^{\frac{2}{\gamma}} - \left(\frac{p}{p_0}\right)^{\frac{\gamma+1}{\gamma}}\right\}\right]} \tag{3.32}$$

Equation (3.31) was used in Model I and equation (3.32) was in Model II for calculating the mass flow rate. $C_d$ is the discharge coefficient which is introduced to take into account the real gas flow effect. $A$ is the instantaneous valve flow area that depends upon the valve lift and the geometric features of the valve head, seat and stem. For flow into the cylinder through the intake valve, $p_0$ is the intake manifold pressure $p_{imf}$ and $p$ is the cylinder pressure. For flow out of the cylinder through the exhaust valve, $p_0$ is the cylinder pressure and $p$ is the exhaust manifold pressure. The critical pressure ratio for the choked flow condition is

$$\frac{p}{p_0} = \left(\frac{2}{\gamma+1}\right)^{\gamma/\gamma-1} \tag{3.33}$$

When $\frac{p}{p_0}$ less than its critical value, the flow is subsonic and the mass flow rate is given by equations (3.31) and (3.32). For critical pressure ratio, the maximum mass flow rate for sonic flow is given by

$$\frac{dM}{dt} = C_d A p_0 \sqrt{\left[\frac{\gamma}{RT}\left(\frac{2}{\gamma+1}\right)^{\frac{\gamma+1}{\gamma-1}}\right]} \tag{3.34}$$

The equations (3.29) and (3.30) can be expressed in the general form:

$\Delta p = Q\Delta t$ with $Q$ being equal to $\frac{dp}{dt}$

Defining a maximum allowable pressure change for every time step in the integration for the exhaust and intake process,

$$\Delta p_{\max} = \frac{p - p_{emf}}{m}(exhaust) \tag{3.35}$$

$$\Delta p_{\max} = \frac{p_{imf} - p}{m}(\text{int}\, ake) \tag{3.36}$$

where, $m$ is some number between 3 and 10 [51, 59]. $p_{emf}$ and $p_{imf}$ are the exhaust and inlet manifold pressures that are considered as reference pressures for the engine exhaust and intake processes.

A maximum allowable time interval $\Delta t_{max}$, the time duration for $n$ degrees of crankshaft rotation is defined for each time step as:

$\Delta t_{max} = \frac{n}{360}\frac{60}{N}$; where, $N$ is the engine rpm. The value of $n$ also chosen between 3 and 10 [51, 59]. For each time step, $\Delta p_{max}$ is calculated first and then mass flow rate $\frac{dM}{dt}$ is calculated using equation (3.31) for Model I and equation (3.32) for Model II, under subsonic conditions or equation (3.34) for both the models, under choked flow conditions. The value of $Q$ is then determined from the given conditions using equations (3.35) for the exhaust process and equation (3.36) for the intake process. The gas flow into and out of the cylinder and the piston movement may oppose each other during the gas exchange processes and it may so happen that either $\frac{dM}{dt}$ predominates over $\frac{dV}{dt}$ or vice versa. Depending on this $Q$ may be positive, negative or zero (very rarely). With the values of $Q$ and $\Delta p_{max}$, $\Delta t$ is computed and then compared with $\Delta t_{max}$. The smaller of the two is used as the time step for the integration process. While following this process of integration it must have some control over it because a uniform $\Delta t$ may lead to values of $\Delta p$ that reduce the cylinder pressure below $p_{emf}$ during the exhaust process and above $p_{imf}$ during the intake. A fixed value of $\Delta p$ also leads to large $\Delta t$ values and these results in overshooting the limits of piston travel. The above mentioned procedure poses no problem for the exhaust process, however, there is problem with the use of equation (3.36) during the early period of the intake stroke as the cylinder pressure may be greater than the intake manifold pressure and in that case $\Delta p$ becomes negative. Therefore, to overcome this problem, the pressure $p$ is decreased by small prescribed amounts after the piston reaches TDC during the exhaust stroke until $p$ becomes less than $p_{imf}$ and the corresponding $\Delta t$ is then calculated.

### 3.7 Valve flow area

Several different valve flow areas are in use for calculating the mass flow rate. They include (i) valve head area $\left(\frac{\pi D_v^2}{4}\right)$, (ii) the port area at the valve seat $\left(\frac{\pi D_p^2}{4}\right)$, (iii) the valve curtain area $(\pi D_v L_v)$ and (iv) geometric minimum flow area [28]. In the expressions for

valve area, $L_v$ , $D_v$ and $D_p$ are the instantaneous valve lift, valve head diameter and valve port diameter respectively. The valve curtain area is convenient to use as it varies linearly with valve lift and is easy to determine. The concept of geometric minimum flow area represents a complex function of valve and valve seat dimensions. In the present analysis, the minimum flow area concept is used.

Depending upon the values of instantaneous valve lift, three different cases of flow area development may arise [28, 59, 73],

$Case I : 0 < \frac{L_v}{D_v} < 0.125$ : The minimum flow area corresponds to the slant surface of a frustum of a right circular cone and perpendicular to the valve seat and is given by,

$$A = 2.22 L_v \left( \frac{7}{8} D_v + \frac{L_v}{2} \right) \tag{3.37}$$

$Case II : 0.125 < \frac{L_v}{D_v} < 0..2735$ : The minimum flow area is still the slant surface but no longer perpendicular to the valve seat and is given by,

$$A = 2.94 D_v \sqrt{\left( L_v^{\,2} - \frac{L_v D_v}{8} + \frac{D_v^2}{128} \right)} \tag{3.38}$$

$Case III : \frac{L_v}{D_v} > 0.2735$ : When valve lift becomes large, the flow area is port flow area minus the sectional area of the valve stem and is given by,

$$A = \frac{\pi}{4} \left[ \left( \frac{D_v}{2} \right)^2 - \left( \frac{D_v}{4} \right)^2 \right] \tag{3.39}$$

It is assumed that the port diameter $D_p = \frac{D_v}{2}$ and the valve stem diameter $D_s = \frac{D_v}{4}$, with a valve seat angle of 45°.

## 3.8 NET WORK DONE AND INDICATED MEAN EFFECTIVE PRESSURE

Net work done in a complete cycle is the integration of $pdV$ work given by,

$$W_{net} = \oint \left( p \pm \frac{\Delta p}{2} \right) \Delta V \tag{3.40}$$

where, $\Delta p$ is the change in pressure inside the cylinder due to piston motion, combustion, heat transfer and flow into and out of the cylinder. The positive (+) sign with $p$ equal to the pressure at the initial CA $(\theta_1)$ is used in Model I while the negative sign (−) with $p$ equal to the pressure at the next CA $(\theta_2)$ is used in Model II. Heat transfer during the gas exchange period is also taken into consideration through a pressure drop given by the equation (3.16) as stated earlier. IP is calculated from the net work done during the cycle and the engine speed. Indicated mean effective pressure (IMEP) is then calculated.

## 3.9 FRICTIONAL LOSSES

Frictional losses affect the maximum brake torque and the minimum BSFC directly and are often a criterion for good engine design. These losses not only reduce the power but also influence the size of the coolant systems [68].The mean effective losses of power due to friction in different moving parts are calculated by using the following empirical relations [51]. Details about these frictional models are available in [74].

(i) Mean effective pressure( MEP ) lost due to friction in the piston and piston rings

$$FMEP1 = 12.85\frac{P_{sl}}{DL} \times \frac{100 \times V_p}{1000} \tag{3.41}$$

where, $P_{sl}$ is the piston skirt length (mm), $D$ is the cylinder bore (m), $L$ is the stroke length (m), $V_p$ is mean piston speed (m/s)

(ii) MEP lost in bearing friction

$$FMEP2 = 0.0564\frac{D}{L} \times \frac{N}{1000} \tag{3.42}$$

where, $N$ is the engine RPM.

(iii) MEP lost in friction in the valve gear

$$FMEP3 = 0.226(30 - \frac{4N}{1000}) \times \frac{nD_{vi}^{1.75}}{D^2 L} \tag{3.43}$$

where, $n$ is the number of intake valve per cylinder, $D_{vi}$ is the inlet valve diameter.

(iv) MEP lost in overcoming inlet and throttling losses

$$FMEP4 = \frac{p_e}{2.75} + p_{imf} \tag{3.44}$$

where, $p_e$ is the exhaust gas back pressure (bar) and $p_{imf}$ is the inlet manifold pressure (bar).

(v) MEP lost in pumping

$$FMEP5 = 0.0275 \times \left(\frac{N}{1000}\right)^{1.5} \tag{3.45}$$

(vi) MEP lost in friction due to gas pressure behind rings

$$FMEP6 = 0.42 \times (p_a - p_{imf}) \times \frac{L}{D^2} \times \left(0.0888 R_c + 0.182 R_c^{1.33 - 0.394 V_p/100}\right) \times 10 \tag{3.46}$$

where, $p_a$ is the atmospheric pressure (bar).

(vii) MEP lost in friction due to wall tension in rings

$$FMEP7 = 10 \times \frac{0.377 L n_{pr}}{D^2} \tag{3.47}$$

where, $n_{pr}$ is the number of piston rings.

(viii) Blow by losses

$$FMEP8 = \sqrt{p_a - p_{imf}} \times \left[0.121 R_c^{0.4} - (0.0345 + 0.001055 R_c) \times \left(\frac{N}{100}\right)^{1.185}\right] \tag{3.48}$$

(ix) MEP lost in overcoming combustion chamber and wall pumping losses

$$FMEP9 = \sqrt{\frac{p_{imep}}{11.45}} \times 0.0915 \times \left(\frac{N}{1000}\right)^{1.7} \tag{3.49}$$

where, $p_{imep}$ is the indicated mean effective pressure.

Another empirical relation for frictional mean effective pressure (FMEP) as a function of compression ratio (CR) and engine speed (N) is also considered as given below [58].

$$FMEP = aCR + bN \tag{3.50}$$

where, $a$ and $b$ are constants that required adjustment. This particular empirical equation is used for the fuel blend "B40" in Model II. The values of the constant $a$ at no load, 25%, 50%, 75% and 100 % (full) loads are taken as 0.123, 0.123, 0.121, 0.118 and 0.123 respectively. Similarly values of the constant $b$ at the corresponding loads are $1.884 \times 10^{-4}$, $1.005 \times 10^{-4}$, $0.001 \times 10^{-4}$, $0.001 \times 10^{-4}$ and $0.574 \times 10^{-4}$.

## 3.10 INPUT PARAMETERS AND OUTPUT VARIABLES FOR THE SIMULATION MODELS

Fuel properties and the engine design and operating parameters are specified as inputs to the models. B20 and B40 blends have been the common fuels for both Models I and II and as such although the chemical formulae for them are same, different calorific values of the

corresponding fuels are used in the two models. The fuel properties are taken from the reference [18] in Model I whereas for Model II the fuel properties are determined as a part of the present study which are discussed in Chapter 5. Model input parameters such as SOI, combustion duration were chosen arbitrarily for diesel and the biodiesel blends (B20, B40 and B60) in Model I at various speeds and different CR. However for Model II, these two input parameters are determined from experiments conducted on a test engine with the tested fuels while operating the engine at various loads. Moreover, combustion duration for the premixed and diffusion combustion phases as required in the double Wiebe function is also calculated separately. The methodologies for calculation of model output parameters in both the models are identical.

IP, BP and BTE are the direct output variables of the models. FMEP is calculated following procedures as already outlined in section 3.9. Brake mean effective pressure (BMEP) is the difference between the IMEP and the FMEP. BP is calculated from known values of BMEP, stroke volume and speed. The BTE is also estimated using values of calculated BMEP, mass flow rate, cylinder stroke volume, and calorific value of the fuel.

# CHAPTER 4

# BIODIESEL PRODUCTION, BLENDING AND CHARACTERIZATION

## 4.1 INTRODUCTION

Biodiesel is an alternative fuel made from plant vegetable oil and animal fats. Vegetable oils are usually viscous with viscosities that range from 10 to 20 times greater than petro-diesel fuel. The major problem with direct use of pure vegetable oils as fuels for diesel engines is caused by high fuel viscosity. Due to their high viscosity and low volatility, they do not burn completely as atomization becomes poor and form deposits in the fuel injector of diesel engines [75]. Dilution, micro emulsification, pyrolysis and transesterification are the four techniques applied to solve problems of high viscosity of vegetable oil. Dilution of pure vegetable oils by blending with diesel and micro emulsion of vegetable oils lowers the viscosity, but some engine performance problems still exist. Micro emulsion is basically the process of colloidal dispersion of fluid microstructures (1-150 nm) in solvent in which two immiscible phases are formed and is a probable solution to the problem of high viscosity of vegetable oil. Pyrolysis or thermal cracking is a process of conversion of one substance into another by application of heat either in absence or presence of a catalyst. The pyrolyzed material can be vegetable oils, animal fats, natural fatty acids or methyl esters of fatty acids. Pyrolysis of vegetable oil gives different lower hydrocarbons that can be used as fuel. The first pyrolysis of vegetable oil was conducted in an attempt to synthesize petroleum from vegetable oil. Schwab et al. [76] has reported in detail on the mechanism of pyrolysis of triglycerides. Catalytic cracking of vegetable oils to produce liquid biofuels has also been studied by Pioch et al. [77]. Among these techniques, transesterification seems to be the best as the physical characteristics of fatty acid esters produced by transesterification are very close to those of diesel and the process is also relatively simple.

## 4.2 TRANSESTERIFICATION

Animal and plant fats and oils are typically made of triglycerides which are esters of free fatty acids (FFAs) with the trihydric alcohol (glycerol). In organic chemistry, transesterification is the process in which the alcohol group of an ester is substituted by another alcohol. The transesterification reactions find its application in many industrial processes, e.g. a large number of acrylic acid derivatives are produced by transesterification of methyl acrylate with different alcohols in the presence of acid catalysts. Production of

PET (polyethylneterephthalate) involves transesterification with ethylene glycol in presence of zinc acetate as catalyst.

## 4.3 TRANSESTERIFICATION OF VEGETABLE OIL

In transesterification of vegetable oils a triglyceride (fat/oil) reacts with three molecules of alcohol in the presence of catalyst to form a mixture of fatty acid alkyl esters and glycerol [78, 79]. Commonly, ethanol or methanol is used. The overall transesterification reaction [79, 80] is the consequence of the following three consecutive reactions in which di- and mono-glycerides are formed as intermediates.

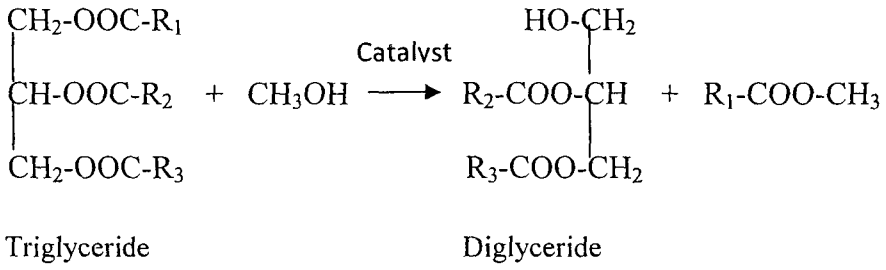


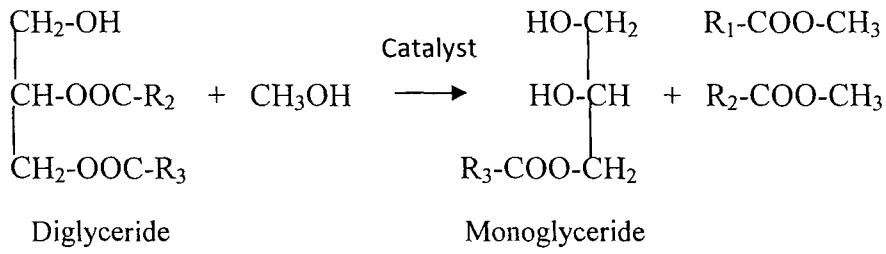


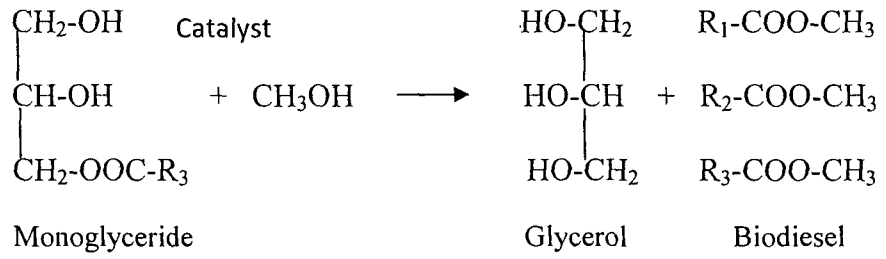


Theoretically, the transesterification reaction is an equilibrium reaction in which excess alcohol is required to shift the reaction equilibrium to the right side and produce more methyl esters as the proposed product. A catalyst is usually used to improve the reaction rate and yield. The overall chemical reaction of the transesterification process is:

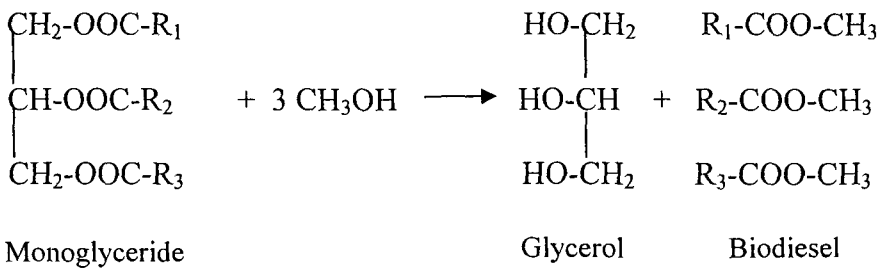


Catalytic transesterification processes are usually of the following types.

a. Direct Acid Catalyzed transesterification of the oil with methanol.

b. Base Catalyzed transesterification of oil with alcohol

c. Two step acid-base Catalyzed transesterification

d. Enzyme Catalyzed transesterification

The most important variables that influence the transesterification reaction are:
(i) reaction temperature (ii) reactant ratio (molar ratio of alcohol to vegetable oil) (iii) type of catalyst (iv) mixing intensity (v) purity of reactants (vi) reaction time (vii) presence of moisture and FFAs.

### 4.3.1 Acid-catalyzed processes

The transesterification process is catalyzed by acids, preferably by sulfonic and sulfuric acids. These catalysts give very high yields in alkyl esters, but the reactions are slow and requires more than 3 hour to reach complete conversion at temperature above 100° C [79]. The molar ratio of alcohol to vegetable oil is one of the main factors that influence the transesterification. An excess of alcohol favors the formation of the products. On the other hand, an excessive amount of alcohol makes the recovery of the glycerol difficult, so that the ideal alcohol to oil ratio has to be established empirically, considering each individual process. Acid catalytic transesterification of vegetable oils was carried out in several studies [81-84]

### 4.3.2 Base (alkaline) catalyzed processes

The majority of the alkyl esters are produced nowadays with the base catalyzed reaction because the base catalyzed transesterification reaction proceeds faster than the acid catalyzed reaction. Among all the processes, it is considered to be the most economical requiring low temperatures and pressures provided the raw oil is low in moisture and FFAs. It requires temperature of around 60-65°C and gives very high yields (about 98%) with minimal side reactions. Undesirable side reaction (saponification) reduces the yields of ester

making recovery of glycerol difficult due to formation of emulsions. Due to these reasons and also due to the fact that bases are less corrosive than acids, base catalyzed transesterification processes are gaining importance in industrial applications. Applications of base catalyzed transesterification of vegetable oils in biodiesel production are found in several studies [18, 85-88].

### 4.3.3 Two step acid base esterification

Canakci and Van [83] found that alkaline transesterification would not occur successfully if the FFA content in the oil is above 3%. Ramadhas et al. [13] also found from their analysis that the base catalyzed transesterification process is not suitable to produce esters from unrefined rubber seed oil and developed a two-step transesterification process for producing biodiesel from crude rubber seed oil. The reaction was carried out at the temperature ranges between 40° C and 50° C with continuous stirring. The two steps involved are:

(i) Acid-esterification: Alcohol to vegetable oil molar ratio of 6:1 and 0.5% sulfuric acid (by volume) is used in acid esterification process. The purified products of this first step are used as triglycerides for the second step.

(ii) Base-esterification: Alcohol to vegetable oil molar ratio of 9:1 and 1% sodium hydroxide (by weight) is used in the second step and the maximum yield is achieved. The products are allowed to separate into two layers; the upper layer which is the biodiesel is purified to remove the impurities.

A two step 'acid–base' process was also followed to produce biodiesel from crude Mahua oil in a laboratory scale processor [14].

### 4.3.4 Enzyme catalyzed processes

Results of enzyme-catalyzed transesterification have also been reported in article [89], although these processes are not yet commercially developed. The common aspects of these studies consist in optimizing the reaction conditions (solvent, temperature, pH, type of microorganism which generates the enzyme etc.) in order to establish suitable characteristics for an industrial application. However, the reaction yields as well as the reaction times are still unfavorable compared to the base-catalyzed reaction systems [90].

### 4.3.5 Non-catalytic supercritical transesterification

The transesterification of triglycerides by supercritical methanol, ethanol, propanol and butanol has proved to be the most promising process [91]. A non-catalytic biodiesel production with supercritical alcohol allows a simple process with high yield because of simultaneous transesterification of triglycerides and methyl esterification of fatty acids [92]. At subcritical state of alcohol, reaction rate is very low and gradually increases as either pressure or temperature rises. Increasing the reaction temperature, especially to supercritical conditions, had a favorable influence on the yield of ester conversion [93-97]. Another major advantage with this method is that the reaction time is very less compared to catalytic transesterification method. In the conventional transesterification, FFA and water always produce negative effects since they cause soap formation, consumes catalyst and reduces catalyst effectiveness which ultimately reduces the yield. However in a non catalytic supercritical method, these have no effect on the yield of ester, 98% ester conversion is observed irrespective of the amount of FFA and water present in the oil [91].

For the present study biodiesel was produced by following a two step acid base transesterification process. Details about the source of biodiesel and its production methodology have been discussed in the following sections.

## 4.4 BIODIESEL FOR THE PRESENT STUDY

### 4.4.1 Selection of oil seeds

There is variety of indigenous oil seeds bearing plant in the forests of North East India. For the present study we selected Koroch (Pongamia Glabra Vent.) seed oil. *Pongamia glabra* vent. trees are found in abundance in this region and is a non edible source of biodiesel containing high percentages of oil. It is a middle size tree with spreading branches. These trees are available in many areas of Assam, Nagaland and Meghalaya. A fully matured tree yields 20-50 kg of seeds per year and the oil content of the seeds varies from 30-35%.

### 4.4.2 Extraction of oil from Koroch seed

About 30 kg of the Koroch seeds were collected from the forest areas of Darrang district, Assam, India in the month of March, 2009 and these were shelled and dried for two days. The dried seeds were then crushed in an oil expeller to extract oils from it. About 5

### 4.4.3 Titration of oil

Titration was done in order to determine the FFA content in the oil. Following are the steps involved in the tritration procedure.

(i) The first step is to prepare an N/10 solution of NaOH in water. This is prepared by adding 4 grams of fresh NaOH in one litre of distilled water in one litre standard flask.

(ii) 25 ml of this N/10 NaOH solution is taken in a clean burette.

(iii) In a 250 ml conical flask, 50 ml of isopropyl alcohol (Rectified spirit) is taken.

(iv) Few drops of N/10 NaOH solution are added to the isopropyl alcohol in the conical flask and this is shaken well.

(v) 10 grams of raw seed oil is then added to the above conical flask and again this is well shaken.

(vi) The mixture in the conical flask is heated to about 50-60°C. and then shaken again and allowed to cool.

(vii) Then 2-3 drops of Phenolphthalein indicator is added to the mixture in the conical flask.

(viii) Next is the titration of this solution in the conical flask with the N/10 NaOH solution in the burette shaking it vigorously until a faint pink colour is obtained. This pink colour should persist for at least one minute. The burrete reading is then noted down.

The following formula was used to calculate % of FFA present in the oil.

$$\%FFA = \frac{28.2 \times Normality\ of\ NaOH\ Solution \times Titrate\ Value}{Weight\ of\ the\ oil}$$

Titrated value is the ml of NaOH consumed during titration. The FFA content of Koroch seed oil was found to be 18.78%. Adequate measures were taken during transesterification process to take care of higher level of FFA content of oil.

### 4.4.4 Production of biodiesel

Since the FFA content in Koroch seed oil was relatively high, biodiesel was produced using a two step acid base esterification process. Firstly, the acid pretreatment followed by main base-transesterification reaction using methanol as reagent and $H_2SO_4$ and NaOH as catalysts for acid and base reactions, respectively. Details of the production process are outlined below.

**The set up**

The production was carried out in a 2 litre capacity glass reactor vessel as shown in the Fig. 4.1. The reactor is basically a three-neck flask equipped with a magnetic stirrer and a condenser for recovering the evaporated methanol. The centre neck was used for connecting the reflux condenser with the water pipe line. The other two necks are there, one for putting the thermometer and the other for adding the mixture of methanol and sodium hydroxide. The set up also had a provision for speed adjustment for the stirrer which is adjusted at 200 RPM for homogeneous heating of the oil. The reactor vessel was placed over a heater. There is a thermostat which is a part of the heater and this is used for maintaining temperature of the reactants at the desired level.

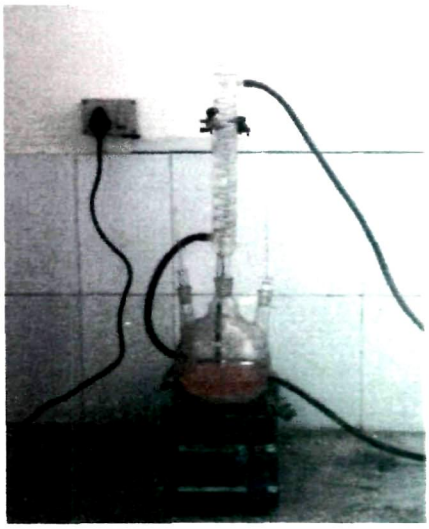

Fig. 4.1: Reactor vessel for transesterification

**Procedure**

Two steps involved in transesterification process of Koroch seed oil are described below:
(i) Acid catalyzed esterification: Crude Koroch seed oil (500 ml) was heated to 60°C in the glass vessel. 150 ml of methanol (in 1: 6 molar ratios) was mixed with 3ml of $H_2SO_4$ and the mixture was added to the heated Koroch seed oil. The reaction was continued for 1 hour and as soon as the reaction time was over, the mixture was placed in a separator funnel and allowed to cool and settle for 2 hours. Two distinct layers were observed. Methanol, water and $H_2SO_4$ rise to the top forming a black layer at the top while bottom layer is oil requiring further treatment. The % of FFA content of bottom layer oil was measured and found as 6.82%. This oil was further treated to bring down the level of FFA of the bottom layer to

acceptable level (below 3%). Finally, the oil with 2.7% FFA was used as triglycerides for the second step.

(ii) Base catalyzed esterification: The acid treated oil was transesterified using NaOH as catalyst. The oil was heated to 63°C and the mixture of methanol (150 ml) and NaOH (4 gm), called methoxide, was added for the reaction to occur continuously for 2 hours. After the reaction was over, the mixture was put in a separating funnel to cool and settle for 2 hours. The glycerol, which formed as a result of reaction, got settled at the bottom and was separated. The biodiesel (methyl ester) thus produced was transferred to the reactor vessel for recovery of methanol by maintaining the temperature at about 70°C. Finally, it was water washed to remove the traces of methanol and NaOH from it and dried to remove the moisture content from the biodiesel.

### 4.4.5 Preparation of biodiesel blends

The pure biodiesel thus produced from Koroch seed oil was mixed with commercial diesel procured from Numaligarh Refinery Limited (NRL), Assam. Four levels of blending were prepared while mixing the biodiesel with diesel in various proportions as follows.

B10: 10% (vol.) biodiesel + 90% (vol.) NRL diesel

B20: 20% (vol.) biodiesel + 80% (vol.) NRL diesel

B30: 30% (vol.) biodiesel + 70% (vol.) NRL diesel

B40: 40% (vol.) biodiesel + 60% (vol.) NRL diesel

The properties of these blending as well as NRL diesel were determined and used as fuels for experimental investigations of engine performance, fuel combustion and emissions characteristics.

### 4.4.6 Determination of fuel properties of the blends

The fuel properties are evaluated at the quality and control laboratory of NRL as per the ASTM standards and these are presented in Table 4.1.

The fatty acid composition, fuel properties of raw Koroch seed oil, refined biodiesel obtained from Koroch seed oil including the various blending up to 50% with diesel were also evaluated and reported in [98]. Slight variation in the properties of the blends has been observed. The properties which are reported in the present study show slight improvement in

Table 4.1: Properties of NRL diesel and the KSOME blends

| Property | NRL diesel | B10 | B20 | B30 | B40 |
|---|---|---|---|---|---|
| Density at 15°C (g/cc) | 0.846 | 0.8500 | 0.8548 | 0.8594 | 0.8661 |
| Kinematic viscosity at 40°C (cSt) | 2.34 | 2.64 | 2.84 | 3.07 | 3.28 |
| Higher heating value (kJ/ kg) | 45553.0 | 45489.9 | 45418.1 | 45348.9 | 45247.4 |
| Cetane Index | 46.60 | 46.34 | 46.50 | 46.34 | 45.39 |
| Flash point (°C) | 46 | 47 | 49 | 53 | 55 |
| Pour point (°C) | +3 | -3 | 0 | +3 | +6 |
| Sulphur content (ppm) | 489 | 440 | 390 | 302 | 274 |
| IBP/FBP (°C) | 147/372 | 148/371 | 148/368 | 149/368 | 149/368 |

terms of viscosity and higher heating value of the blends. These are relative in the sense that comparison is made with the property of diesel which varies from time to time as the refinery producing these petroleum fuels is always engaged in improving its quality. e.g., the kinematic viscosity of NRL diesel has been reported as 2.781 cSt. in [98] as opposed to 2.34 cSt. in the present case. Similarly the higher heating value of NRL diesel was mentioned as 45013 kJ/kg in the report, however for the present study it is found to be equal to 45553 kJ/kg.

It was also observed that the density and kinematic viscosity of the KSOME blends increase with increasing proportion of biodiesel in the blend. On the other hand, the calorific values of the blends were lesser than that of diesel and it decreased with increase in percentage of biodiesel in the blends. Density is a fuel property which influences the fuel consumption characteristics of an engine. Viscosity plays a major rule in the fuel injection system. The changes in fuel viscosity and consequently in bulk modulus affect the speed of sound and are responsible for the difference of injection timing. A higher bulk modulus, caused by increasing the content of biodiesel, leads to more rapid pressure wave propagation from the pump to the nozzle and an earlier needle lift. The higher viscosity of fuel leads to reduced fuel leakage during injection, faster

evolution of pressure and thus injection timing is advanced [99]. Besides, it also leads to poor atomization of the fuel spray leading to poor combustion.

Calorific value of a fuel is the measure of fuel energy input. Higher the calorific value more will be the output for a given amount of fuel consumed. Lower fuel calorific value in case of the blends might result in high rate of fuel consumption during engine operation at a given load producing a given power output.

The flash point is the temperature to which the fuel must be heated such that the mixture of vapor and air above the fuel can be ignited. As reported in literature, the flash point of neat biodiesel is typically greater than 90°C. Fuel with higher flash point is considered as non-hazardous from storage and fire-hazard point of view. Neat Biodiesel is thus safer to storage than conventional diesel. The flash points of the KSOME blends were higher and it increased with addition of biodiesel in the blend.

Presence of sulphur compounds in fuel produces mainly SOx. Sulfur oxides, primarily emitted as sulfur dioxide ($SO_2$), are formed through oxidation of sulfur in fuel during combustion. A small fraction of the $SO_2$ in diesel exhaust is oxidized to sulfur trioxide ($SO_3$). $SO_3$ reacts easily with water to form sulfuric acid ($H_2SO_4$) and sulfate particulate matter. In the diesel exhaust stream, sulfate aerosol is an important initiator of particle formation. Sulfur dioxide is a respiratory irritant and it aggravates existing cardiopulmonary conditions and contributes to respiratory illness and trouble breathing. Sulfuric acid significantly contributes to widespread ecosystem damage. Sulfate particulate matter is a significant health concern as well as one of the primary pollutants responsible for impaired visibility. Sulphur compound are also responsible for corrosion of engine parts and formation of engine deposits. Reducing sulphur content of petroleum based fuel has been a big challenge for the industries as it involves costly processing equipment and high operational cost, therefore the blending of diesel with biodiesel can be a good choice for lowering sulphur content of diesel in order to reduce harmful emissions. Under the Euro II and III norms, the permissible sulphur content is 500 parts per million (ppm) and 350 ppm respectively. With the implementation of Euro IV norms, the permissible sulphur content has come down to 50 ppm. The sulphur content as can be seen from the Table 4.1 reduces significantly in case of the blends.

Cetane index is a tool for estimating cetane number where a test engine is not available for determining this property. It may be employed for approximating cetane number (CN) where the quantity of sample is too small for an engine rating. Diesel engine operation is primarily related to actual CN and cetane index is simply an estimation of the

base CN. The CN may be equal or greater than the Cetane index depending on the amount of additives used. CN of a fuel is the measure of its ignition delay with higher CN indicating a shorter delay period and is one of the prime indicators of the quality of diesel engine fuel. The longer the fatty acid carbon chains and the more saturated the molecules, the higher the CN. The higher the CN, easier the fuel ignites when it is injected into the engine. In the Ref. [98], the CN of the KSOME blends B10, B20, B30 and B40 have been reported as 46.8, 47.6, 48.8 and 49.5, respectively against a CN of 46 of NRL diesel, which clearly indicates the increase in CN with addition of biodiesel in fuel blends. However, the Cetane index of the KSOME blends in the present study was found to be slightly lesser compared to that of diesel fuel.

Two important parameters for low temperature applications of a fuel are cloud point and pour point. The cloud point is the temperature at which the wax present in the fuel first becomes visible when the fuel is cooled. The pour point is the lowest temperature at which the amount of wax out of solution is sufficient to gel the fuel, thus it is the lowest temperature at which the fuel can flow under certain prescribed conditions. Only the pour points have been determined for the present study. It is seen that up to the 30% blending (B30), the blends have pour point close to that of diesel but in case of the blend B40, the pour point was found to be comparatively high. In the thesis [98] also, the pour points of diesel, B10, B20, B30, B40 were all reported to be 0°C while it was 3°C for B50.

As regards the boiling range of the biodiesel blends, the initial boiling point (IBP) and final boiling point (FBP) were determined from distillation analysis. The detailed distillation characteristics of KSOME were presented in [98]. Pure KSOME has a narrow boiling range compared to diesel which implies shortage of lower boiling point hydrocarbons in it. But when it is blended with diesel it shows more or less the same characteristics of diesel fuel as evident from the present results and results in [98]. It is also observed from Table 4.1 that the IBP values of the blends are slightly higher compared to that of NRL diesel while the FBPs are slightly lower. Slightly higher IBP in case of the blends may be due to molecular interaction of the diesel and biodiesel molecules [98]. FBP of unrefined KSOME is reported to be high, but it reduces to the level of diesel when it is further refined by distillation at reduced pressure. The presence of high boiling point components has an effect on the formation of solid combustion deposit [67]. The distillation (volatility) characteristics of hydrocarbon fuel have its implications on the optimum engine performance and safety because it is volatility that measures of the tendency of a liquid fuel to produce potentially explosive vapour and proper air-fuel mixture for combustion.

# CHAPTER 5

# EXPERIMENTATION FOR ENGINE PERFORMANCE AND MODEL VALIDATION

## 5.1 INTRODUCTION

In Chapter 3, formulation of mathematical models using single zone approach for simulating the diesel engine processes was presented. Implementation of such models requires identification of key model parameters and their determination through experiments. For meaningful application of model results it is essential to have validation experiments for improving the reliability and confidence regarding the model predictions, while keeping in mind that the model results are always to be used with caution. The present Chapter focuses on the experimentation for engine performance taking different blends of biodiesel as fuel. Moreover, determination of parameter values for subsequent use in the simulation model and generation of data for model validation are also described in this Chapter.

The following sections describe the computerized test engine set up used for experimentation along with the measurement system and various sensors used for pressure, temperature, and fuel and air flow rate measurement. Furthermore, the results concerning engine performance, fuel combustion and emission characteristics with diesel and biodiesel blends have been discussed and analyzed. Post processing of the raw experimental cylinder pressure data is also discussed separately.

## 5.2 TEST ENGINE SET UP

Tests were performed in a single-cylinder; four-stroke, naturally aspirated, DI diesel engine, and its specifications are given in Table 5.1. The test engine is provided with necessary instrumentation for combustion pressure, fuel pressure and crank angle (CA) measurements. The in-cylinder and the fuel pressure are sensed by two piezo sensors. One sensor was installed in the engine cylinder head to sense combustion pressure and the other in the fuel line to sense the fuel pressure. Signals from these pressure transducers are fed to a charge amplifier. A high precision crank angle (CA) encoder is used to give signals for TDC and the CA. The signals from the charge amplifier and CA encoder are supplied to a data acquisition system (DAQ) which is interfaced through engine indicator to a computer for obtaining pressure crank angle (p- $\theta$ ) diagram. There are also provisions made in set up for interfacing airflow, fuel flow, temperatures, and load measurement. A differential pressure

transducer is used to measure air flow rate. The engine is coupled with an eddy current dynamometer which is used to control the engine torque through computer. Thermocouples are used to measure different temperatures, such as exhaust temperature, coolant temperature, and inlet air temperature. Two rotameters are provided for engine cooling water and calorimeter water flow measurement. A Lab view based Engine Performance Analysis software package is provided for on line performance evaluation. The engine is operated at various loads for all the fuel tested. The test engine set up is shown in Fig. 5.1.

Table 5.1: Engine specifications

| | |
|---|---|
| Make & Model | Kirloskar –TV1 |
| Rated power | 3.5 kW @ 1500 rpm |
| Type of Engine | Single cylinder, four stroke, DI |
| Compression ratio (CR) | 12-18 |
| Type of ignition | Compression Ignition |
| IV Opening | 4.5° before TDC |
| IV Closing | 35.5° after BDC |
| EV Opening | 35.5° before BDC |
| EV Closing | 4.5° after TDC |
| Bore and Stroke | 87.5mm and 110mm |
| Nozzle opening pressure | 200-220 bar |
| Cooling Medium | Water cooled |

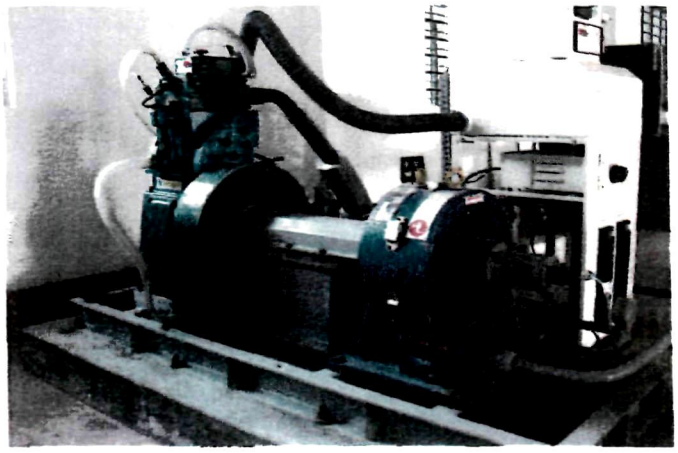

Fig. 5.1: Test engine set up

## 5.3 INSTRUMENTATION AND MEASUREMENTS

Detail information of the engine test instrumentation is shown in Table 5.2.

Table 5.2: Instrumentation list for the test set up

| Signal | Description |
|---|---|
| Pressure sensor<br>• In cylinder<br>• Diesel pressure | Piezo sensor<br>Make PCB Piezotronics<br>Model HSM111A22, Range 5000 psi<br>Diaphragm stainless steel type and hermetic sealed. |
| Temperature sensor<br>• Engine inlet water temperature<br>• Engine outlet water temperature<br>• Calorimeter inlet water temperature<br>• Calorimeter outlet water temperature<br>• Exhaust gas to calorimeter inlet temp.<br>• Exhaust gas from calorimeter outlet temp. | Type RTD, PT100, Range 0–100 deg C, Output 4–20 mA.<br><br>Thermocouple, K type, Range 0–1200 deg C, Output 4–20 mA. |
| Air flow transmitter | Pressure transmitter, Range (-) 250 mm WC |
| Fuel flow transmitter | DP transmitter, Range 0-500 mm WC |
| CA (rotary) encoder | Resolution 1 deg, Speed 5500 RPM with TDC pulse. |
| Load sensor | Load cell, strain gauge( S beam) type , Make Sensotronics, Capacity: 0-50kg |

### 1) Pressure measurement

**In-cylinder pressure and fuel pressure:** The in-cylinder pressure and the diesel pressure are sensed by piezo sensors. These two dynamic pressure sensors with a built in amplifier in each were installed, one in the engine cylinder head to sense combustion pressure and the other in the fuel line to sense diesel pressure. These sensors are supplied with a 2 to 20 mA constant current at +20 to +30 VDC through a current – regulating diode or equivalent circuit. One important characteristic of these signal conditioners is that they have adjustable current features which allow them for a choice of input currents from 2 to 20 mA. Lower current ranges are generally chosen for lowest noise (best resolution). A pressure sensor usually generates an electrical signal in terms of an output voltage related to the

pressure imposed which is then converted to its corresponding physical pressure using proper calibration equation. The dynamic voltage signal from these piezo sensors are scanned with respect to CA signals received from rotary encoder fitted on the engine crankshaft. Both signals are simultaneously scanned by an engine indicator (electronic unit) and communicated to computer which draws the pressure crank angle diagram.

**2) Temperature measurement**

Temperatures of water at inlet to the engine and also at outlet from the engine were measured for calculating the heat lost in cooling the engine with water. The engine set up also consists of a Calorimeter which is basically a parallel flow pipe in pipe type heat exchanger with water flowing through one pipe and exhaust gas through the other. This was provided to find the specific heat of the exhaust gas from a heat balance equation. Water temperatures at calorimeter inlet and outlet were also measured. These were measured using four RTD type temperature sensors. These sensors have platinum resistances which change with temperature. This resistor is connected to the temperature transmitter and proportional signal is scanned by the computer through the data acquisition system. Two K type thermocouples were also installed at the exhaust inlet and outlet of the calorimeter to measure the temperatures of reference. These thermocouples use junction of dissimilar metal which generate voltage proportional to temperature. These are also connected to transmitters.

**3) Measurement of flow rate**

**(A) Air flow rate:** The air consumption in an IC engine can be measured by air box method. In IC engines, as the air flow is pulsating, for satisfactory measurement of air consumption an air tight chamber (air box) of suitable volume is fitted with sharp edged orifice. The orifice is located away from the suction connection to the engine and engine suction causes air flow through the orifice. The volume of the air box is made sufficiently large compared to the swept volume of the cylinder for obtaining steady flow. Also the intermittent suction of the engine will not affect the air pressure in the box and the pressure in the box remains constant. The differential pressure across the orifice is measured with the help of manometer and a pressure transmitter which is installed on the air box with the orifice meter. The air flow rate is calculated using Equation 5.1.

$$\text{Air flow rate} = C_d \times \frac{\pi D^2}{4} \sqrt{2gh \frac{\rho_{water}}{\rho_{air}}} \times \rho_{air} \times 3600 \qquad (5.1)$$

where, $C_d$ = Orifice discharge coefficient
$D$ = Orifice diameter in m
$g$ = Acceleration due to gravity
$h$ = manometer reading (m of water)
$\rho_{water}$ = Water density (kg/m$^3$)
$\rho_{air}$ = Air density at working condition (kg/m$^3$)

**(B) Fuel flow rate:** The fuel consumed by an engine can be measured by methods such as (i) Volumetric method in which the fuel consumed by an engine is measured by determining the volume flow of the fuel in a given time interval (ii) Gravimetric method in which the time to consume a given weight of the fuel is measured. Alternately, differential pressure transmitters working on hydrostatic head principles can also be used for fuel consumption measurement. In the present engine set up, it is measured on the hydrostatic head basis. The fuel flow transmitter measures the hydrostatic head in the fuel measuring unit (Make: Apex Innovations, Model: FF0012) consisting of the glass burette. The difference between two signals in the interval of one minute is converted in to corresponding fuel flow rate.

**(C) Engine cooling water and Calorimeter water flow rate:** Two rotameters ( Make: Eureka, Model PG 5 and PG 6) having the ranges of 25-250 litres per hour (LPH) and 40-400 LPH are provided for calorimeter water and engine cooling water flow rate measurement respectively.

### 4) Measurement of Power

**(A) Brake power (BP):** Measurement of BP involves determination of torque and angular speed of the engine output shaft. The engine speed was measured using a rotary encoder. The engine torque was measured with the help of an eddy current dynamometer. It comprises basically a rotor mounted on a shaft which rotates within a casing supported in ball bearing. In the casing, two field coils (electromagnets) were connected in series. When these coils are supplied with a direct current (DC), a magnetic field is created in the casing across the air gap at either side of the rotor. When the rotor turns in this magnetic field, eddy currents are induced in the casing due to magnetic flux set up by the passage of field current in the electromagnets. These eddy currents oppose the rotor motion, thus loading the engine. These eddy currents are dissipated in producing heat and therefore it requires cooling. The rotational torque exerted on the casing was measured by a strain gauge load cell. The load was controlled by rotating the knob on dynamometer loading unit which actually regulates the current in the electromagnets. The dynamometer arm length (radial distance between

dynamometer centre and the load cell position) was known and the engine torque was measured multiplying the load with the dynamometer arm length.

**(B) Indicated power (IP):** The IP of an engine can be measured either from the indicator diagram or by Morse test in case of multi-cylinder engine. The method used for measuring engine IP in the present case was the indicator diagram method. In this method the pressure CA plot obtained as discussed above is converted into its corresponding pressure volume plots.

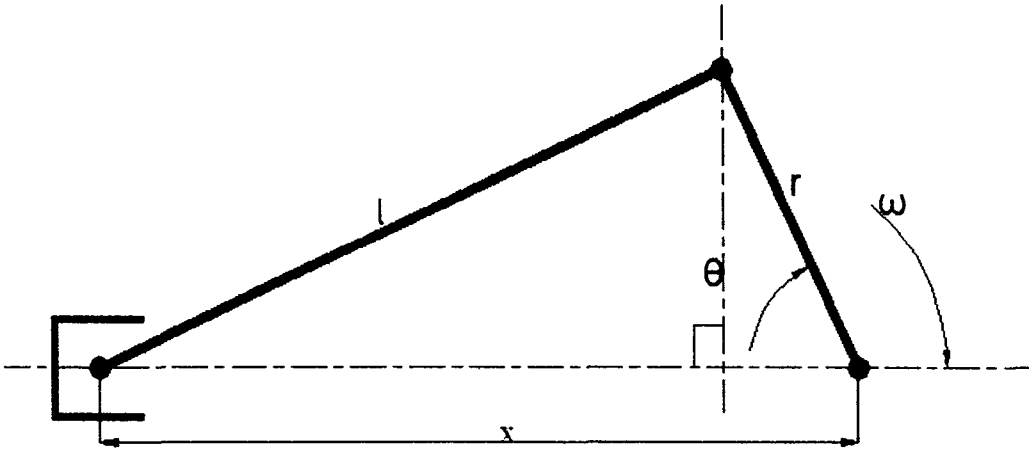


Fig. 5.2: Slider crank mechanism

The approximate position of piston pin end from the centre of crank circle is calculated as:

$$x = r\left[\cos\theta + \frac{l}{r}\left\{1 - \left(\frac{r}{2l}\right)^2 (1 - \cos 2\theta)\right\}\right] \tag{5.2}$$

Where $r$ =crankshaft throw and $l$ = connecting rod length.

Once x is calculated using the above equation, the term $(l + r - x)$ gives the distance traversed by piston from its top most position at any angle $\theta$. The instantaneous cylinder volume on CA basis is thus calculated from the equation given below.

$$V(\theta) = V_c + \frac{\pi D^2}{4}(l + r - x) \tag{5.3}$$

where, $V_c$ is the clearance volume and $D$ is the cylinder diameter.

The pressure volume plot is obtained from known values of instantaneous cylinder pressure and volume. The area of the pressure volume plot (indicator diagram) is found out by algebraic integration of $pdV$ over the whole cycle, which is then multiplied with the engine RPM to calculate IP.

**5) Crank angle encoder**

A CA (rotary) encoder as shown in Fig. 5.3 is fitted on the dynamometer and is connected to the piezo powering unit through cable. Number of pulses received from CA encoder in one revolution is 360.

Fig. 5.3: Crank angle encoder

The function of the encoder is to locate the top dead center of the firing cylinder to calculate CA and provide the trigger timing for DAQ system. This optical type rotary encoder was aligned to the TDC by rotating the flywheel slowly in clockwise direction (viewed from dynamometer end) till the CA mark on the flywheel matches with the reference pointer provided on the engine body. This is confirmed by glowing of the TDC light on the piezo powering unit. There are two types of signal available from the encoder: the TDC signal for every rotation (marker pulse) required for speed measurement and the CA signal. Both of these signals are necessary which are collected and then processed through analog to digital converter (ADC) in the computer, where the data processing by a Lab view program was performed. Improper TDC adjustment leads to faulty pressure CA diagram resulting in faulty IP.

**6) Data acquisition system (DAQ)**

National Instrument hardware was used for all data acquisition components. It is a 16 channel analog input card which is connected to a PC with USB port. The system uses a SCXI signal conditioning box for the high frequency signals such as CA based cylinder pressure. This SCXI interface box protects the noise from ground problem, and amplifies the signals. Then, all the signals come into the computer through the ADC. The ADC card uses 16 bit resolution with a maximum sampling rate of 250 kSample/sec. The sampling rate is influenced by the engine speed, the CA resolution which is 1° CA in the present case and the

number of channels enabled. The Lab view based performance software scans the signals received from all the channels and uses for display and analysis.

## 5.4 ENGINE TEST PROCEDURE AND IDENTIFICATION OF OPTIMUM CR

The engine was first made to run by supplying commercial grade diesel fuel to the engine and the CR was varied from 13 to 18 one by one. This is done first by slightly loosening the Allen bolts which are provided for clamping the tilting block of the engine. There is a CR adjuster with a lock nut in it which can be rotated by loosening the lock nut to set it for the desired CR. At each CR, the load was varied from no load (0 Kg) to over load (12 Kg) in five steps. At each load, the engine speed was measured by the CA encoder; cylinder pressure, fuel injection pressure were measured by the piezo electric sensors. When the load is changed operating the loading knob in the dynamometer loading unit, the fuel flow rate also changes while keeping the engine speed in a very narrow range. The average speed varies slightly from 1616 rpm at no load to 1535 rpm at full load for all the fuel operations. The average engine speeds at 25%, 50% and 75% of full engine loads were found to be 1587, 1569 and 1554 rpm respectively. The average engine torque at various loads ( no load to full load ) were 0.09, 5.44, 10.89, 16.36 and 21.78 Nm respectively with corresponding average BPs being equal to 0.01 kW, 0.91 kW,1.79 kW, 2.66 kW, 3.5 kW. The fuel flow rate is controlled by a governor integrally fitted to the engine. The fuel flow and the air flow rates were measured by the flow transducers as described. The signals obtained from various sensors were fed to the engine indicator for storing the data and interfacing with computer. The stored data were analyzed by using the analysis software package. The engine test results at various CR and load will be discussed later in section 5.9.1. From the results, it was confirmed that the engine performed better at CR 18 and therefore the engine tests for NRL diesel, KSOME and its diesel blends were carried out at a fixed CR of 18 while varying the loads to the engine. For each fuel operation at a particular load, three test runs were performed under identical conditions to check for the repeatability of all the results. The repeatability of the results was found to be within an acceptable limit. The test results were then averaged and the average test results have been reported. In order to take care of the cycle to cycle variation, five cycles were considered and then it was averaged over the cycles. An exhaust gas analyzer was used to measure the concentration of CO, $CO_2$, HC, NOx and $O_2$ emissions. The gas analyzer calibrates automatically every time it is started and display the quantity of exhaust gases.

## 5.5 ENGINE TEST DATA TREATMENT

Accuracy of data acquired from a data acquisition system depends on factors such as resolution of ADC card, numbers of channels being logged, the sampling rate (samples/sec) and the amount of data collected. The in-cylinder pressure is one of the important signals while analyzing combustion inside the engine. The cylinder pressure signal is sometimes noisy. Therefore, this noisy signal needs to be rectified with appropriate methods such as filtering and smoothing algorithm. When a noisy signal is differentiated numerically by looking at the difference in successive values, then the results become very noisy. To mitigate this effect, smoothing of the test data is required before numerical differentiation. Satisfactory results can be obtained by employing higher order finite difference scheme. In this work, a fourth order central difference scheme was used as described by the following equation:

$$\frac{dp}{d\theta,i} = \frac{p_{i-2} - 8p_{i-1} + 8p_{i+1} - p_{i+2}}{12\Delta\theta} \tag{5.4}$$

This first order derivative is required while calculating the net heat release rate (NHRR). The following smoothing equation was applied twice for smoothing the raw cylinder pressure test data before carrying out the numerical differentiation.

$$p_i = \frac{p_{i-1} + 2p_i + p_{i+1}}{4} \tag{5.5}$$

The effect of smoothing on cylinder pressure data, peak cylinder pressure and NHRR can be observed from Fig. 5.4 to Fig. 5.9. Fig. 5.4 shows the raw cylinder pressure data consisting of noise near the peak pressure region. Fig. 5.5 and Fig. 5.6 show the consequence of applying equation (5.4) once and twice respectively to smooth the raw cylinder pressure data. It is seen that the noise present in the raw data have been mitigated and nearly the same peak pressure value as the raw data could be maintained. This is evident from Fig. 5.7 where all three categories of data are shown superimposed. Only a marginal decrease in the peak pressure value was observed. Therefore, a smoothing order of 2 will be used in this study in order to avoid any possible loss of information due to over-smoothing. Smoothing process loses information and the peak pressure may reduce in magnitude. It is observed that the smoothing process keeps the auto ignition point undistorted, which is an important aspect in diesel engine combustion. Moreover, the peak pressure value also remains unaffected.

Additionally, the noise generated during the compression and engine combustion process can be treated.

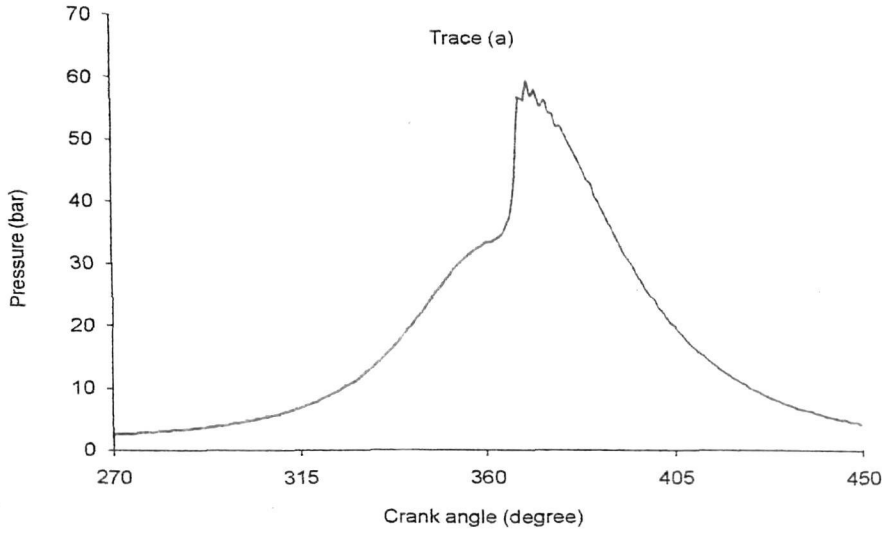


Fig. 5.4: Raw cylinder pressure data recorded every 1° CA from the engine set up at full load and CR 18

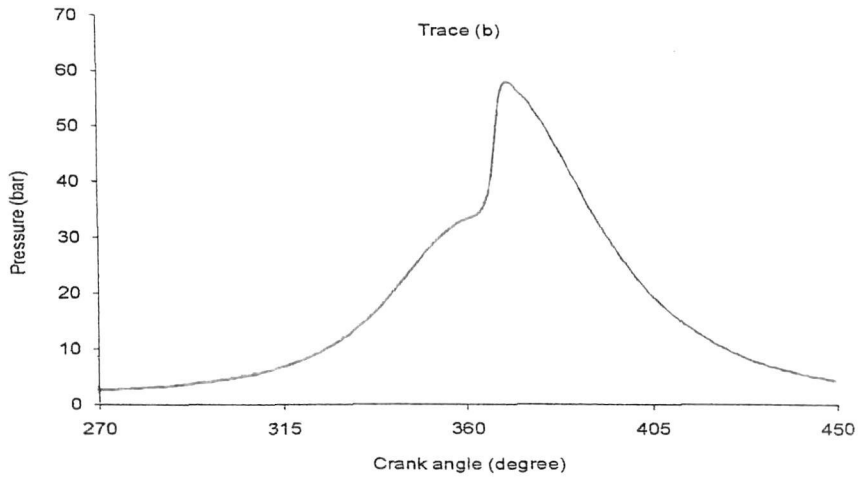


Fig. 5.5: Cylinder pressure data applying equation (5.4) once to smooth the trace

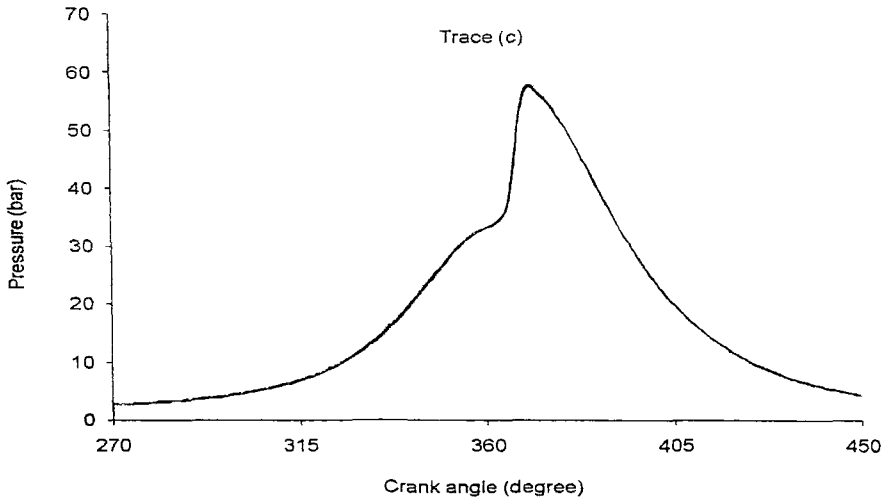


Fig. 5.6: Cylinder pressure data applying equation (5.4) twice to smooth the trace

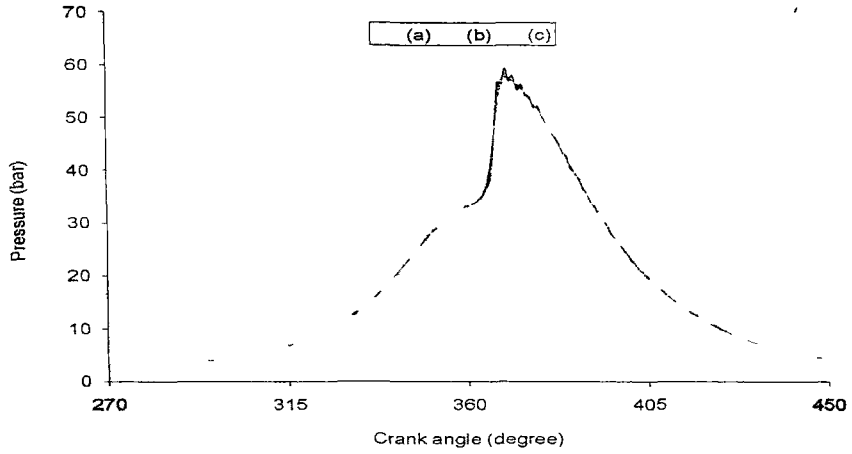


Fig. 5.7: Comparison of treated and untreated cylinder pressure data

The effect of smoothing the cylinder pressure data on the rate of pressure rise can be clearly seen from Fig. 5.8. The peak pressure rise rate reduces significantly and also the noise at the same time, which would have been present otherwise, had the numerical differentiation of pressure with respect CA been done without smoothing of the raw cylinder pressure data. Finally, the NHRR is found out using the treated cylinder pressure and the treated rate of pressure rise. The effect of smoothing on NHRR can be observed from Fig 5.9 (a). This has also been shown separately for the compression stroke, combustion process and the expansion stroke in Fig. 5.9 (b), Fig. 5.9 (c) and Fig. 5.9 (d), respectively for further clarity. As can be seen in Fig. 5.9 (a) and Fig. 5.9 (c), the peak value of raw net heat release rate data is decreased by smoothing. The peak net heat release rate is reduced by 34 %, the raw value is 143.81 J/CA whereas the filtered data reduces to 94.54 J/CA. However, the peak cylinder

pressure value does not change much due to smoothing. It is believed that this peak value is the real data, but the other values resulting from numerical calculation including differentiation is slightly affected by the processing.

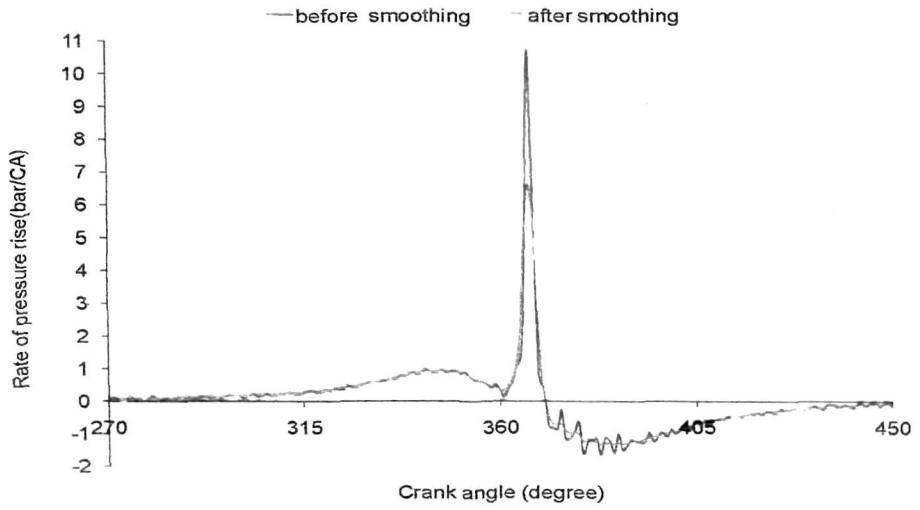


Fig. 5.8: Effect of smoothing on rate of pressure rise

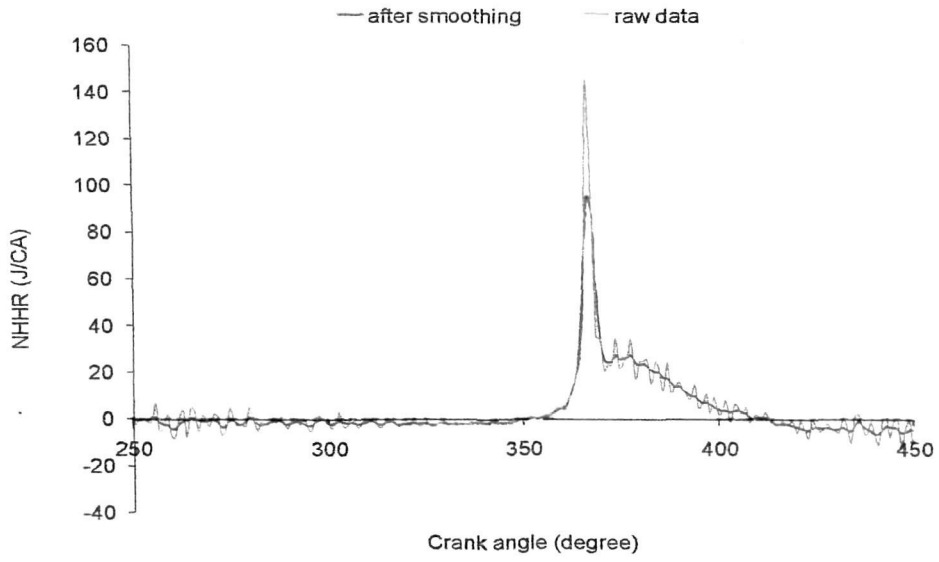


(a) Entire Plot

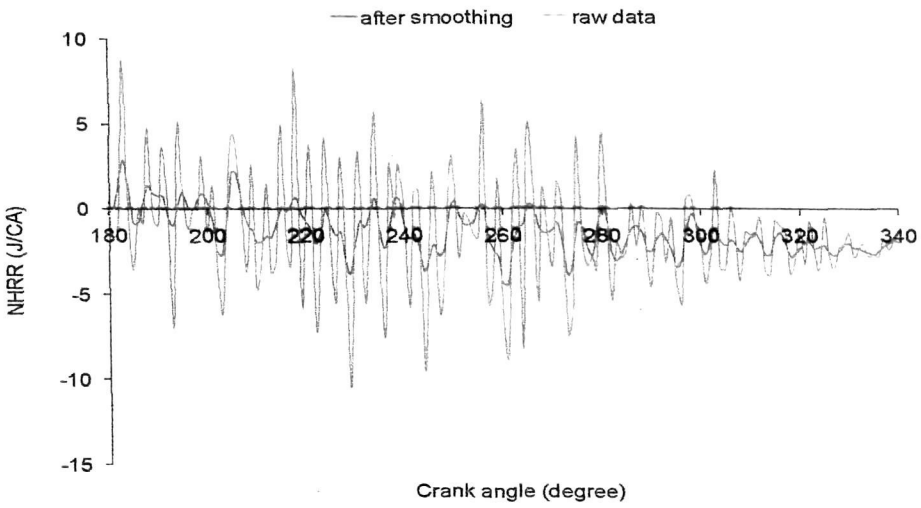


(b) Compression Stroke

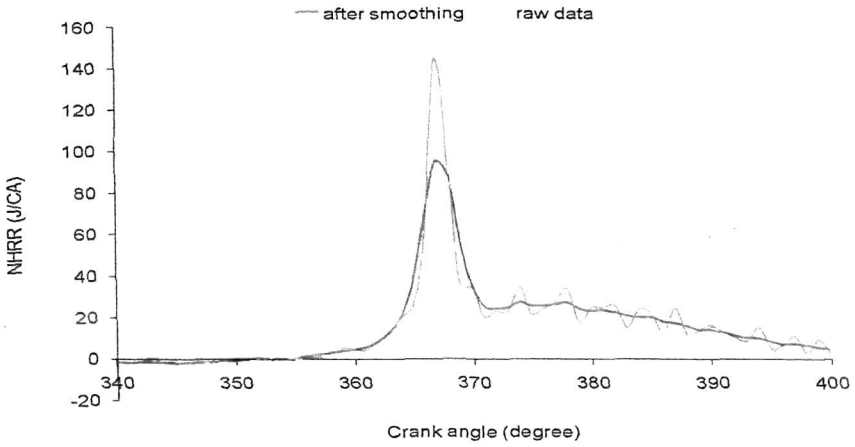


(c) During combustion

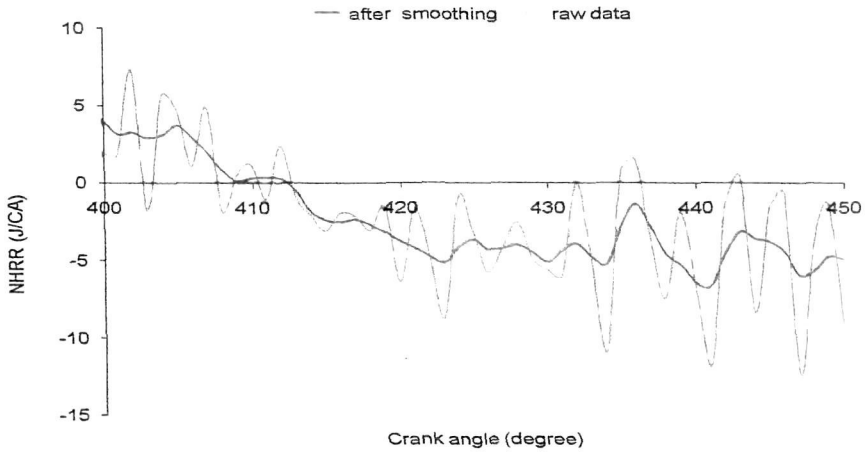


(d) Expansion stroke

Fig. 5.9: Effect of smoothing on NHRR

From the discussion so far, it can be summarized that the cylinder pressure data including the auto-ignition point is no longer distorted in terms of CA degree and the peak pressure is also approximately the same. Therefore, smoothing of the cylinder pressure data with the process described could be done. Especially the cylinder pressure data near the region of peak pressure is greatly improved in its shape while removing the noise present, as it can be seen in the Figs. 5.5 and 5.6. Also observed from Figs. 5.8 and 5.9 (c) that the ignition point seen in the raw data is also approximately the same after smoothing and this is the major advantage of this methodology. This process of smoothing the cylinder pressure test data will be applied to obtain the NHRR curves for other test cases including the different blending of diesel and biodiesel at various loads.

## 5.6 TDC ADJUSTMENT

As already stated, the rotary encoder apart from transmitting one pulse for each degree of CA also transmits one marker pulse for every rotation. Proper matching of the TDC position of the piston and marker pulse position of the encoder is necessary in order to get the reference for obtaining the $p$ - $\theta$ diagram. This can be checked by installing the CA encoder synchronously with engine crank shaft pulley without any phase shift. To ensure this, the CA coordinate is corrected with an offset CA and then the $p$ - $\theta$ diagram is checked for any phase shift. Provision is made to rotate the encoder body about its axis for this adjustment. Once proper adjustment is done, the encoder is clamped at its location on the mounting bracket. This adjustment is done when engine is not in running condition. Under running engine condition the correct TDC position needs to be found out by motoring the engine at the operating speed and matching the encoder marker pulse position with motoring peak pressure position. For SI engines, it is easy to simulate motoring by cutting off the spark. However, for CI engines by the time the fuel supply is cutoff, the speed drops, hence it is difficult to find out the motoring peak. However, from experience and proper judgment, the encoder needs to be adjusted for 2-3 degree before TDC. If the encoder is not installed correctly either in the clockwise or counter-clock wise direction, then it may lead to distortion of the $p$ - $\theta$ diagram. When the encoder is installed in a retarded direction, crossing of the p-V plot may occur near the TDC [44]. Therefore, the correct installation of the CA encoder is an important issue in so far as the phase shift and distortion of the $p$ - $\theta$ and p-V diagrams are concerned. Otherwise, it will result in faulty IP calculation as it depends on the p-V diagram.

## 5.7 DETERMINATION OF START OF INJECTION

Fuel injection timing has significant effect on the combustion characteristics and the exhaust emissions of the engine. Start of fuel injection is an important parameter which is influenced by the fuel properties such as viscosity and compressibility. Determination of the actual point of start of injection (SOI) is inferred from measurement of the fuel injection pressure profile and the needle opening pressure. The injection pressure profile is obtained by post processing of the dynamic signals sensed by a piezo sensor which is scanned with respect to CA signals received from the rotary encoder. The test engine set up uses a single acting cam operated plunger type fuel injection system. During the upward stroke of plunger, suction is created in plunger space and fuel is sucked in through the suction valve. During the downward stroke the fuel below the plunger is compressed, pressure builds up and when it exceeds the pressure required for needle opening, injection begins. The injector manufacturer specifies an approximate value of 210 bar with a tolerance band of $\pm 10$ bar for the nozzle opening pressure while carrying out the calibration test at static condition with reference to atmospheric pressure. However for the present study, since the fuel is injected dynamically into the cylinder at higher pressure, therefore a special procedure was adopted to determine the nozzle opening pressure for the injector. Figs. 5.10-5.13 show the injection line pressures for NRL diesel and the KSOME blends at various loads. SOI is usually taken as the time when the injector needle lifts off its seat. As no needle lift sensor was fitted to the injector, therefore the CA, at which the fuel pressure in the fuel line reached its maximum value followed by a sudden drop in pressure, was considered as the SOI.

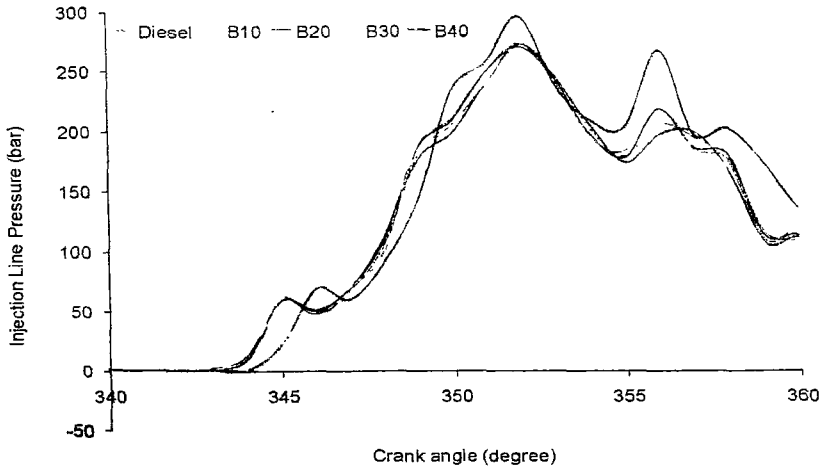


Fig. 5.10: Injection line pressure for the tested fuels at full load

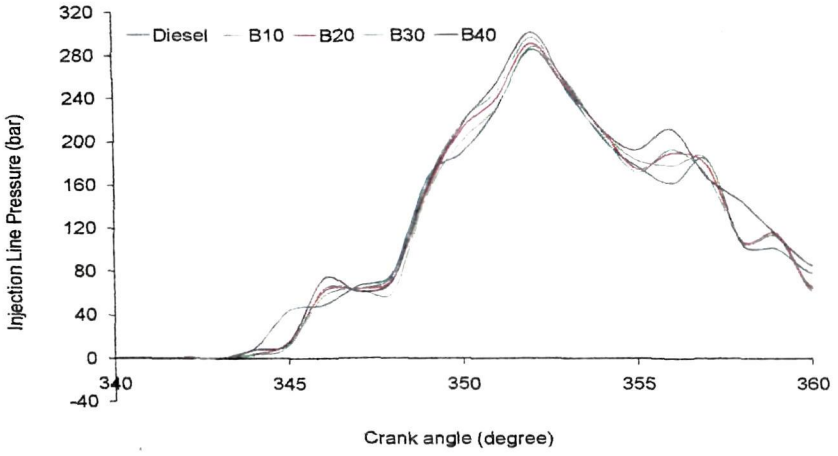


Fig. 5.11: Injection line pressure for the tested fuels at 75% of full load

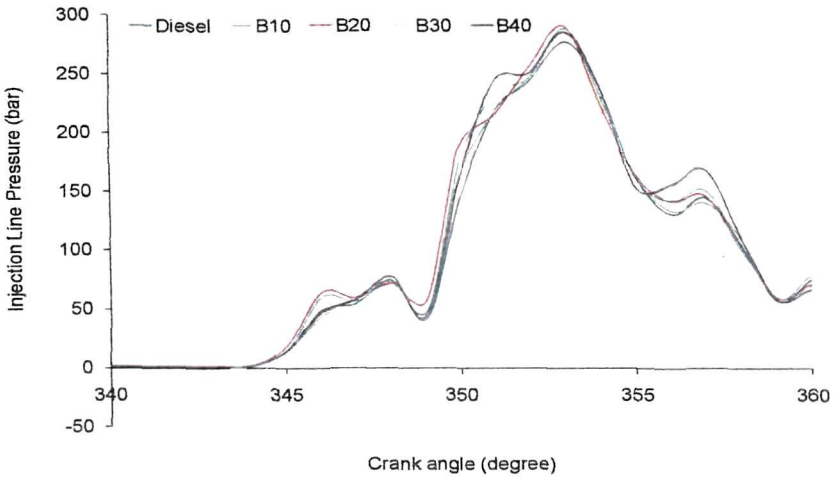


Fig. 5.12: Injection line pressure for the tested fuels at 50% of full load

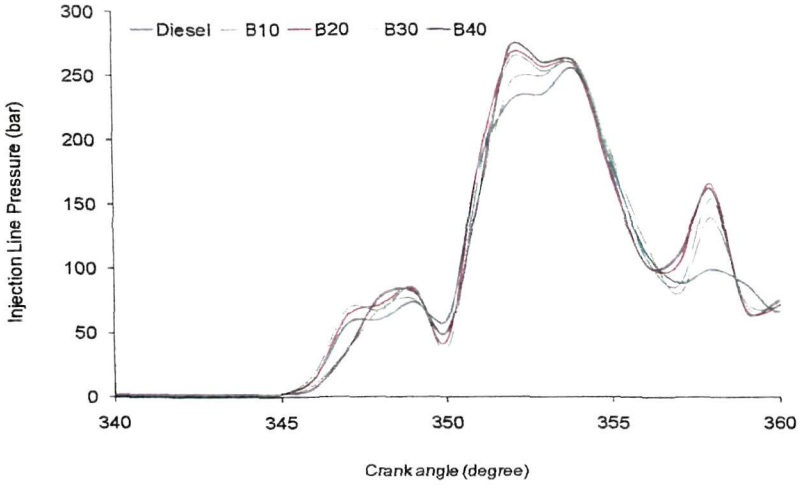


Fig. 5.13: Injection line pressure for the tested fuels at 25% of full load

It was observed that the injection line pressure changing trend for all the fuels was the same at all the loads. In case of the biodiesel blends, the peak fuel pressure at which the fuel is injected to the cylinder was more compared to the diesel peak pressure at all the loads. It could possibly be due to higher bulk modulus of the biodiesel blends. Biodiesel in general are viscous and when blended with diesel it reduces, but still it is slightly higher than that of pure diesel. The waviness in the injector pressure profile after the peak may be due to dribbling of the injector. This was observed more in case of the biodiesel blends. If contaminated fuel gets past the fuel filter, deposits formed due to evaporation of fuel droplets after an engine shuts off, clogs the fuel injector and skew the fuel spray pattern preventing the fuel from vaporizing completely. Sometimes such deposits also prevent the injector needle valve or the pintle from seating completely, so the injector dribbles fuel.

## 5.8 DETERMINATION OF START OF COMBUSTION

It is necessary to define the point of auto ignition for determination of ignition delay period and combustion duration. Identification of actual starting point of combustion in diesel engine is of crucial importance for credible analysis of in-cylinder pressure diagram. Proper definition of start of combustion (SOC) is still an unresolved issue of ignition study. Ignition criteria based on which SOC in diesel engines is normally identified include (i) rapid rise of cylinder pressure gradient[100], (ii) the light emission detected by a photocell [101], (iii) sudden temperature rise due to combustion, (iv) the combustion of a certain mass of fuel, and (v) the change of slope in the heat release rate profile [28, 102] . Out of all these techniques, the pressure-based techniques are more reliable than the light emission technique. More specifically Heywood [28] indicates that a pressure change is often detected before the luminosity detector has noted the appearance of a flame. Actually there exists no exact single point of the SOC if one takes into consideration the effect of combined physical and chemical delay period and the interlacing of the exothermic pre-flame reactions by the endothermic fuel droplet evaporation reactions during the delay period. Criterion based on $\max\left(\frac{d^2p}{d\theta^2}\right)$ presented in [28, 102] is widely used as it predicts SOC with delay and is used in the present study to determine SOC.

## 5.9 TEST RESULTS

### 5.9.1 Test results at variable compression ratio mode

The engine was first tested for its performance varying the CR from 13 to 18 using commercial grade diesel as fuel. At each CR, the load was varied from no load to full load. Fig. 5.14 shows the effect of CR on BTE at various loads. It was observed that the BTE of the engine was the maximum at CR 18 followed by BTE at CR 17 over the entire range of load.

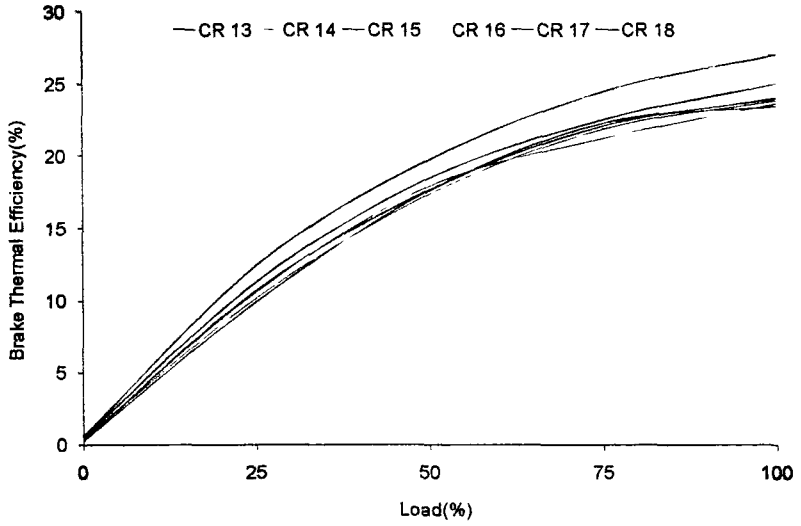


Fig. 5.14: BTE as function of load at various CR

It was observed that at low CR, the fuel consumption of the engine was more and as the CR is increased gradually the fuel flow rate to the engine decreases and this was almost the trend at each and every load. The fuel flow rates e..g. at full load( BP 3.5 kW) at CR 13, 14, 15, 16, 17, 18 were found to be 1.26 kg/h, 1.20 kg/h., 1.18 kg/h, 1.14 kg/h, 1.13 kg/h, 1.11 kg/h respectively. Since the fuel flow rate decreased with increase in CR and the BP and calorific value being the same at a given load at all CR, therefore it resulted in higher BTE at increased CR and hence it was the maximum at CR 18.

Fig. 5.15 presents the variation of BSFC with load at various CR. The fuel consumption characteristic of an engine is generally expressed in terms of SFC in kg/kWh. It is a parameter that reflects how good the engine performance is and this is inversely proportional to BTE of the engine. BSFC decreases with increase in load at all the CRs and the BSFC values were found to be the minimum at CR 18. This is again due to reduction in

fuel flow rate with increasing CR. At full load, the BSFC values at the various CR in increasing order from 13 to 18 were found as 0.36, 0.343, 0.337, 0.326, 0.323, 0.317 kg/kWh respectively.

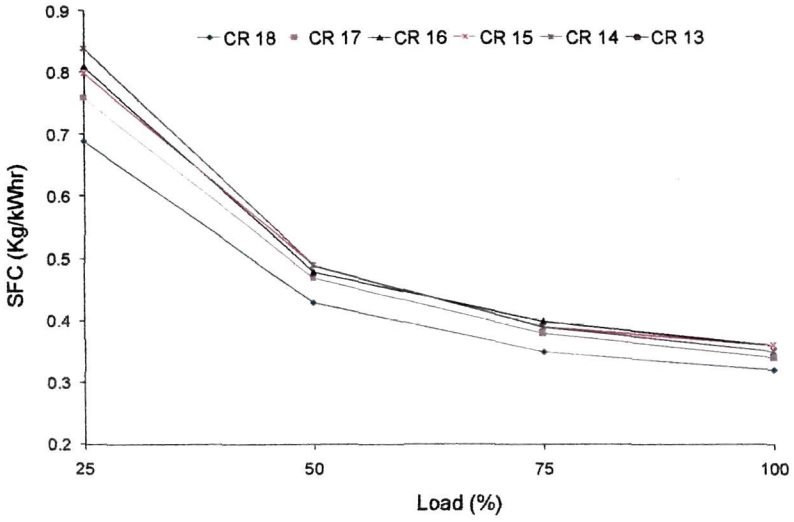


Fig. 5.15: SFC vs load at various CR

Fig. 5.16 represents the pressure-CA variation at different CR under full load condition. Early combustion at higher CR is clearly evident from the figure. With increase in CR, the temperature of compressed air increases and reaches the self ignition temperature of the fuel relatively at a lesser time and hence results in early combustion. Due to early premixed combustion at higher CR, the pressure also rises early and rapidly resulting in a higher peak pressure at higher CR.

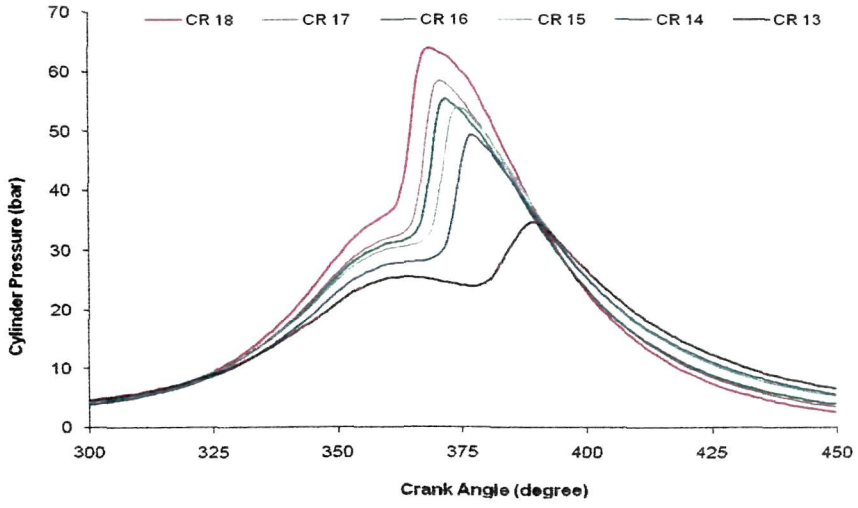


Fig. 5.16: Pressure crank angle diagram at various CR

Based on this study at different CR while operating the engine with commercial grade diesel, it was found that the engine performed better at CR 18 in terms of BTE, BSFC and pressure CA variation and therefore it was decided to carry out experiments for NRL diesel and the various KSOME blends at a fixed CR of 18 while changing the load gradually from no load to full load.

### 5.9.2 Engine performance test results with KSOME blends at CR 18

#### (A) Brake Thermal Efficiency (BTE)

The effect of load on BTE for NRL diesel, B10, B20, B30 and B40 is shown in Fig. 5.17. It was seen that there is a steady increase in efficiency with load in all the fuel operations. This is due to the fact that with increase in load both the BP and fuel flow rate to the engine increase and there is reduction in heat loss. However the rate at which BP increases with load is higher than the rate of increase of fuel flow rate. It was also observed that the thermal efficiencies were closer to each other. With increasing load the engine is required to develop more power meaning thereby more fuel consumption; however, in the process the various losses increase but at a lesser rate and thus BTE increases with load. However there is a slight decrease in BTE in case of the blends at all the loads and it was the lowest for the blend B40. The engine BTE at full load for NRL diesel, B10, B20, B30 and B40 fuels were 25.63%, 24.86%, 24.34%, 24.09% and 22.32% respectively. It was also observed that the rate of fuel consumption was more for the blends and it was the maximum for the blend B40. Higher fuel consumption in case of the KSOME blends may be due to higher injection line pressure and reduced fuel loss which might arise from its higher viscosity and density. If it is attempted to produce a given power output from the engine fuelling the engine with NRL diesel and the various KSOME blends, then the fuel consumption rate becomes higher in case of the bio-diesel blends. The fuel consumption rate at CR 18 and full load (BP 3.5 kW) for NRL diesel, B10, B20, B30 and B40 were found to be 1.15 kg/h, 1.187 kg/h, 1.214 kg/h, 1.228 kg/h and 1.328 kg/h respectively. Since the BTE of an engine is defined as the ratio of BP to the fuel energy input which is the product of fuel calorific value and its flow rate, therefore it depends mainly on the fuel flow rate and its calorific value because the BP remains the same for all the fuels at a particular load. It was seen in Table 4.1 that the calorific values of the blends were lower and it decreased with increase in the percent of bio-diesel in the blend. Again the densities of the blends were more compared to that of NRL diesel. It was observed that the rate at which fuel flow rate

increased with the blends was more compared to the rate of decrease in the calorific value of the blends with increasing proportion of bio-diesel in the blends. Moreover, the unaccounted losses were higher for the biodiesel blends which are described in detail in chapter 6. Hence the BTE of the engine was less in case of the bio-diesel blends.

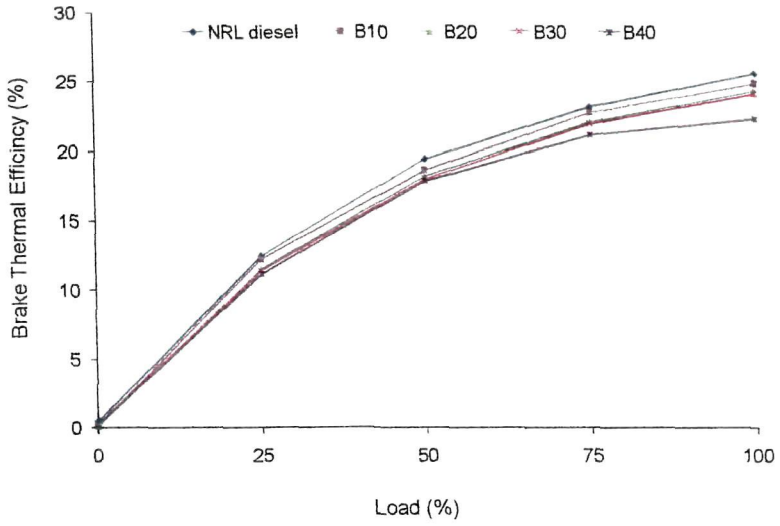


Fig. 5.17: Variation of BTE with load for the tested fuels

**(B) Brake specific fuel consumption (BSFC)**

The BSFC of the engine with the KSOME blends viz. B10, B20, B30 and B40 as fuels are compared with its diesel fuel operation at various loads and this is shown in Fig. 5.18 for CR 18. All the fuels showed similar trend as that of NRL diesel in the entire range of load i.e. for NRL diesel as well as the blends, BSFC of the engine decreased with increase in load. The BSFC decreases with increasing load because of higher BTE as already explained in Section 5.9.1. But the BSFC for the KSOME blends were found to be higher compared to that of NRL diesel at all the loads. This was due to higher fuel consumption of the engine during its operation with the bio-diesel blends, e.g. the BSFC values with NRL diesel, B10, B20, B30 and B40 at full load were found to be 0.3285 kg/kWh, 0.339 kg/kWh, 0.3468 kg/kWh, 0.351 kg/kWh and 0.3794 kg/kWh respectively. BSFC is the defined as the ratio of fuel flow rate to the BP output. In case of engine operation at a particular load, the BP remains the same for all its fuel operations and since the fuel consumption is more in case of the KSOME blends, therefore the BSFC is more for the bio-diesel blends and this applies for the entire range of load. Higher fuel consumption can be attributed to the fact that the

KSOME blends have relatively lower calorific value, although its higher density could somewhat reduce the effect.

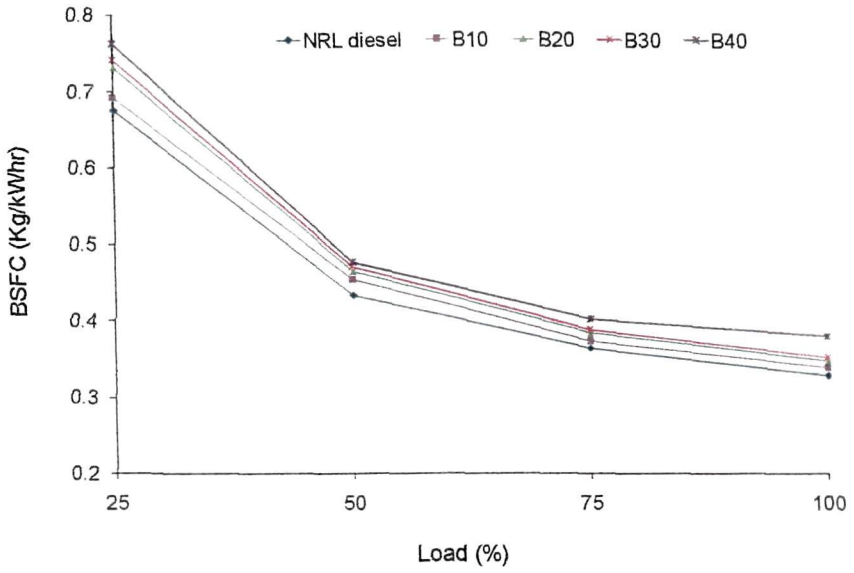


Fig. 5.18: Variation of BSFC with load for the tested fuels

**(C) Indicated power (IP)**

Calculation of IP is based on the integration of the $pdV$ work over the entire cycle, which is then multiplied with the engine speed to determine it. The variation of IP with load at CR 18 and for NRL diesel and the KSOME blends is presented in Fig. 5. 19. It was observed that the IP of the engine operated with the blends up to B30 is slightly more than the engine IP when run with NRL diesel. However, for the blend B40 the IP was less compared to that for NRL diesel over the entire range of load. At full load, the engine IP produced with NRL diesel, B10, B20, B30 and B40 as fuels were found to be 5.6 kW, 5.76 kW, 5.80 kW, 5.92 kW, and 5.42 kW respectively. It was observed that the loop work (the work done during the gas exchange process) and the compression works were less for the blends B10, B20 and B30. Also there was an increase in the combustion and expansion work associated with these blends. Hence the net work done during the cycle was more for these blends and this ultimately resulted in higher IP. Lower IP of the engine with B40 as fuel was due to increase in the compression and loop works and reduction in the combustion and expansion work. The loop works corresponding to fuel operation with B10, B20, B30 and B40 are 20.121 J, 18.319 J, 14.642 J and 42.966 J respectively compared to a loop work of 24.156 J corresponding to diesel fuel operation at full load. Similarly the combustion and expansion works for NRL diesel, B10, B20, B30 and B40 are 724.13 J, 728.18 J, 719.64 J,

743.05 J and 692.86 J respectively. It was seen that there was a significant increase of about 77.9% in the loop work in case of the fuel blend B40 and the combustion and expansion works were also significantly less for this fuel blend as compared to the combustion and expansion works corresponding to the other fuel blends. The compression work required at full load operation for NRL diesel and the various KSOME blends were 309.8 J, 300.51 J, 286.15 J, 294.92 J and 311.35 J respectively. As can be seen from these values that compared to the compression work corresponding to NRL diesel fuel operation, it was less for the blends up to B30 and slightly more in case of the blend B40.

Moreover for a major portion of load, IMEP for B30 has the highest value and hence the corresponding combustion chamber and wall pumping loss (Equation 3.49) is more, while the same for B10 and B20 are very close to each other. Hence the IP- load curves have indicated a merger for B10 and B20. However, the percentage variation of IP values for these fuels at a particular load is very small (2.7% max.).

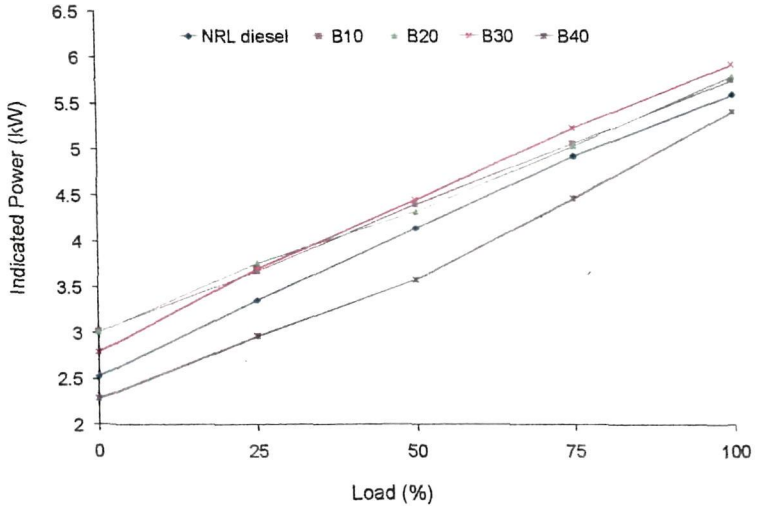


Fig. 5.19: IP vs. load for the tested fuels

**(D) Exhaust gas temperature (EGT)**

EGT is one the important parameter in engine study as it represents the temperature of the fuel mixture after it is burnt in the cylinder. EGT is a direct indication of loading given to an engine and in case, the EGT exceeds the permissible limit it results in severe smoke escaping out the engine. There is a direct proportionality between temperature in the combustion chamber and the nitrogen oxides (NOx) emission also. Since, EGT indicates the temperature that prevails in the combustion chamber, therefore an increase in EGT means

more NOx emission. Biodiesel fueled engines emit more NOx as compared to that of diesel fueled engines [13]. The variation of EGT with load for NRL diesel and the KSOME blends is compared and presented in Fig. 5.20. It was found that the EGT increased with increase in engine loading for all the fuels. With increasing load, the amount of fuel injected to the engine's combustion chamber increases and as a result, more amount of heat is released due to burning of relatively more amount of fuel. This is the reason that EGT is more at higher load. In general, the EGT was found to increase by small values with the increasing concentration of KSOME in the blends at all the loads. At full engine load, the EGT with NRL diesel, B10, B20, B30 and B40 were 333.28, 337.15, 343.6, 344.87 and 340.06°C respectively. This increase in EGT in case of the bio-diesel blends could be due to higher fuel consumption in case of the biodiesel blends and as a result, more heat is released during the late combustion phase. This is described later in the heat release analysis. Slightly lower EGT for B40 compared to B20 and B40 at full load can be due to incomplete combustion of this particular fuel blend. Raheman and Ghadge [14] also observed higher EGT in case of Mahua methyl ester blends with high speed diesel. Higher EGT with the biodiesel blends was explained to be due to increased heat losses associated and the same reasoning was also given for lower BTE with respect to the blends. However Ramadhas et al.[13] observed lower EGT up to B20 with biodiesel from rubber seed oil and the EGT was more for the other fuel blends( B50, B75) and pure biodiesel. Raheman and Phadatare [18] on the other hand, observed slightly lower EGT (with little variation) in case of various blends and pure biodiesel from Karanja oil at all the loads.

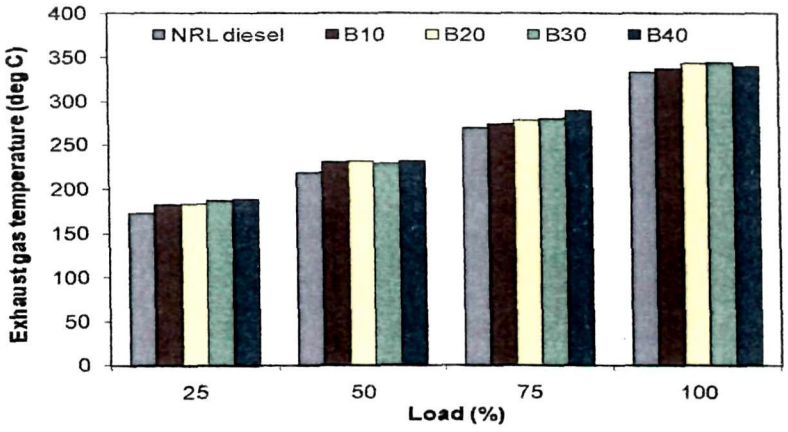


Fig. 5.20: Variation of EGT with load for various fuels

### 5.9.3 Combustion analysis

Combustion characteristics of an engine are very important from the point of view that they provide much important information which help in interpreting engine performance and exhaust emissions. They are also useful from the engine design and optimization point of view. Besides, the combustion characteristics, such as maximum cylinder gas pressure, the heat-release rate can be used to explain the effects of engine-operating conditions on the engine performance or to compare the performance of alternative fuels under the same operating conditions. The combustion characteristics of an engine is usually defined by parameters such as pressure CA diagram, peak pressure, NHRR, cumulative heat release, ignition delay and combustion duration. Since in the present context, there is a greater motivation to utilize biodiesel as a supplementary fuel for diesel in compression ignition engines, it is extremely relevant to assess the combustion characteristics of biodiesel fuelled engine.

**(A) Pressure crank angle diagram and peak pressure**

The pressure CA variation at various engine loads viz. full load, 75%, 50% and 25% of full load are shown in Fig. 5.21-5.24 for NRL diesel and the various blends. Since care was taken during installation for proper matching of TDC position of the piston and marker pulse position of the CA encoder, obtained pressure CA variations take into account the effect of the valve timing as mentioned in the engine specifications. Not much variation was observed; however, early pressure rise for the blends at all the loads was distinct from these figures.

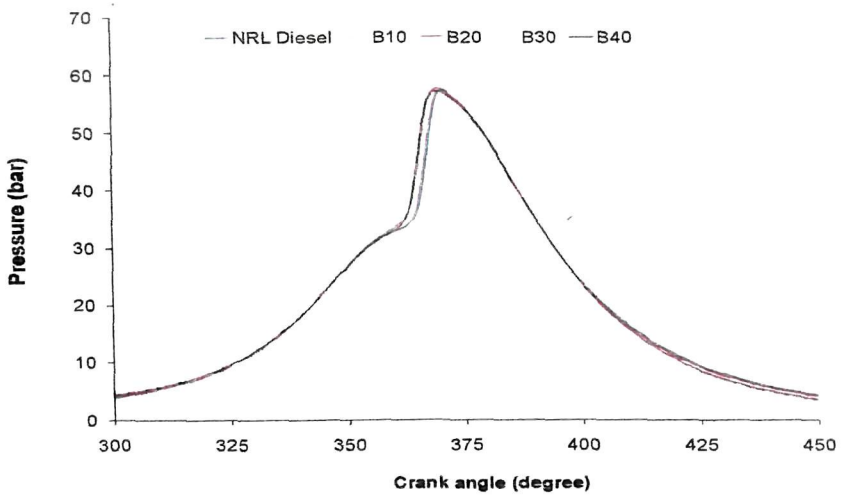


Fig. 5.21: Pressure crank angle variation for the tested fuels at full load

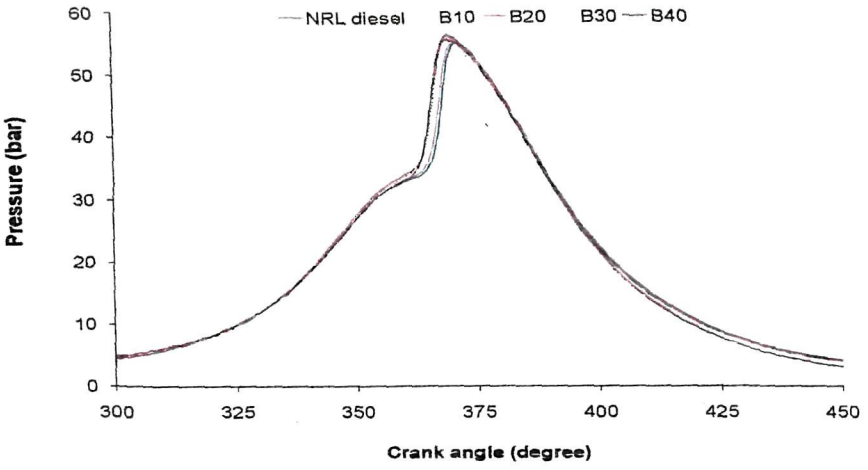


Fig.5.22: Pressure crank angle variation for the tested fuels at 75% load

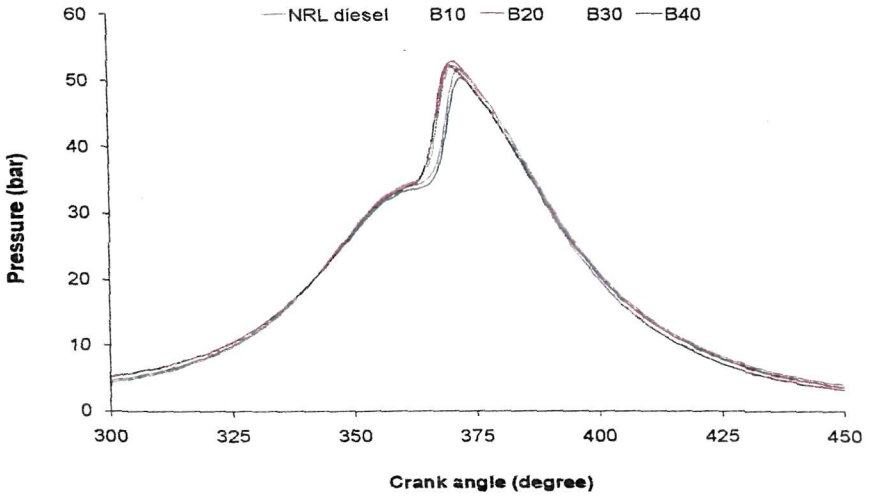


Fig. 5.23: Pressure crank angle variation for the tested fuels at 50% load

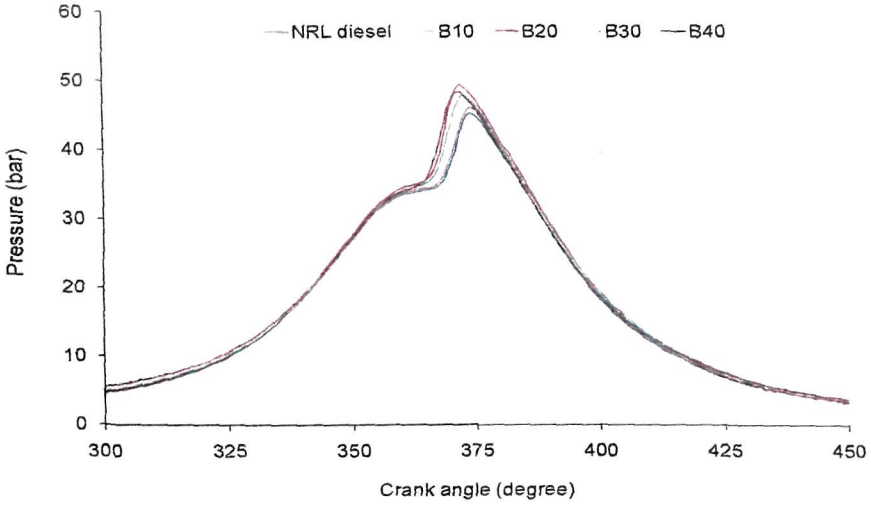


Fig. 5.24: Pressure crank angle variation for the tested fuels at 25% load

Fig. 5.25 shows the peak cylinder pressure for the fuels at various engine loads. The peak pressure depends on the amount of fuel taking part in the uncontrolled combustion phase of combustion, which is governed by the delay period and spray envelope of the injected fuel. It is a measure of the amount of fuel accumulated during the delay period that takes part in the premixed combustion phase. Larger the ignition delay more will be the fuel accumulation, which finally results in a higher peak pressure. It was seen that the peak pressure for NRL diesel as well as the various KSOME blends was almost the same at full load (BP 3.5 kW), the peak pressure values for B10, B20, B30 and B40 being 57.35, 57.62, 57.31 and 57.16 bar respectively as against a peak pressure value of 57.43 bar for NRL diesel. The CAs at which these peak pressures occurred were 370°, 370°, 370° , 369° and 369° for NRL diesel, B10, B20, B30 and B40 respectively. However, at 75%, 50% and 25% engine loads, the peak cylinder pressures for engine operation with the KSOME blends were slightly on the higher side. For example at 50% load, the peak cylinder pressure corresponding to fuel operation with NRL diesel, B10, B20, B30 and B40 are 50.32, 51.65,52.8,52.22 and 52.31 bar respectively. At lower load operations, lower peak in case of all the fuels is due to the combustion of relatively less amount of fuel. With decrease in engine load the in-cylinder gas and wall temperatures decrease and it results in lower charge temperature during fuel injection and thus there is increase in ignition delay [28]. At lower engine loads, due to longer ignition delay, combustion starts later and as a result, the peak cylinder pressure attains a lower value and it occurs at a later CA position away from the TDC. As mentioned earlier, the CA at which peak pressure occurred at full load is 370° for NRL diesel, B10, B20 and it was 369° for B30 and B40. However at 25% engine load, these were 374°, 374°, 372°, 372°, 372° CA for NRL diesel, B10, B20, B30, and B40 respectively.

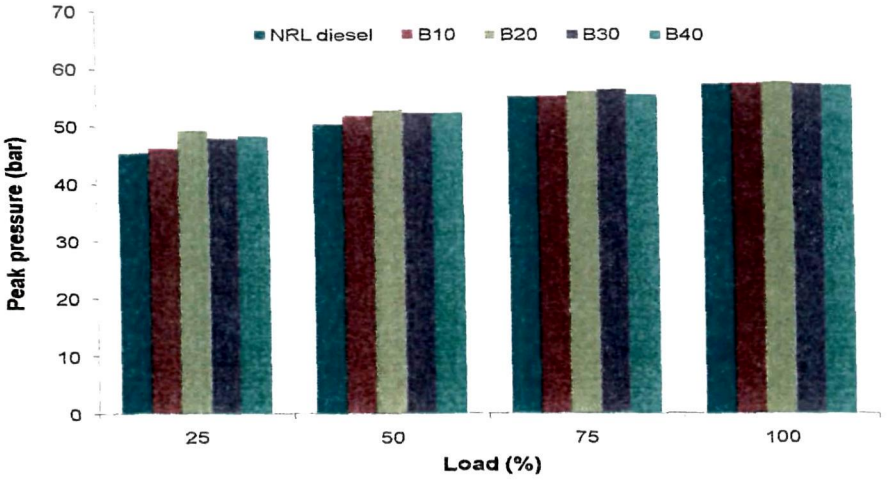


Fig. 5.25: Peak pressure at various loads for the tested fuels

Slightly higher peak pressure in case of the KSOME blends at lower load may be due to increased amount of fuel injected, although the ignition delays were less for these blends which is discussed later in section 5.9.3 (D). This resulted in early rate of pressure rise in case of the blends as compared to that of NRL diesel which can be seen from Fig. 5.26-5.29. It was seen that at lower engine loads the peak rate of pressure rise for the KSOME blends is slightly higher than that for NRL diesel. This may again be due to relatively higher amount of injected fuel and early combustion with respect to the biodiesel blends. However, the peak rate of pressure rise was lower for the blends at higher engine loads in comparison to that of NRL diesel. The rate of pressure rise also decreased with decrease in the load for all the fuels as seen from Fig. 5.30, which shows the rate of pressure rise for NRL diesel specifically at various loads. Analysis of rate of pressure rise is important in engine study because it is possible to determine the smoothness of progress of the combustion process in the engine combustion chamber from the observation of rate of pressure rise. It is necessary that the maximum rate of pressure rise should be as low as possible for reduced engine noise and increased engine life. It was also observed that the peak cylinder pressure increased with load for all the fuel operations. With increasing load, the amount of fuel supplied to the engine increases and due to combustion of relatively more amount of fuel, the peak pressure of the in-cylinder gas is more at higher load. With increase in load, the occurrence of pressure rise was also advanced with respect to the CA and the peak pressure occurred early for all the fuels at higher load. In case of the biodiesel blends the pressure rise and the peak pressure occurred even earlier at all the loads compared to NRL diesel but definitely well after the TDC. The early peaking characteristics of an engine with biodiesel blends need to be considered carefully because a peak pressure occurring very close to TDC or before causes severe engine knock, and thus affects engine durability [103].

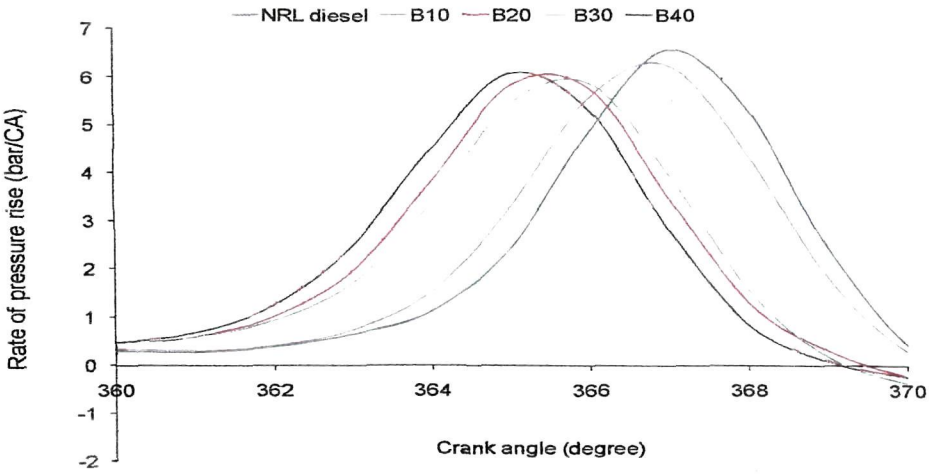


Fig. 5.26: Rate of pressure rise vs. crank angle for the tested fuels at full load

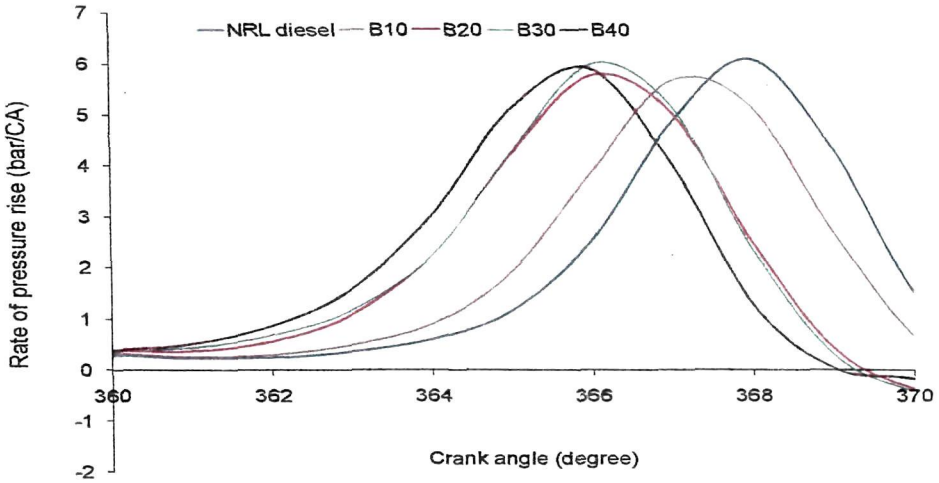


Fig. 5.27: Rate of pressure rise vs. crank angle for the tested fuels at 75% load

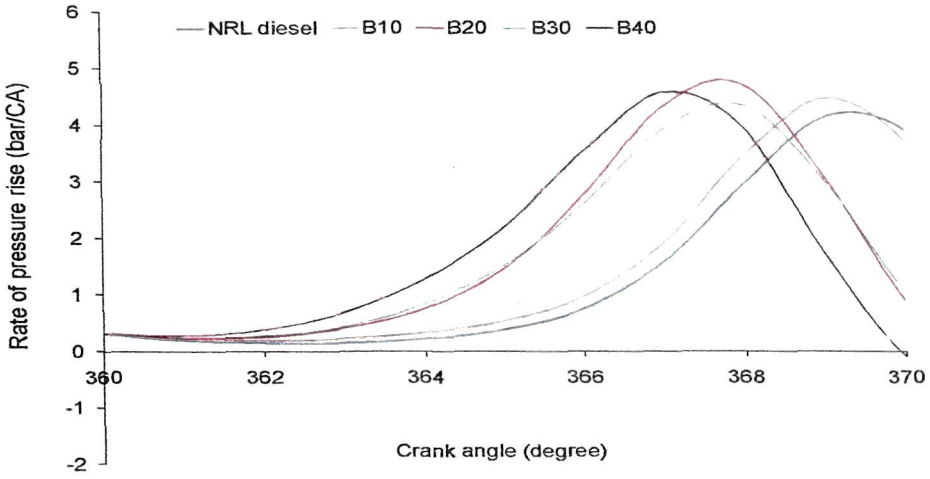


Fig. 5.28: Rate of pressure rise vs. crank angle for the tested fuels at 50% load

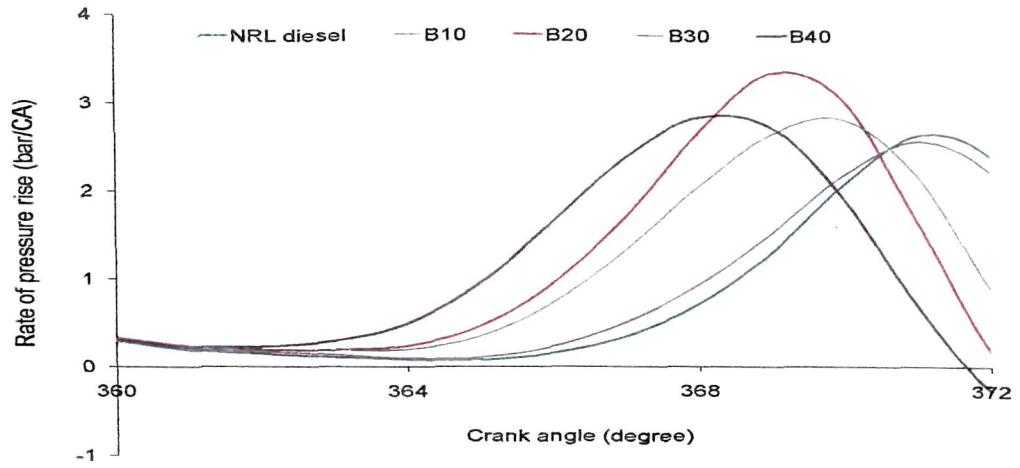


Fig. 5.29: Rate of pressure rise vs. crank angle for the tested fuels at 25% load

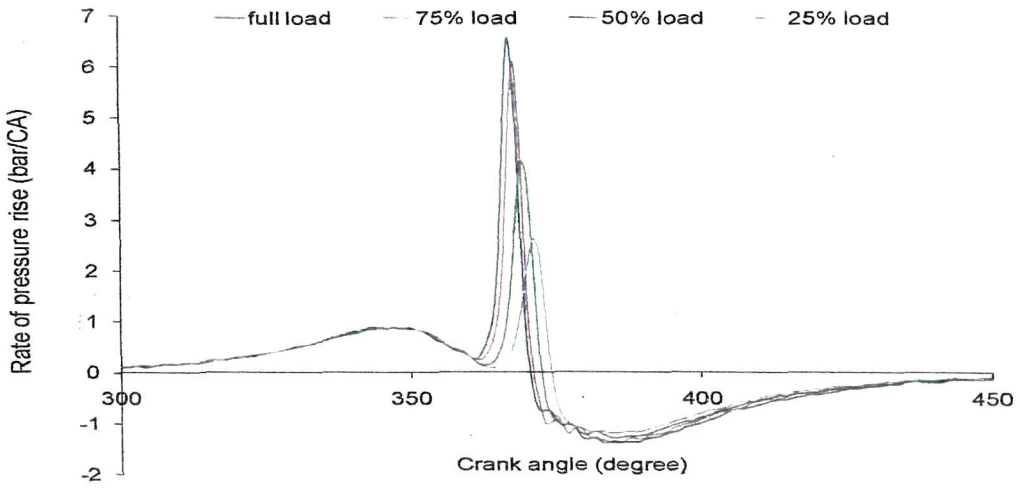


Fig. 5.30: Rate of pressure rise for NRL diesel at various loads

**(B) Net heat release rate (NHRR)**

The heat release analysis compute how much heat would have to be added to the cylinder contents in order to produce the observed pressure variations and is a method used to obtain important combustion information from the cylinder pressure data. It strongly affects the fuel economy, power output and the emissions of the engine. As already mentioned, in-cylinder pressure and TDC signals were acquired and stored on a high-speed computer-based digital data-acquisition system. The data from 5 consecutive cycles were recorded. The NHRR was obtained from first law analysis of the pressure CA data. The apparent NHRR which is the difference between the apparent gross heat release rate and the heat transfer rate to the walls is given by the following equation.

$$\frac{dQ_n}{d\theta} = \frac{dQ_{ch}}{d\theta} - \frac{dQ_{ht}}{d\theta} = \frac{\gamma}{\gamma - 1} p \frac{dV}{d\theta} + \frac{1}{\gamma - 1} V \frac{dp}{d\theta} \tag{5.6}$$

where, $\frac{dQ_n}{d\theta}$, apparent rate of net heat release; $\frac{dQ_{ch}}{d\theta}$, apparent rate of gross heat released by combustion of fuel and $\frac{dQ_{ht}}{d\theta}$, rate of heat transfer from the in-cylinder gas to the cylinder walls. $\gamma$ is the ratio of specific heats. An approximate range for $\gamma$ for diesel engine heat release analysis is 1.3 to 1.35. However the values of $\gamma$ which will give more accurate heat release information are not well defined [28]. In the present analysis value of $\gamma$ for all the fuels were taken as 1.35.

Fig. 5.31-5.34 show net heat release rate for different fuels at full load, 75 %, 50% and 25% of full load respectively. Shorter ignition delay period predicted in case of the blends as explained in the previous section while analyzing the pressure CA diagram for different fuels can now be confirmed from these figures for NHRR vs. CA. Lower peak of heat-release rate was observed in case of KSOME blends at full load and 75% of full load although for B10 it was only marginally less than NRL diesel. However, at 50% load, the magnitude of the peak of the heat release rate was higher for B10 and B20 and same was the case for B20 at 25% load. Saravanan et al. [87] also observed lower heat release rate in case of 20% blending of crude rice bran oil methyl ester with diesel at rated load, the lower calorific value of the blend was stated to be the possible reason for that. Higher peak of heat release rate in case of B10 and B20 at 50% load and B20 at 25% load can again be related to higher peak of the rate of pressure rise for these blends at these two particular loads as can be seen in Fig. 5.28 and 5.29. This is because; the influence of the second term on the right hand side of equation (5.6) is much stronger than the first term over a wide range around TDC [104]. It was further seen that the heat release occurred earlier in the case of KSOME blends at all the loads. Early premixed combustion associated with early heat-release rate in case of KSOME blends signify shorter ignition delay period for these blends. Because of the shorter ignition delay, maximum heat-release rate also occurs earlier for the bio-diesel blends compared to NRL diesel.

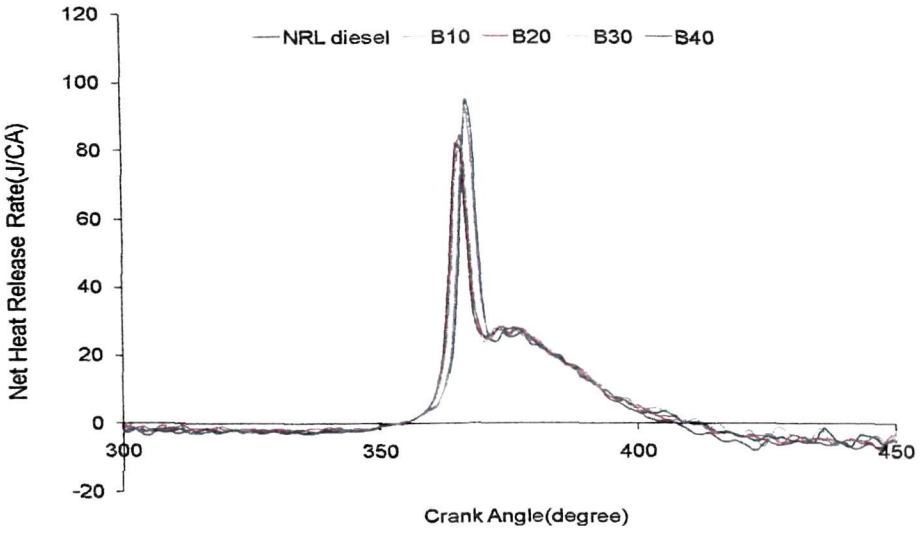


Fig. 5.31: Net heat release rate characteristics of the tested fuels at full load

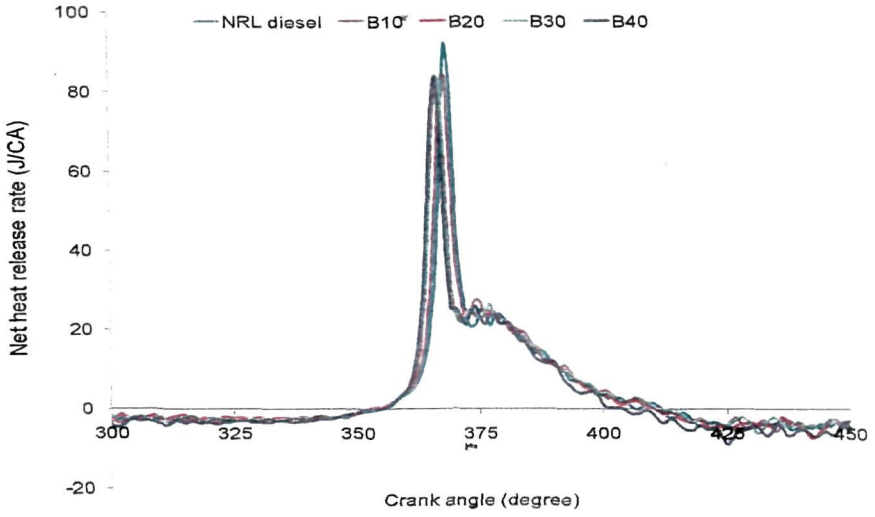


Fig. 5.32: Net heat release rate characteristics of the tested fuels at 75% load

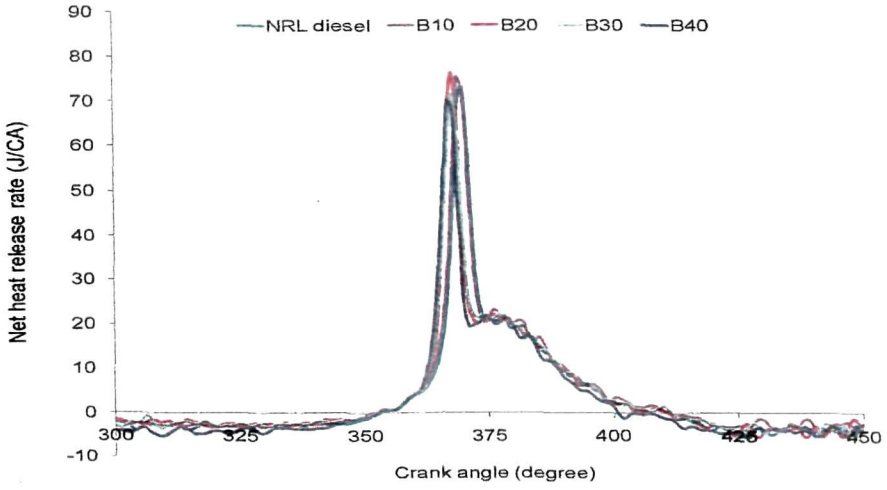


Fig. 5.33: Net heat release rate characteristics of the tested fuels at 50% load

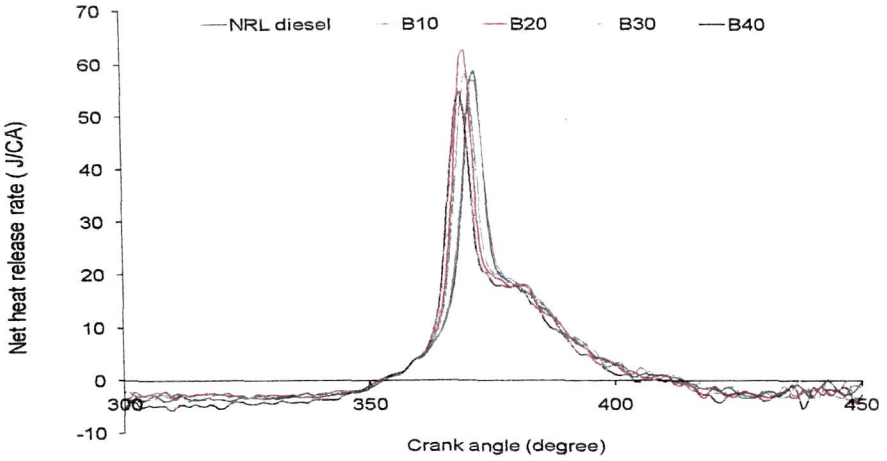


Fig. 5.34: Net heat release rate characteristics of the tested fuels at 25% load

**(C) Cumulative heat release**

Cumulative heat release is the integration of the results presented for NHRR characteristics and it indicates the amount of energy spent for a given output. Cumulative heat release is shown in Fig. 5.35-5.38 for all the tested fuels at full load, 75%, 50% and 25% of full load respectively. It was observed that cumulative heat release increased towards the later part of the combustion processes for the blends up to B30 at all the loads. It means that greater amount of heat is released in order to obtain the given output in case of the blends. This is due to the fact that more amount of fuel was available in the case of KSOME blends to take part in combustion as it progressed. This may also be the reason of higher IP associated with these blend as explained in Section 5.9.2. Although the fuel flow rate for the KSOME blends was higher compared to NRL diesel, but the calorific values of the blends were slightly lower. The lower calorific value of the KSOME blends were compensated by their higher fuel flow rate and hence cumulative heat release increased for the blends up to B30. However, the cumulative heat release for the blend B40 was significantly lower towards the later part of combustion as can be seen from the figures at all the loads even though the fuel consumed was the maximum for this fuel blend. This was due to some other reason and the explanation given for higher cumulative heat release with the blends up to B30 may not be correct for the blend 'B40'. There is not much literature available to compare the present results of cumulative heat release with results already published. It was seen that the viscosities of the KSOME blends were more and may be due to higher viscosity and particularly for this blend; the fuel did not atomize properly leading to poor combustion, which ultimately resulted in lower heat release. The same may also be the reason of lower engine IP produced with this particular blend as fuel to the engine.

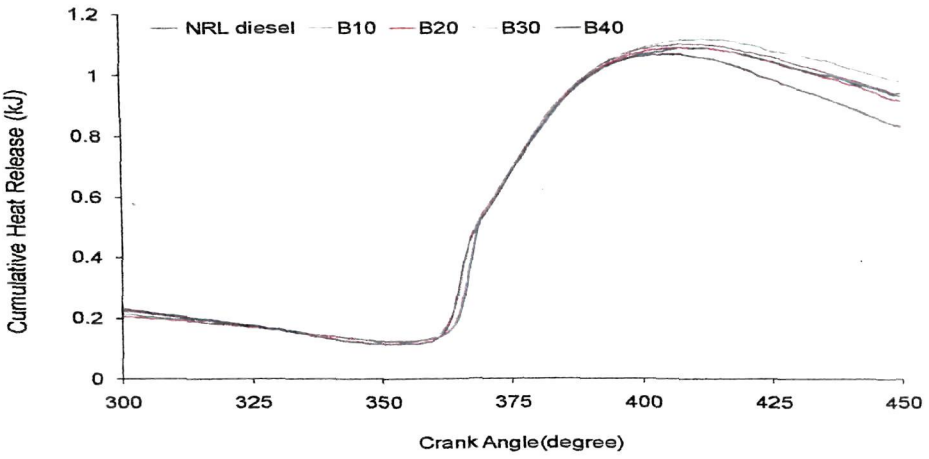


Fig. 5.35: Cumulative heat release characteristics of the tested fuels at full load

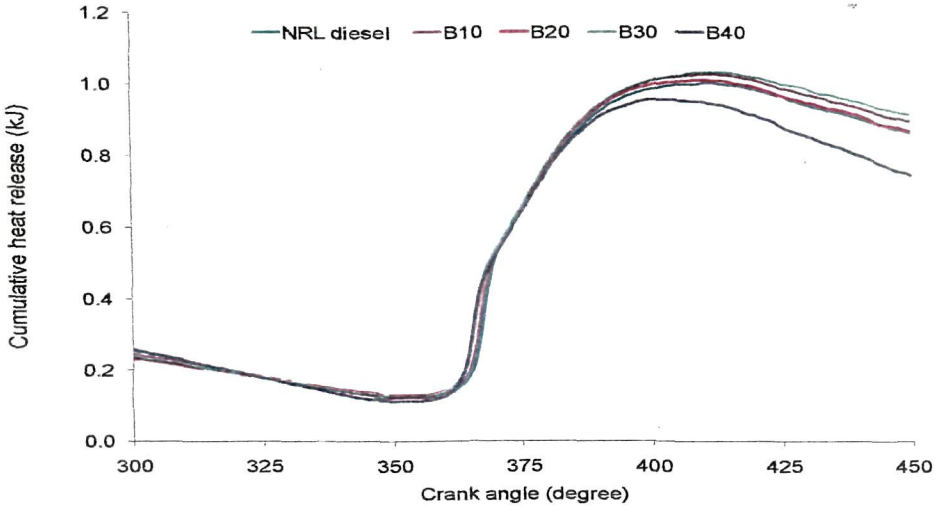


Fig. 5.36: Cumulative heat release characteristics of the tested fuels at 75% load

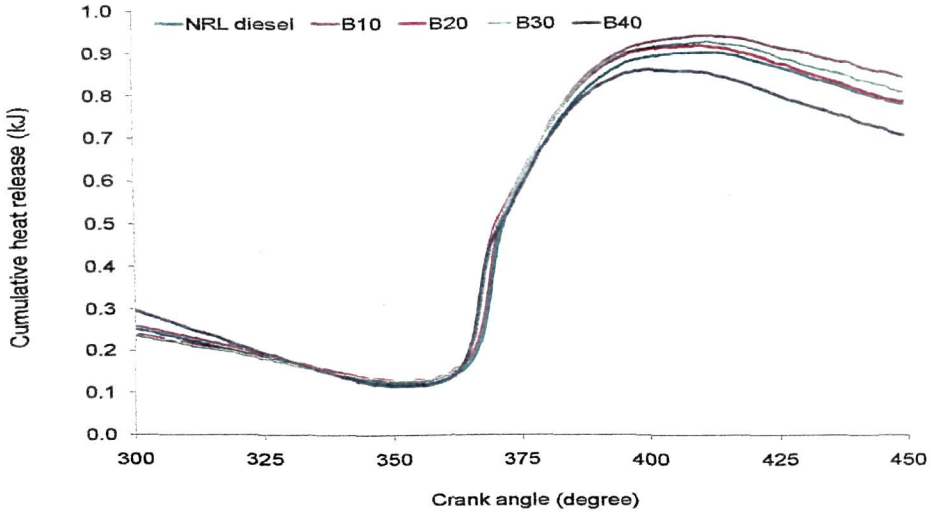


Fig. 5.37: Cumulative heat release characteristics of the tested fuels at 50% load

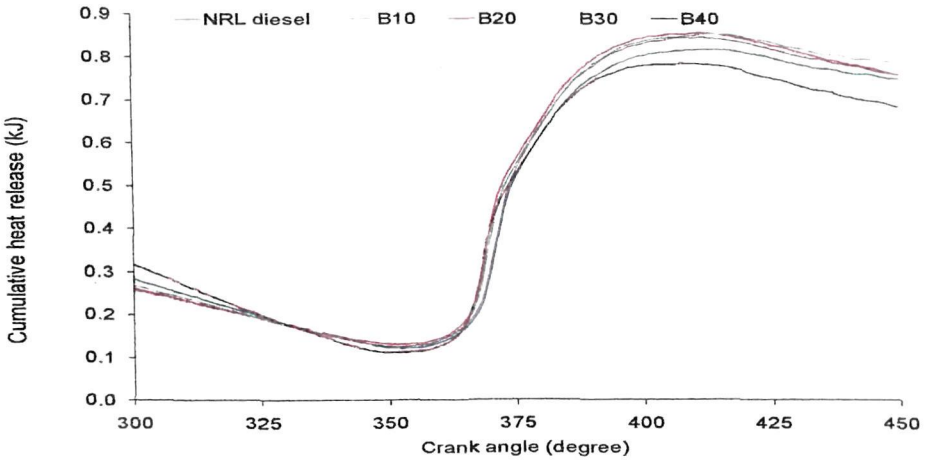


Fig. 5.38: Cumulative heat release characteristics of the tested fuels at 25% load

**(D) Ignition delay**

Ignition delay is the time period between SOI and SOC. Fig. 5.39 shows the ignition delay for NRL diesel and various KSOME blends at full load, 75%, 50% and 25% of full load respectively. It was already explained in the net heat release analysis that shorter ignition delay period was the cause of early heat release in case of the KSOME blends. Ignition delay period was calculated from known values of SOC and SOI and it was found that the ignition delay period for KSOME and its NRL diesel blends was less at all the loads and the prediction made in heat release analysis was found to be correct. Many researchers [87, 103, 105] have analyzed the lower ignition delay with biodiesel in spite of its slightly higher viscosity and lower volatility. Due to rapid and complex pre-flame chemical reaction with high temperature air during injection and also may be due to thermal cracking, the high molecular weight ester (biodiesel) breaks down leading to formation of lighter compounds that ignites earlier resulting in shorter ignition delay. Biodiesel typically contains unsaturated fatty acids, the amount of saturated and unsaturated fatty acids in Koroch seed oil are about 26.7% and 72.86% respectively. Higher percentage of unsaturation in both the oil and the ester enhances its oxidation instability and these unsaturated fatty acids get oxidized when exposed to oxygen environment. May be due to presence of higher oxygen content, biodiesel gets ignited earlier than that of diesel. Further it was observed that the ignition delay period for NRL diesel as well as the KSOME blends decreases with increase in load. At higher loads, due to combustion of relatively more amount of fuel high temperature exists in the combustion chamber and as a result the process of vaporization of fuel is enhanced. The chemical delay period required for the reaction to occur reduces and hence the delay period.

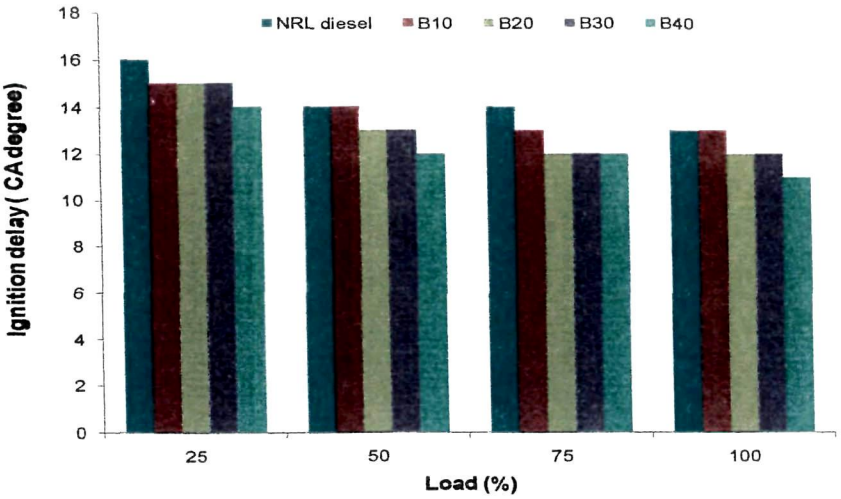


Fig. 5.39: Ignition delay for the tested fuels at various loads

**(E) Combustion duration**

It is very difficult to define exactly the combustion duration of a diesel engine as the total combustion process consists of the rapid premixed combustion, mixing controlled combustion and the late combustion of fuel present in the fuel rich combustion products. The rapid combustion duration is the time interval from the start of rapid pressure rising to the end of rapid pressure rise. The total combustion duration is the time interval from the start of heat release to the end of heat release [103]. Banapurmath et al. [21] have found the combustion duration in a diesel engine from calculations based on the duration between the SOC and 90% cumulative heat release. They observed higher combustion duration with Honge, Jatropha and Sesame oil methyl esters which they attributed to the longer diffusion combustion phase of the esters. Since the cumulative heat release is obtained by integration of NHRR results therefore the integral of NHRR over the combustion process should be approximately equal to the heat released during the combustion process, of course with due consideration of heat transfer from the wall. From this point of view, considering 90% cumulative heat release as the end of combustion is well justified because the total heat released may be correct to within few percent only as the analysis is based on approximation and not exact. However in the present study the CA at which the cumulative heat release becomes maximum has been considered as the end of combustion because these are always based on approximation and calculation of NHRR first and then cumulative heat release are based on cylinder pressure data measured by the dynamic pressure sensor fitted on the combustion chamber of the engine cylinder. Fig. 5.40 shows the combustion duration for NRL diesel and the KSOME blends at various loads. The combustion duration in general

increases with load because with increase in load, the quantity of fuel injected increases and combustion takes place for a longer period. At full load operation, the combustion durations of B30 and NRL diesel were the same (47° CA duration) and it was slightly less for the other blends i.e. B10, B20 and B40. Even though the amount of fuel injected was more for the biodiesel blends but slightly lesser combustion duration in the case of the blends at full load may be due to fact that biodiesel is oxygenated in nature which helps in early completion of combustion of the blends as it was the case for B10. But with the increase in the amount of biodiesel in the blend, combustion duration increased for B20 and B30 which may be due to increase in the amount of fuel injected. But again the combustion duration decreased in case of B40, which was not due to the reason explained for B10, but may be due to higher viscosity of this particular blend as explained in the cumulative heat release analysis. At 75% load, the combustion durations of B10, B20 and B30 were slightly higher than that for NRL diesel and again it was again less for the blend B40. Higher combustion duration of the blends may be due to longer pre mixed and diffusion combustion phases because it was seen that the peak pressure of the combustion gases was also slightly higher for the blends B10, B20 and B30 at 75% load. Longer diffusion combustion of these biodiesel blends at this load can also be seen from Fig. 5.32. At 50% load, the combustion durations of NRL diesel, B10 and B20 were almost the same, being it slightly higher for B30. However, it reduced significantly in case of the blend 'B40' at this load. At 25% load, the trend of combustion duration variations for different fuels was the same with that of the full load condition but the magnitudes were slightly lower. However the combustion duration for B40 at 25% load was more than its value corresponding to 50% load. Overall observation was that the combustion durations were significantly less for the blend 'B40' at 50% and 75% load in comparison to combustion durations for the other blends and NRL diesel.

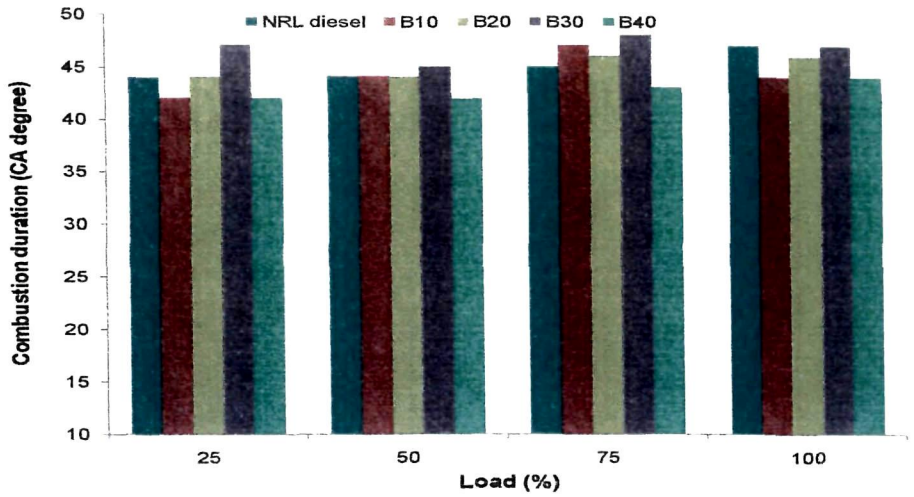


Fig. 5.40: Combustion duration of the tested fuels at various loads

### 5.9.4 Emission Test Results

Table 5.3 below shows the typical emission results for different fuels at various engine loads.

Table 5.3: Emission results at various loads

| Load | Parameter | Unit | NRL diesel | B10 | B20 | B30 | B40 |
|---|---|---|---|---|---|---|---|
| Full load | CO | % | 0.129 | 0.125 | 0.152 | 0.171 | 0.145 |
| | $CO_2$ | % | 7.880 | 8.040 | 8.410 | 8.180 | 8.170 |
| | HC | ppm | 72 | 60 | 94 | 96 | 102 |
| | NO | ppm | 555 | 532 | 543 | 543 | 553 |
| | $O_2$ | % | 10.080 | 9.810 | 9.610 | 9.700 | 9.850 |
| 75% load | CO | % | 0.084 | 0.085 | 0.088 | 0.097 | 0.083 |
| | $CO_2$ | % | 6.480 | 6.630 | 6.800 | 6.690 | 6.730 |
| | HC | ppm | 60 | 56 | 68 | 78 | 72 |
| | NO | ppm | 480 | 477 | 485 | 497 | 466 |
| | $O_2$ | % | 12.14 | 11.99 | 11.96 | 11.95 | 11.92 |
| 50% load | CO | % | 0.106 | 0.093 | 0.089 | 0.104 | 0.089 |
| | $CO_2$ | % | 5.170 | 5.380 | 5.390 | 5.380 | 5.570 |
| | HC | ppm | 62 | 52 | 48 | 60 | 60 |
| | NO | ppm | 286 | 332 | 321 | 348 | 345 |
| | $O_2$ | % | 14.2 | 13.8 | 13.84 | 13.77 | 13.54 |
| 25% load | CO | % | 0.118 | 0.099 | 0.103 | 0.108 | 0.098 |
| | $CO_2$ | % | 4.15 | 4.34 | 4.31 | 4.29 | 4.23 |
| | HC | ppm | 68 | 48 | 50 | 50 | 56 |
| | NO | ppm | 144 | 181 | 191 | 189 | 152 |
| | $O_2$ | % | 15.61 | 15.27 | 15.33 | 15.32 | 15.55 |

**(A) Carbon monoxide**

It was seen from Table 5.3 that CO emission for the KSOME blends were more compared to that of NRL diesel at 75% and full load. However, for B40 at 75% load, CO emission was the same with that of diesel. Again for B10 at full load, it was slightly lesser than that for NRL diesel. At 25% and 50% loads, CO emission for all the KSOME blends was comparatively less. Since biodiesel fuel contains small amount of oxygen, these lower CO emissions of biodiesel blends at lower loads may be due to their more complete oxidation as compared to diesel. Slightly lower CO emission of B10 at full load can also be attributed to complete burning of the air fuel mixture. It was also found that CO emission increases with blending of up to B30 which may be due higher viscosity with blending that led to less homogenous mixtures. CO concentration in the exhaust decreases when a homogeneous mixture is burned at stoichiometric air fuel ratio or on the lean side stoichiometric. Although biodiesel blends contain some amount of oxygen but due to higher fuel consumption the amount of oxygen required for burning may not be sufficient to burn the fuel completely. More CO is formed due to the lack of oxygen. However marginally lower CO emission with B40; compared to the other blends at all the loads could be due to presence of extra oxygen molecules present in this particular blend. At high load, due to the higher viscosity of the KSOME blends, the air–fuel mixing process may be affected by poor atomization and vaporization of blends. CO emission was found to decrease initially with load for all the fuels but it again increased to the maximum at full load for all the fuels. Similar results are reported by Raheman and Ghadge [14], where they have also specifically mentioned about several other research works with similar findings. At medium load range, due to better burning of relatively small amount of fuel at elevated temperature, it resulted in lower CO emission. However at full engine load, the air fuel mixture becomes sufficiently rich and therefore more CO is generated during combustion, due to the lack of locally available oxygen. It was observed that the CO emission was the least in case of B10 at all the loads and therefore, this is the optimum fuel blend for CO emission.

**(B) Carbon dioxide**

The $CO_2$ emissions from a diesel engine indicate the burning efficiency of fuel inside the combustion chamber. More amount of CO2 in the exhaust emission is an indication of the complete combustion of fuel [13]. As seen from the table above, the $CO_2$ emissions increase with load for all the fuels due to higher fuel consumption at increased load. Also $CO_2$

emissions of the KSOME blends were higher than that of the NRL diesel over the entire range of load. The amount of CO emissions for the biodiesel blends was less at 25% and 50% load, therefore higher $CO_2$ emission with them at the above mentioned loads is justified. However, higher $CO_2$ emission at 75% and full load could be due to increased fuel consumption at higher load and presence of higher carbon content in the biodiesel blends. Because otherwise the amount CO formed would have been less at these loads and this was not the case for the biodiesel blends except B10. At full load, the $CO_2$ emission for B10, B20, B30 and B40 were 2.03%, 6.726%, 3.807%, and 3.68% higher than that for NRL diesel. However an opposite trend was observed by some researchers [13, 88] where they have reported about lower $CO_2$ emission from biodiesel fuelled engine.

**(C) Unburned hydrocarbon (HC)**

HC is also an important parameter for determining the emission behavior of the engine. It was seen that the KSOME blends give lower HC emission as compared to NRL diesel at 25% and 50% load. However at 75% and full load, HC emission with KSOME blends except B10 was higher than that of NRL diesel. Same was the case in case of CO emissions too. The HC emission trend with changing load in case of B20-B40 was the same. However for B10, the increase in HC emission with load was not much as compared to the other KSOME blends and also HC emission was less for this blend at all loads. This clearly indicates the efficient combustion with respect to this particular fuel blend and better emission characteristics over the other KSOME blends. There was 16.67% reduction in case of B10 whereas 30.55%, 33.33%, 41.66% increase was observed for B20, B30 and B40 respectively at full load. Exhibition of higher HC emission at higher engine load in case of KSOME blends may be because of relatively less oxygen availability for the combustion reaction when more amount of fuel is injected into combustion chamber at high engine load. Similar results are also reported by Agarwal and Rajamonoharan [106]. Banapurmath et al. [21] also found higher HC emission with methyl esters of Jatropha, Honge and Sesame oil, which they have attributed to higher viscosity, poor atomization and lower volatility in respect of the esters.

**(D) NOx emission**

Nitric oxide (NO) and nitrogen dioxide ($NO_2$) are generally combined together as NO*x*, although NO is the dominant oxide of nitrogen produced within the engine cylinder. NOx emission is the most harmful gaseous emissions from engines. NOx emission reduction

has always been the target for engine researchers and engine makers. Availability of oxygen, local stoichiometry of air fuel mixture, the temperature in the combustion chamber is some of the factors that are important for formation of NOx. Besides engine operating and design parameters also have strong influence on NOx emission. The nitric oxide emissions from KSOME blends and NRL diesel at various engine loads are shown in Table 5.3. $NO_x$ emissions depend upon the origin of biodiesel fuel and are higher for unsaturated biodiesel as compared to its saturated counterpart [107]. As can be seen from the table, NOx emissions increase with load for all the fuels. With increase in load due to combustion of more amount of fuel, and also due to lesser ignition delay, the peak pressure increases resulting in high temperature which causes larger amounts of NOx formation. It was seen that NOx emission with all the KSOME blends were more at 25% and 50% load, it was slightly more with B20 and B30 at 75% load and found to be slightly less for all the blends at full load. It may be due to higher peak pressure in respect of the KSOME blends at lower engine loads compared to the full load, where the cylinder peak pressure was slightly less for the blends. Higher rate of pressure rise in case of blends at 25% and 50% load causes early and rapid premixed combustion and can be the reason of higher NOx emission at lower loads in case of the KSOME blends. NOx emission can be reduced by retarding the injection timing [108] and recirculation of exhaust gases through engine's combustion chamber. At full load the measured values for NRL diesel, B10, B20, B30 and B40 are 555, 532, 543, 543 and 555 ppm respectively. Because of lower heat release during the pre-mixed as well as the mixing controlled combustion phase, the peak combustion chamber temperature is possibly lower for the KSOME blends and this lead to lower NOx formation at full load. Literature often give contradictory results, with some researchers [14, 17, 20] reporting an increase in NOx emission while several others [18, 21, 88, 105, 106] reporting reduction in NOx emission with biodiesel.

**(E) Smoke Opacity**

Smoke opacity is considered to be an indicator of soot emissions [107]. Fig. 5.41 shows the effect of load on smoke opacity level for NRL diesel and the KSOME blends. It was seen that the smoke opacity level increased with increase in load for all the tested fuels. Especially, greater smoke opacity was observed at full load. As the load increases, the fuel injected to the combustion chamber increases and when a larger quantity of fuel are to be burnt by relatively less amount of air, much of the fuel goes unburned into the exhaust leading to increased smoke level at higher load. In case of the KSOME blends, it was seen

that the smoke opacity level of the blend B10 was less at all engine loads. The smoke opacity values for the other KSOME blends were higher than that for NRL diesel at various engine loading conditions, except at 75% engine load where the blends showed slightly lower smoke level. At full load, the smoke opacity values for NRL diesel, B10, B20, B30 and B40 were found to be 49.46, 41.18, 54.78, 58.95 and 56.24 HSU respectively. Higher smoke opacity with methyl esters have been reported in some research works [21, 106]. This was stated to be due to heavier molecular structure, higher viscosity, lower volatility and poor atomization of the esters. However in many other reports [13, 14, 18, 20, 105], it was reported that the level of smoke was less with biodiesel and some of its blends. Oxygenated nature of biodiesel and its complete combustion has been shown as possible reason of lower smoke level in all these reports.

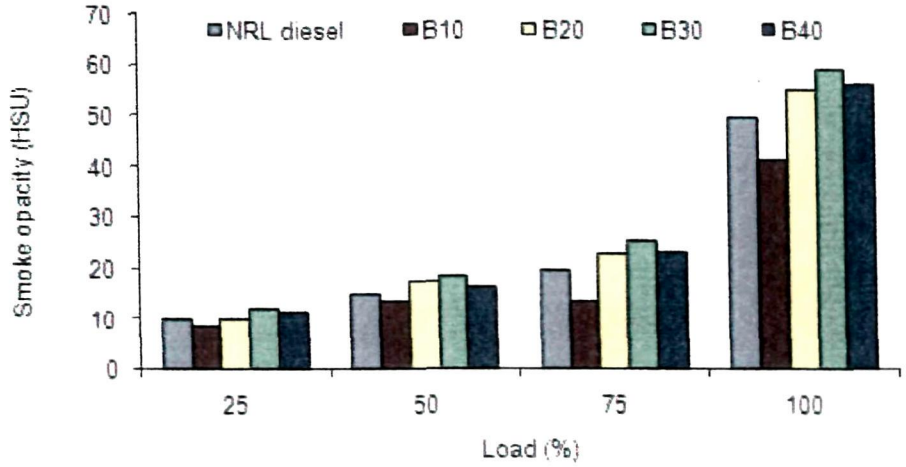


Fig. 5.41: Smoke opacity for the tested fuels at various loads

# CHAPTER 6

# ENERGY AND EXERGY ANALYSES

## 6.1 INTRODUCTION

In a reciprocating internal combustion engine the chemical energy of the fuel is the input energy and not all the input energy is converted into useful work. A major part of the heat energy produced as a result of combustion of fuel is lost in cooling the engine. A significant part of the fuel energy is lost with the exhaust gases. A part of heat energy is consumed by friction in the moving parts and there are unaccounted energy losses which may be due to radiation from high temperature in-cylinder combustion gases and the surface of the combustion chamber. Radiation is considered to be an important source of heat loss in diesel engine mainly caused by presence of high temperature soot particles in the combustion gases. Due to these losses the thermal efficiency of the engine reduces. An energy balance study on an engine helps in understanding how the energy is lost which in turn help in finding means to reduce the same to improve the performance of the engine in terms of efficiency and power output. This is the main reason behind most energy studies performed on engines. Besides, energy balance studies help characterize the effect of changes in engine operating and design parameters on the overall engine system. Once it is identified by the energy balance, one can attempt to either maximize its use for its benefits or oppose due to its drawbacks. If there were significant losses through certain parts of the system, the energy balance study would show this and help identify the cause. However, energy analysis based on first law often fails to provide the engine designer the best insight into the engine's operation. Exergy or second law analysis is must if someone desires to evaluate the inefficiencies associated with the various engine processes. Unlike energy, exergy can be destroyed by way of engine phenomena such as combustion, friction, mixing and throttling. The destruction of exergy is also called irreversibility. It is irreversibility due to which it ultimately leads to defective exploitation of fuel into useful mechanical work in an engine. Any attempt to reduce these irreversibilities would result in better engine performance through a more efficient utilization of fuel. Therefore, to reduce irreversibility, it is necessary to quantify them for which the exergy analysis is needed [109]. Through exergy analysis it is possible to (i) to identify those processes in which destruction or loss of exergy occurs and to detect the sources for these destructions, (ii) to quantify the various losses and destructions, (iii) to analyze the effect of various design, operating and thermodynamic

parameters on the exergy destruction, (iv) to propose methods for reduction of exergy destruction *e.g.* exergy destroyed with combustion, exhaust gas to ambient and heat transfer to cylinder walls.

Canakci and Hosoz [63] have made energy and exergy analyses of a diesel engine fuelled with biodiesel from theoretical calculations of heat transfer. However, results have been reported only for full engine load operation. Similarly, Gokalp et al. [64] also presented results concerning the energetic and exergetic performance of a four cylinder four stroke DI TZDK Basak engine at full throttle condition and rated speed of 1600 rpm. Calculation of heat transfer in their work was based on experimental results, but the frictional power was determined theoretically. Considering the fact that research works on energy and exergy balance studies are relatively scanty [63, 64, 109, 110, 111], particularly with biodiesel and its blends as engine fuels, the present work aims at evaluating performances of a single cylinder four stroke diesel engine in the light of first and second law of thermodynamics.

## 6.2 ASSUMPTIONS MADE

In the energy and exergy balance study, it is assumed that the engine operates at steady state under different fuel operations. Steady state test results consisting of fuel and air flow rate, pressure, temperature, torque, rotational speed, and exhaust emissions are used for the energy and exergy rate balances for the engine. It is also assumed that air and fuel reacts in the combustion chamber of the engine and the combustion products leave the system as exhaust gases to the atmosphere. The combustion air and the exhaust gases each form ideal gas mixtures. Further, the potential and kinetic energy effects of the incoming air and fuel and outgoing exhaust gas streams are ignored. In the exhaust gas streams, total seven species were taken into account (CO, $CO_2$, $O_2$, NO, HC, $H_2O$, and $N_2$) in the calculation of enthalpy and entropy for the purpose of first-law and second-law analyses. It is assumed that the reference environment has a temperature ($T_0$) of 298.15 K and a pressure ($P_0$) of 1 atm. Furthermore, the reference environment is considered a mixture of perfect gases with the following composition on a molar basis: $N_2$, 75.67%; $O_2$, 20.35%; $CO_2$, 0.03%; $H_2O$, 3.12%; other gases, 0.83% [63]. Ambient temperature ($T_{amb}$) is assumed to be equal to the standard environment temperature $T_0$ and energy input accompanying the incoming air stream is ignored.

## 6.3 ENERGY ANALYSIS

The detailed methodology of calculation of various terms associated with energy balance study is described in this section. Two approaches were considered for determination of exhaust gas energy viz. (i) energy balance of exhaust gas through exhaust gas calorimeter and ii) exhaust gas enthalpy approach. However the method based on exhaust gas enthalpy is preferred and employed in the present study.

Fuel input energy is the product of its flow rate and calorific value.

Fuel Energy Input (kW) = $\dot{m}_f$ × Calorific Value (6.1)

Where $\dot{m}_f$ is the fuel flow rate of the engine at a given load in kg/s.

Engine BP is calculated using equation (6.2). This was also discussed in Chapter 5.

$$BP\ (kW) = \frac{2\pi NT_q}{60000} \tag{6.2}$$

Where $N$ is the engine rpm, $T_q$ is the engine output torque (N-m) measured by the eddy current dynamometer.

Frictional power (kW), $FP = IP - BP$ (6.3)

Heat lost to water in cooling the engine (kW) is calculated using equation (6.4).

$$\dot{Q}_W = \dot{m}_{w\ engine} C_{pw} (T_2 - T_1) \tag{6.4}$$

In this equation, $\dot{m}_{w,engine}$ is the mass flow rate of engine cooling water. The volume flow rate of cooling water is measured by the rotameter (engine) and this is multiplied with the density of water to obtain $\dot{m}_{w,engine}$

$T_1$ and $T_2$ are the engine cooling water inlet and outlet temperatures respectively. $C_{pw}$ is the specific heat of water evaluated at the mean of the temperatures, $T_1$ and $T_2$. The density of water is also evaluated at this mean temperature.

(i) Energy balance in the exhaust gas calorimeter

The test engine set up is provided with facilities for calculation of the exhaust heat loss as given below.

Heat lost with exhaust gas (kW),

$$\dot{Q}_{ex} = (\dot{m}_a + \dot{m}_f) C_{pex} (T_5 - T_{amb}) \tag{6.5}$$

As can be seen, it requires the specific heat of the exhaust gas which can be calculated from an energy balance in the exhaust calorimeter as follows.

$$C_{pex} = \frac{\dot{m}_{w,cal} C_{pw} (T_4 - T_3)}{(\dot{m}_a + \dot{m}_f)(T_5 - T_6)} \tag{6.6}$$

In the above equation, $\dot{m}_{w,cal}$ is the water flow rate through the calorimeter which is measured by adjusting the flow rate of the rotameter (calorimeter). $T_3$ and $T_4$ are the calorimeter water inlet and outlet temperatures. $T_5$ and $T_6$ are the exhaust gas temperatures at calorimeter inlet and outlet respectively. Determination of exhaust gas energy using heat balance in the exhaust gas calorimeter is possible as Yuksel and Ceviz [111] also adopted this method for determination of the same, while carrying out a thermal balance study of a four stroke SI engine operating on hydrogen as a supplementary fuel. However, in the present work, it was seen that there was variation in the values of $C_{pex}$ calculated at a given load for a particular fuel. Moreover, there was uncertainty in the exhaust energy results obtained because the heat loss from the calorimeter was totally ignored in the calculation of $C_{pex}$. Besides, the exhaust losses calculated using the average specific heat values were found to be high for their use in the energy balance calculations as it led to some unrealistic results on the part of unaccounted miscellaneous losses. Therefore, the exhaust energy was calculated from the enthalpies of products following Gokalp *et al.* [64] as follows.

(ii) Exhaust gas enthalpy approach

Based on the experimental emission results obtained at various loads and considering equilibrium of these species in the combustion products, the molar based reaction equation can be expressed as follows:

$$C_x H_y O_z + \lambda(O_2 + 3.76N_2) \rightarrow a_1 CO + a_2 CO_2 + a_3 H_2O + a_4 O_2 + a_5 C_\lambda H_y + a_6 NO + a_7 N_2 \tag{6.7}$$

The values of the coefficients in equation (6.7) per mole of fuel were calculated at various loads and the exhaust energy in kW was calculated using the following equation.

$$\dot{E}_{ex} = \dot{n}_f \sum_{i=1}^{n} a_i \Delta\bar{h}_i \tag{6.8}$$

In the above equation, $\Delta\bar{h}_i$ is enthalpy change of the $i$ th product corresponding to the states of EGT and the reference temperature. This is expressed as $\Delta h = h(T) - h(T_0)$ and $\dot{n}_f$ is the molar fuel flow rate. $a_i$ is the molar amount of the $i$ th component (i.e., the coefficient of the component $i$ in the reaction equation). $n$ is the number of products considered in the exhaust

gases. The values of the coefficients for different fuels at various loads are shown in Table 6.1.

The remainder of the energy which can be found from energy balance is termed as unaccounted miscellaneous losses $(\dot{Q}_{misc})$.

Table 6.1: Values of molar coefficients at various loads (Eqn. 6.7)

| Load | Coefficients | NRL diesel | B10 | B20 | B30 | B40 |
|---|---|---|---|---|---|---|
| Full load | $a_1$ | 0.2230 | 0.2199 | 0.2619 | 0.2998 | 0.2443 |
| | $a_2$ | 13.6268 | 14.1487 | 14.4884 | 14.3392 | 13.7656 |
| | $a_3$ | 11.4004 | 11.7537 | 12.0745 | 12.4656 | 12.8931 |
| | $a_4$ | 17.4311 | 17.2635 | 16.5557 | 17.0036 | 16.5962 |
| | $a_5$ | 0.0249 | 0.0211 | 0.0324 | 0.0336 | 0.0344 |
| | $a_6$ | 0.09597 | 0.09362 | 0.09354 | 0.09520 | 0.09317 |
| | $a_7$ | 121.915 | 124.033 | 121.457 | 123.585 | 118.788 |
| 75% load | $a_1$ | 0.1743 | 0.1749 | 0.1856 | 0.2061 | 0.1869 |
| | $a_2$ | 13.4486 | 13.6439 | 14.3416 | 14.2118 | 15.1554 |
| | $a_3$ | 11.4004 | 11.7459 | 12.0893 | 12.4674 | 12.9023 |
| | $a_4$ | 25.1954 | 24.6742 | 25.2240 | 25.3858 | 26.8429 |
| | $a_5$ | 0.0249 | 0.02305 | 0.02868 | 0.03314 | 0.032428 |
| | $a_6$ | 0.09962 | 0.09816 | 0.10229 | 0.10558 | 0.10494 |
| | $a_7$ | 146.327 | 145.0869 | 148.6997 | 149.7757 | 158.77 |
| 50% load | $a_1$ | 0.2722 | 0.2488 | 0.2383 | 0.2847 | 0.2459 |
| | $a_2$ | 13.2774 | 14.3926 | 14.4292 | 14.7288 | 15.3898 |
| | $a_3$ | 11.3726 | 11.7269 | 12.1012 | 12.4686 | 12.8994 |
| | $a_4$ | 36.468 | 36.918 | 37.050 | 37.698 | 37.411 |
| | $a_5$ | 0.03184 | 0.02782 | 0.0257 | 0.032852 | 0.033156 |
| | $a_6$ | 0.07345 | 0.08880 | 0.08593 | 0.09527 | 0.09532 |
| | $a_7$ | 181.0975 | 188.6331 | 188.7654 | 193.0420 | 194.8181 |
| 25% load | $a_1$ | 0.3861 | 0.3497 | 0.3357 | 0.3874 | 0.3421 |
| | $a_2$ | 13.5790 | 15.3316 | 14.0482 | 15.2475 | 14.7675 |
| | $a_3$ | 11.3220 | 11.7043 | 12.0736 | 12.4578 | 12.8756 |
| | $a_4$ | 51.0769 | 53.9432 | 49.9672 | 54.4504 | 54.2873 |
| | $a_5$ | 0.0445 | 0.0339 | 0.0326 | 0.0355 | 0.0391 |
| | $a_6$ | 0.04712 | 0.06394 | 0.06225 | 0.06717 | 0.05306 |
| | $a_7$ | 230.7615 | 249.1289 | 229.8552 | 250.6456 | 246.2068 |

### 6.3.1 Fuel energy

The fuel energy input to the engine for the five different tested fuels at various loads is shown in Fig. 6.1. The KSOME and its diesel blends provide slightly higher energy input to the engine than NRL diesel fuel in order to produce the same BP output at different loads. This was due to higher fuel consumption in respect of the KSOME blends. Although the calorific values of the KSOME blends were less but increase in rate of fuel consumption resulted in higher fuel energy input. Due to higher fuel consumption, BTE in case of KSOME and its diesel blends were lower. This was discussed in Section 5.9.2 (A) in Chapter 5.

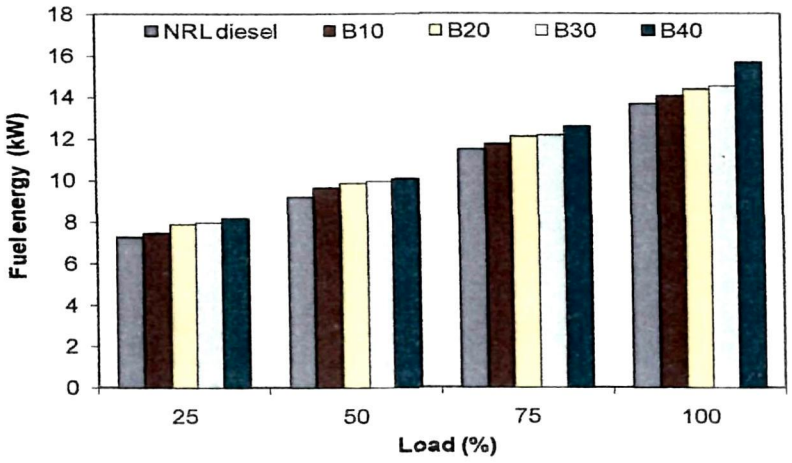


Fig. 6.1: Fuel energy input for the tested fuels at various loads

### 6.3.2 Energy loss in engine cooling

Fig. 6.2 shows the loss of energy in cooling the engine by cold water which was circulated through the engine jacket. The heat carried away by a coolant medium generally consists of heat transferred to the combustion chamber walls from the gases in the cylinder, heat transferred to the exhaust valve in the exhaust process, and a substantial fraction of the friction work [28]. It was seen that the energy lost to the coolant increases with increasing load for all the fuels. Due to burning of relatively more amount of fuel at higher load, the in-cylinder temperature increases and therefore the temperature of engine cooling water leaving the engine jacket ($T_2$) also becomes high. Since the flow rate of engine cooling water is maintained at the same level at all engine loads, therefore with increase in the value of $T_2$, the heat lost to the coolant increases. Heat lost to coolant for engine cooling was in general found to be more for the KSOME blends at all the loads. Early premixed combustion and

subsequent heat release in the late combustion phase in case of the biodiesel blends may have resulted in slightly higher overall cylinder temperatures than NRL diesel due to which more heat was absorbed by the engine cooling water. It could also be due greater radiation heat loss from the combustion gases due to presence of the soot particles. Since the energy absorbed by the coolant also accounts for the energy transferred to the lubricating oil from friction of moving engine components, higher frictional losses in case of the blends may have also added to the increase in temperature of coolant leaving the engine. However, in case of the blend B40 cooling loss was significantly less than the other fuels at 75% load and full engine load. This may be due to reduction in the cylinder temperature resulting from incomplete combustion of this particular fuel blend owing to its higher viscosity, poor atomization and lack of available oxygen for burning a rich fuel mixture. At full engine load, there was 2.89%, 4.23%, 9.37% increase in energy loss to the coolant with B10, B20 and B30, respectively as against a reduction of 4.89% in case of B40 compared to cooling loss with respect to NRL diesel. This may be noted that cooling losses may be optimized by careful control of the coolant mass flow rate.

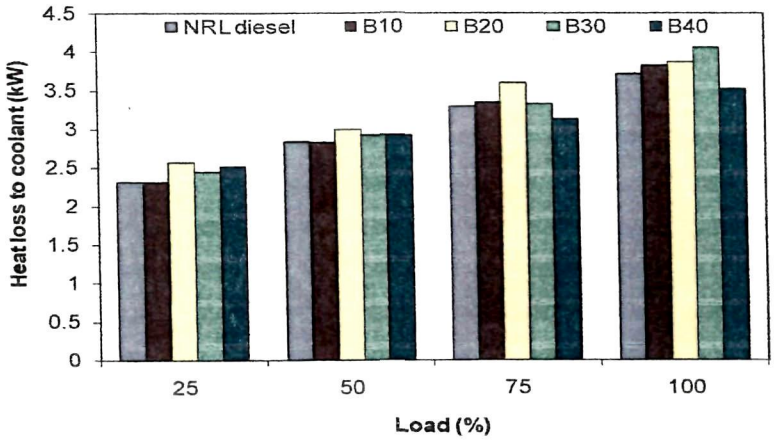


Fig. 6.2: Energy loss in cooling for the tested fuels at various loads

### 6.3.3 Exhaust energy loss

A major part of the input energy not available for useful work is the energy carried away by the exhaust gases. The energy loss accompanying the exhaust gases is shown in Fig. 6.3. There was increase in the exhaust loss with increasing load in almost all the fuel operations. With the increase in load the amount of fuel injected to the combustion chamber increases while the amount of air inducted is more or less constant with load. The heat release increases with load due to combustion of higher amount of fuel and as a result the

temperature of the products of combustion increases. Higher the temperature of combustion gases more is the EGT and hence the loss of energy accompanying exhaust gas is also more at higher engine load. It was seen that the EGT was more for the KSOME blends therefore the energy loss accompanying exhaust gas was also found to be slightly higher for the blends at 25% and 50% load. At 75% load the exhaust loss was almost the same for NRL diesel, B10 and B20. At full engine load operation, the energy loss accompanying exhaust gas was slightly more with B10 and B20 as compared to NRL diesel fuel. However, with B30 and B40 at full load engine operation, the exhaust loss decreased slightly. The calculated losses were 3.02, 3.08, 3.04, 3.00, 2.95 kW for NRL diesel, B10, B20, B30 and B40, respectively which were almost comparable even though the EGTs for the blends were more. Reduction in exhaust loss with B40 particularly at full load was mainly due to lower values of EGT and the molar coefficients of $O_2$ and $N_2$ in the combustion products as compared to the other blends. Canakci and Hosoz [63] found 13.98%, 11.86%, 12.71%, 6.35% reduction in exhaust energy loss with B100 SME, B20 SME, B100 YGME and B20 YGME with respect to No. 2 diesel (D2) at full load operation.

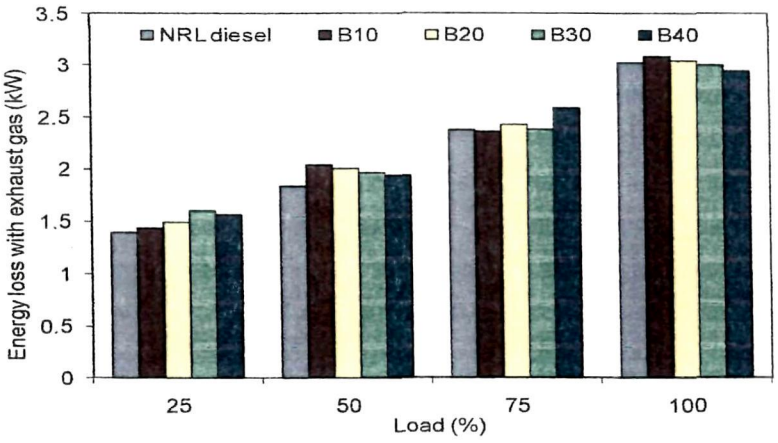


Fig. 6.3: Exhaust energy loss for the tested fuels at various loads

### 6.3.4 Energy loss in friction

This friction power is basically the difference between IP and BP. A substantial part of the friction power is dissipated between the piston and piston rings and cylinder wall and is transferred as thermal energy to the cooling medium [109]. The remainder of the friction power is dissipated in the bearings, valve mechanism, or drives auxiliary devices, and is transferred as thermal energy to the lubricating oil or surrounding environment as

unaccounted miscellaneous losses $(\dot{Q}_{misc})$. Fig. 6.4 shows the frictional power loss at various loads for the tested fuels. It was observed that the frictional power losses decrease with increase in load. When the load to the engine was gradually increased, the engine speed decreased from an average 1622 rpm at no load to 1535 rpm at full load. Since the engine speed decreases with load, therefore the friction losses are less at higher load. In the case of KSOME blends, the frictional power losses were more for the blends up to B30 at all engine loads compared to NRL diesel. This was due to higher engine IP associated with these blends as already explained in section 5.9.2 (C). However, for the blend B40, it was seen that the friction losses were significantly less over the entire load ranges. This was obvious because the engine IP produced with this fuel blend was less compared to IP produced with NRL diesel as fuel at various loads. It could be due to better lubricating property of B40 with higher amount of biodiesel in the blend. As mentioned earlier, the engine BP at a given load for different fuel operations was the same.

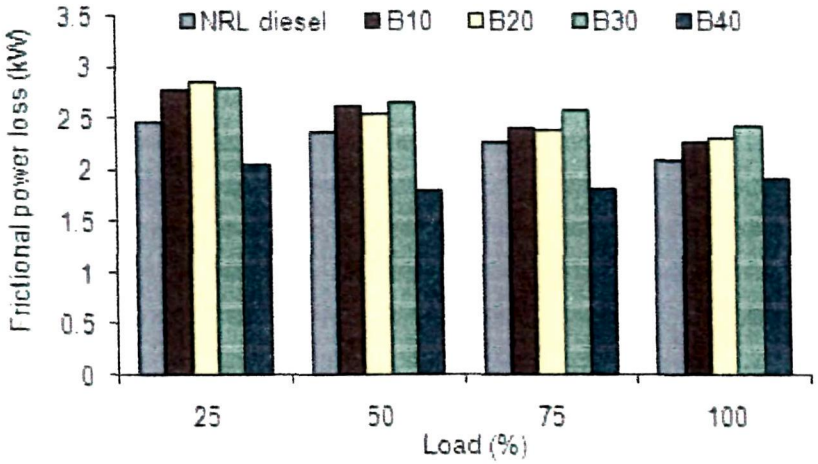


Fig. 6.4: Frictional loss for the tested fuels at various loads

### 6.3.5 Unaccounted miscellaneous losses

As stated earlier, the unaccounted losses may include thermal energy transferred to the lubricating oil or the surrounding environment due to convective and radiation heat transfer from the engine's external surface. These may also include the losses resulting from incomplete fuel combustion. These losses at various engine loads for all the tested fuels are presented in Fig. 6.5. It was observed that these losses were more in case of the KSOME blends at all the loads except for the blend B10 at 25% and 50% load and B20 at 25% load. More significantly, these losses were fairly high for the blend B40 at all engine loads.

Therefore, higher unaccounted losses in case of B40 at various loads and more particularly at full engine load imply that a significant portion of these losses may be either due to combustion inefficiency or may be due to higher convective and radiation heat transfer from in-cylinder surface. Radiation heat transfer in diesel engine is mainly from the in-cylinder soot particles and smoke opacity indicates the presence of soot particles in the exhaust gases. Since the increase in smoke opacity level for this blend was not significantly different from the other KSOME blends, the additional losses could mainly be due to inefficient combustion. Higher combustion losses as well as lower engine IP in respect of B40 clearly indicates the problem relating to the combustion of this particular KSOME blend. Unaccounted losses for NRL diesel, B10, B20, B30 and B40 at full engine load were 1.32, 1.42, 1.67, 1.55 and 3.78 kW respectively and account for 9.7%, 10.10%, 11.63%, 10.67% and 24.13% of the fuel energy input. It was also seen that these losses increased with load for all the fuels which may be due to increase in soot emission (smoke opacity) with increasing load or may be due to combustion inefficiency at higher load resulting from incomplete combustion of relatively rich fuel air mixture.

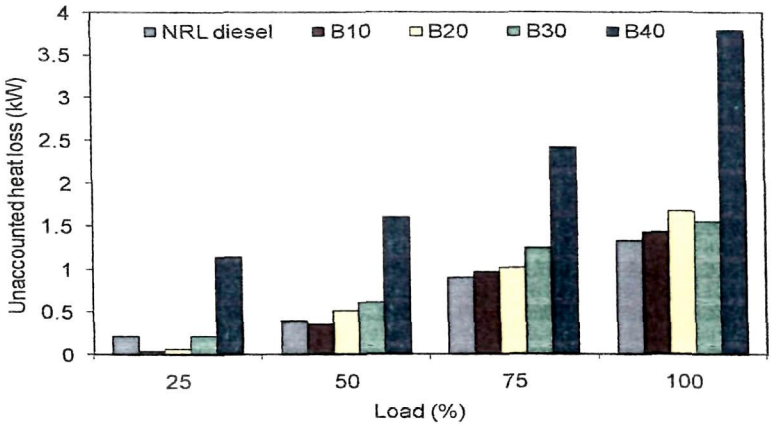


Fig. 6.5: Unaccounted heat loss for the tested fuels at various loads

In Sections 6.3.2-6.3.5 so far, a comparative analysis of the various losses for engine operation with NRL diesel and KSOME blends was made. As the fuel energy input for NRL diesel and the KSOME blends was different, so, all these losses for a particular fuel can be shown as percentage of its fuel energy input. Fig. 6.6 shows the distributions of the fuel energy specifically at full load. Energy loss due to cooling was less in case of B40. Exhaust loss as percentage of fuel energy decreased with increasing biodiesel content. Percentage unaccounted heat loss was however more in case of KSOME blends and more specifically in case of B40.

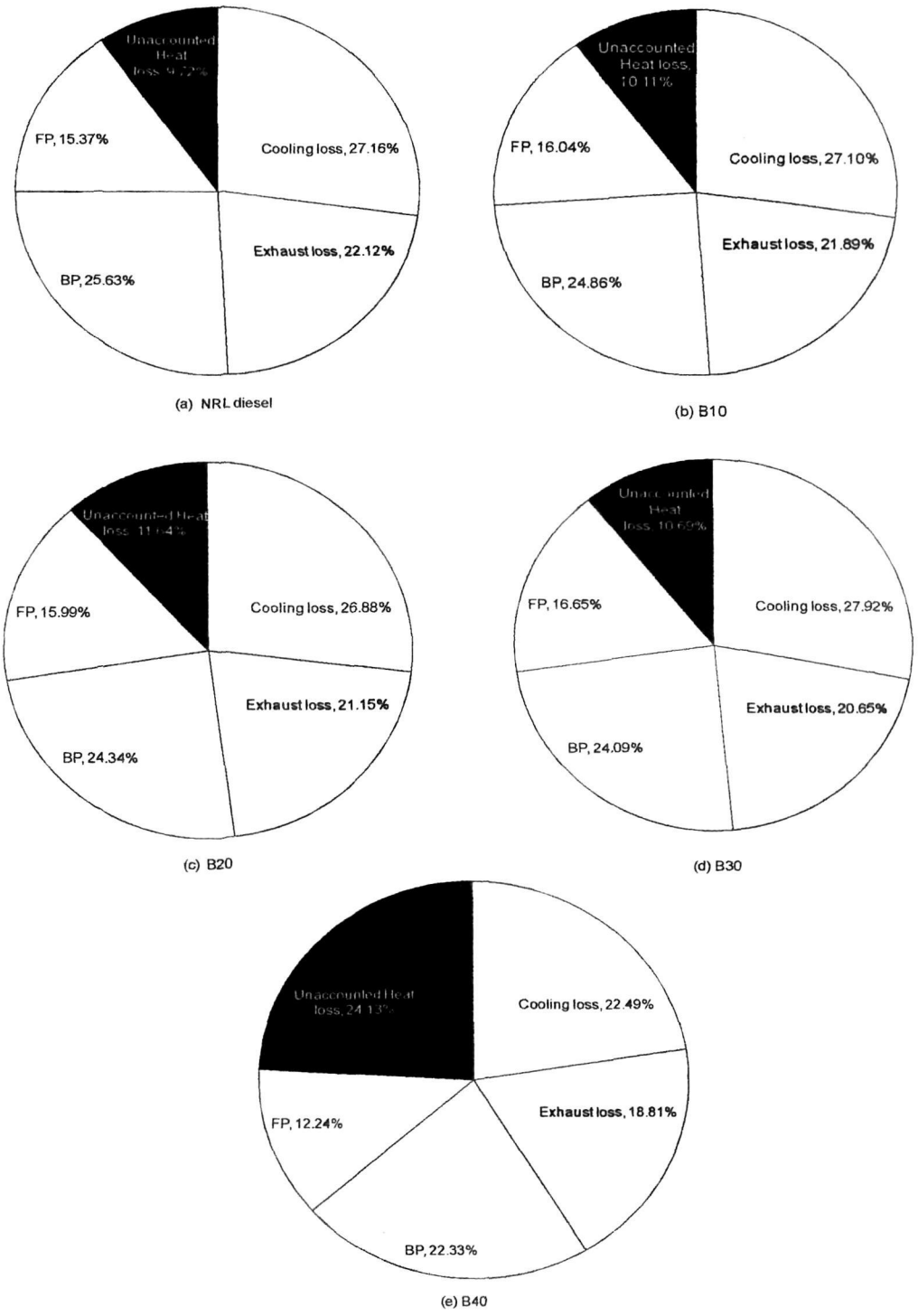


Fig. 6.6: Distribution of fuel energy at full load

### 6.3.6 Combustion efficiency

Another important criterion that measures the energetic performance of an engine is the combustion efficiency. Chemical energy of fuel is not fully released during the

combustion process and hence it is important that the combustion efficiency needs to be evaluated. Presence of smoke and other incomplete combustion products such as unburned hydrocarbon, carbon monoxide in the engine exhaust gases represent combustion inefficiency. Considering the engine as an open system involving work and heat transfer with the surrounding, the combustion efficiency is defined as [28],

$$\eta_c = \left| \frac{\bar{h}_P - \bar{h}_R}{LHV} \right| \tag{6.9}$$

$$\text{and } \bar{h}_P - \bar{h}_R = \sum_{i,products} a_i \left( \bar{h}_f^0 + \Delta\bar{h} \right) - \sum_{i,reactants} a_i \left( h_f^0 + \Delta h \right) \tag{6.10}$$

where, $\bar{h}_P$ and $\bar{h}_R$ are the enthalpies of the products and reactants per mole of fuel respectively. $h_f^0$ is the standard enthalpy of formation of the species in the products and the reactants. Enthalpy of formation of certain compounds is available in thermodynamics property table. However, enthalpy of formation of various fuels is determined from its enthalpy of combustion and it is usually the LHV, which is known. This is defined as the difference between the enthalpy of the products and reactants in the general stoichiometric reaction equation at the reference pressure and temperature. Combustion efficiency defined in this form takes into account not only the power output but also the rate of heat transfer.

Fig. 6.7 shows the combustion efficiency at various engine loads for the tested fuels. Combustion efficiency for engine operation with the biodiesel blends was higher for the blends B10, B20 and B30 at various loads compared to that of NRL diesel except for the blend B30 at full load. A marked reduction in combustion efficiency was observed in case of the blend B40 at all the loads. At full load, the combustion efficiency was slightly more for B10 and B20 while it was less for B30 and B40. The values of combustion efficiency at full load for NRL diesel, B10, B20, B30 and B40 are 87.30%, 88.00%, 87.97%, 85.28% and 81.92% respectively. Possible incomplete combustion with B40 was stated to be the reason of lower cumulative heat release, IP and BTE earlier which is now confirmed by evaluating its combustion inefficiency. Canakci and Hosoz [63] however, reported higher combustion efficiency at full load operation with pure B100 SME, B100 YGME, B20 SME, and B20 YGME compared to D2 fuel. Combustion efficiency depends upon the enthalpy difference per mol of fuel and lower heating value of the fuel in kJ/mol. Higher combustion efficiency in case of the blends up to B30 was due to increase in the enthalpy difference of the product and reactants relative to the increase in the fuel lower heating value in kJ/mol. Although the

LHV of the KSOME blends was less and decreased with increasing proportion of KSOME in the blend; but due to their higher molecular weight, the LHV in kJ/mol was more for the blend. Lower combustion efficiency in case of B40 could be attributed to its higher viscosity, poor atomization and lower volatility.

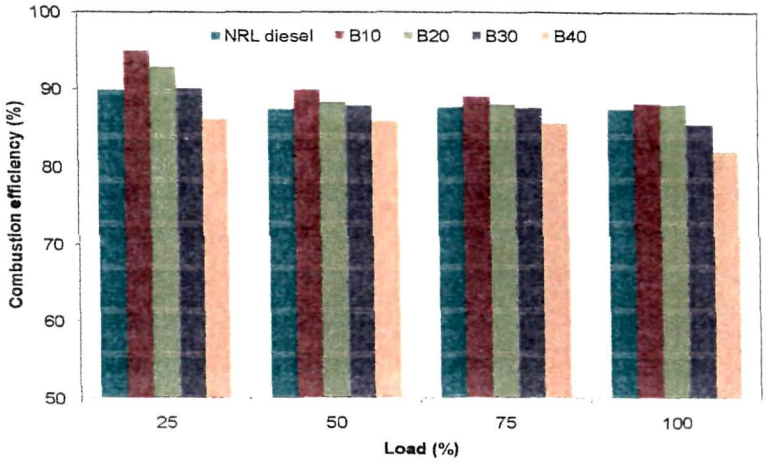


Fig. 6.7: Combustion efficiency for the tested fuels at various loads

## 6.4 EXERGY ANALYSIS

In the exergy analysis, focus is given on calculation of both thermo-mechanical and chemical exergy of the constituents of the exhaust gases and the fuels. Besides, exergies accompanying heat transfer is also calculated. Exergy of power is equal to the magnitude of power itself regardless of the temperature and pressure of the environment. The specific chemical exergies of liquid fuels can be evaluated from the following equation on a unit mass basis [63] while the thermo-mechanical exergy of the fuels are considered to be zero.

$$b_f^{ch} = |LHV| \left[ 1.0401 + 0.1728\frac{h}{c} + 0.0432\frac{o}{c} + 0.2169\frac{s}{c}\left(1 - 2.0628\frac{h}{c}\right) \right] \qquad (6.11)$$

where, $h$, $c$, $o$, and $s$ are the mass fractions of hydrogen, carbon, oxygen and sulphur respectively. The chemical exergy of NRL diesel and various KSOME blending were computed using equation (6.11) multiplied with corresponding fuel flow rate. Since the state of air entering the engine's combustion chamber is close to the reference state, it is assumed that it is in thermal, mechanical and chemical equilibrium with the reference environment and both the thermo-mechanical and chemical contributions to exergy are equal to zero. The specific flow exergy of exhaust gas can be expressed as sum of the thermomechanical and the chemical exergy as follows.

$$b_{ex} = b^{tm} + b^{ch}$$

where, $b_{ex}$ is the specific flow exergy of exhaust gas.

Thermo-mechanical exergy of the exhaust gases (ideal gas mixture) at the temperature $T$ and pressure $p$ and containing $n$ components is given by

$$b^{tm} = \sum_{i=1}^{n} a_i \left[\bar{h}_i(T) - \bar{h}_i(T_0) - T_0\left(\bar{s}_i(T) - \bar{s}_i(T_0)\right)\right] \tag{6.12}$$

On further simplification

$$b^{tm} = \sum_{i=1}^{n} a_i \left[\bar{h}_i(T) - \bar{h}_i(T_0) - T_0\left(\bar{s}_i^{\,0}(T) - \bar{s}_i^{\,0}(T_0)\right) - \bar{R}\ln\frac{p}{p_0}\right] \tag{6.13}$$

where, $\bar{s}_i^{\,0}$ is the absolute entropy at the standard pressure, and $\bar{R}$ is the universal gas constant. On the other hand, the chemical exergy of the exhaust gas constituents can be found out using equation (6.14).

$$b^{ch} = \bar{R}T_0 \sum_i a_i \ln\frac{x_i}{x_i^0} \tag{6.14}$$

This is a simplified form of equation (2.10) mentioned in Chapter 2.

The maximum amount of power that can be extracted from the exhaust gas stream at the specified condition is found out using equation (6.15) given below.

$$\dot{B}_{ex} = \dot{n}_f b_{ex} \tag{6.15}$$

where, $\dot{n}_f$ is molar fuel flow rate.

The general exergy balance relations for an open system undergoing any process where work, heat and mass transfers across the system boundary occur can be written as:

$$\Delta B = B_{in} - B_{out} + B_{heat} - B_{work} - B_{destroyed} \tag{6.16}$$

and $$\Delta B = B_2 - B_1 \tag{6.17}$$

where $B_{in}$ and $B_{out}$ represent exergy transfers into and out of the system across the boundary due to mass influx and efflux respectively. $B_{heat}$ is the exergy transferred accompanying heat transfer, $B_{work}$ is the exergy transfer with work and $B_{destroyed}$ is the exergy which is destroyed due to system irreversibility. $B_1$ and $B_2$ are the total system exergy at the initial and final states, respectively. For a closed system, the exergy terms $B_{in}$ and $B_{out}$ should be omitted from equation (6.16). The equation (6.16) in the rate form can be expressed as:

$$\frac{dB_{CV}}{dt} = \sum_{in} \dot{m}_{in} b_{in} - \sum_{out} \dot{m}_{out} b_{out} + \sum_{J} \left(1 - \frac{T_0}{T_J}\right) \dot{Q}_J - \left(\dot{W} - p_0 \frac{dV_{CV}}{dt}\right) - \dot{B}_{destroyed} \quad (6.18)$$

where, the terms $b_{in}$ and $b_{out}$ refer to the flow exergy of the incoming and the outgoing stream in the cylinder per unit mass of flow rate, respectively. $T_J$ indicates the absolute temperature at the location on the boundary where the heat transfer occurs. The term $\left(1 - \frac{T_0}{T_J}\right)\dot{Q}_J$ gives the rate of exergy accompanying heat transfer. $\dot{W}$ and $p_0 \frac{dV_{CV}}{dt}$ are the terms corresponding to work transfer. $\dot{B}_{destroyed}$ represents the rate of exergy destroyed due to irreversibilities. Finally, the exergy rate balance for the engine operating at a steady state can be expressed as:

$$0 = \sum_{in} \dot{m}_{in} b_{in} - \sum_{out} \dot{m}_{out} b_{out} + \sum_{J} \left(1 - \frac{T_0}{T_J}\right) \dot{Q}_J - \dot{W} - \dot{B}_{destroyed} \quad (6.19)$$

The above equation in a simplified form can be written as:

$$0 = \dot{m}_f b_f^{ch} - \dot{B}_{ex} + \left(1 - \frac{T_0}{\overline{T}_W}\right) \dot{Q}_W + \left(1 - \frac{T_0}{\overline{T}_W}\right) \dot{Q}_{misc} - IP - \dot{B}_{destroyed} \quad (6.20)$$

The absolute temperature at the location on the boundary, where the heat transfers occur, is considered as the mean coolant temperature and calculated as

$$\overline{T}_W = \frac{T_1 + T_2}{2}$$

The values of $\overline{T}_W$ at various loads and for the various fuels are shown in Table 6.2.

Table 6.2: Mean coolant temperature in Kelvin at various loads

| | Temperature, K | | | | |
|---|---|---|---|---|---|
| Load | NRL diesel | B10 | B20 | B30 | B40 |
| 25% | 302.295 | 302.695 | 299.420 | 301.485 | 300.955 |
| 50% | 303.305 | 302.760 | 300.405 | 302.190 | 301.865 |
| 75% | 303.925 | 302.880 | 301.710 | 302.740 | 301.840 |
| Full | 304.485 | 304.000 | 302.280 | 303.795 | 301.455 |

The exergetic efficiency of the engine is the ratio of BP output to the fuel exergy input.

The energetic performance of the engine operated with NRL diesel and various KSOME blends at various engine loads has already been explained while discussing IP and BTE in Chapter 5 and also discussed are the various losses in section 6.3 in this Chapter. The results of exergetic performance of the engine are discussed in the following subsections.

### 6.4.1 Fuel exergy

The chemical exergy of the fuels at various engine loads is shown in Fig. 6.8. Fuel exergy was more for the KSOME blends than NRL diesel at all loads. This was due to presence of higher carbon, hydrogen atoms and additional oxygen atoms in the blended biodiesel which together with the higher fuel flow rate in respect of the blends ultimately gave higher fuel exergy for the blends. Fuel exergy inputs were 6.34%, 6.39%, 6.44%, 6.49% and 6.54% higher than the corresponding fuel energy inputs of NRL diesel, B10, B20, B30 and B40 respectively at all the loads.

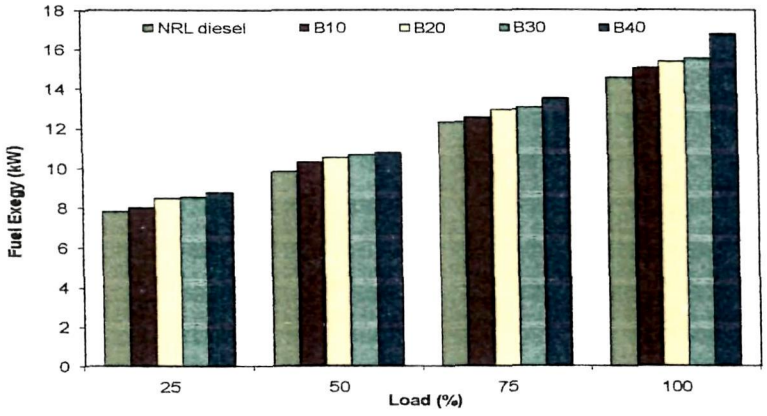


Fig. 6.8: Fuel exergy at various loads

### 6.4.2 Exergy loss with heat transfer

Fig 6.9 shows the exergy loss with heat transfer from the engine. More the rate of heat rejection more is the exergy loss with heat transfer. It depends upon the cylinder wall temperature, the higher the temperature of the engine surface from where heat loss occurs, the higher is the exergy loss accompanying it. The total heat loss i.e. the sum of heat loss to engine cooling water and the unaccounted heat loss was more in case of the KSOME blends except for the blend B10 at 25% and 50% load which can be seen in Fig. 6.2 and Fig. 6.5. It was also seen that the loss of exergy with heat transfer in case of the KSOME blends were in general less compared to that in case of NRL diesel. The exergy of heat transfer for the blends B10 and B40 at 25% load, B40 at 50% load, B30 at full load were almost same with

that of NRL diesel at the respective engine loads. For the blend B20 at all engine loads, the exergy of heat transfer was the least and this was due to cylinder wall temperature which was slightly less in respect of this blend at all the loads as compared to the other fuel blends. Although the total heat loss was more for the KSOME blends, lower exergy of heat transfer was due to lower cylinder surface temperature in respect of the biodiesel blends. Same was the reason that exergy of heat transfer was the minimum for the blend B20. The test diesel engine set up used in the present study was a small single cylinder four stroke engine with a rated power of 3.5 kW, therefore the exergy loss with heat transfer was not so significant as opposed to results presented in [63, 64]. In these two works, the test engines used for experimentation were four cylinder four stroke diesel engines having different configuration and the engine rated powers were 57.1 kW and 40 kW respectively.

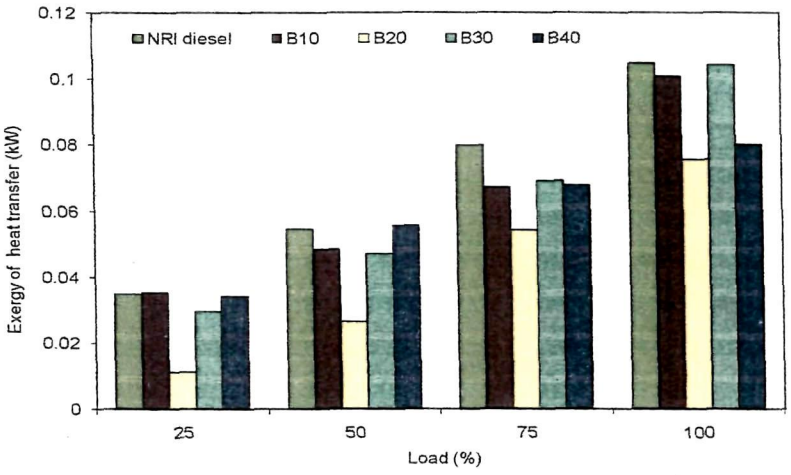


Fig. 6.9: Exergy of heat transfer at various loads

### 6.4.3 Exhaust exergy

Exergy loss accompanying exhaust gas for different fuel operations at various engine loads is shown in Fig. 6.10. The exhaust exergy losses for the KSOME blends were marginally higher in comparison to that of NRL diesel at all engine loads. However, no specific trend of change with increasing biodiesel concentration in the blend was observed. Higher exhaust exergy in case of the KSOME blends was due to higher EGT for the biodiesel blends. The enthalpy of exhaust gas constituent's increases with the increase in EGT. It was also due to combination of factors such as (i) higher values of the coefficients (Table 6.1) which were used in the calculation of thermo-mechanical and chemical exergy of the exhaust gases and (ii) higher molar fuel flow rate in respect of the blends. The molar specific thermo-

mechanical and chemical exergy values for various fuels at full load are shown in Table 6.3 below. It was seen that thermo-mechanical and chemical exergies in case of the KSOME blends up to B30 were more compared to NRL diesel. These exergy values however reduced in case of the blend B40 which again could be due to lower EGT value for this blend at full load compared to the other blends. Moreover, loss of exhaust exergy increases with load which is again due to higher EGT at increased load. Higher EGT resulted in increase of $h_i(T) - h_i(T_0)$ and $s_i^0(T) - s_i^0(T_0)$ values for the different exhaust gas constituents and the chemical exergy values.

Table 6.3: Molar specific themo-mechanical and chemical exergy of various fuels at full load

| Exergy | NRL diesel | B10 | B20 | B30 | B40 |
|---|---|---|---|---|---|
| $b^{tm}$ (kJ/mol) | 499186.8 | 519235.7 | 533353.8 | 543628.3 | 512695.4 |
| $b^{ch}$ (kJ/mol) | 175462.3 | 183363.0 | 188713.7 | 187712.4 | 181908.5 |

Similarly at full load, the exhaust exergy values with NRL diesel, B10, B20, B30 and B40 were 1.290 kW, 1.329 kW, 1.337 kW, 1.309 kW and 1.282 kW respectively with insignificant variation. It is seen that exhaust exergy in KW is less in case B40 compared to that of NRL diesel. Canakci and Hosoz [63] also found the same exhaust exergy of 14.9 kW each with D2 and B20 YGME; and 15 kW each for B100 SME, B20 SME and B100 YGME respectively at full load. Higher exhaust exergy values reported in their results compared to the results presented in this thesis is obvious from the point of view that they used multi-cylinder engine of larger size. Gokalp *et al.* [64] reported exhaust exergy values of 12.04 kW, 12.12 kW, 12.17 kW and 13.64 kW respectively for B5 SME, B20 SME, B50 SME and B100 SME against an exergy value of 11.73 kW with D2 for full load operation of the test engine at 1600 rpm. Exhaust exergy was more in case B100 SME and it increased with increasing concentration of SME in the blend. Higher exhaust exergy loss with higher blending and pure SME was attributed to higher EGT as a result of longer ignition delay and slower combustion in case of biodiesel due to its lower cetane number. Ignition delay, however with KSOME blends was less due to oxygenated nature of the blends and its higher cetane index. Higher EGT in case of KSOME blends were already explained in Chapter 5 [Section 5.9.2 (D)] which was explained to be due to higher amount of heat release in late

combustion phase. Loss of exhaust exergy, therefore, depends upon EGT. To some extent, it also depends upon the concentration of unburned combustion products in the exhaust gas.

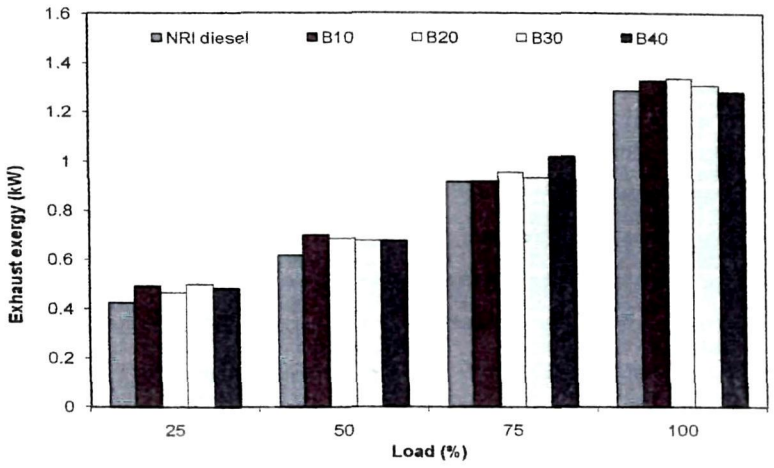


Fig. 6.10: Exhaust exergy at various loads

### 6.4.4 Exergy destruction by mixing and combustion

The rate of exergy destructed with various fuels at different engine loads is presented in Fig. 6.11. It is seen that the exergy destroyed with the fuels increase with increasing load. It was observed that the exergy destroyed in case of engine operation with the KSOME blends was more compared to NRL diesel fuel operation at all engine loads, with an exception in case of B10 at 25% load. Exergy destruction also increased with increasing biodiesel in the blend at various loads. The most important observation was the rate of exergy destroyed for operation with B40 which was the maximum at all loads. Since the exergy of IP was the minimum at various loads with B40 and also the fuel exergy input being higher for this particular blend, therefore it resulted in higher destruction of exergy. Canakci and Hosoz [63] however found lower exergy destruction with B100 SME, B100 YGME, B20 SME and B20 YGME. Gokalp et al. [64] observed higher exergy destruction with B5 SME compared to that of D2 and exergy destruction was comparatively less for B20 SME, B50 SME, and B100 SME. Similarly the exergy destruction was more in case B5 SME and B20 SME when it was blended with marine fuel (MF), while it was lower in case of B50 SME and B100 SME compared to that of MF. Moreover the variation of fuel exergy and exergy destruction with biodiesel addition to D2 and MF was the same. In the present study too, fuel exergy was more in case of the KSOME blends at various load and hence, the exergy destruction was also more in case of the KSOME blends. But compared to the fuel exergy

input, exergy destruction was relatively higher and it was the maximum in case of B40. The rate of exergy destroyed in a process represents the irreversibility associated with it. Hence, there is scope of further improvement in case of fuel operation with the KSOME blends. The exergy destroyed with heat transfer and friction being calculated separately, the exergy destruction described in this section represents the rate of exergy destroyed mainly due to irreversibility of phenomenon of air fuel mixing and combustion.

Biodiesel has a lower calorific value than petro-diesel; fuel consumption of engine operated with biodiesel is more. Different physical properties, most notably viscosity alters fuel atomization and combustion behavior. These are some the factors that intensifies the need for efficient design with biodiesel fuel operation. Once fuel is released from an injection nozzle, its combustion efficiency is influenced by the droplet size. Fuel injector with a given design using higher viscosity fuel produces droplets of bigger diameters. However, smaller droplets vaporize more quickly than larger ones, so they generally enable more rapid and efficient combustion. Incomplete combustion with B40 due to its higher viscosity was confirmed from its lower combustion efficiency; also the unaccounted heat loss and exergy destruction by mixing and combustion was more for this particular fuel blend. Higher injection pressure should be employed so that the injected liquid fuel jet can enter the combustion chamber with high velocity. This will help in early atomization of the fuel jet into small sized droplets to enable rapid evaporation and also to traverse the combustion chamber in the time available and fully utilize the air charge. On the other hand, proper air fuel mixing is sensitive to the nature of in-cylinder gas motion which is strongly influenced by the configuration of both the induction system and the combustion chamber. In larger engines mixing rate requirements are least stringent and additional organized motion is not required. However in case of engines of smaller size, increasing amounts of air swirl are required to achieve adequate fuel distribution and faster mixing of fuel with the air. Air swirl can be generated by suitable design of the inlet port (e.g. deflector wall port, helical port) and using bowl-in-piston type of combustion chamber. The test engine which was used for experimentation in the present study has a piston bowl (hemisphere; 52 mm diameter) type of combustion chamber and the injection system comprises of a single cylinder fuel pump with a multi hole nozzle (3 Orifice) having nozzle diameter of 9.2 mm and length of 17 mm respectively. Use of proper inlet manifold and swirl combustion chamber in the test engine that would generate swirl during induction and combustion could be a solution of improper mixing of air and fuel in case of higher percentage blend or neat biodiesel. Nozzle orifice

diameter also plays a major role in the spray combustion characteristics. The fuel injection rate and hence the total mass of injected fuel increases with increase in orifice diameter. With a smaller orifice, smaller liquid penetration length can be achieved thus decreasing the chances of piston and wall impingements. The fuel evaporation is also enhanced around the end of injection with orifice of smaller diameter. Hence, nozzle with smaller orifice could be tried for enhancement of fuel evaporation. Canakci and Hosoz [63] recommended for preheating of combustion air and reduction in excess air as a measure to reduce exergy destruction with combustion, however at the same time, also opined that any such attempt would lead to increase in EGT which in turn may increase the exhaust energy, exergy and heat transfer.

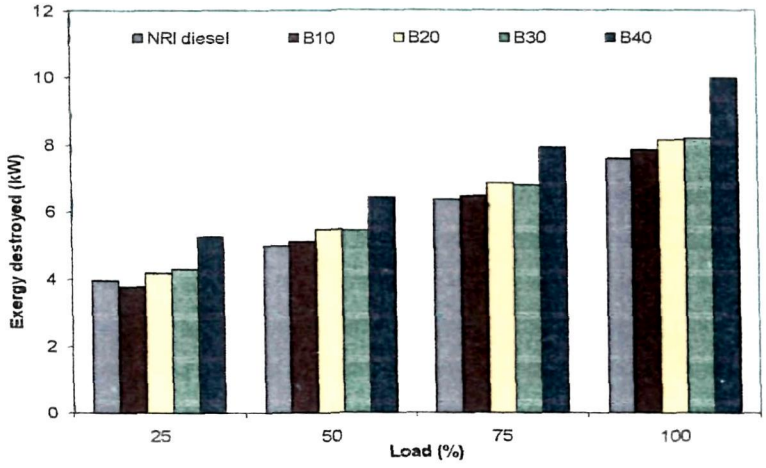


Fig. 6.11: Exergy destruction with different fuels at various loads

### 6.4.5 Exergetic efficiency

The exergetic efficiency at various engine loads for the fuels is presented in Fig. 6.12. Since fuel exergy input was higher compared to the fuel energy input in case of all the fuels at various loads, therefore the exergetic efficiencies are lower than the corresponding energetic first law efficiencies (BTEs). At full engine load operations with NRL diesel, B10, B20, B30 and B40, the exergetic efficiencies were 6.29%, 6.36%, 6.40%, 6.44% and 6.50% lower than the corresponding BTEs. The percentage reductions at the other loads were also almost in the same range. It is the exergetic efficiency that provides a better measure of the performance for a thermal system. Therefore lower exergetic efficiency in case of the KSOME blends at all the loads and particularly with B40, clearly indicates the room for improvements in the system operations with the biodiesel blends.

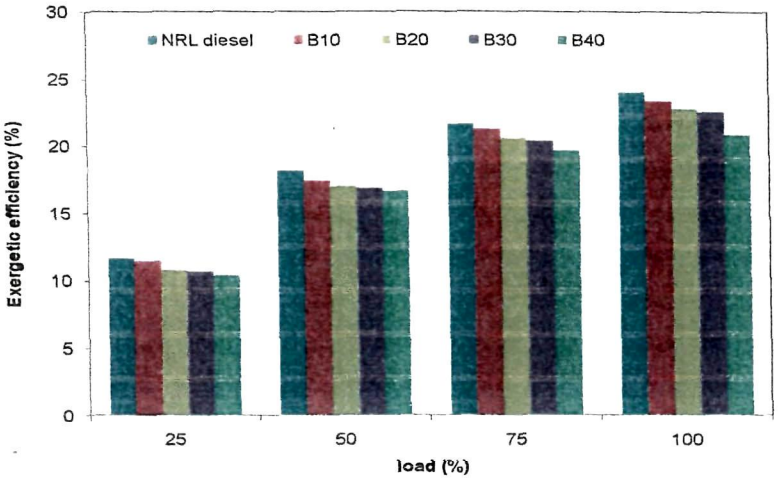


Fig. 6.12: Exergetic efficiency for the tested fuels at various loads

### 6.4.6 Exergy distributions at full load

Fig. 6.12 shows the distributions of the fuel exergy for NRL diesel and the KSOME blends at full load. Exhaust exergy in percentage was marginally less for the biodiesel blends at full load. The percentage exergy destruction was more in case of KSOME blends and particularly for B40. In case of B40, it accounts for 59.57% of fuel exergy as compared to 52.01% corresponding to that of NRL diesel. This was the reason that exergetic efficiencies were less for the biodiesel blends compared to NRL diesel. Fuel exergy input was the maximum for B40 and destruction of a major part fuel exergy clearly indicates the inefficiency of engine operation with this particular biodiesel fuel blend.

It can be mentioned that the energy and exergy analyses on diesel engine operations with biodiesel fuel blends presented in this chapter was based on experimental performance and emission results obtained from the fully automated engine test set up.

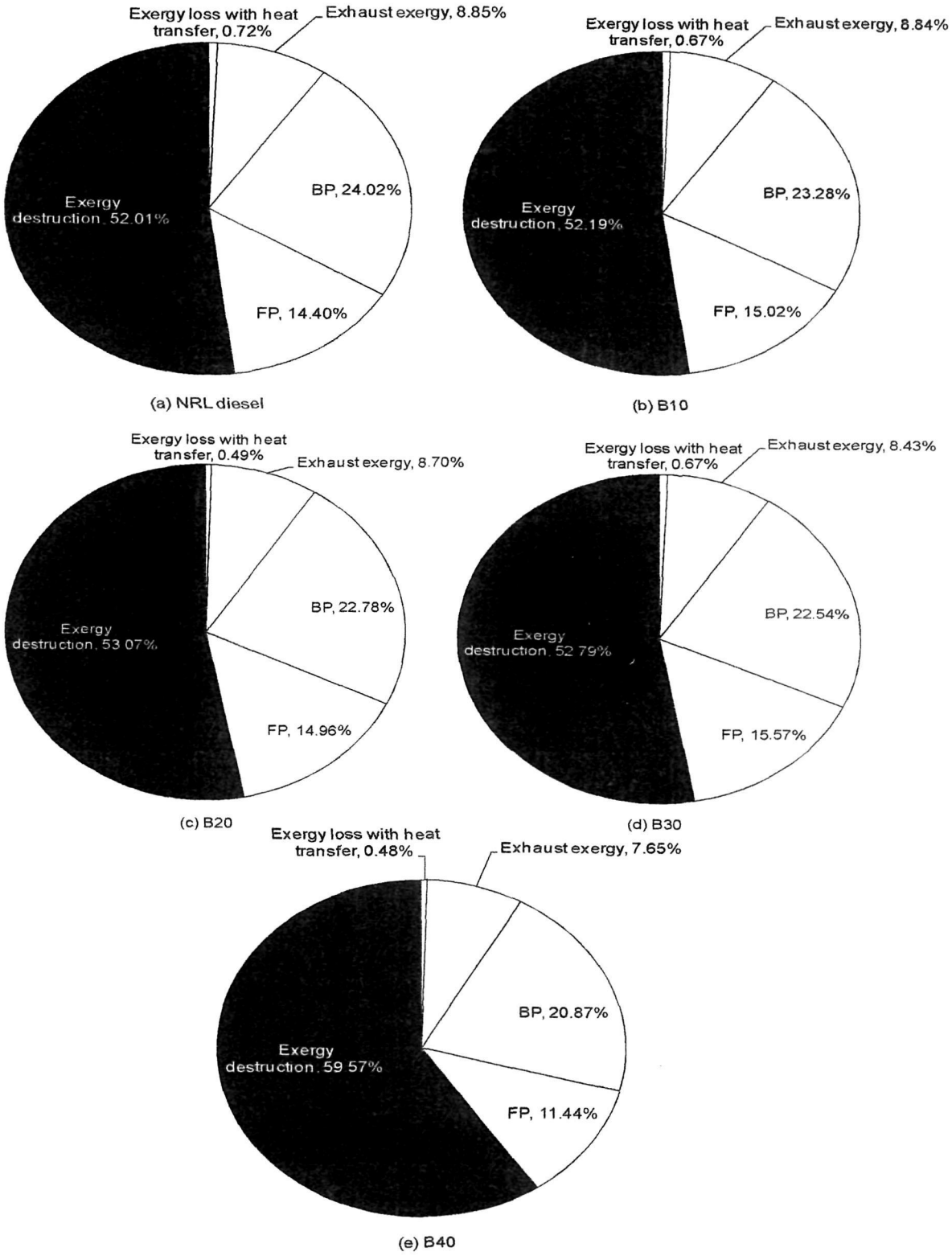


Fig.6.13: Distribution of fuel exergy at full load

# CHAPTER 7

# MODEL RESULTS AND VALIDATION

## 7.1 INTRODUCTION

The diesel cycle simulation models that have been developed for the present work are detailed in Chapter 3. Model I was developed initially to study the effect of variation of engine speed and CR on power and efficiency with diesel and various blends of diesel and biodiesel viz. B20, B40 and B60 as fuels. The speed was varied from 800 to 1800 rpm and the CR from 12 to 18.5.

However, certain modifications were done to this model afterwards. For instance, the simple Wiebe function was used in Model I for calculation of heat release rate due to combustion of fuel, but the simple Weibe function is replaced by the double Wiebe function in Model II. Similarly for the calculation of pressure and temperature during the compression and the expansion phase, the procedure outlined by Rakopoulos et al. [71] has been followed in Model II. This has been discussed in section 3.4.3 in chapter 3. Whereas these were calculated in Model I simply by using the polytropic relations of pressure and temperature with cylinder volume and considering a pressure drop due to heat transfer given by equation (3.16) in Chapter 3. Further, the relative air fuel ratio was considered to be 1.5 for all the fuels at all speeds in Model I, although in the real engine situation it varies with fuel, speed and other operating parameters. These issues are taken care of in Model II. Moreover, the cycle simulation Model II has been used to investigate the effect of variation of load at a fixed CR of 18. Because the diesel engine set up which was used for experimentation had the provision for changing the load from no load to full load and the engine was run with fuels such as NRL diesel and the biodiesel blends viz. B10, B20, B30 and B40 at a fixed CR of 18. Air fuel ratio (AFR) for a particular fuel at a given load is known from experiment. The stoichiometric AFR was calculated from the chemical reaction involving the given fuel. Thus, the RAF for the fuel at the given load was determined and was given as input to the model to take into consideration the effect of load to the engine.

Comprehensive experimental tests for validation of Model II were carried out and the detailed experimental results were presented and discussed in Chapter 5. Simulation results of Model I and Model II along with comparison of results of Model II with experiment have been presented and discussed in this chapter. Parameter identification process has an

important role in the overall model structure. For the purpose of Model II, model inputs were derived from experimental data and relevant parameters used in the various sub-models were identified and computed using experimental data and discussed in this chapter.

## 7.2 RESULTS AND DISCUSSION FOR MODEL I

### 7.2.1 Effect of speed on brake power

Figs. 7.1–7.3 show the variations of BP with speed for CR 14, 15.5 and 17.5. The results show that BP increases with the increase in speed for all the fuel, the peak power occurs at a particular speed and further increase in speed results in decrease of BP. Peak power at a particular speed is a characteristic of diesel engine. At speeds above the one at which peak power occurs, the frictional losses increase very rapidly and hence the BP decreases. From the figures, increased BP is evident in case of the blends B40 and B60. The BP output in case of the blend B20 is slightly lower than diesel at all speeds and CR. Rehman et al. [112] also on a variable speed TD43F engine obtained higher performance with Karanja methyl ester and its blends B40 and B60 and lower BP in case of B20. According to their report, the increased power in case of the blends B40 and B60 was due to complete combustion of oxygenated fuel, and the lower power output in case of B20 was due to increased viscosity and presence of relatively less oxygen. However, they varied the speed from 1200 rpm to 2400 rpm and the power values were found at a CR of 18. Moreover, the engine design parameters were also different from the ones that are considered in the present study. Fig. 7.1 presents that at CR 14, the peak power occurs at 1400 rpm for all the fuels. The peak power values for diesel, B20, B40 and B60 are 4.321, 3.954, 4.366, and 4.961 kW respectively. Fig. 7.2 shows that at CR 15.5, the peak power occurs for diesel, B20 and B60 at 1400 rpm and for B40, it occurs at 1500 rpm. At CR 17.5 (Fig. 7.3.), the peak power values occur at 1500 rpm for diesel (4.69 kW), B20 (4.517 kW), B40 (4.927) with peak BP values within the bracket, except for B60, it occurs at 1400 rpm (5.512 kW). From analysis of the model results it was found that the increased power with B40, B60 is due to increase in the combustion and expansion works and reduction in the compression work. As a result, the net work done during the cycle increases and hence, the power increases. The net work done during the cycle is the sum of the combustion and expansion work minus the compression work and the loop work (work done during the gas exchange process). In the model, early injection was considered for the biodiesel blends because the injection timing is advanced due to higher sound velocity and bulk modulus of biodiesel at low pressure [113]. At 1500

rpm and CR of 17.5, the injection timing for diesel, B20, B40 and B60 were considered 17, 18, 19 and 20° CA before TDC respectively. Higher cetane number of the blends led to the decrease of ignition delay and with slightly more combustion durations [114]; this ultimately resulted in higher combustion work in case of the blends (B40 and B60). It can also be seen from Fig. 7.4 and Fig. 7.5 that the gas temperature is more during combustion in case of the blends and hence it results in a higher pressure during the combustion phase except for the blend B20 that shows slightly less pressure in the later stages of combustion. This is the reason that combustion works were more in case of the blends. For B40 and B60, the combustion works were 514.829 and 529.244 J at 1500 rpm and at CR 17.5 as against 505.358 J with respect to diesel. For B20 it was slightly less than diesel. The expansion works predicted for diesel, B20, B40, B60 were 381.381, 380.132, 392.606, 415.718 J respectively. Slightly less BP in case of the blend B20 was due to reduced combustion and expansion work.

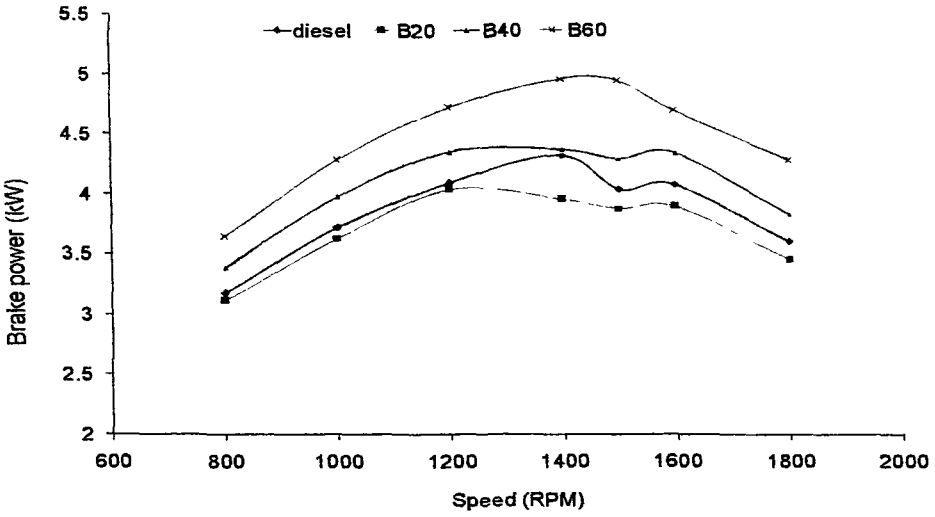


Fig. 7.1: BP vs. speed at CR 14

BP increases with speed for all the fuels up to a certain limit and then decreases, as a general trend for all the fuels, as expected. However, it is observed from the figure that the BP output decreases locally in and around a speed of 1400 rpm for diesel, B20 and B40. For each fuel, a combustion completeness parameter '*a*' was chosen in the model for determining the heat release. It is quite possible that a proper tuning of the parameter '*a*' could remove this kink in the graph which needs further investigation.

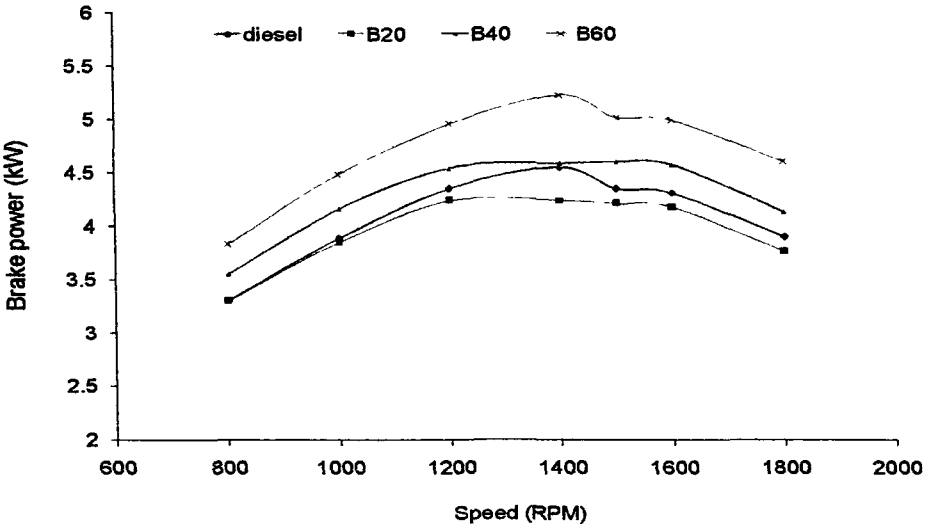


Fig. 7.2: BP vs. speed at CR 15.5

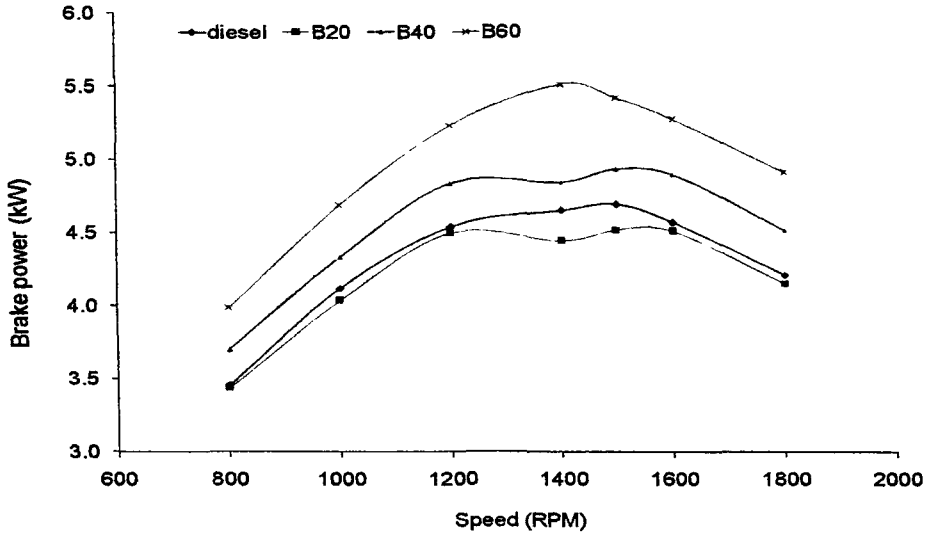


Fig. 7.3: BP vs. speed at CR 17.5

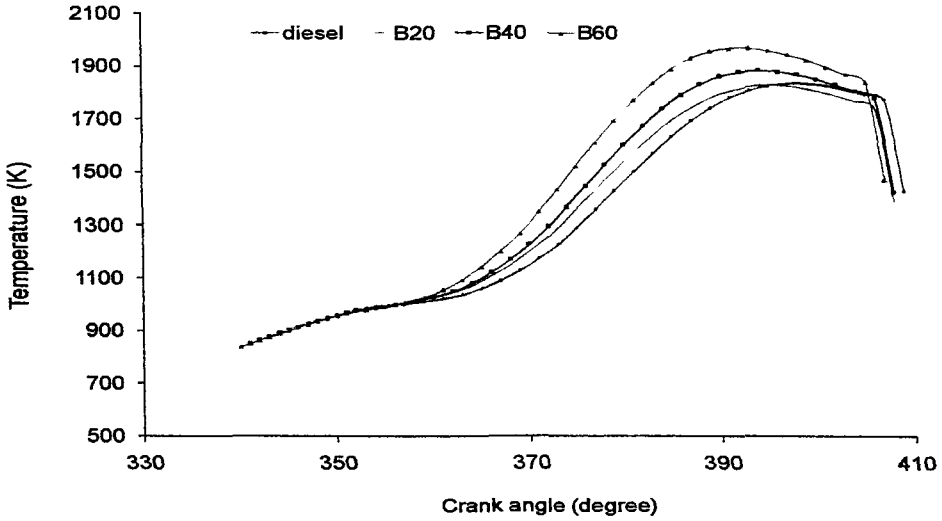


Fig. 7.4: Temperature vs. crank angle during combustion at 1500 rpm and CR 17.5

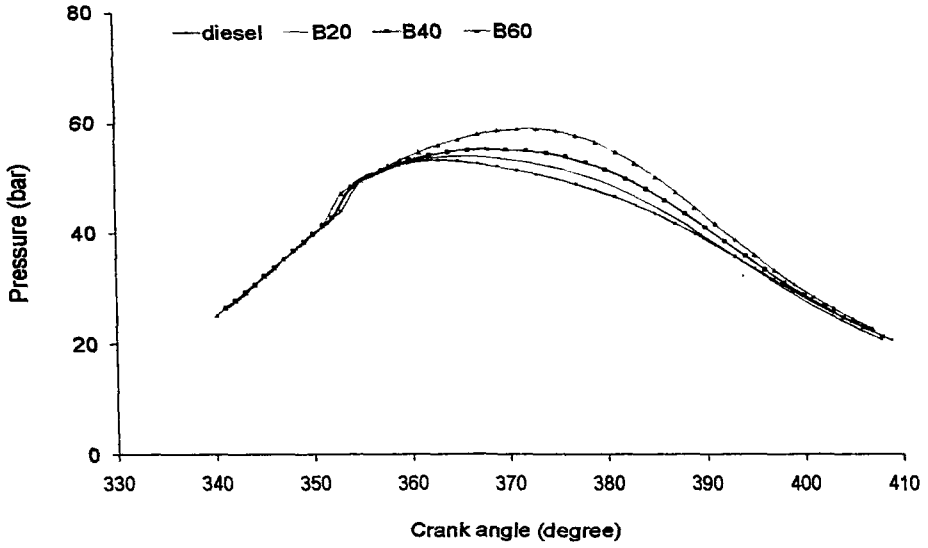


Fig. 7.5: Pressure vs. crank angle during combustion at 1500 rpm and CR 17.5

### 7.2.2. Effect of CR on brake power

Fig. 7.6 and Fig. 7.7 summarize the predicted effect of CR on engine BP at two different speeds, viz. 1400 and 1500 rpm. With increasing CR, the BP increases for all the fuels. With the change in CR, engine processes that influence its performance and efficiency, namely, combustion rate, heat transfer and friction, also vary. As the CR is increased, the heat loss to the combustion chamber wall and frictional losses decrease [69]; hence, there is an improved performance at higher CR. However, there is a limit at which further increase in CR would not be beneficial as it may lead to increasing surface to volume ratio and slower combustion; because at higher CR, the height of the combustion chamber becomes very small. The BP results predicted by Model I also show an increasing trend with CR for all the fuels. At 1400 rpm as shown in Fig. 7.6, the BP values for diesel fuel varied from a minimum of 3.894 kW (at CR 12) to a maximum of 4.731 kW (at CR 18.5). The corresponding minimum and maximum values for B20, B40 and B60 are (3.512 kW, 4.599 kW); (4.138 kW, 4.984 kW) and (4.489 kW, 5.651 kW) respectively. Fig. 7.7 presents the BP values as a function of CR at 1500 rpm. The minimum and maximum BP values at 1500 rpm for these fuels i.e. diesel, B20, B40, B60 are (3.794 kW,4.779 kW); (3.505 kW, 4.631 kW); (3.899

kW, 5.059 kW) and (4.429 kW, 5.5 kW), respectively. Higher BP for B40 and B60 and slightly lower BP for B20 compared to diesel are also evident from these figures. This is because these two figures correspond to a particular constant speed and at constant speed (1400 rpm and 1500 rpm) the BP for B40 and B60 is more and it is slightly less for B20 in comparison to the BP obtained for diesel. But for all the fuels the BP increased with CR.

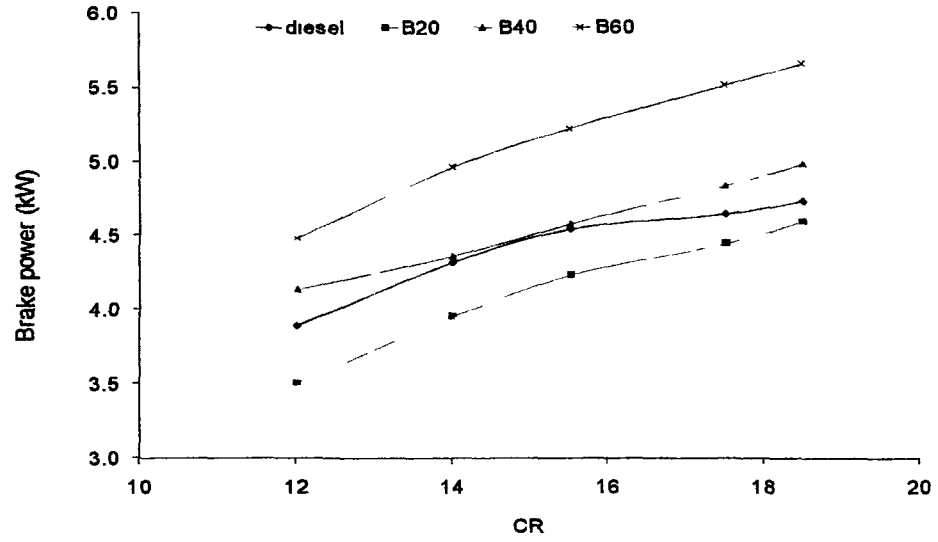


Fig.7.6: BP vs. CR at 1400 rpm

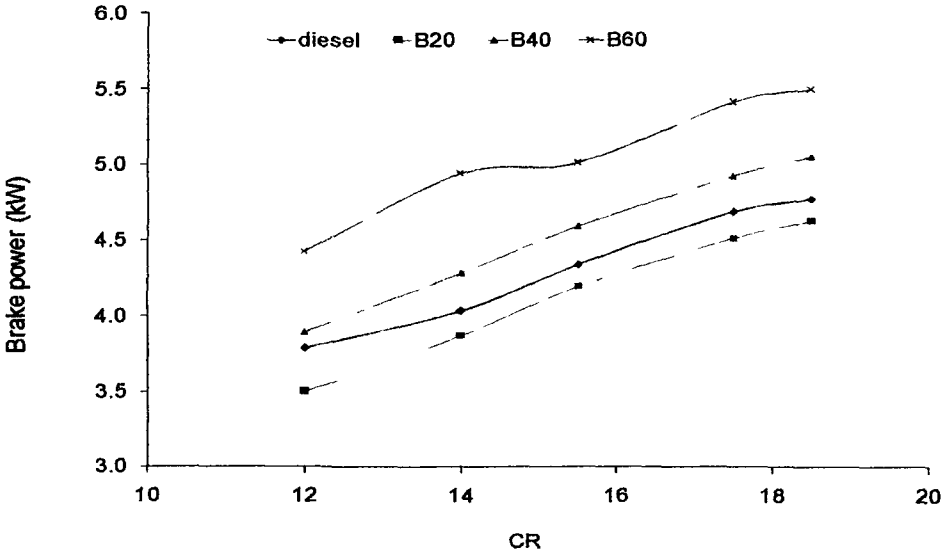


Fig. 7.7: BP vs. CR at 1500 rpm

It was observed from the model results that at CR 17.5 and 1500 rpm, the peak power values for diesel, B20, B40 and B60 are 4.69 kW, 4.517 kW, 4.927 kW and 5.418 kW

respectively. It is generally at this speed, the rated power of a small conventional diesel engine under consideration is specified which is of the order of 4.0 kW at CR of 17.5 and at 1500 rpm. The Model I predicted slightly higher BP in case of diesel and hence the error is marginal.

### 7.2.3. Effect of speed on brake thermal efficiency

Fig. 7.8 represents the predicted trend of BTE as a function of speed at CR 17.5. BTE decreases with speed for all the fuels. The blends B20, B40 and B60 present an increase in BTE compared to diesel. Since BTE is the ratio of BP to the fuel energy input, therefore, due to increased BP and less fuel energy input with biodiesel blends, the BTE is more in case of the blends. Higher BTE with pure biodiesel was reported by Murrilo et al. [25], who compared the performance of a three-cylinder variable speed (2000–3500 rpm) diesel engine running on blends of diesel and biodiesel derived from used cooking oil. However, they observed similar behavior in case of the blends B10, B30 and B50, but slightly less efficiently in comparison to diesel, which they attributed to fuel atomization during injection and its stability during storage, pumping and injection. Raheman and Phadatare [18] obtained higher BTE with blends B20 and B40, almost similar performance with B60 and lower BTE with B80 and B100. Lower calorific value of the blends B60 – B100 together with increased fuel consumption were reported as reasons for lower BTE. Although these BTE results were obtained for karanja methyl ester, but the engine that was used for evaluating the performance was different with rated output of 7.5 kW at a speed of 3000 rpm and CR of 16. Moreover, the results were obtained as a function of load at an average speed of 2525 rpm. In the present work, the increased BTE in case of the blends (B40 and B60) is due to comparatively higher BP and lower calorific value of these blends. In case of the blend B20, even if the BP is slightly less, increased BTE may be due to calorific value of the blend, which is significantly lower than that of diesel.

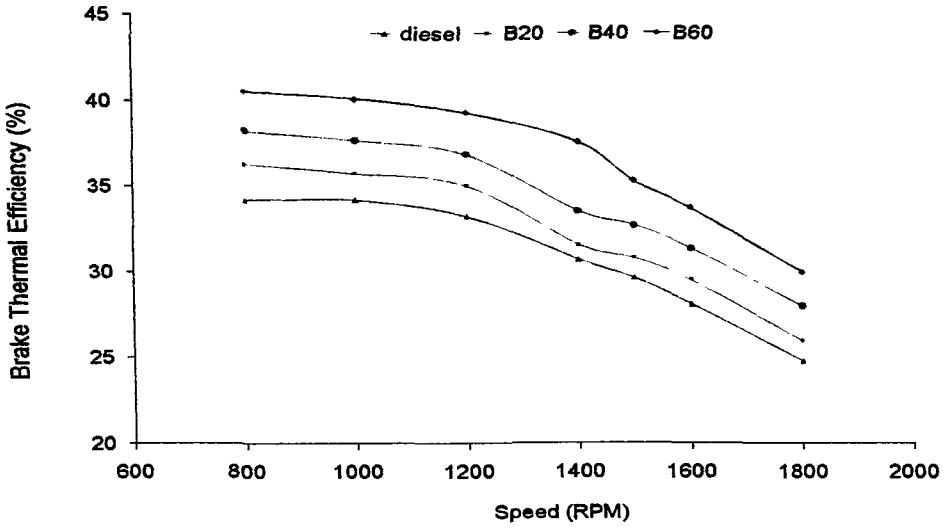


Fig. 7.8: BTE vs. speed at CR 17.5

Considering the fact that the scope of Model I was to predict the BP and BTE trend, it was found that the Model I has been successful in predicting the trend correctly for BP and BTE at various speeds and CRs for diesel as well as the blends of diesel and biodiesel.

## 7.3 PARAMETER IDENTIFICATION FOR SUBMODELS OF MODEL II

We discuss various sub-models used in Model II while identifying the parameters and their determination from experimental data and then present the results with experimental validation in the following subsections.

### 7.3.1 Ignition model

Ignition is one of the most important parameter in diesel engine combustion and therefore it needs to be modeled and predicted as accurately as possible. Actually the fuel, immediately after injection to the combustion chamber experiences a series of processes such as break-up, atomization, droplet formation, and wall impingement, vaporization, mixing with surrounding air, and ignition when it reaches the auto-ignition temperature. The subsequent phenomenon such as heat release, pressure rise, heat transfer etc. could be determined by the ignition. Ignition phenomenon can be considered either from the mechanical aspect by consideration of processes such as evolution of the fuel spray,

evaporation and fuel air mixing in detail or simply by considering the delay in the chemical reaction. There are certain limitations with the use of the detailed and complete ignition model as mentioned earlier in section 3.4.4. In the single zone combustion model approach, it is assumed that fuel is evaporated and completely mixed with necessary oxygen as soon as it is injected. Therefore, only the chemical reaction side is usually considered in most ignition models when using a simple combustion model. The ignition delay model that was used in the present study is equation (3.26), expressed as function of cylinder pressure and temperature, fuel cetane number and the fuel air equivalence ratio:

$$\tau_{id} = \frac{A}{p^n \phi^{02}} \exp\left(\frac{16550 - 20CN}{RT}\right)$$

The SOI in terms of CA is known from experimental test data for different fuel operations at various loads. Determination of SOI was discussed in section 5.7 in chapter 5. The SOI determined from experimental results is given as input to the model. Similarly, the SOC, as discussed in section 5.8 in chapter 5 is also known for all fuel operations at various loads. The CA duration between SOC and SOI is the ignition delay. The value of parameter $A$ is considered as 2.4 for all the fuel operations at all the loads except for B20 at 75% load, where it is considered as 1.9. A fixed exponent of 0.2 (standard value) was used for the fuel air equivalence ratio $(\phi)$ for all the fuels at various loads. The fuel air equivalence ratio was incorporated in the expression for ignition delay in order to take into consideration the effect of load and fuel consumption which varies with type of fuel used. Then from known experimental values of ignition delay period with different fuels at various loads, the exponent $n$ was determined by matching the calculated ignition delay with that of the experimental test data. The values of the exponent $n$ for different fuels at various engine loads are summarized in Table 7.1. The proposed ignition model predicts the ignition timing and the SOC precisely without posing much problem.

Table 7.1: Ignition model parameters

| | | | Parameters | | Test | Model | Test | Model |
|---|---|---|---|---|---|---|---|---|
| Load (%) | Fuel | SOI | A | n | SOC | SOC | ID | ID |
| % | | CA | | | CA | CA | CA | CA |
| 25 | NRL diesel | 353 | 2.4 | 0.62 | 369 | 369 | 16 | 16 |
| 50 | | 352 | 2.4 | 0.64 | 367 | 366 | 15 | 14 |
| 75 | | 352 | 2.4 | 0.6 | 366 | 366 | 14 | 14 |
| 100 | | 352 | 2.4 | 0.6 | 365 | 365 | 13 | 13 |
| 25 | B10 | 354 | 2.4 | 0.68 | 369 | 369 | 15 | 15 |
| 50 | | 353 | 2.4 | 0.66 | 367 | 367 | 14 | 14 |
| 75 | | 352 | 2.4 | 0.66 | 365 | 365 | 13 | 13 |
| 100 | | 352 | 2.4 | 0.63 | 365 | 365 | 13 | 13 |
| 25 | B20 | 352 | 2.4 | 0.65 | 367 | 367 | 15 | 15 |
| 50 | | 353 | 2.4 | 0.66 | 366 | 366 | 13 | 13 |
| 75 | | 352 | 1.9 | 0.64 | 364 | 364 | 12 | 12 |
| 100 | | 352 | 2.4 | 0.64 | 364 | 364 | 12 | 12 |
| 25 | B30 | 352 | 2.4 | 0.66 | 367 | 367 | 15 | 15 |
| 50 | | 353 | 2.4 | 0.66 | 366 | 366 | 13 | 13 |
| 75 | | 352 | 2.4 | 0.66 | 364 | 364 | 12 | 12 |
| 100 | | 352 | 2.4 | 0.64 | 364 | 364 | 12 | 12 |
| 25 | B40 | 352 | 2.4 | 0.66 | 366 | 364 | 14 | 12 |
| 50 | | 353 | 2.4 | 0.67 | 365 | 365 | 12 | 12 |
| 75 | | 352 | 2.4 | 0.66 | 364 | 364 | 12 | 12 |
| 100 | | 352 | 2.4 | 0.62 | 363 | 363 | 11 | 11 |

### 7.3.2 Heat release based combustion model

The combustion process in Model II is simulated by using a double Wiebe function. In a double Wiebe function the total heat release rate is shown as the sum of heat release rates during its premixed phase (suffix 1) and diffusion combustion phase (suffix 2) as described below. Rewriting equation (3.7)

$$\frac{dQ_f}{d\theta} = \frac{dQ_{f,1}}{d\theta} + \frac{dQ_{f,2}}{d\theta}$$

Where, $$\frac{dQ_{f,1}}{d\theta} = a_1(m_1+1)\left(\frac{Q_{f,1}}{\Delta\theta_1}\right)\left(\frac{\theta-\theta_{0,1}}{\Delta\theta_1}\right)^{m_1}\exp\left[-a_1\left(\frac{\theta-\theta_{0,1}}{\Delta\theta_1}\right)^{m_1+1}\right]$$

With $\theta_{0,1} \le \theta \le \theta_{0,1} + \Delta\theta_1$

And $$\frac{dQ_{f,2}}{d\theta} = a_2(m_2+1)\left(\frac{Q_{f,2}}{\Delta\theta_2}\right)\left(\frac{\theta-\theta_{0,2}}{\Delta\theta_2}\right)^{m_2} \exp\left[-a_2\left(\frac{\theta-\theta_{0,2}}{\Delta\theta_2}\right)^{m_2+1}\right]$$

With $\theta_{0,2} \le \theta \le \theta_{0,2} + \Delta\theta_2$

$Q_{f,1} = xQ_{f,total}$ and $Q_{f,2} = (1-x)Q_{f,total}$

The meaning and significance of the parameters $a_1$, $a_2$, $m_1$, $m_2$ and $x$ used in the above equations were already explained in chapter 3. The values of all these parameters for NRL diesel as well as the various blending of biodiesel are shown in Table 7.2. A computer program was developed specifically for the net heat release rate to determine the values of these parameters for the fuels at various loads by using equation (5.6). The comparison of the experimental and the theoretical net heat release rates are shown in the Fig. 7.9 through Fig. 7.13. The limitation of the double Wiebe function in its inability to explain the effect of load and speed could be understood in the process of choosing values of the parameters and also from these figures. It was mainly the relative air fuel ratio (RAF) and the speed that vary with load and fuels used. The total combustion duration for different fuel operations at various loads was known. The combustion duration for the premixed and diffusion combustion phase separately i.e. $\Delta\theta_1$ and $\Delta\theta_2$ were also calculated from the net heat release rate and cumulative heat release analyses as described in section 5.9.3 (B) and 5.9.3 (C) in chapter 5. These values obtained from the heat release analysis are inputs for the cycle simulation Model II. The procedure for combustion efficiency evaluation is described in section 6.3.6 in chapter 6. The combustion efficiency is also an input to the model that is used in the calculation of $Q_{f,total}$ . In Model I, combustion efficiency values for the tested fuels were chosen arbitrarily whereas in Model II, calculated combustion efficiency values are considered as model input. The values of various parameters used in the combustion model for different fuels at various loads are given in Table 7.2. The parameter $a$ in the Table 7.2 represents the values of $a_1$ and $a_2$, which are same.

Table 7.2: Combustion model parameters (Model II)

| | | parameters | | | | premixed | Diffusion |
|---|---|---|---|---|---|---|---|
| Load | Fuel | $a$ | $m_1$ | $m_2$ | $x$ | $\Delta\theta_1$ | $\Delta\theta_2$ |
| % | | | | | | CA | CA |
| 25 | NRL diesel | 4.000 | 1.1 | 0.75 | 0.546 | 9 | 35 |
| 50 | | 6.500 | 1.5 | 1.00 | 0.548 | 9 | 35 |
| 75 | | 6.000 | 1.1 | 1.00 | 0.504 | 8 | 37 |
| 100 | | 5.000 | 1.2 | 0.75 | 0.420 | 5 | 42 |
| 25 | B10 | 5.000 | 1.1 | 1.00 | 0.579 | 9 | 33 |
| 50 | | 5.000 | 1.1 | 0.50 | 0.479 | 7 | 37 |
| 75 | | 5.000 | 1.0 | 0.50 | 0.483 | 8 | 39 |
| 100 | | 4.000 | 1.1 | 0.75 | 0.406 | 5 | 39 |
| 25 | B20 | 6.000 | 1.1 | 1.00 | 0.552 | 9 | 35 |
| 50 | | 5.500 | 1.1 | 1.00 | 0.465 | 7 | 37 |
| 75 | | 5.000 | 1.1 | 0.75 | 0.468 | 8 | 38 |
| 100 | | 4.000 | 1.1 | 0.75 | 0.403 | 7 | 38 |
| 25 | B30 | 5.000 | 1.2 | 1.00 | 0.543 | 9 | 38 |
| 50 | | 5.000 | 1.1 | 0.50 | 0.451 | 7 | 38 |
| 75 | | 5.000 | 1.0 | 1.00 | 0.456 | 8 | 40 |
| 100 | | 5.000 | 1.0 | 0.75 | 0.362 | 6 | 41 |
| 25 | B40 | 5.000 | 1.0 | 1.00 | 0.586 | 10 | 32 |
| 50 | | 5.000 | 1.2 | 0.50 | 0.470 | 7 | 35 |
| 75 | | 3.000 | 1.0 | 0.50 | 0.480 | 8 | 32 |
| 100 | | 2.000 | 0.8 | 0.25 | 0.436 | 8 | 36 |

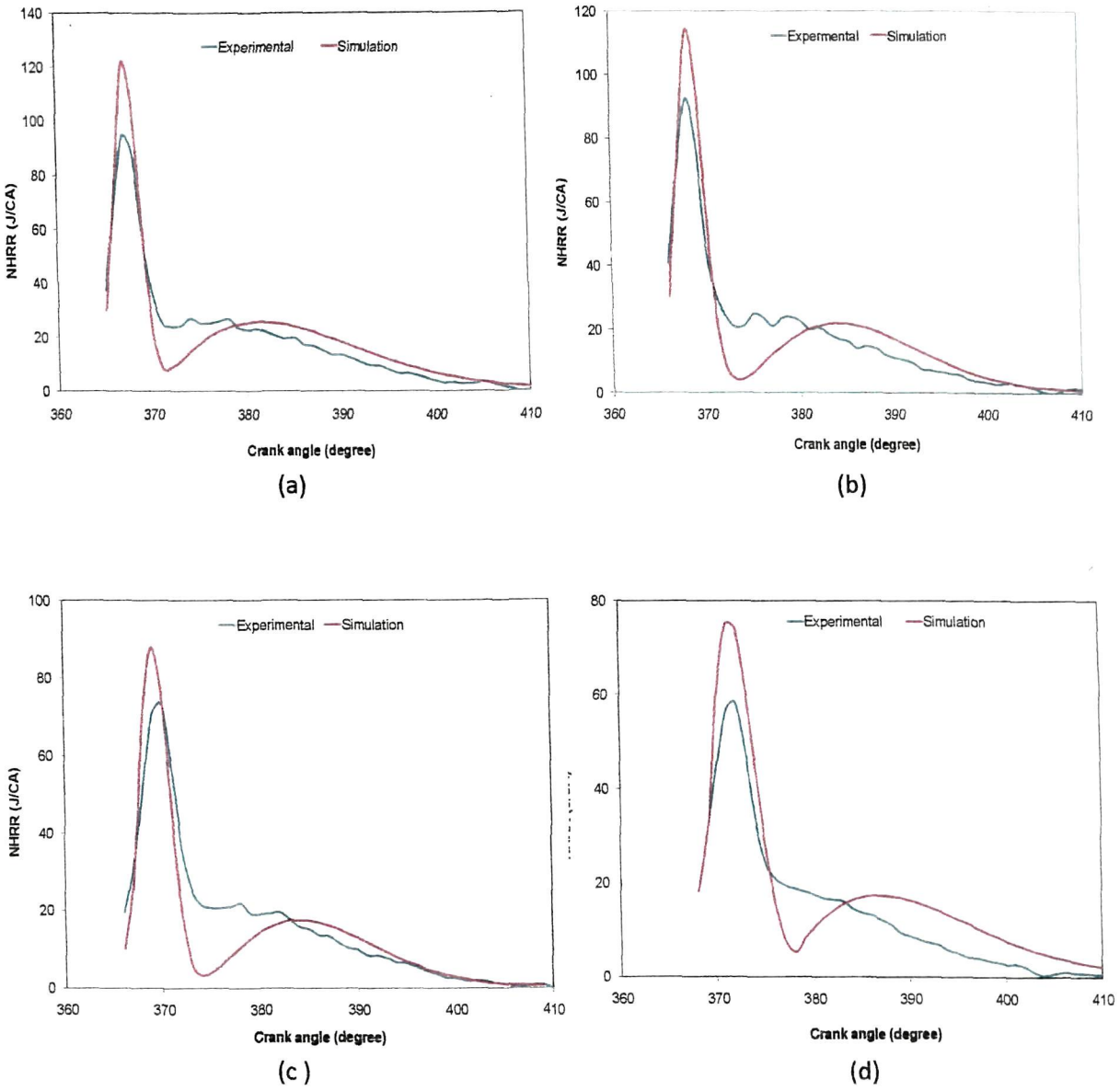


Fig. 7.9: Comparison of net heat release rate for NRL diesel (a) at full load (b) at 75% of full load (c) at 50% of full load (d) at 25% of full load

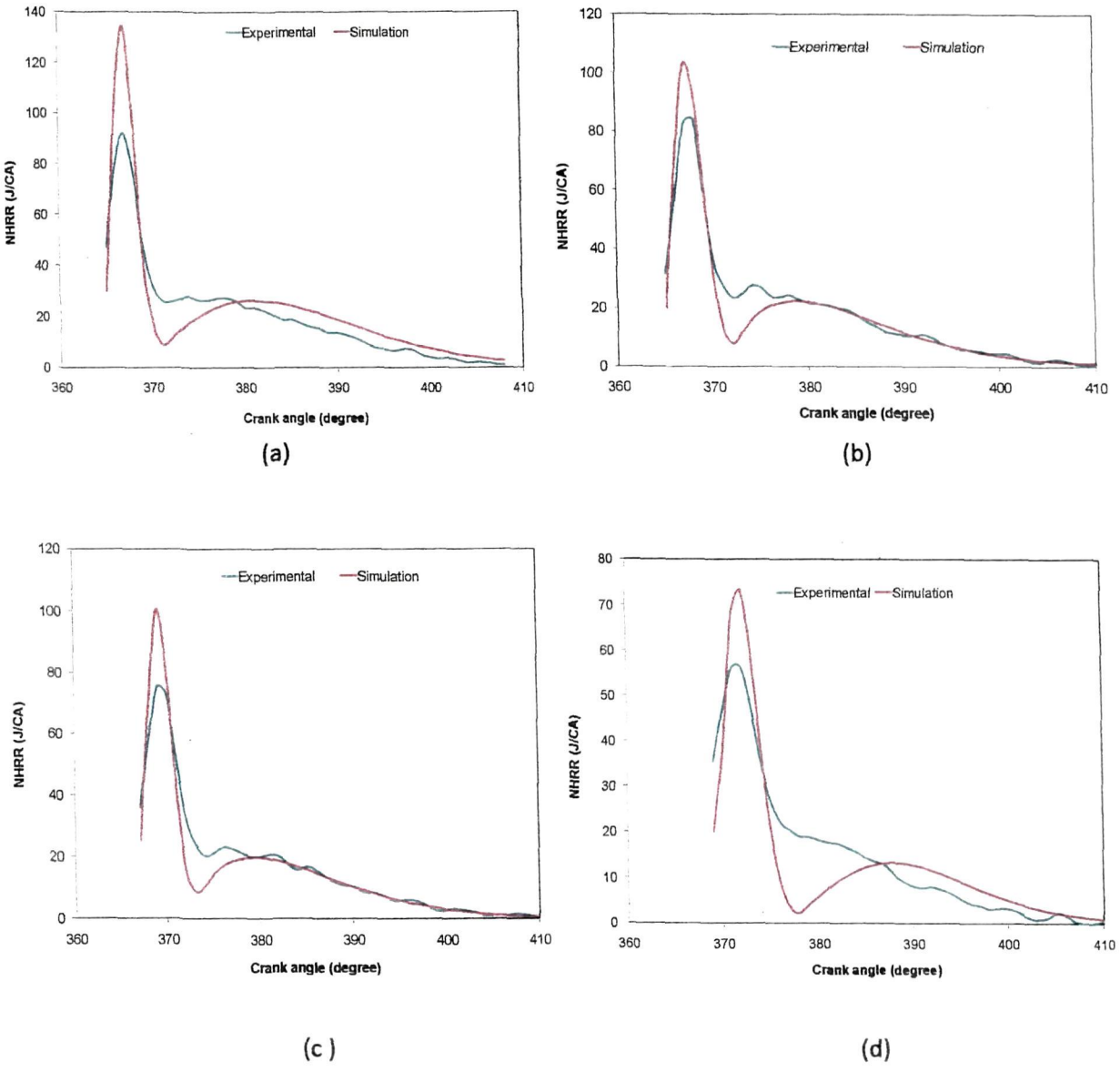


Fig. 7.10: Comparison of net heat release rate for B10 (a) at full load (b) at 75% of full load (c) at 50% of full load (d) at 25% of full load

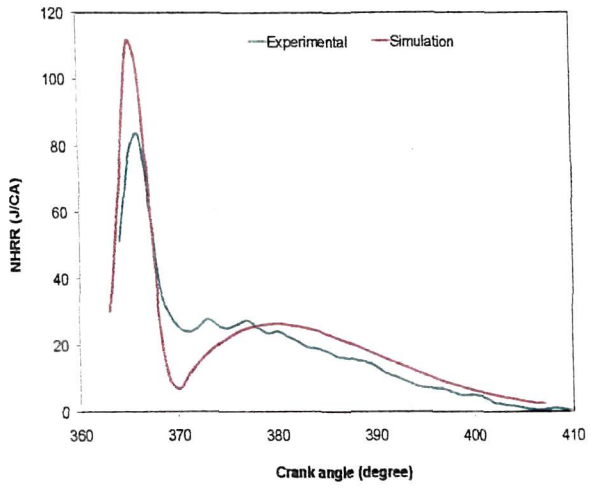


(a)

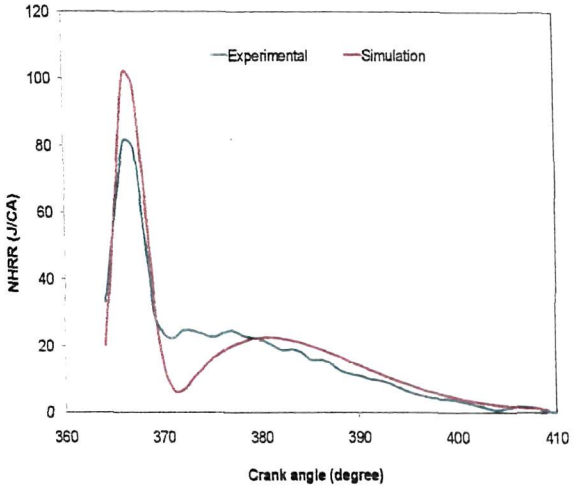


(b)

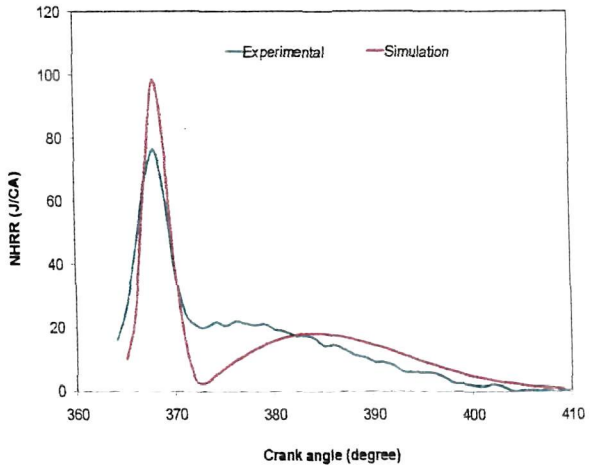


(c)

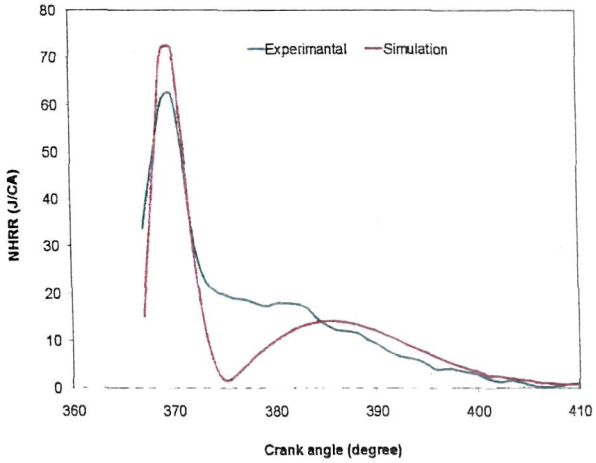


(d)

Fig.7.11: Comparison of net heat release rate for B20 (a) at full load (b) at 75% of full load (c) at 50% of full load (d) at 25% of full load

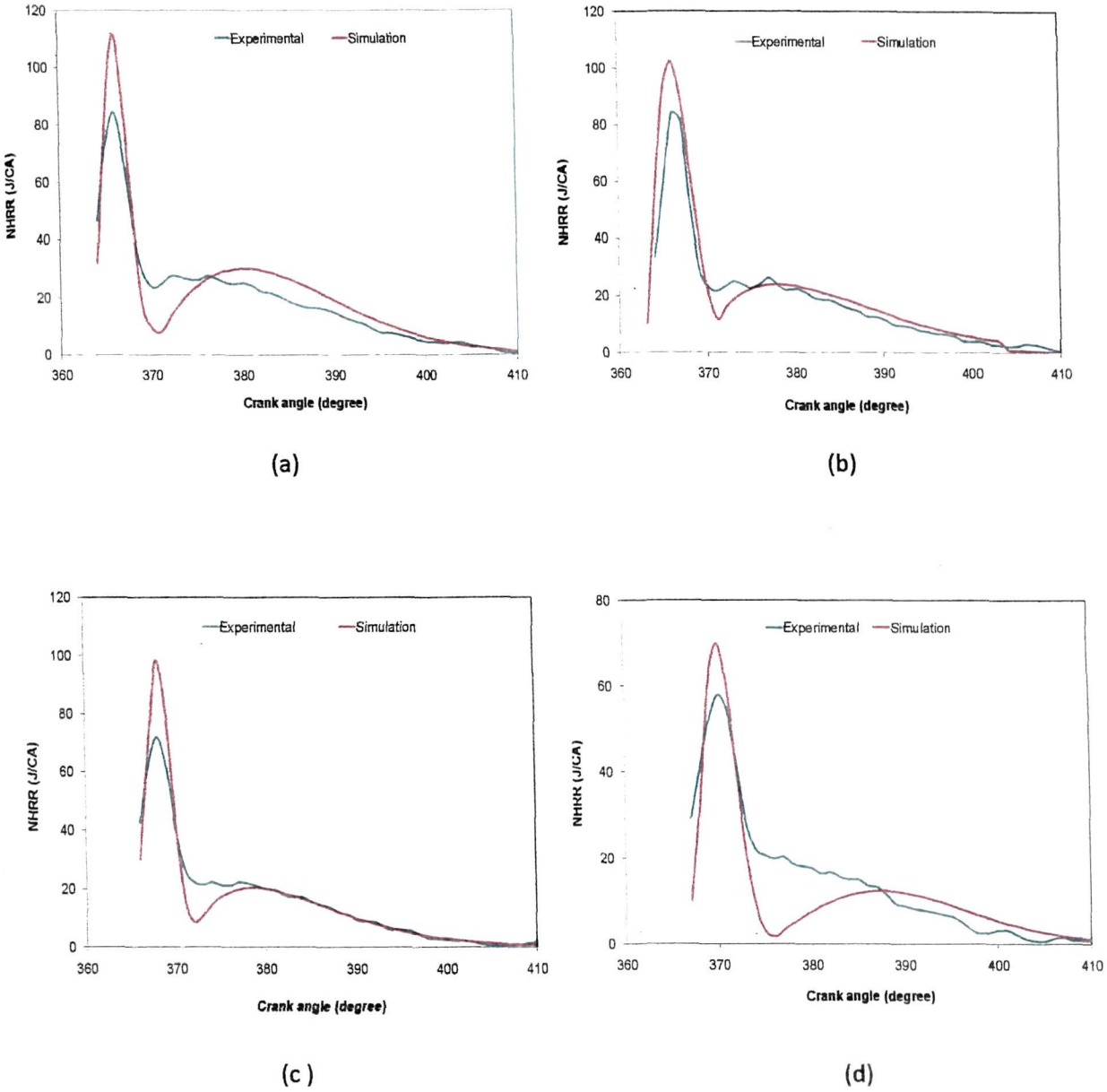


Fig. 7.12: Comparison of net heat release rate for B30 (a) at full load (b) at 75% of full load (c) at 50% of full load (d) at 25% of full load

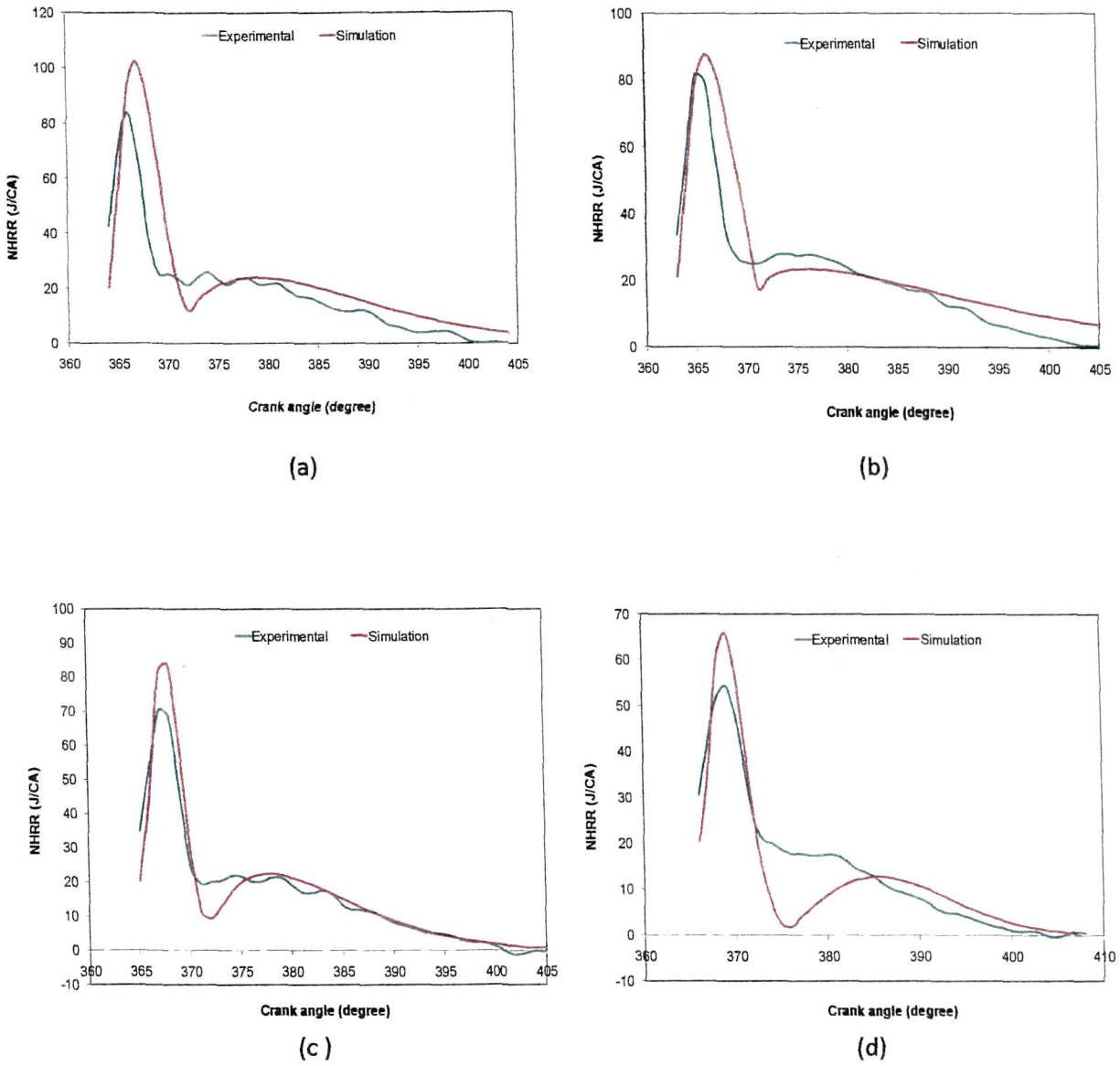


Fig.7.13: Comparison of net heat release rate for B40 (a) at full load (b) at 75% of full load (c) at 50% of full load (d) at 25% of full load

### 7.3.3 Heat transfer

In the Annand's equation (Equation (3.8)) used for calculating heat transfer, three constants were involved. Rewriting the equation,

$$\frac{dQ_h/d\theta}{A} = a\frac{k}{D}\mathrm{Re}^b(T_w - T) + c(T_w{}^4 - T^4)$$

Range of standard values for the constant $a$ and the standard values for the other constants i.e. $b$ and $c$ were mentioned in chapter 3. In Model II, a value of 0.35 was considered for the constant $a$. Values for the constants $b$ and $c$ were taken as 0.1 and $3.3\times10^{-8}$ W/m$^2$K$^4$ respectively for all the fuels at various loads. Cylinder wall temperature $(T_w)$ values at various loads for the different fuels were considered from mean coolant temperature values as reported in Table 6.2 of Chapter 6.

### 7.4 Comparison of Model II and experimental results -Discussion

Model II with the use of parameters identified for various sub-models was tested for prediction of engine performance with different fuels viz. NRL diesel, B10, B20 and B30 and B40 at various loads. The results predicted by the model are compared with the results derived from the experimental investigation in this section in order to test the accuracy of the model in predicting the performance of the engine. The effects of two major parameters i.e. (i) biodiesel addition in diesel in various proportions and (ii) load are examined. The results are presented for the various fuels at CR 18 and loads corresponding to 25%, 50%, 75% and full (100%) load.

Figs. 7.14-7.17 show the experimental and calculated cylinder pressure vs. crank angle diagrams at various loads for NRL diesel, B10, B20, B30 and B40 respectively. The quality of the model prediction capability was analyzed by calculating the RMS errors of the cylinder pressure residual for different test cases which are summarized in Table 7.3.

In the table, *error* $\Delta P_{cyl}$ is the root mean square (RMS) error of the cylinder pressure during the CA interval shown in the pressure crank angle diagrams whereas the *error* $\Delta P_{cy2}$ is the RMS error of the cylinder pressure during the combustion period. These are described by the following equations:

Error, $\Delta P_{cyl} = \sqrt{\sum_{i=1}^{N_1} \frac{(P_{est} - P_{test})^2}{N_1}}$ where, crank angle range is 250° to 500° with increment of 1° as shown in the pressure crank angle diagram, meaning $N_1$=251.

Error, $\Delta P_{cy2} = \sqrt{\sum_{i=SOC}^{N_2} \frac{(P_{est} - P_{test})^2}{N_2}}$ ; where, $N_2$ corresponds to the combustion duration.

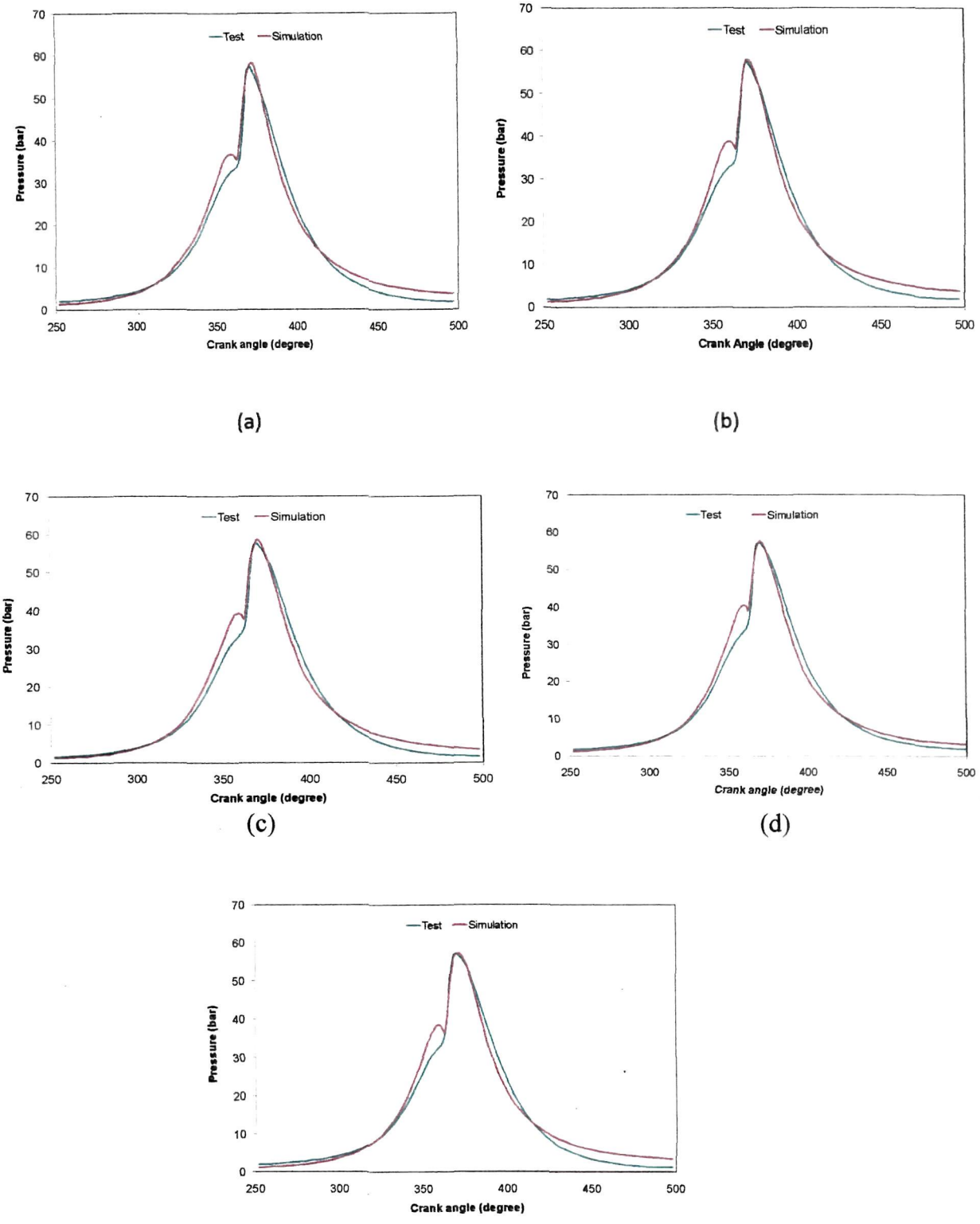


Fig. 7.14: Comparison of pressure crank angle variations (a) NRL diesel (b) B10 (c) B20 (d) B30 and (d) B40 at full load

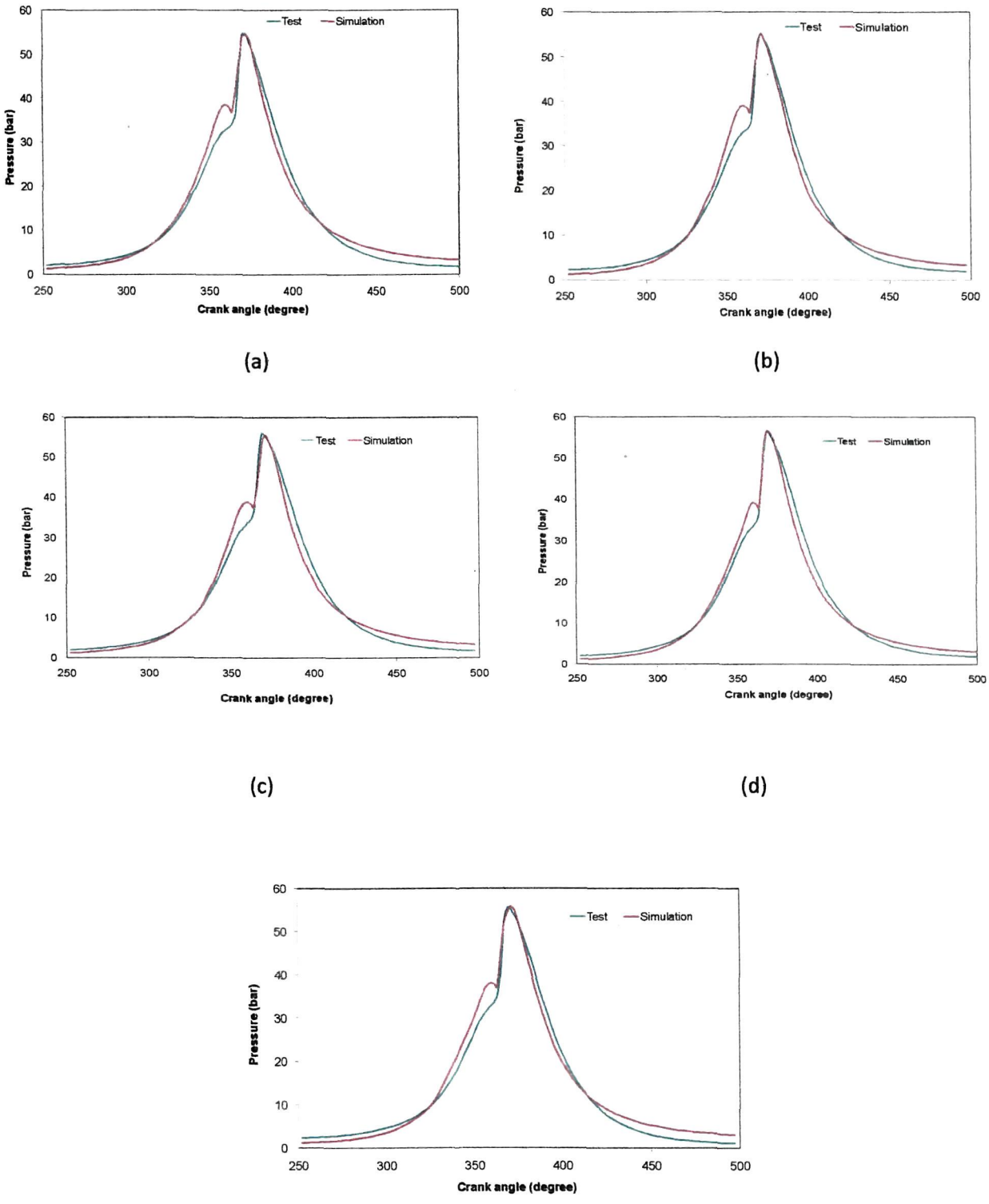


Fig. 7.15: Comparison of pressure crank angle variations (a) NRL diesel (b) B10 (c) B20 (d) B30 and (d) B40 at 75% of full load

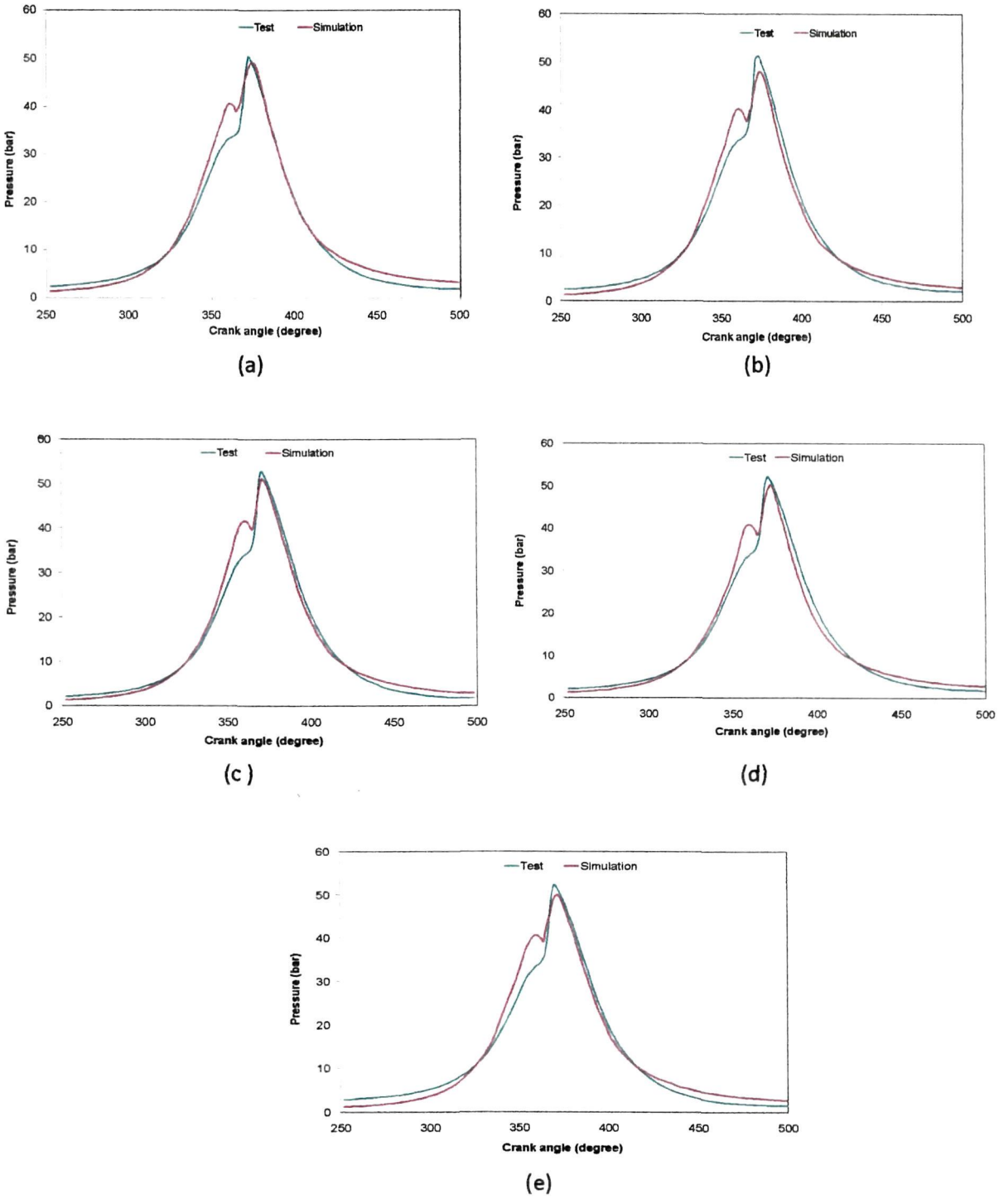


Fig. 7.16: Comparison of pressure crank angle variations (a) NRL diesel (b) B10 (c) B20 (d) B30 and (e) B40 at 50% of full load

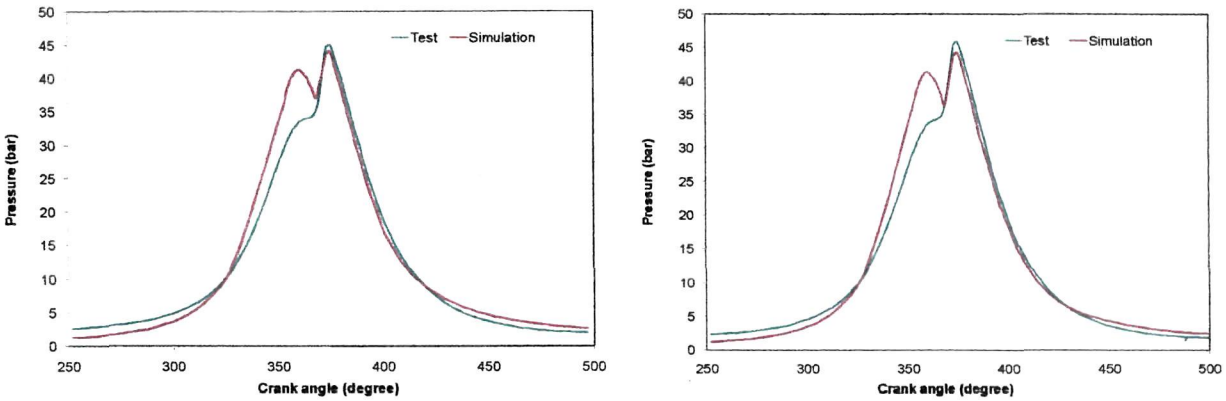


(a)




(b)

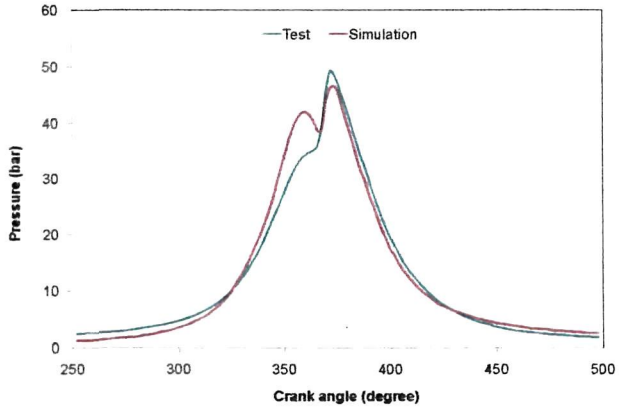


(c)

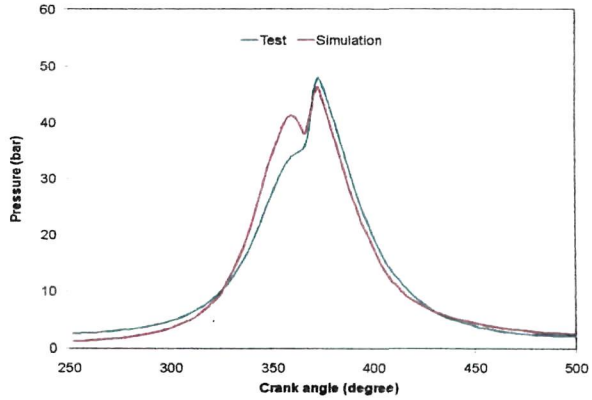


(d)

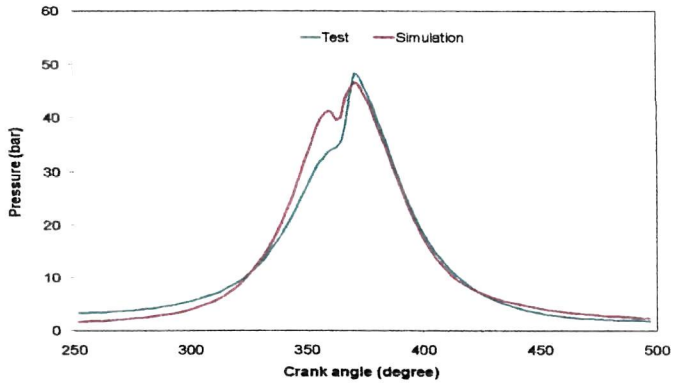


(e)

Fig. 7.17: Comparison of pressure crank angle variations (a) NRL diesel (b) B10 (c) B20 (d) B30 and (e) B40 at 25% of full load

Table 7.3: RMS error of cylinder pressure during the interval from 250-500° CA and the combustion period

| | | Load | | | |
|---|---|---|---|---|---|
| | | % | | | |
| Fuel | Error | 25 | 50 | 75 | 100 |
| NRL diesel | $\Delta P_{cyl}$ | 3.27 | 2.58 | 2.62 | 2.33 |
| | $\Delta P_{cy2}$ | 1.44 | 1.39 | 2.67 | 2.49 |
| B10 | $\Delta P_{cyl}$ | 3.02 | 2.73 | 2.66 | 2.64 |
| | $\Delta P_{cy2}$ | 1.42 | 2.58 | 2.33 | 2.12 |
| B20 | $\Delta P_{cyl}$ | 3.25 | 2.85 | 2.61 | 2.69 |
| | $\Delta P_{cy2}$ | 1.98 | 1.76 | 2.96 | 2.46 |
| B30 | $\Delta P_{cyl}$ | 3.04 | 2.87 | 2.67 | 2.84 |
| | $\Delta P_{cy2}$ | 2.2 | 2.87 | 3.2 | 2.59 |
| B40 | $\Delta P_{cyl}$ | 3.1 | 3.01 | 2.57 | 2.69 |
| | $\Delta P_{cy2}$ | 2.4 | 1.89 | 2.42 | 2.52 |

The average prediction error of the cylinder pressure at various loads for the different fuel operations is 2.80 bar corresponding to $\Delta P_{cyl}$ and 2.28 bars with respect to $\Delta P_{cy2}$ Slightly higher prediction error is due to over prediction by the model well before TDC during the compression phase up to SOC. Moreover, the predicted cylinder pressure traces at all loads for all the fuels shows two peaks, one for compression and the other for the combustion. The two peaks were more significant at lower loads and particularly at 25% of full load. The exact reproduction of the cylinder pressure trace with the use of double Wiebe function was not possible because the parameters $a_1$, $a_2$, $m_1$ and $m_2$ etc. were adjusted by trial and error and visually from a program developed specifically for the net heat release rate. Determination of parameters by trial and error is time consuming and mathematical methods such as method of least square and some other curve fit software can be used for determining the parameters more accurately. The method of least square using linear regression was tried to find the parameters, however the values that were obtained from regression analysis were found to be significantly different from the standard already reported values. Other combustion models such as the one proposed by Watson et al. [47] could be a choice for future work for more precise results. The objective of the developed model was to check whether it could predict IP, BP and BTE etc. accurately and it was found that the model could calculate these process data in good agreement with reality. This is discussed in a later section. Accurate estimation

of cylinder pressure is important from the point of view of emission modeling. Figs. 7.18-7.22 show the variation between experimental and calculated engine IP and BP results at various loads for NRL diesel and the four level of blending considered, at the CR examined. Existences of satisfactory coincidence between the experimental and calculated values once again confirm the validity of the model. It may be noted that calculated IP and BP values are the direct outcome of the developed model, while the experimental BP values are derived from the torque applied to the engine through the eddy current dynamometer and hence these values (experimental) are the same for all the fuels at a given load. For almost the same values of both experimental and calculated BP, the calculated IP values also match well with its experimental counterpart for all the fuels considered. As is quite obvious that both IP and BP increase almost linearly with increasing load. The quality of the model prediction capability was also analyzed by calculating the arithmetic percentage error of the estimated IP and BP with respect to the test data. The detailed results of estimation of these two performance parameters are summarized in Table 7.4. As can be seen in Table 7.4, the RMS error of IP prediction is 4.4% when the model is applied to the 25 test cases comprising of five different loads and five tested fuels, which means a relatively accurate estimation with the cycle simulation model approach. Similarly the RMS error of BP prediction is 1.3%, when applied to 20 test cases excluding the error corresponding to no load condition in which the calculated arithmetic percentage error is relatively high. Since the performance of the engine at no load condition is not of practical importance, hence it was neglected in calculating the RMS error in percentage and same was the reason why most of the results have been reported for the other loading conditions i.e. 25% load, 50% load, 75% load and full load conditions. In most of the test cases, the IP is overestimated by Model II which could be due to higher values of estimated combustion and expansion works in comparison to that of the experimental counterparts. The estimated net work done during the cycle which is the algebraic sum of the compression, combustion, expansion and the loop works, was more in case of these test cases. The fact that the model has predicted the engine IP at various loads accurately for NRL diesel and the various blending can also be seen from Fig. 7.23. The comparison between the experimental and calculated engine IP results at various loads for all the fuels is also shown in Fig. 7.24. As can be seen from the figure, the $R^2$ value ranges between 0.998-0.999 for all the fuels which implies a good coincidence between the experimental and calculated results.

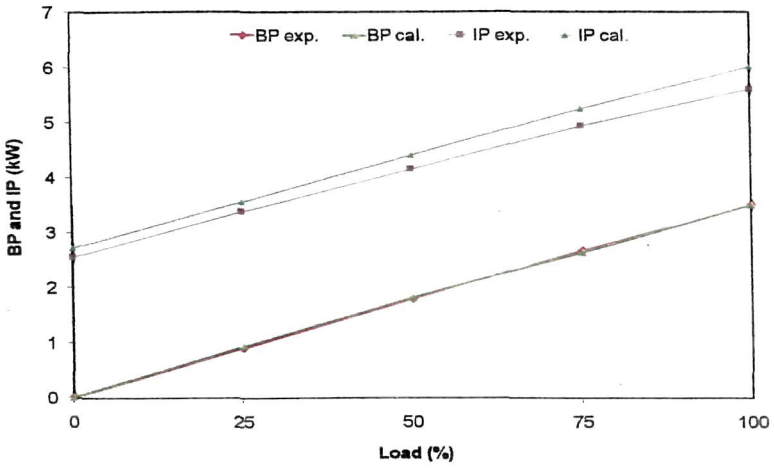


Fig. 7.18: Experimental and calculated BP and IP for NRL diesel

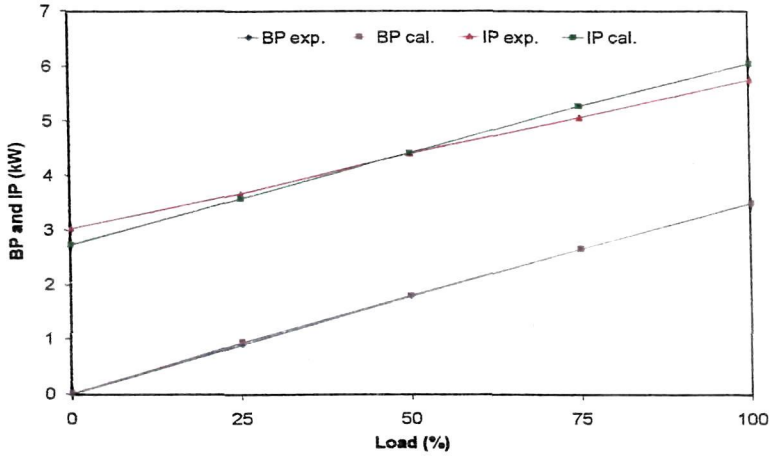


Fig. 7.19: Experimental and calculated BP and IP for B10

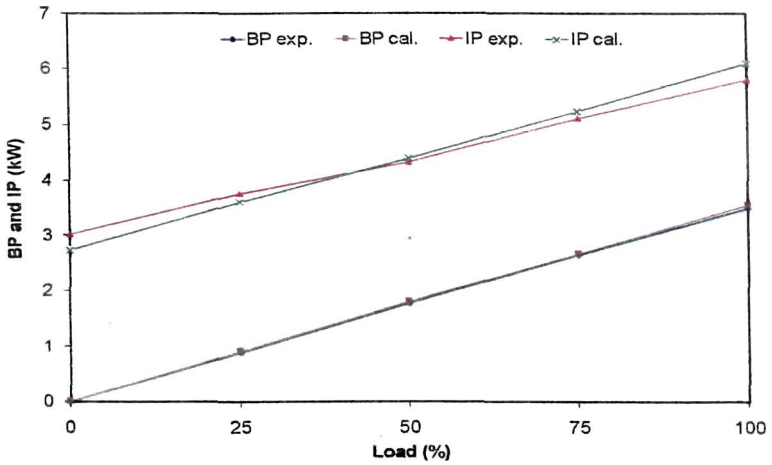


Fig. 7.20: Experimental and calculated BP and IP for B20

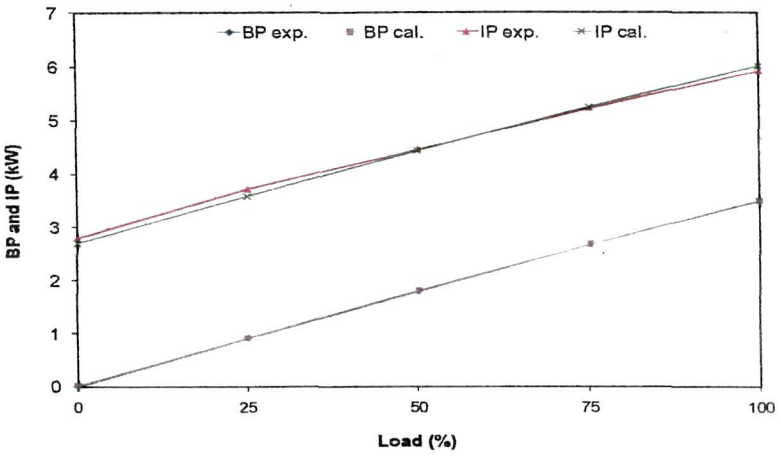


Fig. 7.21: Experimental and calculated BP and IP for B30

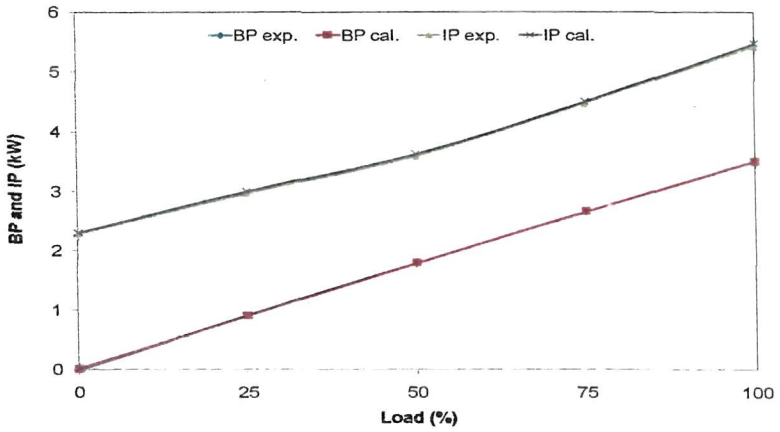


Fig. 7.22: Experimental and calculated BP and IP for B40

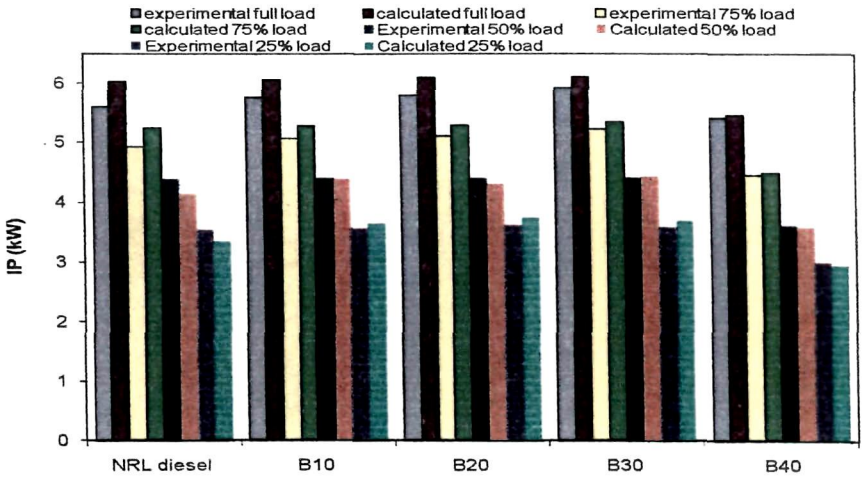


Fig. 7.23: Experimental and calculated IP for different fuels at various loads

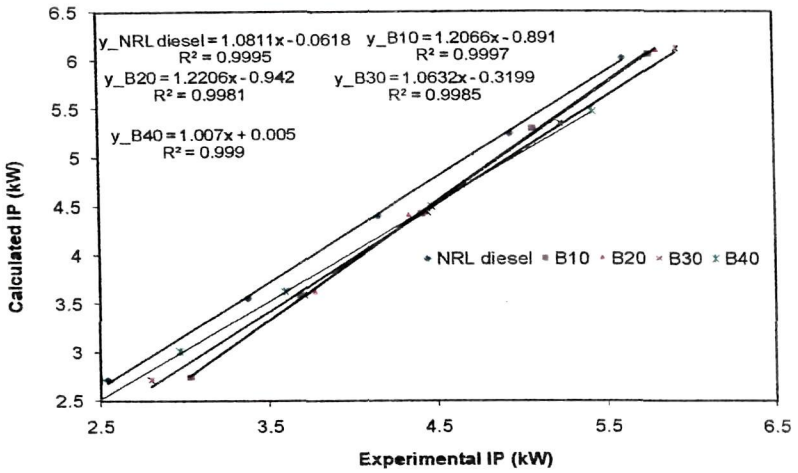


Fig. 7.24: Comparison of experimental and calculated IP

Table 7.4: Comparison of estimated IP and BP with experimental data

| | | IP | | Error | BP | | Error |
|---|---|---|---|---|---|---|---|
| Load (%) | Fuel | Est. | Test | | Est. | Test | |
| % | | kW | kW | % | kW | kW | % |
| 0 | NRL diesel | 2.710 | 2.54 | 6.693 | 0.016 | 0.01 | 60.000 |
| 25 | | 3.560 | 3.37 | 5.638 | 0.932 | 0.91 | 2.417 |
| 50 | | 4.407 | 4.15 | 6.193 | 1.821 | 1.79 | 1.732 |
| 75 | | 5.245 | 4.93 | 6.389 | 2.639 | 2.66 | -0.789 |
| 100 | | 6.025 | 5.60 | 7.589 | 3.505 | 3.50 | 0.143 |
| 0 | B10 | 2.742 | 3.03 | -9.505 | 0.018 | 0.01 | 80.000 |
| 25 | | 3.587 | 3.68 | -2.527 | 0.951 | 0.91 | 4.505 |
| 50 | | 4.418 | 4.41 | 0.181 | 1.817 | 1.79 | 1.508 |
| 75 | | 5.286 | 5.07 | 4.260 | 2.651 | 2.66 | -0.338 |
| 100 | | 6.056 | 5.76 | 5.139 | 3.491 | 3.50 | -0.257 |
| 0 | B20 | 2.753 | 3.02 | -8.841 | 0.014 | 0.01 | 40.000 |
| 25 | | 3.615 | 3.77 | -4.111 | 0.932 | 0.91 | 2.417 |
| 50 | | 4.411 | 4.33 | 1.871 | 1.813 | 1.79 | 1.285 |
| 75 | | 5.304 | 5.12 | 3.593 | 2.676 | 2.66 | 0.601 |
| 100 | | 6.099 | 5.80 | 5.155 | 3.560 | 3.50 | 1.714 |
| 0 | B30 | 2.715 | 2.80 | -3.036 | 0.015 | 0.01 | 50.000 |
| 25 | | 3.592 | 3.71 | -3.180 | 0.916 | 0.91 | 0.659 |
| 50 | | 4.434 | 4.45 | -0.359 | 1.807 | 1.79 | 0.949 |
| 75 | | 5.254 | 5.23 | 0.459 | 2.661 | 2.66 | 0.037 |
| 100 | | 6.112 | 5.92 | 3.243 | 3.484 | 3.50 | -0.457 |
| 0 | B40 | 2.307 | 2.29 | 0.742 | 0.016 | 0.01 | 60 |
| 25 | | 3.007 | 2.97 | 1.246 | 0.901 | 0.91 | -0.98901 |
| 50 | | 3.627 | 3.59 | 1.030 | 1.788 | 1.79 | -0.11173 |
| 75 | | 4.497 | 4.47 | 0.604 | 2.662 | 2.66 | 0.075188 |
| 100 | | 5.472 | 5.42 | 0.959 | 3.501 | 3.50 | 0.028571 |

Figs. 7.25-7.29 show experimental and calculated BTE trend with the change in load at CR 18 for various fuel. Steady increase in efficiency with load was observed in case of predicted BTE results too as was observed in case of experimental results. Experimental BTE values in case all the fuels are closer to estimated model results and the model has been successful in predicting the trend correctly for BTE at various loads for NRL diesel as well as the various biodiesel blends.

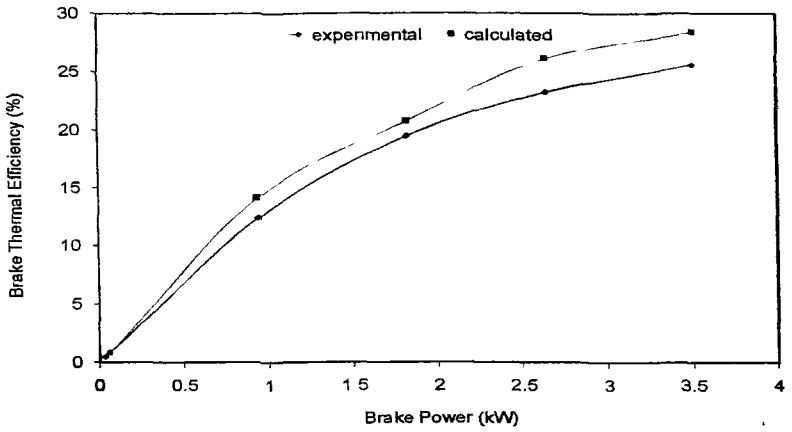


Fig. 7.25: Experimental and calculated BTE at various BPs (loads) for NRL diesel

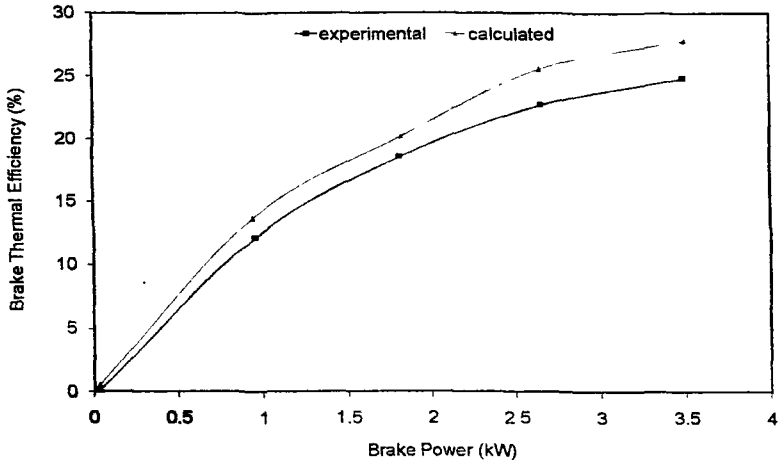


Fig. 7.26: Experimental and calculated BTE at various BPs (loads) for B10

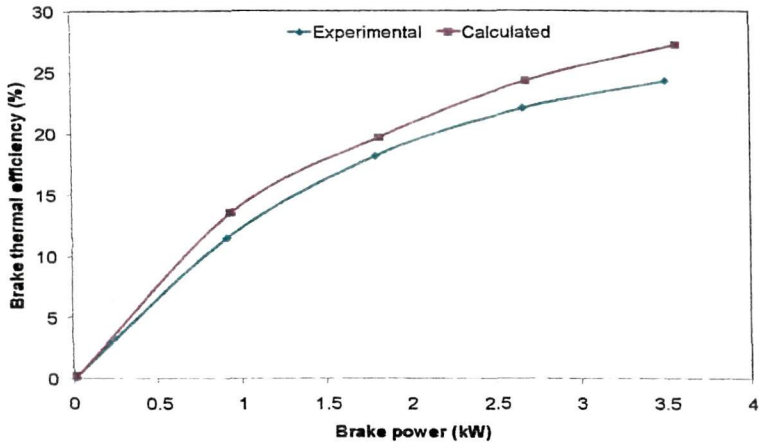


Fig. 7.27: Experimental and calculated BTE at various BPs (loads) for B20

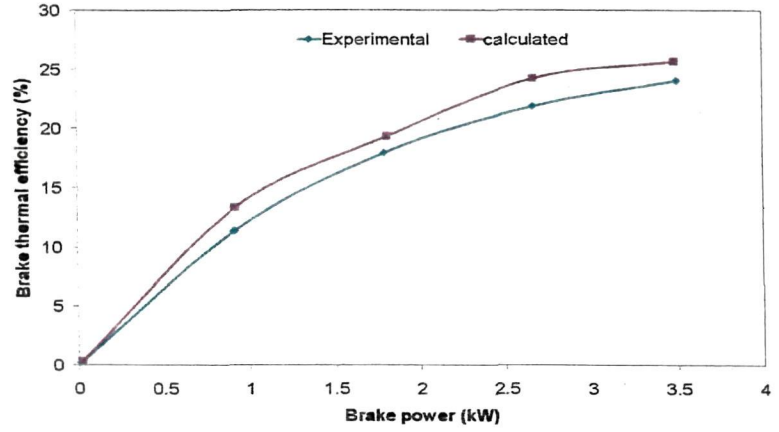


Fig. 7.28: Experimental and calculated BTE at various BPs (loads) for B30

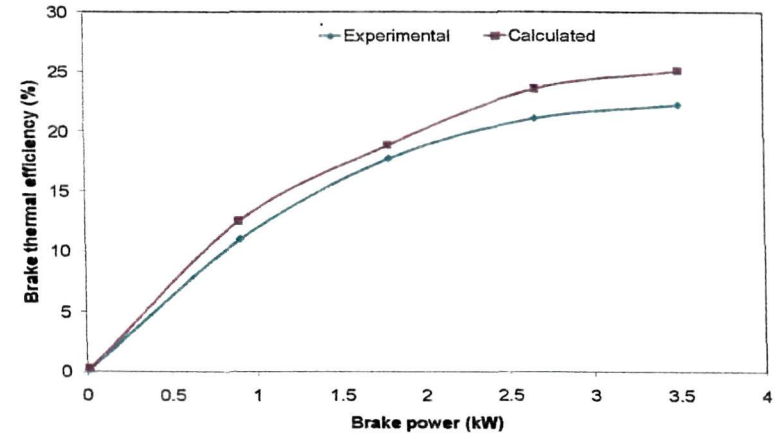


Fig. 7.29: Experimental and calculated BTE at various BPs (loads) for B40

The accuracy of the BTE results predicted by the model was also checked by calculating the arithmetic percentage error of the estimated BTE results with respect to the test data. These are summarized in Table 7.5. The RMS error of BTE prediction is 5.3% when the model is applied to the 25 test cases as mentioned before. For nearly same values of estimated and experimental BP results, slightly over BTE prediction by the model is due to the uncertainty involved in the theoretical calculation of number of moles of fuel. It was assumed in both the models that the fuel mass is injected instantaneously and calculation of fuel mass that takes part in chemical reaction during combustion is based on number of moles of air trapped in the engine cylinder at the IVC event. However, an approach that is more realistic is the incorporation of a fuel injection rate profile in the model with a finite injection duration period. The effect of biodiesel addition on BTE can be seen separately from Fig. 7.30. BTE decreases with increasing proportion of biodiesel in the blends. This is modeled and experimentally validated. Fig. 7.31 shows the comparison between the experimental and calculated BTE results at various loads for NRL diesel and the KSOME blends. Once again the $R^2$ values in the range of 0.997-0.998 clearly depict a fairly accepted proximity between experimental and calculated BTE results.

Table 7.5: Comparison of estimated BTE with test data

| | | | Load | | | | |
|---|---|---|---|---|---|---|---|
| | | | % | | | | |
| Fuel | BTE | | 0 | 25 | 50 | 75 | 100 |
| NRL diesel | Est. | % | 0.562 | 14.103 | 20.699 | 26.111 | 28.367 |
| | Test | % | 0.500 | 12.460 | 19.430 | 23.210 | 25.630 |
| | Error | % | 12.4 | 13.18 | 6.53 | 12.49 | 10.67 |
| B10 | Est. | % | 0.150 | 13.705 | 20.180 | 25.549 | 27.855 |
| | Test | % | 0.130 | 12.180 | 18.570 | 22.740 | 24.860 |
| | Error | % | 15.38 | 12.52 | 8.67 | 12.35 | 12.04 |
| B20 | Est. | % | 0.180 | 13.601 | 19.678 | 24.318 | 27.245 |
| | Test | % | 0.150 | 11.520 | 18.180 | 22.100 | 24.340 |
| | Error | % | 20.00 | 18.06 | 8.24 | 10.03 | 11.93 |
| B30 | Est. | % | 0.353 | 13.344 | 19.309 | 24.226 | 25.649 |
| | Test | % | 0.280 | 11.400 | 17.950 | 21.914 | 24.090 |
| | Error | % | 26.07 | 17.05 | 7.57 | 10.55 | 6.47 |
| B40 | Est. | % | 0.306 | 12.579 | 18.884 | 23.704 | 25.219 |
| | Test | % | 0.240 | 11.106 | 17.800 | 21.170 | 22.320 |
| | Error | % | 27.50 | 13.26 | 6.09 | 11.97 | 12.98 |

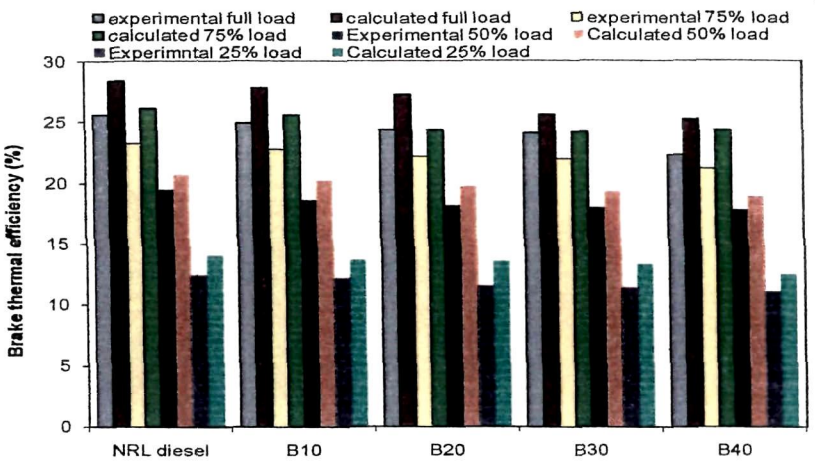


Fig. 7.30: Experimental and calculated BTE for different fuels at various loads

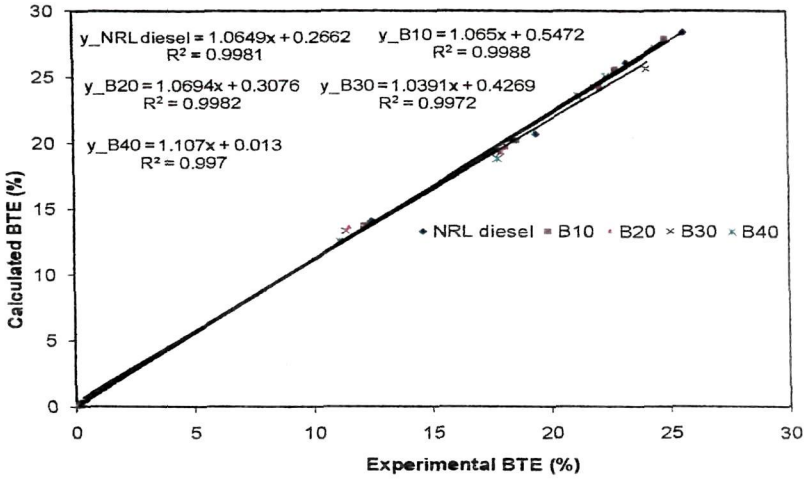


Fig. 7.31: Comparison of experimental and calculated BTE

# CHAPTER 8

# SUMMARY, CONCLUSIONS AND RECOMMENDATIONS FOR FUTURE WORK

## 8.1 SUMMARY

Public awareness for protecting the global environment and the concern for long-term supplies of conventional diesel fuel has motivated extensive research into the development of alternative fuels that are renewable, less polluting and give engine performance at par with diesel. Among the alternative fuels, biodiesel and its blends are gaining importance as diesel engine fuel due to its favorable attributes with properties almost similar to that of petro-diesel. Biodiesel from edible oil sources as substitute to diesel fuel may lead to the concept of self-sufficiency in vegetable oil production, which India has not attained yet. Therefore, biodiesel from non-edible oil sources are considered suitable for use in CI engine compared to their edible counterpart. There is ongoing research to find new non edible sources which can contribute to the local production of biodiesel, but their suitability as diesel engine fuel must be tested.

Many different conclusions have been made by researchers on engine performance, emissions and fuel combustion with blended and pure biodiesel. These results vary considerably depending upon the type of biodiesel used, engine configurations, test condition, and the method of analysis. The appropriate blend that would give optimum engine performance and best combustion characteristics may vary from biodiesel feedstock to feedstock, its production processes and the type of engine in which it is used. Of course, there are concerns about use of higher percentage blends or biodiesel in its pure form to reduce dependence on conventional diesel fuel. However this would necessitate for engine modification to overcome difficulties associated with the use of pure biodiesel. Future research must be carried out by researchers to develop new engine design concept, to make dedicated engine for biodiesel use in its pure form. But from the short term perspective, it is extremely necessary to identify locally available new variety of biodiesel and evaluate its characteristics as fuel in order to find out the optimized blend that can be used in a diesel engine without any appreciable drop in performance.

It is always advantageous to use biodiesel fuel in an unmodified diesel engine without affecting the engine performance and its durability. However, experimental investigations concerning fuel combustion vis-à-vis engine performance, with comprehensive

representation of the system, are sometimes expensive and also time consuming. A realistic numerical simulation model could reduce such effort. Therefore, development of a diesel cycle simulation model for predicting engine performance fuelled with biodiesel blends was one objective of this study. Prediction of diesel engine performance using cycle simulation program is very common in so far as diesel engine research and development is concerned. However, diesel engine cycle simulation modeling using biodiesel blends as fuels is either not available or even though there are models but these have not been validated so far for biodiesel blended fuel and hence a new development as far as research on biodiesel is concerned. Consequently two models (Model I and Model II) were developed during the course of the present research work.

Model I was developed for prediction of engine performance theoretically in terms of BP and BTE with changing speed and CR with diesel, B20, B40 and B60 as fuels, while Model II predicts engine performance in terms of IP, BP and BTE etc., but with changing load at a fixed CR of 18 for fuel operations with NRL diesel, B10, B20, B30 and B40. Air fuel ratio (AFR) for a particular fuel at a given load was obtained from experiment. The stoichiometric AFR was calculated from the chemical reaction involving the given fuel. Thus, the RAF for the fuel at the given load was determined and was given as input to the model to take into consideration the effect of load to the engine. Moreover, Model II has been validated using experimental results.

Both Model I and Model II used a single-zone approach for simulating various engine processes. These two models were supplemented with many sub-models for the estimation auto-ignition delay, heat release rate, heat transfer, valve flow area and frictional power etc.

For the heat release rate model, simple Wiebe function was used in Model I and the double Wiebe function was used in Model II. In double Wiebe function, the total heat release rate was calculated by superimposition of two simple Wiebe functions with subdivision of the energy shares of the premixed and diffusion phases of fuel combustion.

For the prediction of the auto-ignition timing, an Arrhenius type of ignition model was used in both the models. The values of the constant $A$ and the exponent $n$ used in the model were chosen arbitrarily for the tested fuels at different speed and various CR in Model I, whereas in Model II, the values of these parameters were calibrated and validated based on experimental ignition delay results obtained for different fuels at various loads.

The heat transfer between the in-cylinder gas and the surrounding wall is calculated by using Annand's equation.

Parameter values used in the model equations pertaining to fuel properties and operating conditions were based on some realistic conditions and relevant data as available in standard literature in Model I. However for the parameterizations and validation of Model II, extensive experiments were conducted in a single cylinder four stroke DI diesel engine while operating the engine with diesel and specific biodiesel blends at various loads.

It is not possible to find out the effect of biodiesel properties on engine performance and fuel combustion behavior unless a comprehensive engine performance analyses is done to draw any conclusion out of it. Therefore bio-diesel was produced from locally available Koroch seed oil and the properties of various blending (B10-B40) of biodiesel with NRL diesel were determined. Extensive engine tests were performed operating the engine at various loads with NRL diesel and the Koroch seed oil methyl ester (KSOME) fuel blends to evaluate the engine performance and combustion characteristics of the biodiesel blends. Emission tests were also conducted to evaluate the emission characteristics of the tested fuels in the test engine at various loads. Experimental results thus obtained have been thoroughly analyzed and the results concerning performance have been used for parameterization of model equations and validation of Model II.

From the literature survey conducted, it was also realized that a detailed engine performance analysis (apart from using it for model parameterization and validation) in the light of both first and second law of thermodynamics involving a new biodiesel could be useful in understanding the details of engine operation with biodiesel blends in an unmodified diesel engine. Therefore, a comprehensive first and second law analyses have also been made in the present work. Various losses such as heat loss in engine cooling, exhaust loss, frictional loss and unaccounted miscellaneous losses have been determined from the energy balance study. Second law (exergy) analysis is a powerful tool for assessing and improving efficiency through identification of processes accompanying exergy destruction and thus gives a better insight to the various engine operations. Hence, an exergy balance study was carried out and exergy destroyed with various engine processes for all the fuel operations at various loads are determined.

## 8.2 CONCLUSIONS

Within the broad framework of the thesis presented above, the following specific contributions were made:

1. Model I developed for predicting some aspect of diesel engine performance was tested for investigating the effect of variation speed and CR on BP and also the effect of speed on BTE at fixed CR of 17.5. The speed was varied from 800 to 1800 rpm and the CR from 12 to 18.5.

(i) It was found that the BP of the engine increased with speed, the peak power occurred at a particular speed and further increase in speed beyond that value resulted in decrease of power. At CR of 17.5, the engine peak power occurred at 1500 rpm for diesel, B20 and B40; however, for B60 it occurred at 1400 rpm. Predicted BP at various speed was more in case of B40 and B60, whereas it was slightly lower in case of B20 compared to that of diesel. It was observed that at CR 17.5 and speed 1500 rpm, the peak power values for diesel, B20, B40 and B60 were 4.69 kW, 4.517 kW, 4.927 kW and 5.418 kW respectively. It is generally at this speed, the rated power of the diesel engine under consideration is specified to be about 4.0 kW at CR of 17.5 and at 1500 rpm. The Model I predicted slightly higher BP in case of diesel and hence the error is marginal.

(ii) The blends B20, B40 and B60 also presented an increase in BTE when compared to diesel. Predicted increased BTE in case of B40 and B60 was due to comparatively higher BP and lower calorific value of these blends. In case of the blend B20, although the BP was slightly less, higher BTE may be due to calorific value of the blend, which was also lower than that of diesel. The model also predicted higher rate of pressure and temperature rise for the blends during combustion as compared to diesel. The model outputs are analyzed in terms of corresponding experimental results available in the literature.

(iii) Considering the fact that the scope of Model I was to predict the BP and BTE trend, it was found that the model had been successful in predicting the trend correctly for BP and BTE at various speeds and CRs for diesel as well as biodiesel blends. However, any possible error in model predictions could be due to the use of (i) simple Wiebe function (ii) constant fuel air equivalence ratio at all speed and (iii) arbitrary model parameters.

2. Parameter identification process has an important role in the overall model structure. The ignition and the combustion model parameters in Model II was done with the knowledge of

known standard values and adjustment of parameters made visually from a program developed specifically for the net heat release rate to match the experimental apparent net heat release rate curve. To the author's knowledge, it is the first time that such an approach was applied to model the heat release with biodiesel blends at various loads using double Wiebe function. The model was used to predict in-cylinder pressure evolution as a function of crank (CA), IP, also BP and BTE for a large number of cases corresponding to different fuel operations at various engine loads. Experimental data such as speed, RAF, injection timings, combustion durations etc. obtained from experiments have been used as inputs for Model II. However, the exact reproduction of the cylinder pressure trace with the use of double Wiebe function was not possible particularly at lower loads and more significantly at 25% of full engine load. It may be due to the limitation of the Wiebe function that it cannot explain the effect of speed and load properly. Overall, the agreement of model predictions with experimental data was very good in terms of peak pressure, location of peak pressure, resulting IP, BP and BTE etc. despite the relative simplicity of the model.

3. For experimentation in the engine with biodiesel fuel blends it necessitated the production of biodiesel. Therefore biodiesel was produced from Koroch seed oil following a two step acid base transesterification and the pure biodiesel thus obtained was mixed with NRL diesel in various proportions to prepare the blends viz. B10, B20, B30 and B40. A comparison of physical and fuel properties of different KSOME blends with pure NRL diesel fuel indicated that the blends were quite similar in nature to diesel fuel. However, viscosities of the blends were found slightly higher and calorific values were lower than that of NRL diesel.

4. Although the experimental results were used for model validation, but at the same time these also revealed some interesting features of engine operation with the biodiesel blends. Based on the comprehensive experimental engine performance, combustion and emission studies conducted in the computerized, fully instrumented test engine, the characteristics of various KSOME blends were evaluated and compared with that of NRL diesel fuel. The following observations were made from the performance, combustion and emission analyses.

(i) BTE of the engine operated with KSOME blends was found lower than NRL diesel. BSFC was more in the case of KSOME blends compared to BSFC of NRL diesel at all loads.

(ii) IP produced by the engine was higher when run on the KSOME blends up to B30 compared to its NRL diesel operation over the entire range of load. However, it showed lower engine IP with B40. Observed lower engine IP for B40 at all the loads was due to poor atomization and incomplete combustion of this particular fuel blend because of its higher viscosity that finally resulted in lower pressure variation and heat release. Use of fuel injection pump employing higher injection pressure or introduction of additives to lower the viscosity could be a solution to this problem relating to use of higher level of biodiesel blending.

(iii) Combustion analysis revealed almost the same pressure crank angle characteristics for the KSOME blends and NRL diesel. Early pressure rise was observed in case of the KSOME blends at all the loads which were due to early premixed combustion of the blends. Peak pressure of the combustion gases in the engine with NRL diesel and the KSOME blends as fuels was more or less same at full load. At the other loads however, the peak pressure was slightly higher for the blends compared to the peak pressure corresponding to NRL diesel fuel operation.

(iv) Heat release characteristics showed that the heat release occurred earlier in the case of KSOME blends at all the loads which confirms the shorter ignition delay period with respect to the blends. Due to shorter ignition delay, maximum heat release rate also occurred earlier for the KSOME blends at all the loads. Compared to NRL diesel, the cumulative heat release was higher for the blends B10, B20 and B30 and it was significantly less for the blend B40 at all the loads. With 40% KSOME in the fuel blend, observed lower cumulative heat release as well lower engine IP clearly puts a question mark to the suitability of this particular blend as fuel to the engine in so far as the engine performance and combustion characteristics are concerned.

(v) Ignition delay period was less for the KSOME blends at all the loads. Combustion duration of the KSOME and its diesel blends up to 30% blending was more or less the same with slight decrease in case of B10 and B20 at full load and 25% load. Slight increase in ignition delay for B30 was observed at these loads. At 75% load, the duration was more for the blends B10, B20 and B30 and these were almost the same at 50% load. However for B40, it was slightly less at full and 25% load as compared to the other fuels but a marked decrease in combustion duration was observed at 75% and 50% load. The reduction in combustion

duration had a direct consequence on the heat release and the combustion work which ultimately affected the engine IP for B40 blend.

(vi) EGT of the KSOME blends were found to be higher compared to NRL diesel at various loads due to higher heat release during the late combustion phases of biodiesel fuel blends.

(vii) Exhaust emissions from engine are extremely important in engine emissions study. Emission characteristics of the KSOME blends showed the superiority of the blend B10 over NRL diesel and the other biodiesel blends. Except $CO_2$ emission, all other emissions were less for B10 at all the engine loads studied. In case of the other biodiesel fuel blends, the emissions of CO, HC and smoke opacity were found to be higher than that of NRL diesel at relatively higher load.

(viii) At lower loads, CO emission for all the KSOME blends was comparatively less than that of NRL diesel. However at higher load, CO emission for the KSOME blends was more. $CO_2$ emissions in case of all the KSOME blends were slightly higher than that of NRL diesel in the entire range of engine load. This was due to presence of higher carbon content in the biodiesel blends.

(ix) KSOME blends produced lower HC emission as compared to NRL diesel at 25% and 50% load. However at 75% and full engine load, HC emission with KSOME blends except for B10 was higher than that of NRL diesel. HC emission with B10 was comparatively less at all engine loads which confirmed the efficient combustion and better emission characteristics of this particular fuel blend over the other KSOME blends.

(x) NOx emission for the KSOME blends at higher load was almost comparable whereas at lower loads, it was more. Moreover, NOx emissions increased with load for all the fuels. The same was the trend with the smoke opacity level, especially, greater smoke opacity was observed at full load. It was seen that the smoke opacity level of the blend B10 was lesser than that of NRL diesel at all engine loads. However for the other KSOME blends, it was higher than that of NRL diesel at various engine loading conditions, except at 75% load where the blends showed slightly lower smoke level.

5. From the energy balance study it was found that fuel energy input was more for the KSOME blends at various loads despite the lower heating value of the blends. This was due

to increased fuel consumption associated with the biodiesel blends. It was seen that the energy lost to the coolant increased with load for all the fuels. Heat losses for engine cooling were slightly more for the KSOME blends at all the loads. However, in case of B40 heat loss for cooling reduced at 75% load and full engine load which could be due to reduction in the cylinder temperature resulting from incomplete combustion of this particular fuel blend arising out of its higher viscosity, poor atomization and lack of oxygen available for burning a rich fuel mixture. The energy loss accompanying exhaust gas was also found to be slightly higher for the KSOME blends at lower engine loads. However, at 75% load the exhaust gas losses were almost found to be same for NRL diesel, B10 and B20 and slightly higher for B30 and B40. At full engine load operation, these losses were marginally higher with B10 and B20 and slightly lower with B30 and B40 as compared to NRL diesel fuel operation. The frictional losses were significant for the blends from B10 to B30 at all engine loads. For B40, it was less compared to that of NRL diesel. A very important observation was that the unaccounted heat losses with respect to the fuel blend B40 was significantly high at all engine loads. This was the reason that the IP and BTE of the engine were lower at various engine loads when operated with the blend B40. The viscosity was more for the blends and due to higher viscosity and particularly for this blend; the fuel did not atomize properly leading to poor combustion, which ultimately resulted in higher combustion losses and lower IP and BTE. The combustion efficiency was also evaluated for the tested fuels at various engine loads considering that it is also an important parameter that measures the energetic performance of an engine. Combustion efficiency was higher for the blends B10, B20 and B30 at all the loads. However there was a marked reduction in case B40 at all loads.

6. It was seen that the fuel exergy was more for the KSOME blends than NRL diesel at all the loads due to presence of higher carbon, hydrogen and extra oxygen atoms in the blended biodiesel. This together with the higher fuel flow rate in respect of the blends ultimately gave higher fuel exergy for the blends. The exergy losses with heat transfer in case of the KSOME blends were in general less compared to that of NRL diesel. Although the total heat loss i.e. the sum of heat loss in engine cooling and the unaccounted heat loss was more for the KSOME blends, exergy of heat transfer in case of the blends was less due to lower cylinder surface temperatures in respect of the blends. Moreover the exergy loss with heat transfer as percentage of fuel exergy input was very small. The loss of exergy with heat transfer was the minimum for the blend B20 at all engine loads compared to the other fuel blends.

The exhaust exergy losses for the KSOME blends were slightly higher compared to that of NRL diesel at all engine loads which was due to a combination of factors such as (i) higher EGT with the blends (ii) slightly higher values of the coefficients (Table 6.2) used in the calculation of thermo-mechanical and chemical exergy of the exhaust gases (ii) higher molar fuel flow rate in respect of the blends. Exhaust exergy increased with load for all the fuels. From the exergy balance study when the exergy destroyed for engine operation with various fuels were evaluated it was observed that the exergy destroyed with the KSOME blends was more compared to NRL diesel fuel operation at all engine loads, only slight reduction was observed in case of B10 at 25% load. Most significantly, the rate of exergy destroyed for fuel operation with B40 was the maximum at all loads. The evaluated exergy destruction mainly represented the rate of exergy destroyed due to irreversibility of phenomenon of air fuel mixing and combustion. The exergetic (IInd law) efficiencies were also evaluated and it was found that these were lower for all the fuels than the corresponding energetic (Ist law) efficiencies (BTEs). Compared to diesel fuel operation, exergetic efficiencies were lower for engine operation with the KSOME blends at all the loads and particularly with B40.

From all these analyses based on extensive experimentation it was found that the engine performance with KSOME blends up to 30% was favourable whereas the behavior of the 40% blend was quite different from the other fuel blends from the point of view that due to incomplete burning it resulted in lower heat release leading to lower engine IP and BTE. This has been confirmed from the various analyses made in this thesis. Fuel calorific value decreases with increasing concentration of biodiesel in the blend and therefore fuel consumption of engine operated with higher percentage blends is more. Moreover viscosity of the blends which increases with biodiesel addition also leads to poor atomization, delayed evaporation, and incomplete combustion. Incomplete combustion with B40 due to its higher viscosity was confirmed from its lower combustion efficiency. Increasing amounts of air swirl can be generated by suitable design of the inlet port and using bowl-in-piston type of combustion chamber for better fuel distribution and faster mixing of fuel with the air. It is the 10% blending (B10) that was found to be the most appropriate blend in so far as engine emissions are concerned.

## 8.3 RECOMMENDATIONS FOR FUTURE WORK

Recommendations for future work include the following.

1. Performing engine testing with various levels of biodiesel blending including higher percentage blends and pure biodiesel from various sources over a wide range of engines having different engine configurations. In the present study the experiments were confined only to 10% to 40% blending of KSOME with NRL diesel while experiments can be performed for blends and pure biodiesel from other potential sources. Study on the performance of biodiesel over a wider range of speeds and CR conditions can also be made which can later be used for validation of diesel cycle simulation model results.
2. The calorific value, density, cetane number and the composition of the fuels are some of the parameters that were taken into consideration while defining the characteristics of the fuel. However, viscosity, bulk modulus and surface tension are also important properties that play a major role particularly in the injection, fuel atomization, spray evolution, air fuel mixing and in the engine combustion processes. The effect of these properties are best understood if the fuel injection system, atomization, evaporation and the fuel spray combustion characteristics are considered in details and particularly for biodiesel it may reveal many interesting results. Further, it was assumed that the fuel mass was injected instantaneously and calculation of fuel mass that takes part in chemical reaction during combustion is based on complete combustion of the fuel. However, an approach that is more realistic is the incorporation of a fuel injection rate profile in the model with a finite injection duration period.
3. In this study, Annand's equation was used to simulate the instantaneous spatially averaged heat transfer between cylinder trapped mass and surrounding walls. Although this empirical correlation developed by Annand is based on extensive experiments done on diesel engine and considers the conditions present in a diesel engine, yet may not be sufficient for estimating heat transfer rate accurately, particularly the radiative heat transfer rate which is significant in diesel engine and therefore heat transfer modeling considering radiation from the in-cylinder gases and the luminous flame during combustion can be a future scope of research in order to evaluate the surface heat flux, heat flux on cylinder head and piston top with biodiesel as fuel.

4. The assumption that dissociation of combustion products does not have much effect on engine performance made in the present analysis can be removed and dissociation of combustion products can be taken into consideration to represent a more realistic cycle.

5. Extending the modeling not only for performance prediction but also to include emission modeling of NOx, HC, CO, soot etc. However for this, a correct estimation of cylinder pressure is required as the model cylinder pressure results are used in these emission modeling. In the present modeling approach an exact reproduction of cylinder pressure trace was not possible with the use of double Wiebe function, therefore other combustion models can be employed as a part of future research work in order to obtain more precise cylinder pressure results.

6. Developing a computer analysis for studying the exergetic performance of a diesel engine, operating on biodiesel fuel under both steady and transient load conditions.

7. Modeling combustion using Muti-zone and Multi-dimensionsal (CFD) combustion modeling with biodiesel as fuels.

References:

[1] Agarwal A.K., Biofuels (alcohols and biodiesel) applications as fuels for internal combustion engines. Progress in Energy and Combustion Science 2007; 33: 233–71

[2] Ma F., Hanna M.A., Biodiesel production: a review. Bioresource Technol. 1999; 70: 1-15

[3] Twaiq F.A., Mohamed A.R., Bhatia S., Liquid hydrocarbon fuels from palm oil by catalytic cracking over aluminosilicate mesoporous catalysts with various Si/Al ratios. Microporous and Mesoporous materials 2003; 64: 95-107

[4] Raphael O.I., Katikaneni, Sai P.R., Bakhshi N.N., Catalytic conversion of canola oil to fuels and chemicals: roles of catalyst acidity, basicity and shape selectivity on product distribution. Fuel processing Technology 1997; 51:101-25

[5] Niehaus R.A., Goering C.E., Savage Jr L.D., Sorenson S.C., Cracked soybean oil as fuel for a diesel engine. Trans Am Soc. Agric Eng 1986; 29: 683–89.

[6] Schwab A.W., Bagby M.O., Freedman B., Preparation and properties of diesel fuels from vegetable oils. Fuel 1987; 66: 1372–78

[7] Ziejewski M., Kaufman K.R., Schwab A.W., Pryde E.H., Diesel engine evaluation of a non-ionic sunflower oil-aqueous ethanol microemulsion. J. Am. Oil Chem. Soc. 1984; 61:1620-26

[8] Leung D.Y.C., Wu X., Leung M.K.H., A review on biodiesel production using catalyzed transesterification. Applied Energy 2010; 87: 1083–95

[9] Lotero E., Liu Y., Lopez D.E., Suwannakarn K., Bruce D.A., Goodwin Jr. J.G., Synthesis of Biodiesel via Acid Catalysis. Ind. Eng. Chem. Res. 2005; 44 (14): 5353–63

[10] Moser B.R., Biodiesel production, properties, and feedstocks. In Vitro Cell.Dev.Biol.—Plant 2009; 45: 229-66.

[11] Canakci M., Sanli H., Biodiesel production from various feedstocks and their effects on the fuel properties. J Ind Microbiol Biotechnol 2008; 35: 431–41.

[12] Knothe G., Dependence of biodiesel fuel properties on the structure of fatty acid alkyl esters. Fuel Processing Technology 2005; 86: 1059–70

[13] Ramadhas A.S., Muraleedharan C, Jayaraj S. Performance and emission evaluation of a diesel engine fueled with methyl esters of rubber seed oil. Renewable Energy (AiP) 2005; 30(12):1789–800.

[14] Raheman H.,Ghadge S.V., Performance of compression ignition engine with mahua (Madhuca indica) biodiesel. Fuel 2007; 86: 2568–73

[15] Labeckas G., Slavinskas S., The effect of rapeseed oil methyl ester on direct injection Diesel engine performance and exhaust emissions. Energy Conversion and Management 2006; 47: 1954–67

[16] Cetinkaya M., Ulusoy Y., Tekin Y., Karaosmanoglu F., Engine and winter road test performances of used cooking oil originated biodiesel. Energy Conversion and Management 2005; 46: 1279–91

[17] Usta N., An experimental study on performance and exhaust emissions of a diesel engine fuelled with tobacco seed oil methyl ester. Energy Conversion and Management 2005; 46: 2373–86

[18] Raheman H., Phadatare A.G., Diesel engine emissions and performance from blends of karanja methyl ester and diesel. Biomass and Bioenergy 2004; 27: 393 – 97

[19] Pramanik K., Properties and use of jatropha curcas oil and diesel fuel blends in compression ignition engine. Renewable Energy 2003; 28: 239–48

[20] Sahoo P.K., Das L.M., Babu M.K.G., Arora P., Singh V.P., Kumar N.R., Varyani T.S., Comparative evaluation of performance and emission characteristics of jatropha, karanja and polanga based biodiesel as fuel in a tractor engine. Fuel 2009; 88: 1698–1707

[21] Banapurmath N.R., Tewari P.G., Hosmath R.S., Performance and emission characteristics of a DI compression ignition engine operated on Honge, Jatropha and sesame oil methyl esters. Renewable Energy 2008; 33: 1982-88

[22] Agarwal D., Agarwal A.K., Performance and emissions characteristics of Jatropha oil (preheated and blends) in a direct injection compression ignition engine. Applied Thermal Engineering 2007; 27: 2314–23

[23] Puhan S., Vedaraman N., Bharat Ram B. V., Sankarnarayanan G., Jeychandran K., Mahua oil (Madhuca Indica seed oil) methyl ester as biodiesel-preparation and emission characterstics, Biomass and Bioenergy 2005; 28: 87–93

[24] Canakci M., Combustion characteristics of a turbocharged DI compression ignition engine fueled with petroleum diesel fuels and biodiesel. Bioresource Technology 2007; 98: 1167–75

[25] Murillo S., Miguez J.L., Porteiro J. , Granada E., Moran J.C., Performance and exhaust emissions in the use of biodiesel in outboard diesel engines. Fuel 2007; 86: 1765–71

[26] Rao G.L.N, Sampath S., Rajagopal K., Experimental Studies on the Combustion and Emission Characteristics of a Diesel Engine Fuelled with Used Cooking Oil Methyl Ester

and its Diesel Blends. International Journal of Engineering and Applied Sciences 2008; 4 (2): 64-70

[27] Hiroyasu H., Diesel engine combustion and its modeling, in: Diagnostics and Modeling of Combustion in Reciprocating Engines. COMODIA 85, Proceeding of Symposium; Tokyo 1985: 53–75.

[28] Heywood, J.B. Internal combustion engine fundamentals. McGraw-Hill, New York, 1988.

[29] Oh T.S., Yang J.S., Oh S.Z., Study of prediction of four stroke diesel engine performance –Cycle simulation using heat releases model- in: Diagnostics and Modeling of Combustion in Reciprocating Engines. COMODIA 85, Proceeding of Symposium; Tokyo 1985: 563-69

[30] Arregle J., Lopez J.J., Garcia J.M., Fenollosa C., Development of a zero-dimensional Diesel combustion model. Part 1: Analysis of the quasi-steady diffusion combustion phase. Applied Thermal Engineering 2003; 23: 1301−17

[31] Z.Bazari, A DI diesel combustion and emissions predictive capability for use in cycle simulation, SAE 1992: 747–70

[32] Jung D., Assanis D.N., Multi-Zone DI Diesel Spray Combustion Model for Cycle Simulation Studies of Engine Performance and Emissions. SAE 2001; 2001-01-1246

[33] Rakopoulos C.D., Rakopoulos D.C., Kyritsis D.C., Development and validation of a comprehensive two zone model for combustion and emissions formation in a DI diesel engine. Int. J. Energy Res. 2003; 27: 1221-49

[34] Ishida M., Chen Z.L., Ueki H., Sakaguchi D., Combustion analysis by Two zone model in a DI diesel engine, in: International symposium COMODIA 1994: 309-314

[35] Rakopoulos C.D., Hountalas D.T., Taklis G.N., Tzanos E.I., Analysis of combustion and pollutants formation in a direct injection diesel engine using a multi-zone model, Int. J. Energy Res. 1995; 19: 63-88

[36] Jung D., Assanis D.N., Quasi-dimensional Modeling of Direct Injection Diesel Engine Nitric Oxide, Soot, and Unburned Hydrocarbon Emissions. Journal of engineering for gas turbines and power 2006; 128: 388-396

[37] Sahin Z., Durgun O., Multi-zone combustion modeling for the prediction of diesel engine cycles and engine performance parameters. Applied Thermal Engineering 2008; 28: 2245–56

[38] Gosman A.D., Computer Modeling of Flow and Heat Transfer in Engines, Progress and Prospects, in: Proceedings of International Symposium on Diagnostics and Modeling of Combustion in Reciprocating Engines, COMODIA 85: 15-26

[39] Takagi T., Fukuyama Y., Okamoto T., Nakano Y., Numerical Simulation of Mixing and Combustion in Transient Sprays, in: Proceedings of International Symposium on Diagnostics and Modeling of Combustion in Reciprocating Engines, COMODIA 1994: 397-402

[40] Wakisaka T., Shimamoto Y., Isshiki Y., Noda T., Matsui A., Akamatsu S., Numerical Analysis of Spray Phenomena in Fuel Injection Engines, in: Proceedings of International Symposium on Diagnostics and Modeling of Combustion in Reciprocating Engines, COMODIA 1994: 403-9

[41] Tatschl R., Pachler K., Winklhofer E., A Comprehensive DI Diesel Combustion Model for Multidimensional Engine Simulation, in: The Fourth International Symposium COMODIA 98: 141-48

[42] Kleemann A.P. , Gosmany A.D., Binder K.B., Heat Transfer in Diesel Engines: A CFD Evaluation Study, in: Proceedings of International Symposium on Diagnostics and Modeling of Combustion in Reciprocating Engines, COMODIA 2001: 123-31

[43] Bianchi G.M., Cantore G., Parmigianino P., Michelassi V., On Application of Nonlinear k –ε Models for Internal Combustion Engine Flows. Journal of Engineering for Gas Turbines and Power 2002; 124: 668-77

[44] Kim C.G., A Crank Angle Resolved CIDI Engine Combustion Model With Arbitrary Fuel Injection For Control Purpose, Ph. D.Thesis, The Ohio State University, 2004

[45] Lakshminarayanan P.A., Aghav Y.V., Modelling Diesel Combustion (Mechanical Engineering Series), Springer, New York, 2010

[46] Ferguson C. R., Internal Combustion Engines, Applied Thermodynamic, John Wiley and Sons, New York, NY, 1986.

[47] Watson N., Pilley A. D., A Combustion Correlation for Diesel Engine Simulation. SAE 1980: 800029

[48] Merker G.P., Schwarz C., Stiesch G., Otto F., Simulating Combustion, Simulation of Combustion and Pollutant Formation for Engine Development, Springer-Verlag Berlin Heidelberg, 2006

[49] Yasar H., Soyhan H.S., Walmsley H., Head B., Sorusbay C., Double-Wiebe function: An approach for single-zone HCCI engine modeling. Applied Thermal Engineering 2008; 28: 1284–90

[50] Sanli A., Ozsezen A.N., Kilicaslan I., Canakci M., The influence of engine speed and load on the heat transfer between gases and in-cylinder walls at fired and motored conditions of an IDI diesel engine. Applied Thermal Engineering 2008; 28: 1395–1404

[51] Ganesan V., Computer simulation of CI engine process, University press (India) Ltd, 2000

[52] Cengel Y.A., Boles M.A., Thermodynamics, an engineering approach, New Delhi: Tata Mcgraw-Hill; 2006

[53] Bejan A., Advanced engineering thermodynamics. New York: Wiley; 1988.

[54] Moran MJ, Shapiro HN., Fundamentals of engineering thermodynamics. New York: Wiley; 2000.

[55] Caton J.A., A Review of Investigations Using the Second Law of Thermodynamics to Study Internal Combustion Engines, SAE 2000: 2000-01-1081

[56] Rakopoulos C.D., Giakoumis E.G., Speed and Load Effects on the Availability Balances and Irreversibilities Production in a Multi-Cylinder Turbocharged Diesel Engine. Applied Thermal Engineering 1997; 17(3): 299-313

[57] Rakopoulos C.D., Giakoumis E.G., Development of Cumulative and Availability Rate Balances in a Multi-Cylinder Turbocharged Indirect Injection Diesel Engine. Energy Convers. Mgmt. 1997; 38: 341-69

[58] Rakopoulos C.D., Giakoumis E.G., Simulation and exergy analysis of transient diesel engine operation. Energy 1997; 22 (9): 875-85

[59] Kumar S.V., Minkowycz W.J., Patel K.S., Numerical Simulation of the thermodynamic, fluid flow, and heat transfer processes in a diesel engine. Numerical Heat transfer part A 1990; 17: 143-66

[60] Caton J.A., On the destruction of availability (exergy) due to combustion processes with specific application to internal combustion engines. Energy 2000; 25: 1097-1117

[61] Rakopoulos C.D., Giakoumis E.G., Second-law analyses applied to internal combustion engines operation. Progress in Energy and Combustion Science 2006; 32: 2–47

[62] Som S.K., Dutta A., Thermodynamic irreversibilities and exergy balance in combustion processes, Progress in Energy and Combustion Science 2008; 34: 351–76

[63] Canacki M., Hosoz M., Energy and exergy analyses of a diesel engine fuelled with various biodiesel. Energy sources part B 2006; 1: 379-94

[64] Gokalp B., Soyhan H.S., Sarac H.I., Bostan D., Sengun Y., Biodiesel addition to standard diesel fuels and marine fuels used in a diesel engine: effects on emission characteristics and first and second law efficiencies. Energy and fuel 2009; 23: 1849-57

[65] Diesel-Wikipedia, the free encyclopedia (en.wikipedia.org/wiki/Diesel)

[66] Gogoi T.K., Baruah D.C., A cycle simulation model for predicting the performance of a diesel engine fuelled by diesel and biodiesel blends. Energy 2010; 35: 1317–23

[67] Sarma A.K., Konwer D., Bordoloi P.K., A Comprehensive Analysis of Fuel Properties of Biodiesel from Koroch Seed Oil. Energy and Fuels 2005; 19: 656-57

[68] Ramadhas A.S., Jayaraj S., Muraleedharan C., Theoretical modeling and experimental studies on biodiesel fueled engine. Renewable Energy 2006; 31: 1813-26

[69] Rakopoulos C.D., Antonopoulos K.A., Rakopoulos D.C., Giakoumis E.G., Study of combustion in a divided chamber turbocharged diesel engine by experimental heat release analysis in its chambers. Applied Thermal Engineering 2006; 26: 1611-20

[70] Rakopoulos C.D., Giakoumis E.G., Availability analysis of turbocharged diesel engine operating under transient diesel load conditions. Energy 2004; 29: 1085-1104

[71] Rakopoulos C.D., Rakopoulos D.C., Kyritsis D.C., Development and validation of a comprehensive two zone model for combustion and emissions formation in a DI diesel engine. Int. J. Energy Res. 2003; 27: 1221-49

[72] Bibic D., Filipovic I., Hribernik A., Pikula B., Investigation into the effect of different fuels on ignition delay of M type diesel combustion process. Thermal science 2008; 12 (1): 103-14

[73] Kastner L.J., Williams T.J., White J.B., Poppet Inlet valve Characteristics and their influence on the Induction Process. Proc. Instn. Mech. Engrs part 1 1963-64; 178 (36): 955-78

[74] Bishop I.N., Effect of Design Variables on Friction and Economy, SAE Transaction, 1965; 73: 334-358

[75] Demirbas A., Biodiesel fuels from vegetable oils via catalytic and non-catalytic supercritical alcohol transesterifications and other methods: A survey. Energy Conversion and Management 2003; 44: 2093–2109

[76] Schwab A.W., Dykstra G.J., Selke E., Sorenson S.C., Pryde E.H., Diesel fuel from thermal decomposition of soybean oil. JAOCS 1988; 65:1781–6

[77] Pioch D., Lozano P., Rasoanatoandro M.C., Grailla J., Geneste P., Guida A., Biofuels from catalytic cracking of tropical vegetable oils. Oleagineux 1993; 48: 289–91

[78] Agarwal A.K., Das L.M., Biodiesel development and characterization for use as a fuel in compression ignition engine. J Eng Gas Turbines Power 2001; 123: 440–7

[79] Gupta V., Biodiesel Production from Karanja Oil. Journal of Scientific and Industrial research 2004; 63: 39-47

[80] Barnwal B.K., Sharma M.P., Prospects of biodiesel production from vegetable oils in India. Renewable and Sustainable Energy Reviews 2005; 9: 363–78

[81] Zhang Y., Dub M.A., McLean D.D., Kates M., Biodiesel production from waste cooking oil: 1.Process design and technological assessment. Bioresource Technol 2003; 89: 1-16

[82] Zhang Y, Dub M.A., McLean D.D., Kates M., Biodiesel production from waste cooking oil: 2. Economic assessment and sensitivity analysis. Bioresource Technol 2003; 90: 229–40

[83] Canakci M., Van G.J., Biodiesel production via acid catalysis. Trans. Am. Soc. Agric. Eng.1999; 42(5): 1203–10

[84] Guan G., Kusakabe K., Sakurai N., Moriyama K., Transesterification of vegetable oil to biodiesel fuel using acid catalyst in the presence of dimethyl ether. Fuel 2009; 88(1): 81-86

[85] Agarwal D., Sinha S., Agarwal A.K., Experimental investigation of control of NOx emissions in biodiesel-fueled compression ignition engine. Renewable Energy 2006; 31: 2356–69

[86] Ahmad M., Rashid S., Khan M.A., Zafar M., Sultana S., Gulzar S., Optimization of base catalyzed transesterification of peanut oil biodiesel. African Journal of Biotechnology 2009; 8 (3): 441-46

[87] Saravanan S., Nagarajan G., Lakshmi Narayana Rao G., Sampath S., Combustion characteristics of a stationary diesel engine fuelled with a blend of crude rice bran oil methyl ester and diesel. Energy 2010; 35: 94–100

[88] Kocak M.S., Ileri E., Utlu Z., Experimental Study of Emission Parameters of Biodiesel Fuels Obtained from Canola, Hazelnut, and Waste Cooking Oils. Energy & Fuels 2007; 21: 3622–26

[89] Ali Y, Hanna M.A., Cuppett S.L., Fuel properties of tallow and soybean oil esters. J Am Oil Chem Soc 1995; 72: 1557–64.

[90] Bala B.K., Studies on biodiesels from transformation of vegetable oils for diesel engines. Energy Edu Sci Technol 2005; 15: 1–43.

[91] Demirbas A., Biodiesel production via non-catalytic SCM method, and biodiesel fuel characteristics, Energy Conversion and Management 2006; 47: 2271–82

[92] Cardone M., Mazzoncini M., Menini S., Rocco V., Senatore A., Seggiani M., Vitolo S., Brassica carinata as an alternative oil crop for the production of biodiesel in Italy: agronomic evaluation, fuel production by transesteri!cation and characterization, Biomass and Bioenergy 2003; 25: 623 – 36

[93] Kusdiana D., Saka S., Kinetics of transestrification in rapseed oil to biodiesel fuel as trested in supercritical methanol. Fuel 2001; 80: 693–98

[94] Saka S., Kusdiana D., Biodiesel fuel from rapeseed oil as prepared in supercritical methanol. Fuel 2001; 80: 225–31

[95] Demirbas A., Biodiesel from vegetable oils via transesterification in supercritical methanol. Energy Conversion and Management 2002; 43: 2349–56

[96] Demirbas A., Biodiesel production from vegetable oils by supercritical methanol. Journal of Scientific & Industrial Research 2005a; 64: 858–65

[97] Demirbas A., Biodiesel production from vegetable oils via catalytic and non-catalytic supercritical methanol transesterification methods. Progress in Energy and Combustion Science 2005; 31: 466–487

[98] Sarma A.K., Biodiesel Production from Mesua Ferrea L. (Nahar) and Pongamia Glabra Vent. (Koroch) Seed Oil, Ph D thesis, Department of Energy, Tezpur University, 2006

[99] Kegl B., Hribernik A., Experimental Analysis of Injection Characteristics Using Biodiesel Fuel. Energy & Fuels 2006; 20: 2239-48

[100] Wong C.L., Steere D.E., The Effects of Diesel Fuel Properties and Engine Operating Conditions on Ignition Delay. SAE 1982; 821231

[101] Pischinger F., Reuter U., Scheid F., Self Ignition of Diesel Sprays and Its Dependence on Fuel Properties and Injection Parameters. J. Eng. Gas Turbines Power 1988; 110: 399-404

[102] Assanis D.N., Filipi Z. S., Fiveland S. B., Syrimis M., A Predictive Ignition Delay Correlation Under Steady-State and Transient Operation of a Direct Injection Diesel Engines. J. Eng. Gas Turbines Power 2003; 125: 450-57

[103] Sahoo P.K., Das L.M., Combustion analysis of Jatropha, Karanja and Polanga based biodiesel as fuel in a diesel engine. Fuel 2009; 88: 994–99

[104] Katrasnik T., Trenc F., Opresnik S.R., A New Criterion to Determine the Start of Combustion in Diesel Engines. J. Eng. Gas Turbines Power 2006; 128: 928-33

[105] Qi D.H., Geng L.M., Chen H., Bian Y.ZH., Liu J., Ren X.CH., Combustion and performance evaluation of a diesel engine fueled with biodiesel produced from soybean crude oil. Renewable Energy 2009; 34: 2706–13

[106] Agarwal A.K., Rajamanoharan K., Experimental investigations of performance and emissions of Karanja oil and its blends in a single cylinder agricultural diesel engine. Applied Energy 2009; 86: 106-12

[107] Lapuerta M., Fernandez J. R., Oliva F., Canoira L,. Biodiesel from Low-Grade Animal Fats: Diesel Engine Performance and Emissions. Energy & Fuels 2009; 23: 121–29

[108] Jindal S., Effect of engine parameters on NOx emissions with Jatropha biodiesel as fuel. International journal of energy and environment 2010; 1: 343-50

[109] Taymaz I., An experimental study of energy balance in low heat rejection diesel engine. Energy 2006; 31: 364–71

[110] Wallace S. J., Diesel engine energy balance study operating on diesel and biodiesel fuels. M.S. thesis. 2007, Russ College of Engineering and Technology of Ohio University

[111] Yuksel F., Ceviz M. A., Thermal balance of a four stroke SI engine operating on hydrogen as a supplementary fuel. Energy 2003; 18: 1069–80

[112] Rehman A., Sarviya R.M., Pandey R.K., Investigation to ascertain the possibility of using non edible Karanja oil in CI engine with various oil modification. Conf. on Advances in Energy Research 2007; IIT Mumbai, India

[113] Kegl B., Numerical analysis of injection characteristics using biodiesel fuel. Fuel 2006; 85: 2377–87

[114] Narayana Rao G.L., Prasad B.D., Sampath S., Rajagopal K., Combustion analysis of diesel engine fuelled with jatropha oil methyl ester-diesel blend. International Journal of Green Energy 2007; 4: 645–58

List of Publications:

1. T.K. Gogoi, D.C. Baruah, "A Cycle Simulation Model for Predicting Performance of a Diesel Engine Fuelled by Diesel and Bio-diesel Blends"; published in the journal "Energy" , Vol. 35, Issue 3, March 2010, Pages 1317-1323.

2. T.K. Gogoi, D.C. Baruah, "The use of Koroch seed oil methyl ester blends as fuel in a diesel engine"; published in the journal "Applied Energy", Vol. 88, Issue 8, August 2011, pages 2713-2725.

3. T.K. Gogoi, D.C. Baruah, "Performance and Energy Analyses of a Diesel Engine Fuelled with Koroch Seed Oil Methyl Ester and its Diesel Fuel Blends", Accepted for publication in International Journal of Energy Technology and Policy, Inderscience enterprises ltd.

4. T.K. Gogoi, D.C. Baruah, "Energetic Performance Analysis of a Diesel Engine Fuelled With Koroch Seed Oil Methyl Ester and Its Diesel Blends" ; in the proceedings of International Conference on Thermal Energy and Environment (INCOTEE), 24-26$^{th}$ March, 2011 held in Kalasalingam University, Tamilnadu, India.

5. T.K. Gogoi, S. Talukdar, D.C. Barauah, "Comparative Analysis of Performance and Combustion of Koroch Seed Oil and Jatropha Methyl Ester blends in a Diesel Engine."; in the proceedings of World Renewable Energy Congress (WREC) 2011 held in Linkoping, Sweden from 8-13$^{th}$ May, 2011.